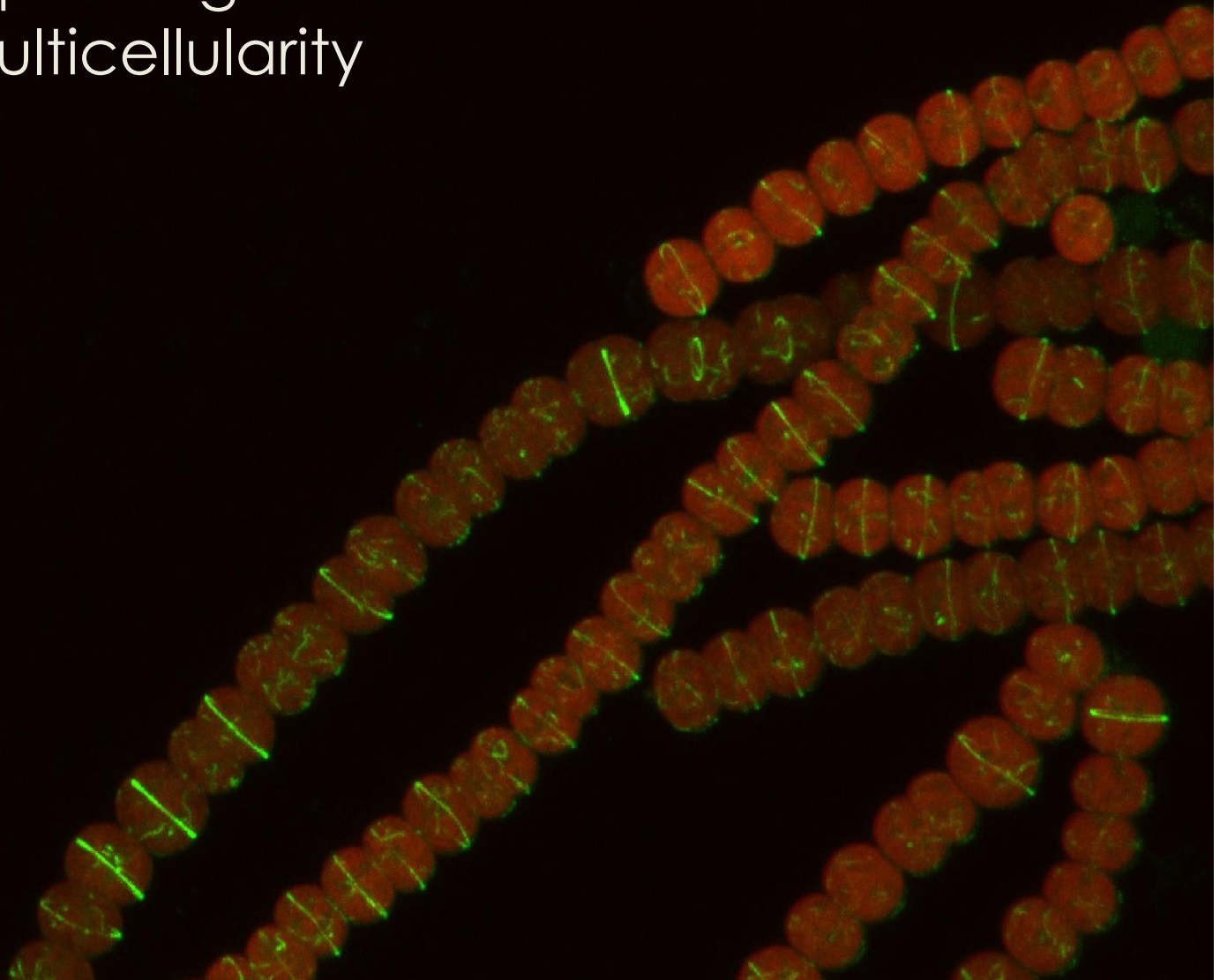# Regulation of cell size and cell division in the filamentous cyanobacterium *Anabaena*: a paradigm of bacterial multicellularity

Cristina Velázquez Suárez
Sevilla, 2023

Instituto de Bioquímica Vegetal y Fotosíntesis
Departamento de Bioquímica Vegetal y Biología Molecular
Consejo Superior de Investigaciones Científicas – Universidad de Sevilla

TESIS DOCTORAL

Regulation of cell size and cell division in the filamentous cyanobacterium *Anabaena*: a paradigm of bacterial multicellularity

Trabajo presentado para optar al grado de Doctora en Biología por la graduada
Cristina Velázquez Suárez

Directora

Dra. Antonia Herrero Moreno
Profesora de Investigación del CSIC

Director

Dr. Ignacio Luque Romero
Científico Titular del CSIC

Tutora

Dra. Mercedes García González
Profesora Titular de Bioquímica y Biología Molecular – Universidad de Sevilla

FUNDING

A los tres pilares de mi vida:
mi padre, mi madre y mi hermana

AGRADECIMIENTOS

Ahora que esta tesis llega a su fin quiero agradecer a todas las personas que han permanecido a mi lado, a los que han llegado y a los que se han ido antes de tiempo. A todos: GRACIAS.

En primer lugar, quiero dar las gracias a mis directores de tesis, los Dres. Antonia Herrero e Ignacio Luque, por darme la oportunidad de formarme y de crecer como científica y como persona en su grupo. Por la paciencia, la dedicación y la motivación durante todos estos años, gracias de corazón.

Al grupo de Biología de Cianobacterias Multicelulares: a Enrique por su visión crítica; a Ana y Gracia por cuidarme siempre; a Rocío, por ser como una hermana mayor; a Mercedes, Mireia, Sergio, Alicia, Miguel Ángel y Cristina-Zgz por aguantar mis dramas. A todo el personal de mi segunda casa, el IBVF, con una mención especial a Alicia Orea, a José Enrique, a Ana Jurado y a Toñi.

I would like to thank Dr. Dennis Nürnberg for hosting me in his laboratory and thanks to Laura, Vera, Xiaoran, Shujie, Claudia, Kalman and Janis for the help during those months. A special thanks to Viktor and Mini, for making my stay in Berlin an unforgettable experience.

Me gustaría agradecer a la primera persona que confió en mí en la ciencia, Eva Valdivia, que diez años después sigue siendo mi amiga y una fuente de inspiración. Por supuesto, a todos los que forman el BIO160 del departamento de Microbiología de la UGR y que prestan su apoyo desde la distancia: Rubén, Manolo, Platero, Sonia y Pirri. Sin mi formación con vosotros, no habría sido lo mismo.

Mil gracias a mis amigas, por demostrar que los kilómetros que nos separan a todas, si se quiere, pueden ser solamente una cifra. Por las risas y por los llantos, por los consejos y por escucharme aunque no entendáis de qué hablo. María Isabel, Virginia, Cristina, Marién y Jesús. A bebé Blanca que me esperó hasta la vuelta de Berlín, algún día te lo contaremos. Gracias a Susana, a quien la microbiología trajo a mi vida y nos hemos visto crecer hasta compartir año de defensa de tesis.

Gracias a mis primos, a mis tíos, a Mangel. Y, en especial, a mis abuelos por el amor incondicional y ser un ejemplo de superación y valentía; sé que estaréis orgullosos de mí. A Javi y a su familia, por haber sido parte de la mía durante tanto tiempo.

Las últimas líneas de estos agradecimientos son para las tres personas más importantes de mi vida: mi padre, mi madre y mi hermana. Por el apoyo, por escuchar mis monólogos, por la confianza siempre, por creer en mí, por secar mis lágrimas y reír con mis tonterias. Gracias por hacer del pequeño renacuajo que fui la persona que hoy soy.

INDEX

INTRODUCTION

1. BACTERIAL CELL MORPHOLOGY

Billion years of evolution have made bacteria largely diverse, showing wide variations in lifestyle, metabolism and ultrastructure. The information for these particular characteristics is genome encoded and defines the identity of each phylogenetic group or species. Likewise, the morphology of bacterial cells is genetically encoded and it is an intrinsic feature of each bacterial species inherited from the mother cell. Thus, since all individuals of a particular species show a similar morphology, for more than a century microbiologists have used this trait as a taxonomic criterion.

Cell size and cell shape contribute importantly to cell morphology, although other features (i.e. the existence of surface extensions or appendages) can also influence it. Despite the great progress made in the last decades, more research is still needed to elucidate in full the mechanisms of determination of bacterial cell morphology.

1.1. Cell size

In the domain Bacteria, the variation in cell size expands more than four orders of magnitude, ranging from the 0.2 µm of *Mycoplasma pneumoniae* to the 1000 µm in length of the recently discovered giant bacteria. The fact that these giant bacteria are visible by the naked eye has challenged the concept that bacteria are microbes (Figure 1). The largest known giant bacteria are the free-living *Thiomargarita namibiensis* and *T. magnifica*, and *Epulopiscium fishelsoni*, a symbiont of the surgeonfish (Levin and Angert, 2015; Volland *et al.*, 2022)*.

Size variation in bacteria is limited by some constraints. The lower limit is dictated by the minimum space needed to house biochemical components such as proteins, lipids and nucleic acids, essential for survival and reproduction (Koch, 1996). The upper limit is thought to be set by the ratio between the cell surface and the cell volume (the S/V ratio). For spherical cells, the larger the cell, the lower its S/V ratio. Because the cell surface mediates the molecular exchange with the surrounding medium, large cells have, in relation to its volume, less surface for exchange with the environment than small cells, which would be detrimental beyond certain limits. However, rather than the surface size itself, the real limit appears to be imposed by the number of transporters to transfer nutrients and waste into and out of the cytoplasm than can be accommodated in the available envelope space (Young, 2006; Westfall and Levin, 2017). Cell size is also restricted by the limitations of molecular diffusion within the cytoplasm, which largely impinges on biochemical reactions, growth and reproduction (Beveridge, 1988; Schulz and Jørgensen, 2001). Nonetheless, bacteria have evolved different ways to overcome such limitations, such as adopting a shape that maximizes the surface area, i.e. the spiral shape of Spirochaetes or *Helicobacter pylori*, or the extensive vesiculation of the inner membrane of the giant bacterium *E. fishelsoni* (Young, 2006; Levin and Angert, 2015). The also giant *T. namibiensis*

shows a large vacuole at the center of the cytoplasm and confines the metabolic activity to peripheral vesicular compartments (Volland *et al.*, 2022).

Notwithstanding that cells of the same strain have the same average size, this parameter can change to some extent depending on certain conditions. The growth law proposed in 1958 by Schaechter was based on empirical observations in *Salmonella thyphimurium* and postulates that the cell size increases linearly with the growth rate and inversely correlates to the duplication time (reviewed in Morcinek-Orlowska *et al.*, 2019). Thus, environmental conditions such as the availability of carbon, phosphate or nitrogen, which determine the growth rate, influence cell size in a variety of species (Levin and Angert, 2015). Some evidence indicates that in some rod-shaped bacteria such as *Caulobacter crescentus*, *Escherichia coli* or *Listeria monocytogenes*, the alarmone guanosine tetraphosphate (ppGpp) could play an important role on cell size determination (Büke *et al.*, 2022). Also, a threshold of unincorporated cell wall precursors appear to signal the time of cell division initiation, which impacts on cell size (Chen and Good, 2016; Harris and Theriot, 2016). However, in general terms, the molecular mechanisms by which variations in bacterial cell size are determined remain largely unknown.
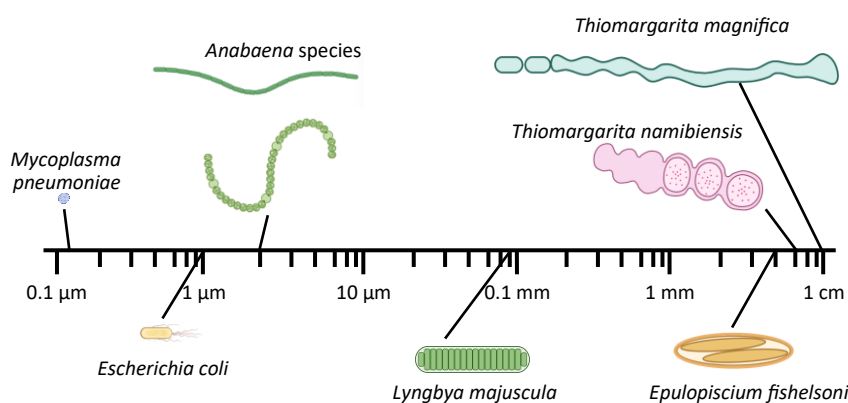
Figure 1. Variation of bacterial size. The scheme is aimed to illustrate the different sizes of bacteria, from the smallest species of the genus *Mycoplasma* to the giant bacteria of the genus *Thiomargarita*. Figure generated with Biorender (https://biorender.com/).

1.2. Cell shape

Species of the Bacteria domain exhibit an astonising vast variety of shapes (Figure 2). The bacterial cell shape is genetically determined and maintained through generations, although some modifications can take place throughout the cell cycle (van Teeseling *et al.*, 2017). Although the most common shapes are cocci and rods, there are many other cell forms, including those resembling spirals or comma, lemon or teardrops, thin circular disks, hexagons or stars (Figure 2). There are also irregular morphologies derived from asymmetric cell division or the presence of appendages, which are used for attachment to surfaces or to increase the cell surface (Young, 2006; Willis and Huang, 2017).

The cell shape is important for different features of bacteria. For instance, as mentioned above, some shapes maximize the S/V ratio providing an adaptative advantage by increasing the accessibility to nutrients. Thin flat shapes provide maximal S/V ratio, but such morphology is not the most abundant, indicating that other parameters also influence on the evolution of cell morphology (Young, 2006; Ojkic and Banerjee, 2021). Cell shape is also important for the colonization of surfaces, as in *C. crescentus*; for biofilm formation, which requires a certain surface for contact with the substratum and the adjacent cells; for motility in social groups or as single cells, or for pathogenicity, as certain cell shapes may contribute to motility in viscous media and evasion from host defenses (van Teeseling *et al.*, 2017). Also, the cell shape can impact antibiotic resistance by limiting the flow of antibiotics into the cell (Ojkic *et al.*, 2022).
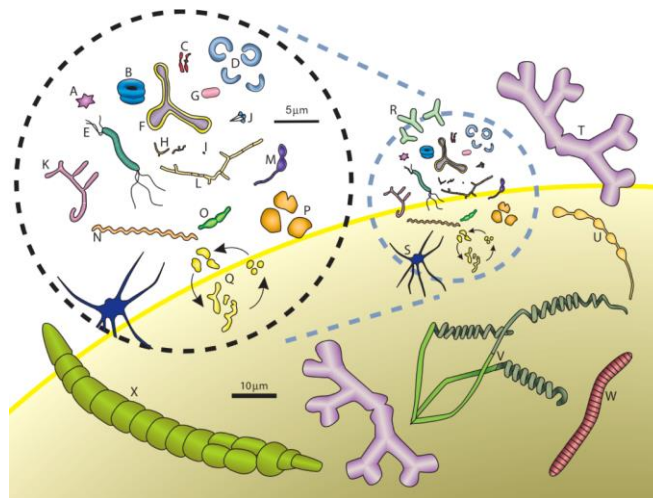
Figure 2. Diversity of bacterial shapes. Although the most common bacteria are cocci, ovococci or bacilli, there are lemon-shaped, teardrop-shaped, curved, helical-shaped, star-shaped or irregularly-shaped cells, among others. Figure from Young, (2006).

All bacterial cells show variations of their shape, including changes in cell length and width, troughout the cell cycle (Young, 2006). Changes associated with growth and division are in general moderate and the overall shape of the cell is maintained. However, some species undergo large alterations. For instance, some species exhibit morphological changes that involve the generation of new regions or appendages (van Teeseling *et al.*, 2017). Besides, the so-called polymorphic, or dimorphic, bacteria show distinct shapes along their life cycle. A well-studied case is *C. crescentus,* which is dimorphic and whose cell cycle is dependent on morphological changes produced by an asymmetric division that gives rise to a stalked sessile cell and a flagellated swarmer cell, whose function is to search new places to colonize (Young, 2006; van Teeseling *et al.*, 2017). The cell shape can also be altered by nutrient availability, leading to the formation of swarming motile cells that show a rounded shape (i.e. rod-shaped cells can turn into coccoids). In other cases, nutrient limitation induces a state of dormancy defined as *viable but not culturable* (VBNC) and the differentiation of spores, which are metabolically inert and show smaller size and rounder shape than normal cells (van Teeseling *et al.*, 2017). Furthermore, shorter or longer cells can be generated when cell division and cytokinesis are altered, as

observed e.g. in *E. coli* mutants that form minicells or filaments by overexpression or downexpression of FtsZ, the protein initiating cell division (see below), respectively (Ward and Lutkenhaus, 1985; Dai and Lutkenhaus, 1991).

Regarding the mechanisms of determination of cell shape, it is well known that the peptidoglycan (PG) sacculus that surrounds the cytoplasmic membrane is responsible for the specific shape of each bacterial species. Indeed, upon isolation, the sacculus of different bacteria maintains the cell shape. Furthermore, PG-less cells (spheroplasts) generated by treatment with hydrolases can synthesize their cell wall *de novo* and restore the original cell shape after a few generations (Ranjit and Young, 2013). This important observation indicates that the formation of the sacculus and in turn the determination of the cell shape does not require a preexisting template, but depends on biosynthetic complexes and their dynamics and topology (van Teeseling *et al.*, 2017).

2. THE BACTERIAL CELL ENVELOPE AND ITS EVOLUTION

The bacteria cell envelope is constituted by the external layers of the cell and plays a fundamental role in the determination of the cell shape. Besides, the cell envelope is responsible for other functions, such as exchanges with the environment, including nutrient uptake and waste disposal, energy production, protection from mechanical stress or aggressions and adhesion to surfaces (Strahl and Errington, 2017; Egan *et al.*, 2020; Sun *et al.*, 2022).

Bacteria have long been classified into two groups according to the structure of their envelope. Such classification was based on the differential staining of cells with the technique developed by Gram in 1884, but it was not until 1964 that the correlation between the differential staining pattern and the structure of the cell envelope was established (Megrian *et al.*, 2020). Gram-positive bacteria have an inner plasma membrane and a thick PG wall composed of multiple layers, decorated with teichoic and lipoteichoic acids facing the external medium. Gram-negative bacteria contain a thin layer of PG in between the inner membrane and an asymmetric outer membrane (OM), in the so-called periplasmic space or periplasm (Figure 3). The Gram test is based on staining with crystal violet followed by washing with ethanol and staining with safranin. Gram positive bacteria retain the crystal violet in its thick PG wall, thus appearing violet. In contrast, after the treatment with the alcohol, which degrades the OM and also makes their PG wall more porous, Gram-negative bacteria cannot retain the crystal violet in its thin PG; however, they can retain the safranin dye, thus appearing pink (Kumar *et al.*, 2022). This nomenclature is still extensively used in the scientific literature, but since a major difference between these two groups of bacteria is the existence of one or two membranes in the cell envelope, a current tendency is to refer them as 'monoderm' or 'diderm' bacteria.
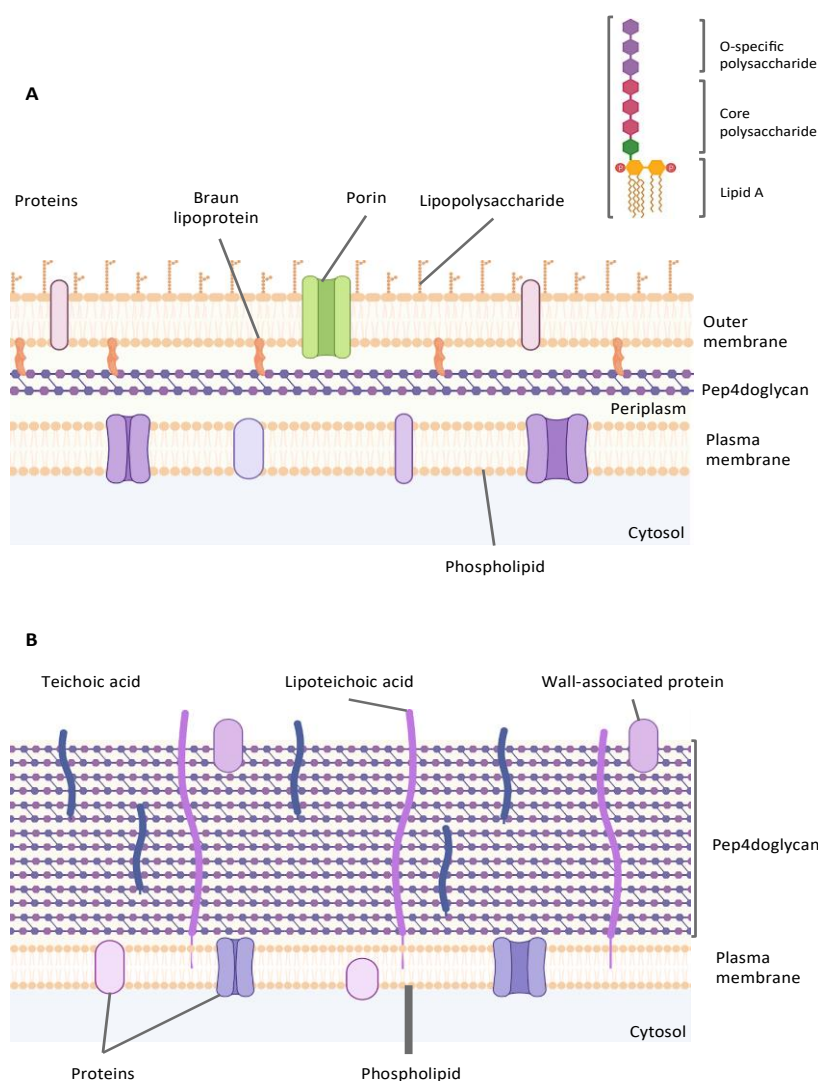
Figure 3. Types of bacterial cell envelopes. (A) Schematic of the cell wall of *E. coli*, a representative of Gram-negative or diderm bacteria, with a thin layer of peptidoglycan and an outer membrane, with lipopolysaccharides in its outer face, bound to the peptidoglycan by the Braun lipoprotein. A variety of proteins are embedded in the plasma membrane and the outer membrane. (B) Representation of the envelope of Gram-positive or monoderm bacteria containing a thick multilayered peptidoglycan sacculus in which teichoic and lipoteichoic acids are embedded. Both, the plasma membrane and the peptidoglycan present associated proteins. Figure generated with Biorender (https://biorender.com/).

The basis for the existence of these two types of bacteria is a major question in Biology. It has been long assumed that monoderm and diderm bacteria are distinct phylogenetic groups, and an intense debate on their origin and evolution has led to propose that monoderm bacteria derived from diderm ones or vice-versa (Cavalier-Smith, 2002; Lake, 2009; Gupta, 2011; Tocheva *et al.*, 2016). Recent investigations have provided a solid support for the notion that diderms were the first bacteria to evolve (Coleman *et al.*, 2021; Witwinowski *et al.*, 2022). Coleman and collaborators have accurately located the root of the bacterial evolutionary tree between two large phylogenetic groups known as 'Gracilicutes' and 'Terrabacteria', respectively. Gracilicutes include the vast majority of diderm bacteria, whereas Terrabacteria include phyla of diderm and monoderm bacteria (Figure 4), suggesting that the common ancestor of both groups was a diderm organism. Based on the analysis of the evolutionary path of bacterial genes, this study proposed that the *Last Bacterial Common Ancestor* (LBCA) was a rod-shaped, diderm bacteria (Coleman *et al.*, 2021).

In addition, some monoderm or diderm bacteria have an outermost envelope layer, the so-called S-layer. The S-layer is a paracristalline monolayer of proteins or glycoproteins that may have different roles such as anchoring to surfaces or structural strengthening, and even can serve as a sort of cell wall in some bacteria lacking it (Missiakas and Schneewind, 2017).
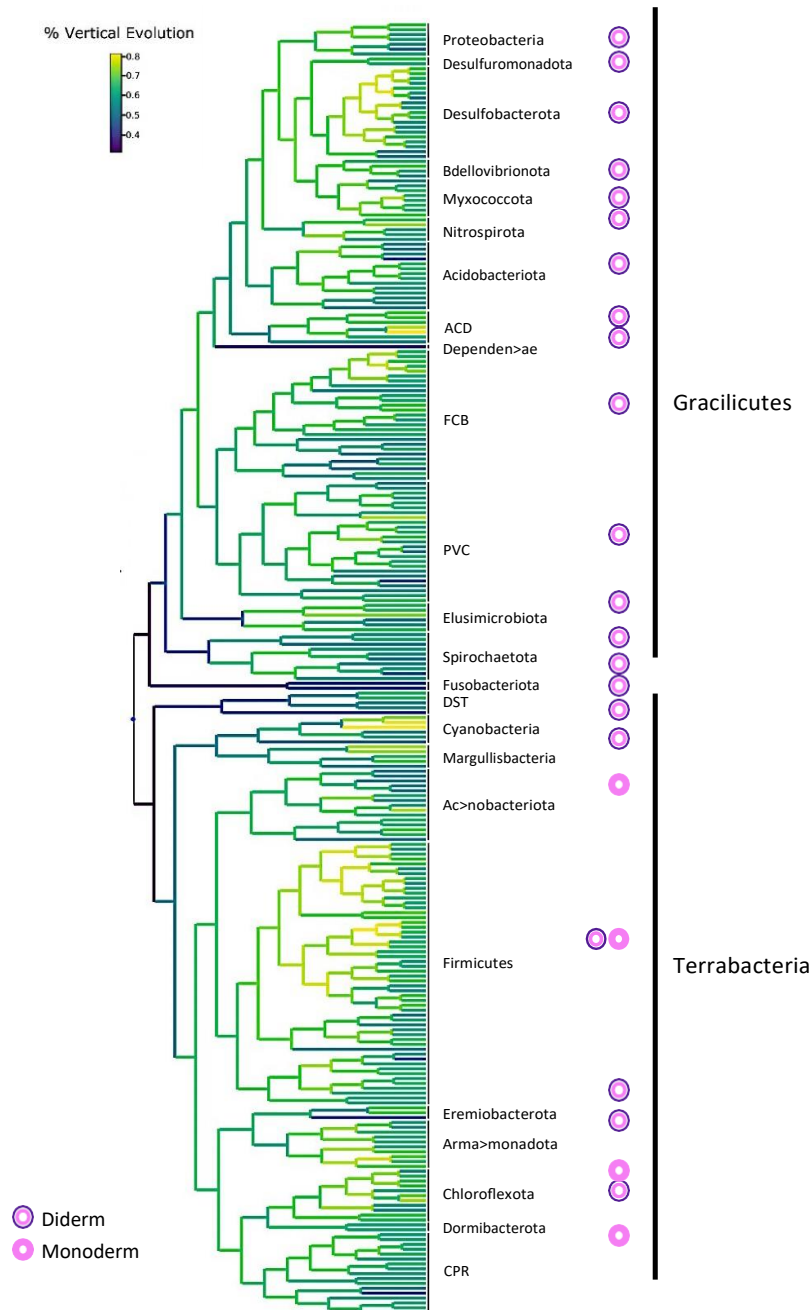
Figure 4. Bacterial cell envelope evolution. Phylogenetic tree of bacteria showing division into two major groups, the so-called Gracilicutes and the Terrabacteria. For each phylum, the structure of the cell envelope is shown at the right side. Figure adapted from Coleman *et al.*, (2021).

2.1. The plasma membrane

The innermost envelope layer that surrounds the cytoplasm and separates it from the environment is the cytoplasmic or inner or plasma membrane (PM). The bacterial PM is a lipid bilayer, the major constitutents of which are phosphatidylethanolamine, phosphatidylglycerol and cardiolipin (Epand and Epand, 2009; Sohlenkamp and Geiger, 2015). Proteins partially or completely embedded, or located at its periphery are also important constituents (Figure 3). The major function of the PM is to mediate the exchange of the cell with the environment, acting as a selective permeability barrier for the passage of molecules through it. The ability to traverse the PM is mainly dictated by the nature of molecules, in such a way that lipophylic and small neutral molecules can diffuse in a gradient-dependent manner. Other molecules pass through the PM by means of protein systems that allow their transport to the inside or the outside of the cell. The transport of nutrient and waste substances through the PM is essential and bacterial cells dedicate a plethora of systems to this role. Transport systems may mediate facilitated diffusion of molecules, which always happens in a gradient-dependent manner, or the transfer of substrates against a concentration gradient (active transport). Transport systems can be constituted by a single transmembrane protein or may be complex structures involving several proteins, such as those of the large category of ABC (ATP-binding cassette) transporters, which normally include a periplasmic substrate-binding protein. Energy for the transport of substances against a concentration gradient can be provided by the disipation of an ion gradient, the proton motive force or, as in the case of ABC transporters, ATP (Konovalova *et al.*, 2017).

Molecules exported from the cytoplasm are either secreted to the periplasm or to the extracellular medium and include waste molecules, constituents of the outermost layers of the cell envelope and molecules with signalling functions, mediating intercellular interactions or devoted to the scavenging of nutrients (i.e. siderophores). Some proteins of the PM may also participate in sensing environmental stimuli and signal transduction.

2.2. The outer membrane

In diderm bacteria, the outermost layer of the cell envelope is the OM, which is a lipid bilayer but, at difference with the PM, it is asymmetric, being constituted by phospholipids, in its inner leaflet, and glycolipids, known as lipopolysaccharide (LPS), in its outer leaflet. In addition, the outer membrane possesses lipoproteins, with a lipid portion embedded in the membrane, and transmembrane proteins called outer membrane proteins (Konovalova *et al.*, 2017; Choi and Lee, 2019; Macnair and Brown, 2020; Sun *et al.*, 2022). The LPS is constituted by three components: a lipidic part, known as lipid A, a conserved core polysaccharide and the O-specific polysaccharide ('O-antigen'), which is variable and possesses repeating units of different structures that can be linear or branched (Raetz and Whitfield, 2002) (Figure 3A). LPS molecules

are cross-linked by divalent cations, which contribute to reinforce the OM structure and somehow compensates for the weakness of the thin PG layer of diderm bacteria (Konovalova *et al.*, 2017; Sun *et al.*, 2022). The anchoring of the OM to the PG has traditionally been thought to be carried out by the Braun's lipoprotein (Lpp). However, recent research has revealed that Lpp is restricted to the Proteobacteria clade, whereas the vast majority of bacteria use alternative anchoring proteins; e.g., OmpA (see below) and OmpM in Gracilicutes and Terrabacteria, respectively (Witwinowski *et al.*, 2022).

The OM also acts as a permeability barrier and delimits the periplasm, where numerous reactions take place. The OM is impermeble to large molecules, such as some antibiotics, but allows the pass of small hydrophilic molecules such as sugars and amino acids, which traverse the OM through porins (Choi and Lee, 2019; Macnair and Brown, 2020). Porins are transmembrane proteins with a β-barrel structure, which forms a channel through which the substrate can traverse. Porins are classified in monomeric, dimeric o trimeric, according to their functional structure; and in non-specific or specific according to their range of substrates. OmpA is the most studied porin; it is anchored to PG by a non-covalent bond and has a role in maintenaince of the integrity of the cell envelope (Choi and Lee, 2019). Other substrates are transported through the OM in an energy-dependent manner by dedicated TonB-dependent transporters (Silale and van den Berg, 2023).

2.3. The cell wall

Bacterial cell morphology is dictated and maintained by the PG layer that composes the cell wall. This structure, also called the sacculus, surrounds the plasma membrane (it is located in the periplasmic space in diderm bacteria) and provides mechanical strength that precludes cells from bursting by turgor pressure. As explained above, the cell wall can be multilayered, as in monoderm bacteria, or monolayered as in canonical diderm bacteria (see section 2 and Figure 3). The specific arrangement of the cell wall components provides this structure with strength as well as flexibility (Egan *et al.*, 2020; Rohs and Bernhardt, 2021; Kumar *et al.*, 2022).

2.3.1. Structure of the cell wall

The PG layer is a giant mesh-like molecule whose structure is based on long chains of alternating *N*-acetylglucosamine (Glc*N*Ac) and *N*-acetylmuramic acid (Mur*N*Ac) units linked by β-1,4 bridges. In rod-shaped bacteria, the glycan chains are oriented perpendicular to the longitudinal axis of the cell. Each Mur*N*Ac amino sugar is covalently linked to a pentapeptide that is cross-linked to the pentapeptide of an adjacent glycan chain, which actually confers to PG its mesh-like structure (Figure 5). In diderm bacteria, the pentapeptide composition is usually L-Ala-γ-D-Glu-*m*DAP-D-Ala-D-Ala, where *m*DAP is meso-diamino pimelic acid. In monoderm bacteria, the

amino acid at the second and third positions are usually D-Gln and L-Lys, respectively. Crosslinking commonly occurs between the fourth and the third amino acids of different peptides (4-3 cross-link) or between amino acids at the third positions (3-3 cross-link); the proportion of each type varying between species and as function of the cellular state (Rohs and Bernhardt, 2021; Aliashkevich and Cava, 2022; Kumar *et al.*, 2022). For instance, in *E. coli* the most common (90-98%) cross-link is 4-3, whereas in *Agrobacterium tumefaciens* 30% of cross-links are 3-3 (Morè *et al.*, 2019; Williams *et al.*, 2021). In *E. coli*, 3-3 cross-links increase when the outer membrane is compromised or during PG maturation in the stationary phase of growth (Glauner *et al.*, 1988; Typas *et al.*, 2012; Morè *et al.*, 2019).
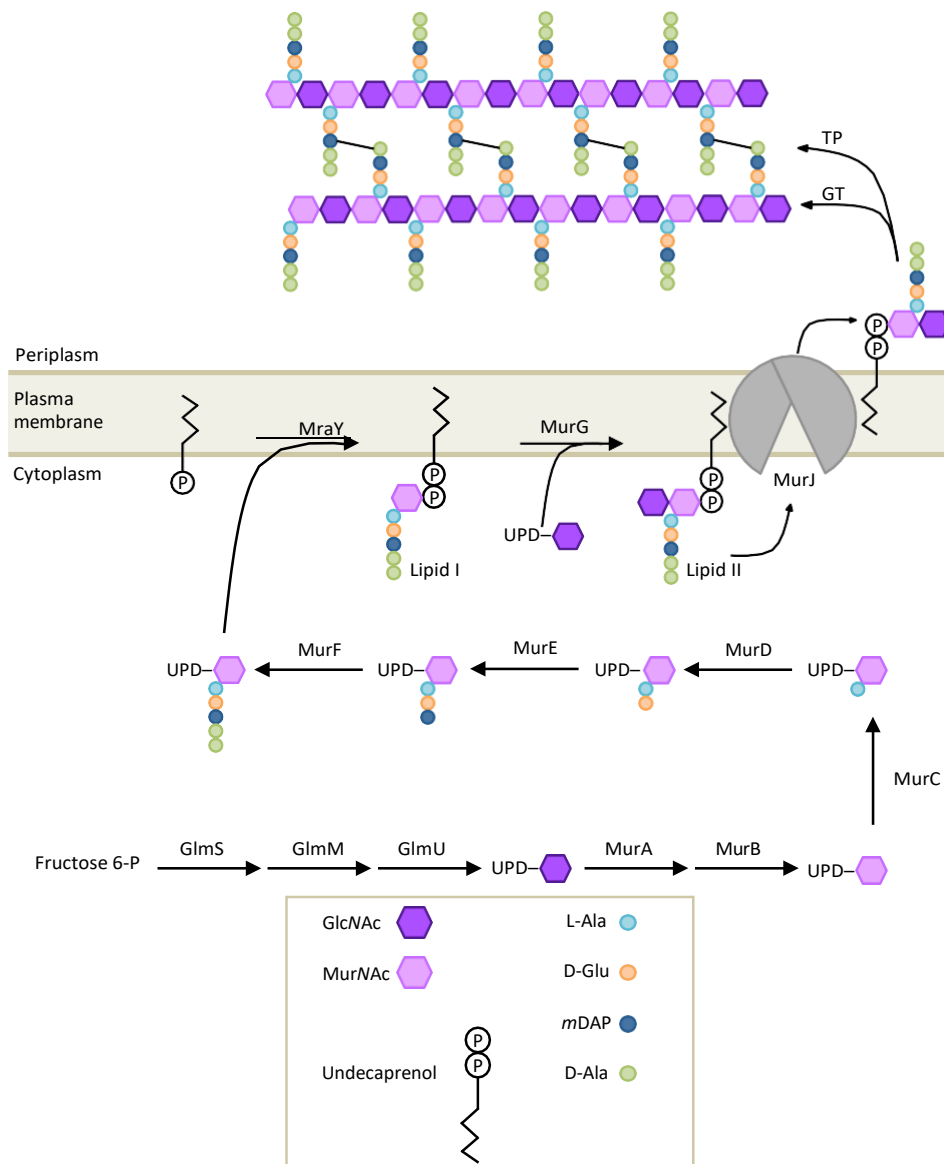
Figure 5. Peptidoglycan synthesis pathway and its cellular compartmentalization. Cell wall precursors and components are represented according to the code shown at the bottom. Arrows represent enzymatic reactions, where either the specific enzyme or the enzyme family is indicated. GlcNAc, *N*-acetylglucosamine; GT, glycosyltransferase enzymes; *m*DAP, *meso*-diaminopimelic acid; MurNAc, *N*-acetylmuramic acid; TP, transpeptidase enzymes. See the text for further details.

2.3.2. Patterns of growth of the cell wall

Growth of the cell wall must be spatiotemporally controlled in order to maintain and pass to the next generations the species-specific cell morphology (Vollmer, 2012). Being a rigid structure, the sacculus hinders cell enlargement, as the exoskeleton of arthropods or the skin of reptiles limits their growth. To allow cell enlargement, bacterial PG grows by addition of new material at positions where previous breaks have been introduced. Hydrolases and synthases play key roles in breaking down the existing PG and inserting new material, respectively (Typas *et al.*, 2012; Vollmer, 2012; Egan *et al.*, 2020). Most of the data available on cell wall synthesis is based on studies in two rod-shaped models, the diderm *E. coli* and the monoderm *Bacillus subtilis* (Rohs and Bernhardt, 2021). The following sections mostly refer to these model organims, although in the last years other diverse bacteria are being investigated. PG growth requires a large number of enzymes and it is initiated in the cytoplasm to proceed at both sides of the plasma membrane (Lovering *et al.*, 2012) (Figure 5).

In model rod-shaped bacteria, PG growth occurs mainly at two cellular locations: at midcell to build the new poles of the daughter cells during cell division (septal PG synthesis), and at the cylindrical part of the cell (lateral or peripheral PG synthesis), which allows cell elongation during cell growth in between cell division events (Typas *et al.*, 2012; Rohs and Bernhardt, 2021). Septal and peripheral PG synthesis are mediated by distinct protein complexes known as the divisome and the elongasome, respectively, that will be described below. It is worth mentioning that PG synthesis at other locations has been reported in different bacterial species (Table 1). For instance, in *E. coli* new PG is synthesized in two belts close to midcell during the initiation of cell division. This is known as pre-septal PG growth and is promoted by divisome proteins, FtsZ, ZipA and FtsN (see below) (Pazos *et al.*, 2018). *C. crescentus* shows a long pre-septal growth phase requiring FtsZ (van Teeseling, 2021), and in *Streptococcus pneumoniae* pre-septal growth adjacent to mid-cell produces the slight enlongation of its ovoid cells (Daniel and Errington, 2003). In *Staphylococcus aureus,* post-septal growth occurs after cytokinesis, with synthesis of PG from the division site to one of the cell poles (Monteiro *et al.*, 2015). Besides, some rod-shaped bacteria elongate through polar PG growth, which can be unipolar, as in *A. tumefaciens*, or bipolar, as in *Corynebacterium glutamicum* (Daniel and Errington, 2003; Cameron *et al.*, 2014).

Table 1. Modes of peptidoglycan growth based on its localization.

PG growth mode		Bacteria	Proteins (complexes) involved	Reference
Lateral		Rod-shaped	Elongasome	Typas *et al.*, (2012)
Septal		Rod-shaped Coccoid Ovoid	Divisome	Typas *et al.*, (2012)
Pre-septal		*E. coli*	FtsZ, ZipA, FtsN, aPBPs	Pazos *et al.*, (2018)
		C. crescentus	FtsZ	van Teeseling, (2021)
		S. pneumoniae		Daniel and Errington, (2003)
Post-septal		*S. aureus*		Monteiro *et al.*, (2015)
Polar		*A. tumefaciens*	FtsZ, FtsA	Cameron *et al.*, (2014)
		C. glutamicum		Daniel and Errington, (2003)

aPBPs, class A penicillin-binding proteins.

2.3.3. Synthesis of PG

PG growth takes place by the incorporation of new PG units, synthesized in the cell cytoplasm, into the preexisting periplasmic PG chains at points of break introduced by PG hydrolases.

2.3.3.1. Synthesis of PG precursors

The synthesis of the lipid II that constitutes the monomeric unit of PG include multiple enzymatic steps that, according to its subcellular localization could be separated into three parts (Figure 5). First, the nucleotide precursors, UDP-Glc*N*Ac and UDP-Mur*N*Ac-pentapeptide are synthesized in the cytoplasm. Second, the UDP-Mur*N*Ac-pentapeptide is bound to an isoprenoid lipid (undecaprenyl pyrophosphate, Und-PP) that acts as a carrier and anchors UDP-Mur*N*Ac-pentapeptide to the inner face of the plasma membrane. This monomeric subunit (UDP-

Mur*N*Ac-pentapeptide-Und-PP) is known as lipid I. Third, UDP-Glc*N*Ac is bound to lipid I, generating a disaccharide-pentapeptide-Und-PP molecule, lipid II. Finally, lipid II is flipped to the outer face of the PM, where PG synthases use the disaccharide pentapeptide moiety as a building block to expand the existing PG chains liberating the lipid carrier, which is recycled. Enzymes encoded by *glm* and *mur* genes catalyze the synthesis of UDP-Mur*N*Ac-pentapeptide. MraY binds undecaprenyl phosphate to UDP-Mur*N*Ac-peptapeptide producing lipid I and MurG subsequently incorporate lipid I to UDP-Glc*N*Ac to produce lipid II (Lovering *et al.*, 2012; Rohs and Bernhardt, 2021; Kumar *et al.*, 2022).

In this complex synthetic process, a distinct enzyme is MurJ, which flips lipid II from the inner to the outer leaflet of the plasma membrane (Rohs and Bernhardt, 2021). MurJ is a flippase of the Multidrug/Oligosaccharidyl-lipid/Polysaccharide (MOP) exporter superfamily, and, in *E. coli*, its deletion leads to the accumulation of PG precursors in the cytoplasm (Ruiz, 2008; Qiao *et al.*, 2017; Egan *et al.*, 2020; Kumar *et al.*, 2022). MurJ is conserved in evolutionarily distant bacteria, but is missing in several monoderm bacteria such as *B. subtilis*, which uses an essential non-homologous protein named AmJ as an alternative flippase (Lovering *et al.*, 2012; Egan *et al.*, 2020; Kumar *et al.*, 2022). The structure of MurJ consists of twelve transmembrane helices organized in two halves, which confers a V-shape to this molecule. During the transport cycle, MurJ oscillates between an inward-open conformation, that allows recruiting cytoplasmic lipid II, and an outward-open conformation that allows the release of lipid II in the periplasm (Figure 5) (Kumar *et al.*, 2022).

2.3.3.2. Incorporation of PG precursors into the cell wall

Once in the periplasm, assembly of building blocks into nascent glycan chains is catalyzed by glycosyltransferase (GT) enzymes, and cross-linking of stem peptides from adjacent glycan strands is catalyzed by transpeptidase (TP) enzymes (Figure 5).

In recent years, new data have led to a change in the concept of the enzymatic complement catalyzing the bacterial cell wall assembly process, attributing its main role to proteins of the SEDS (shape, elongation, division and sporulation) family. These proteins are the core cell wall synthases in both cell elongation and division (Cho *et al.*, 2016; Meeske *et al.*, 2016). The SEDS proteins involved in cell wall synthesis are RodA and FtsW, acting in cell elongation and cell division, respectively. Initially, RodA and FtsW were thought to work as lipid II translocases. However, although there is still some debate on wheter they can play some role at this step, since the identification of their GT activity it is widely accepted that their major role is in PG polymerization (Mohammadi *et al.*, 2011; van der Ploeg *et al.*, 2013; Egan *et al.*, 2020; Liu *et al.*, 2020; Mueller and Levin, 2020). FtsW and RodA act in concert with penicillin binding proteins (PBPs) that provide the catalytic TP activity required for PG synthesis.

PBPs are the target of antibiotics of β-lactam family, which includes penicillin, and due to the fact that they were traditionally considered the main PG synthases, these enzymes have been thoroughly characterized (Lovering *et al.*, 2012; Kumar *et al.*, 2022). PBPs have been classified in three classes according to their structure and catalytic activity. PBPs of the A class (aPBPs) are bifunctional enzymes with GT and TP activities; class B PBPs or bPBPs are monofunctional transpeptidases and class C PBPs, cPBPs, are enzymes with carboxypeptidase or endopeptidase activity (Egan *et al.*, 2020).

bPBPs are the enzymes that work together with SEDS proteins in the pairs SEDS/bPBP (exhibiting a catalytic activity similar to that of bifunctional aPBPs) (Rohs and Bernhardt, 2021; Kumar *et al.*, 2022). In *E. coli*, the pair RodA/PBP2 synthetize PG during cell elongation, whereas FtsW/PBP3 (FtsI) synthetize septal PG during cell division. However, these pairs are responsible for only about 20% of the PG biogenesis in this bacterium, while most of the synthesis relies on aPBPs (Kumar *et al.*, 2022). Cho and colleagues have proposed that SEDS/bPBPs and aPBPs are two independent systems, both with essential roles, of which the former would build the foundation structure of the PG matrix, while the latter would fill in the gaps both during normal growth and, mainly, during damage repair (Cho *et al.*, 2016). In line with this, aPBPs do not seem to participate in cell shape maintenance but are essential to maintain the mechanical integrity of the cell wall (Morè *et al.*, 2019; Vigouroux *et al.*, 2020). Finally, it should be stressed that the specific roles of aPBPs and bPBPs described above apply to *E. coli*, but can be different in other organisms. For instance, in *Mycobacterium* and other actinobacteria, PBP1a is important for maintenance of the rod-shape; and in the rod-shaped *A. tumefaciens,* PBP1a, rather than the pair RodA/PBP2, is the PG synthase that drives cell elongation (Williams *et al.*, 2021). On the other hand, PBP1a of *Acinetobacter baumannii* interacts with the division-specific PBP3 and promotes septation (Kang and Boll, 2022).

As mentioned above, an obligate step for expansion of the cell wall is the generation of gaps by hydrolase-mediated cleavage, which is essential to allow the insertion of new material without increasing the thickeness of the sacculus (Rohs and Bernhardt, 2021). DD-endopeptidases are the enzymes that specifically hydrolyze the 4-3 bridges between peptide chains to allow the interstitial growth of the cell wall, whereas DD-carboxypeptidases remove the terminal D-Ala from the pentapeptides (González-Leiza *et al.*, 2011; Singh *et al.*, 2012; Vollmer, 2012). The bonds between Mur*N*Ac and Glc*N*Ac are hydrolyzed by lytic transglycosilases (Rohs and Bernhardt, 2021). Since the hydrolase activity must be accurately spatiotemporally regulated to avoid cell damage, the 'space-maker' functions of DD-endopeptidases and DD-carboxypeptidases are negatively controlled by proteases (Singh *et al.*, 2012; Jeon and Cho, 2022).

3. THE ELONGASOME

Non-spherical bacteria have to grow laterally before cell division. This requires elongation of the rigid cell wall in the direction of the longitudinal cell axis concomitantly with the increase in cell biomass. In rod-shaped bacteria, the protein complex involved in cell wall elongation is known as the *elongasome* or the *rod-system*, which inserts newly synthetized PG in the cylindrical part of the cell wall. In model bacteria, depletion of elongasome components induces loss of the rod shape and growth retardation, whereas their inactivation commonly provokes cell death (den Blaauwen *et al.*, 2008; Typas *et al.*, 2012; Rohs and Bernhardt, 2021). Importantly, several publications have shown that the elongasome is not only responsible for maintaining a rod shape during normal growth but it is also capable of re-establishing a shape, meaning that it can regenerate a rod shape in cells forced to grow as spheres (Billings *et al.*, 2014; Hussain *et al.*, 2018; Rohs and Bernhardt, 2021). The elongasome is a dynamic complex compossed of regulatory and enzymatic proteins (Figure 6A,B). MreB, MreC and MreD are major components that contribute to the spatial localization of lateral PG synthesis activity including the recruitment of the enzymatic components involved.
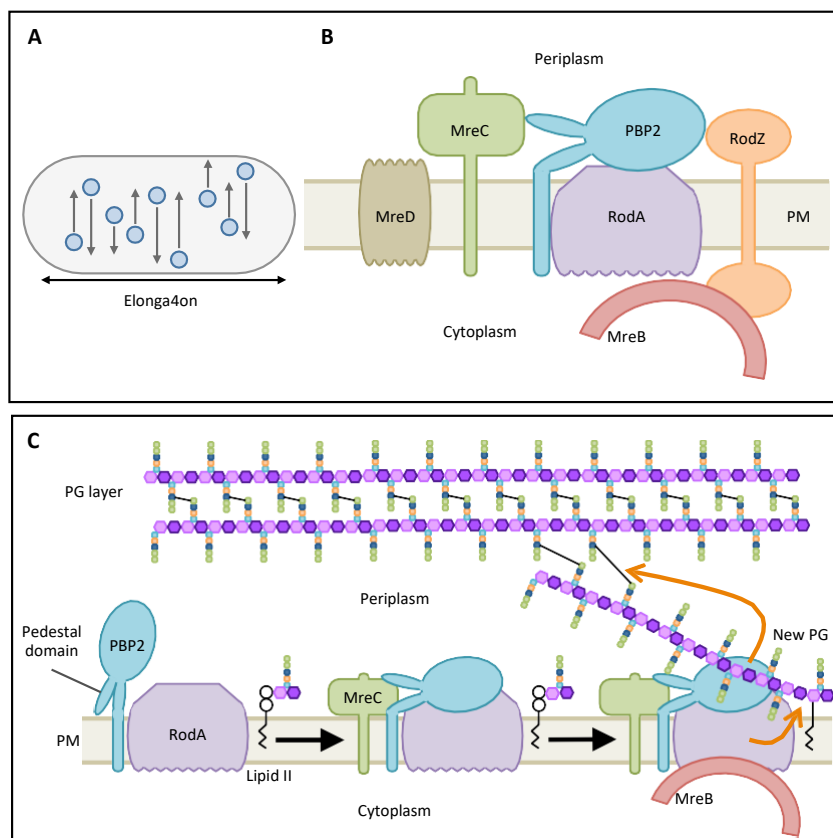
Figure 6. The elongasome and the peptidoglycan elongation process. (A) Schematic of a rod-shaped cell with circles representing elongasome complexes and arrows indicating the direction of rotation. (B) Schematic of the elongasome complex indicating the topology of the components in the plasma membrane (PM). (C) Schematic of PG synthesis by the elongasome. The PBP2 pedestal domain changes its conformation to the active state. The sequence of events is indicated by black arrows. Orange arrows connect PG synthesis enzymes with the sites where catalysis occurs (see the text for further details).

3.1. Elongasome components

3.1.1. MreB

MreB was identified by the characterization of *E. coli* mutants that showed altered cellular morphology (Wachi *et al.*, 1987). At present, MreB is recognized as a characteristic component of the elongasome (Pogliano, 2008; Busiek and Margolin, 2015; Wagstaff and Löwe, 2018; Egan *et al.*, 2020). As such, it is absent in non-cylindrical bacteria and generally present in rod-shaped species, except in the actinobacteria and rhizobiales groups (Busiek and Margolin, 2015). In model organisms like *E. coli*, *B. subtilis* and *C. crescentus*, the *mreB* gene is located in a *mreBCD* operon. Nonetheless, whereas in diderm bacteria there is usually a single *mreB* gene, in monoderms there are multiple homologues, normally encoded in different chromosomal locations (e.g. *B. subtilis* contains three genes: *mreB*, *mbl* and *mreBH*) (Cabeen and Jacobs-Wagner, 2010; Busiek and Margolin, 2015). MreB is an actin-like protein with ATPase activity that can form polymers. Although it was first thought to form continuous filaments that followed a helical path along the periphery of the cell, more recently MreB has been found to polymerize into short, double stranded filaments that in most bacteria show a patchy distribution along the long cell axis (Cabeen and Jacobs-Wagner, 2010; Busiek and Margolin, 2015; see Errington, 2015). MreB associates with the PM using species-specific determinants, corresponding to a N-terminal amphipathic helix in the *E. coli* protein (Salje *et al.*, 2011; Busiek and Margolin, 2015; Egan *et al.*, 2020). MreB protofilaments can associate as pairs in an antiparallel orientation, interacting through their flat surface, which ensures that the amphipathic helix of each subunit is exposed for interaction with the PM (van den Ent *et al.*, 2014). In most bacteria, MreB sits on the inner surface of the cilindrical part of the membrane, being absent from the cell poles, where anionic phospholipids contribute to exclusion of assembled molecules (Billings *et al.*, 2014; Ursell *et al.*, 2014; Kawazura *et al.*, 2017; Wong *et al.*, 2019; Rohs and Bernhardt, 2021). In model bacteria, MreB filaments rotate in a direction perpendicular to the longitudinal cell axis directed by the coupling to the PG synthesis activity (Dominguez-Escobar *et al.*, 2011; Garner *et al.*, 2011; van Teeffelen *et al.*, 2011; Hussain *et al.*, 2018), with the rotation speed being dictated by the fluidity of the PM (Ouzounov *et al.*, 2016; Hussain *et al.*, 2018; Egan *et al.*, 2020; Kurita *et al.*, 2020). The emerging picture on the function of MreB is that it guides the elongasome to synthetize PG in bands that are perpendicular to the long cell axis.

3.1.2. MreC

The *mreC* gene is normally located downstream from *mreB* in the *mreBCD* operon (Dye *et al.*, 2005; Kruse *et al.*, 2005; Leaver and Errington, 2005). MreC is widely conserved and essential in most rod-shaped bacteria, and it is also present in some coccoidal species, suggesting a general

role in cell morphogenesis (Divakaruni *et al.*, 2007; Egan *et al.*, 2020). Its main function is to regulate PG synthesis directed by the elongasome complex. In many bacteria including *E. coli*, MreC is a bitopic protein with a transmembrane α-helix in the N-terminal part and an extensive periplasmic domain, although in *C. crescentus* it is a soluble periplasmic protein (Divakaruni *et al.*, 2005; 2007; Kruse *et al.*, 2005). MreC is organized into patches of short filaments that co-localize with MreB and interact with periplasmic synthetic enzymes including PBP2 (Divakaruni *et al.*, 2005; 2007; Contreras-Martel *et al.*, 2017; Martins *et al.*, 2021). In *Pseudomonas aeruginosa*, it has been shown that MreC self-associates in a head-to-tail fashion through interaction interfaces that are conserved in proteobacteria, alternating between self-association and interaction with the PG-synthesis machinery (Martins *et al.*, 2021; see Rohs and Bernhardt, 2021; Xu *et al.*, 2022). It has been suggested that the transition between monomeric and polymeric states could represent a regulatory mechanism for MreC function (see below) (Rohs *et al.*, 2021).

3.1.3. MreD

The *mreD* gene is usually the last gene of the *mreBCD* operon. This gene is not always conserved; hence, some rod-shaped bacteria contain an *mreBC* operon. When present, MreD is involved in rod shape maintenance (Kruse *et al.*, 2005; Leaver and Errington, 2005; den Blaauwen *et al.*, 2008; Typas *et al.*, 2012; Egan *et al.*, 2020; Liu *et al.*, 2020). It is a PM integral protein with five or six predicted transmembrane α-helices flanked by N- and C-terminal extensions located in the cytoplasm (Kruse *et al.*, 2005; Leaver and Errington, 2005). *In vitro*, MreD interacts with MreC and PBP2, but not with MreB or itself (Kruse *et al.*, 2005; Liu *et al.*, 2020).

3.1.4. RodZ

The *rodZ* gene, which was previously named *yfgA,* encodes a bitopic membrane protein that is widely conserved in rod-shaped bacteria, but is non-essential in *E. coli* (Newitt *et al.*, 1999; Alyahya *et al.*, 2009; Bendezú *et al.*, 2009; Ago and Shiomi, 2019; Egan *et al.*, 2020). Deletion of *rodZ* produces spherical cells with altered curvature and shape, a phenotype that can be supressed by high doses of the cell division protein FtsZ (Bendezú *et al.*, 2009; van den Ent *et al.*, 2010; Bratton *et al.*, 2018; Liu *et al.*, 2020). RodZ is thought to act as a scaffolding protein for the elongasome, being able to interact with itself and with MreB, MreC, RodA and PBP2 (Bratton *et al.*, 2018; Egan *et al.*, 2020; Liu *et al.*, 2020; Özbaykal *et al.*, 2020). The RodZ N-terminal domain is cytoplasmic and contains a helix-turn-helix motif for interaction with MreB, whereas the C-terminal domain is periplasmic and interacts with the PG synthesis machinery (van den Ent *et al.*, 2010; Bratton *et al.*, 2018; Rohs and Bernhardt, 2021). RodZ binds to monomeric and polymeric MreB and regulates MreB polymerization. In *E. coli,* the interaction with RodZ

contributes to anchor MreB to the PM and modulates its physical properties, influencing the curvature of MreB protofilaments (van den Ent *et al.*, 2010; Typas *et al.*, 2012; Morgenstein *et al.*, 2015; Bratton *et al.*, 2018; Shi *et al.*, 2020). *In vivo*, the interaction of RodZ with MreB does not require the presence of other proteins, suggesting that RodZ may represent a link between MreB and other elongasome components (van den Ent *et al.*, 2010; Egan *et al.*, 2020; Özbaykal *et al.*, 2020; Rohs and Bernhardt, 2021). Finally, in *E. coli*, in addition to being part of the elongasome, RodZ has been proposed to have a role in cell division, facilitating the polymerization of the division ring, which is dependent on the interaction of its cytoplasmic domain with FtsZ (Ago and Shiomi, 2019; Yoshii *et al.*, 2019).

3.1.5. <u>RodA and PBP2</u>

In *E. coli*, RodA and PBP2 form the catalytic subcomplex of the elongasome (Liu *et al.*, 2020; Mueller and Levin, 2020). The *rodA* gene forms an operon with the upstream *pbpA* gene encoding PBP2 (Matsuzawa *et al.*, 1989). RodA was identified because its mutations produced round cells (de Pedro *et al.*, 2001; Figge *et al.*, 2004). It is an integral membrane protein, with multiple transmembrane domains, essential and widely conserved in rod-shaped bacteria (Kruse *et al.*, 2005; Leaver and Errington, 2005; van den Ent *et al.*, 2010; Mohammadi *et al.*, 2011; Egan *et al.*, 2020). Besides with PBP2, RodA also interacts with MreB and with itself, whereas PBP2 interacts with itself and with PBP1A, MreC and MreD (Egan *et al.*, 2020; Liu *et al.*, 2020; Chaudhary *et al.*, 2021).

In addition to the RodA-PBP2 pair, aPBPs may play a role in lateral PG synthesis (see paragraph 2.3.3.2. above). In both, monoderm and diderm bacteria, aPBPs interact with proteins of the elongasome, as MreB in *B. subtilis* or PBP2 in *E. coli*, although in both models aPBPs do not rotate with the elongasome and their inactivation affects neither PG synthesis by the elongasome nor the elongasome dynamics (Cho *et al.*, 2016; Meeske *et al.*, 2016).

3.2. Regulatory role of MreC and MreD in PBP2-RodA activity

Recent data indicate that in *T. thermophilus* and *E. coli*, PBP2 oscillates between an inactive and an active state in which the so-called pedestal domain is in its open conformation. In the RodA-PBP2 subcomplex, PBP2 in its open conformation interacts with RodA, promoting activation of its GT activity (Sjodt *et al.*, 2020). Interestingly, in the co-crystal of MreC and PBP2 from *H. pylori*, MreC interacts with the pedestal domain of PBP2 leading to an opening of the two pedestal-interacting subdomains (Contreras-Martel *et al.*, 2017; Rohs *et al.*, 2018). All these results have led to a current model in which the interaction of MreC with PBP2 changes the conformation of the latter, which in turn is communicated to RodA to stimulate PG synthesis by the elongasome (Contreras-Martel *et al.*, 2017; Rohs *et al.*, 2018; Rohs and Bernhardt, 2021) (Figure 6C). For its

part, MreD has been described as a negative regulator of the activity of the elongasome by interaction with MreC and PBP2, preventing the conformational change of the latter and, therefore, the activation of RodA and PG synthesis (Liu *et al.*, 2020). Hence, MreC and MreD would play opposite roles in modulation of the interaction between the components of the bPBP-SEDS pair of the elongasome (Liu *et al.*, 2020; Rohs *et al.*, 2021).

3.3. Relationships of endopeptidases with the elongasome

Endopeptidase enzymes that cleave the crosslinks in the PG and could function in association with the elongasome have been identified. However, the coordination between these enzymes and the elongasome is not yet well defined. In diderm bacteria, little is known about endopeptidases, with some data available in *E. coli* and *Vibrio cholerae* (Rohs and Bernhardt, 2021). By contrast, in monoderm bacteria like *B. subtilis,* the LytE and CwlO endopeptidases have been studied in depth in regard to their regulation and connection with the elongation machinery (Rohs and Bernhardt, 2021). LytE appears to act in concert with the MreB isoform, whereas CwlO have an apparent relationship with Mbl (Carballido-López *et al.*, 2006; Domínguez-Cuevas *et al.*, 2013; Meisner *et al.*, 2013). However, the simultaneous inactivation of CwlO and LytE does not affect the circumferential movement of the elongasome, illustrating that many aspects concerning the role of PG hydrolytic enzymes in cell wall elongation still need clarification (Meisner *et al.*, 2013).

3.4. Elongasome dynamics

In vivo, MreB form short filaments, with disperse localization in the PM, that rotate uncoordinately, and often in opposite orientations, perpendicular to the long axis of the cell (Dominguez-Escobar *et al.*, 2011; Garner *et al.*, 2011; van Teeffelen *et al.*, 2011). The other components of the elongasome also rotate in the same direction with a similar speed, indicating that it is the whole complex that rotates. The observation that inhibition by antibiotics, or by depletion or mutation of PG synthesis enzymes provoked cessation of elongasome movement led to the notion that PG synthesis fuels the motion of the entire elongasome complex (Dominguez-Escobar *et al.*, 2011; Garner *et al.*, 2011; van Teeffelen *et al.*, 2011). This raises the question on the role of MreB in the elongasome. A critical point being that synthesis of new PG must occur in a direction perpendicular to the long cell axis, the emerging picture is that MreB governs the orientation of the elongasome, ensuring that its rotation, and thus PG synthesis, occurs in the correct direction. Crucial for this is the intrinsic curvature of MreB filaments, which makes energetically favorable their alignment along the greatest principal membrane curvature, which in rod-shaped bacteria occurs around the rod circumference (Hussain *et al.*, 2018; Wong *et al.*, 2019; Rohs and Bernhardt, 2021) (Figure 6A).

4. THE DIVISOME

Cell division is a fundamental process governed by a multiprotein complex known as the *divisome* that involves numerous components, including scaffolding proteins, regulatory factors and PG synthesis enzymes. This complex coordinates chromosome segregation with the formation of the new poles of the resulting daughter cells, envelope constriction and daughter cell separation. In diderm bacteria, the divisome expands the three layers of the cell envelope, so that the dynamics of the OM is coordinated to the re-modelling of the PG and the constriction of the PM (Du and Lutkenhaus, 2017; Barrows and Goley, 2021; Levin and Janakiraman, 2021). The structure and function of the divisome has been studied mainly in *E. coli* and *B. subtilis*, although in recent years a good deal is being learned on other model bacteria.
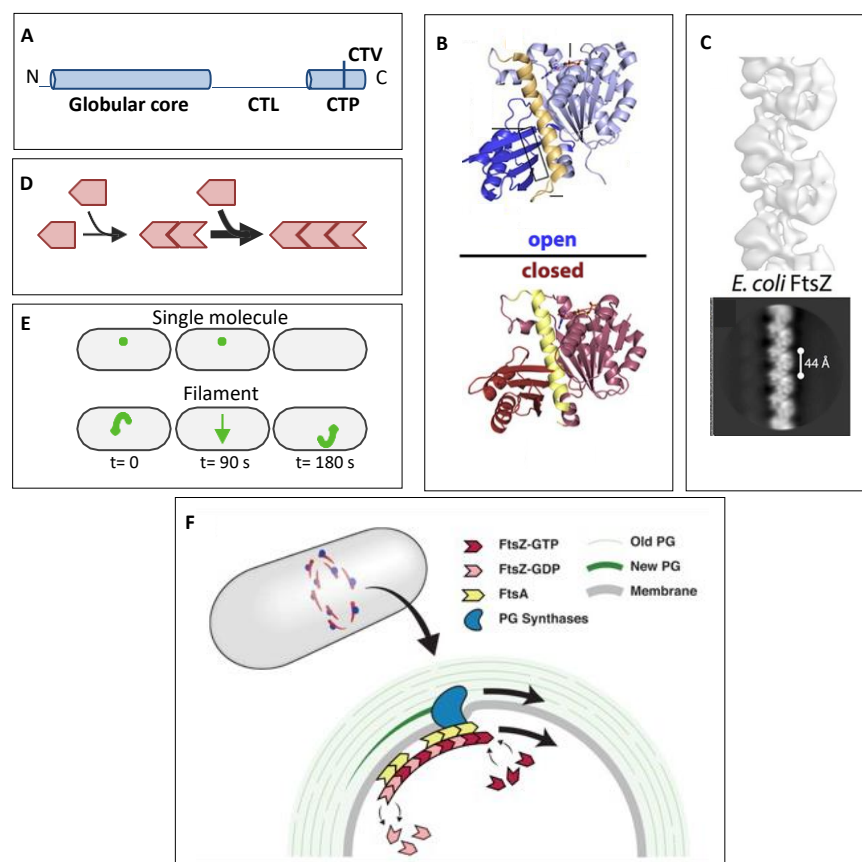
Figure 7. FtsZ, the initial protein of the divisome. (A) Linear representation of FtsZ with its different domains depicted as lines or cylinders. C-terminal linker (CTL), C-terminal peptide (CTP), C-terminal variable region (CTV). Note that the CTV is included in the CTP domain. (B) Crystal structure of FtsZ from *S. aureus* in its open and closed conformations. (C) Model of a single-stranded FtsZ filament from *E. coli*. Note that subunits are in their open conformation. (D) Scheme of the cooperativity between subunits during FtsZ polymerization. Association of monomers in a closed state promote a conformational change to an open state that fosters further recruitment of subunits with increased affinity. (E) Scheme of the movement of the divisome driven by the treadmilling dynamics of FtsZ. (F) Representation of the apparent rotation of FtsZ-GFP fusion proteins. Note that FtsZ subunits are static during treadmilling. (B) and (C) adapted from Wagstaff *et al*., 2017; (E) adapted from Lamanna & Maurelli, (2022); (F) adapted from Bisson-Filho *et al*., (2017).

4.1. FtsZ structure and dynamics

One of the main proteins of the divisome is FtsZ, which is conserved in bacteria, chloroplasts and some archaea and mitochontria (Levin and Janakiraman, 2021). FtsZ is homologous to the eukaryotic cytoskeletal protein tubulin, showing a similar three-dimensional structure in the common core domain (Löwe and Amos, 1998). Much of the divisome functioning depends on the physico-chemical properties and the dynamics of FtsZ.

FtsZ has been mainly studied in *E. coli* and *B. subtilis* and it has been shown to contain five domains (Levin and Janakiraman, 2021) (Figure 7A). The N-terminal part shows a variable length depending on the species, ranging from 10, in *E. coli*, to 68 amino acids in some cyanobacteria (see below) (Corrales-Guerrero *et al.*, 2018; Levin and Janakiraman, 2021). The next domain is a tubulin-like core with GTP binding and hydrolytic activity (Schumacher *et al.*, 2020). The C-terminal linker (CTL) is the domain that binds the proteins that anchor FtsZ to the membrane (Buske and Levin, 2012; Levin and Janakiraman, 2021). Finally, the C-terminal peptide (CTP) is widely conserved and interacts with some proteins that participate in cell division. CTP comprises the domain known as the C-terminal variable region (CTV), which varies in length according to species and seems to mediate self-interactions between FtsZ protofilaments (Buske and Levin, 2012; Ortiz *et al.*, 2015).

FtsZ is a soluble protein that *in vitro* polymerizes in different forms (single-stranded filaments, sheets, bundless or rings) depending on buffer conditions. However, it does not polymerize with the typical microtubular structure of tubulin. *In vivo*, FtsZ is a cytoplasmic protein that at the initiation of cell division gets anchored to the PM by interaction with a variety of PM-located proteins, such as FtsA and ZipA (see below), which also promote FtsZ polymerization into filaments near the inner layer of the PM. Filaments eventually aggregate into a structure known as the Z-ring that enciles the cell around the circumference of the division plane and acts as a scaffold for the recruitment of further divisome proteins. FtsZ polymerization is spatiotemporally regulated and occurs at specific times in the cell cycle prior to cell division (Bramhill and Thompson, 1994; Du and Lutkenhaus, 2017; Levin and Janakiraman, 2021). Z-ring assembly requires a threshold concentration of FtsZ protein above its average cytoplasmic concentration, which is otherwise very stable. Local variations of the FtsZ concentration are observed due to crowding of FtsZ molecules, particularly at the future septal site. The increase of FtsZ concentration and the subcellular localization of Z-ring assembly are key events in cell division, and these events are extensively regulated by both negative (e.g., the Min and nucleoid occlusion systems) and positive (e.g., Ter-MatP-linkage) regulatory circuits (Si *et al.*, 2019; Barrows and Goley, 2021; Levin and Janakiraman, 2021). FtsZ polymerization relies on its dynamic oscillation between two conformational states, a closed state, commonly adopted in individual monomers, and an open state that favours interaction between monomers and is commonly found in the subunits of filaments (Figures 7B and 7C).

As it is the case with tubulin, FtsZ polymerizes by head-to-tail interactions between subunits and, importantly, polymerization is associated to a phenomenon of cooperativity such that, whereas individual FtsZ monomers in the closed conformation show little affinity for each other, once polymerization has started binding of new monomers occurs with higher affinity (Figure 7D) (Michie and Löwe, 2006; Wagstaff *et al.*, 2017). Also similar to tubulin, FtsZ filaments exhibit 'treadmilling' dynamics, which consists in the polymerization of FtsZ GTP-bound monomers at one end of the filament (plus end) and simultaneous dissociation of subunits at the other end (minus end) (Mukherjee and Lutkenhaus, 1998; Loose and Mitchison, 2014; Bisson-Filho *et al.*, 2017; Yang *et al.*, 2017; Ramirez-Diaz *et al.*, 2018). Treadmilling of FtsZ depends on its GTPase activity, which active site is assembled from two consecutive subunits in the filament (Scheffers *et al.*, 2002; Oliva *et al.*, 2004). This way, recently incorporated subunits maintain for some time its GTP-bound state at the plus end of filamens. Hydrolysis of GTP favor the conformational change of the subunits to a closed state, which is prone to dissociation. Treadmilling give rise to the apparent rotational movement of FtsZ-GFP fusions observed *in vivo*; however, it has been shown that individual subunits in the filaments remain static (Figure 7E). This dynamic property of some cytoskeletal proteins is useful to direct the movement of accompanying molecules without the action of motor proteins. Indeed, in *E. coli* and *B. subtilis*, FtsZ has been shown to direct the movement of the divisome complex to ensure the correct building of the septum. It has been propossed that the FtsZ GTPase activity and treadmilling affect the spatiotemporal distribution of PG synthesis to initiate constriction, rather than the PG synthesis rate (Yang *et al.*, 2017; Whitley *et al.*, 2021). In *B. subtilis*, FtsZ treadmilling also appears essential for the initial condensation of the Z-ring (Whitley *et al.*, 2021).

It should be pointed out that, notwithstanding the conservation of the basic composition of the divisome in most bacterial species, whether FtsZ treadmilling is always required for the localization and dynamics of the septal PG synthesis machinery is a matter of current debate. Thus, in contrast to its essential role in *B. subtilis*, in *S. pneumoniae* the constriction mechanism is independent of FtsZ, being instead directed by the TG and TP activities of the PG synthesis machinery. There are also organisms with a biphasic division process, whereby a first part is dependent on treadmilling and a second part independent of it. *S. aureus* and *E. coli* have been described to show this biphasic behavior, although in the latter this issue is currently under debate (Lamanna and Maurelli, 2022).

4.2. Divisome assembly

The *E. coli* divisome is composed of 36 proteins, among which a dozen are essential and widely conserved in bacteria. Divisome components are found in the cell in almost constant amounts, but concentrate at the site of the future septum for divisome assembly (Du and Lutkenhaus, 2017; Levin and Janakiraman, 2021). The assembly of the divisome is considered to take place

stepwise, with an early phase, where the Z-ring is formed by FtsZ polymerization and tethering to the PM, and a later phase where the rest of the proteins join to organize the divisome.
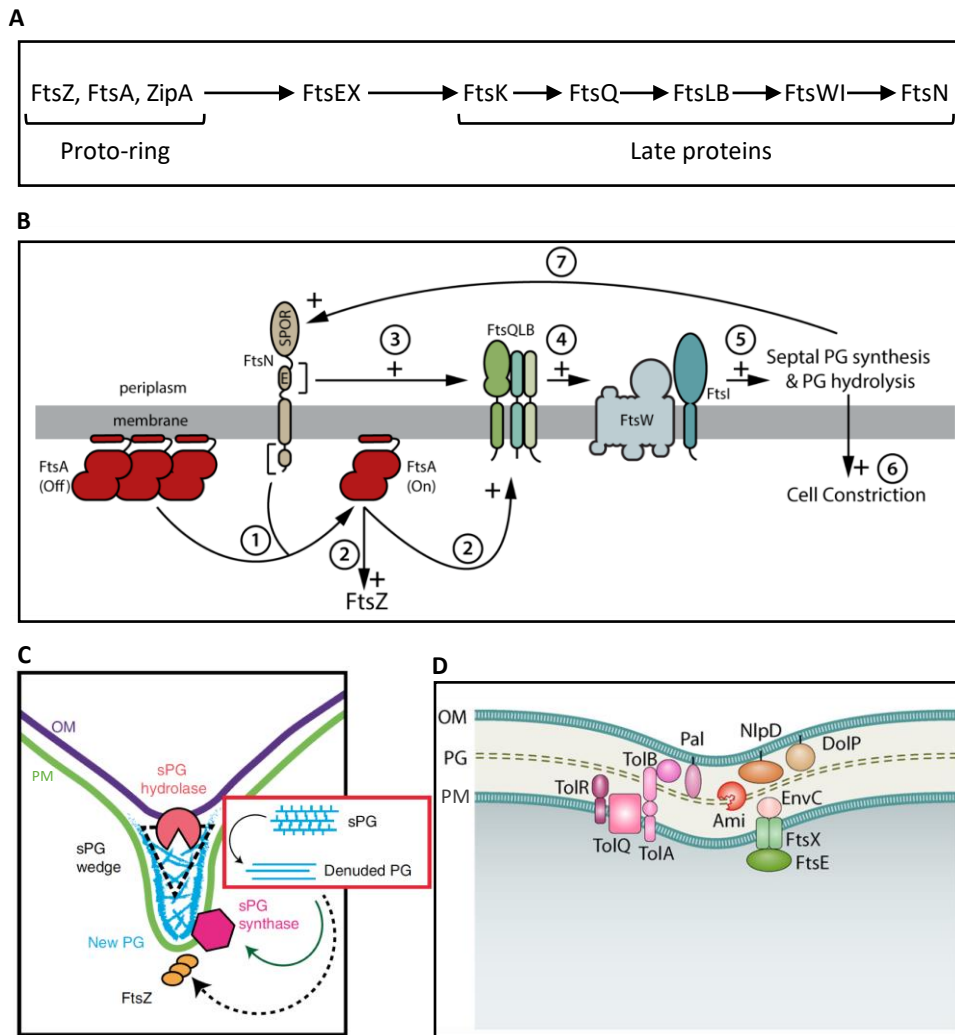
Figure 8. Assembly and activation of the divisome and envelope constriction. (A) The proposed linear hierarchical pathway for divisome assembly is depicted, with arrows separating sequential steps. (B) Scheme of the regulatory events that promote divisome activation. Arrows connect the components involved, and numbers indicate the temporal order of events. (C) Scheme of peptidoglycan remodeling at the septum. The action of PG hydrolases, including PG amidases cleaving septal peptidoglycan (sPG) and producing denuded PG is depicted in the inset. Green and dashed arrows indicate activation by denuded glycans. (D) Representation of the proteins required for constriction of the cell envelope and separation of the daughter cells, including PG amidases and the Tol-Pal complex. (A) adapted from Attaibi & der Blaauwen, (2022); (B) from Tsang & Bernhardt, (2015); (C) adapted from Navarro *et al.*, (2022); (D) adapted from Levin & Janakiraman, (2021).

Many data about the order in which proteins are assembled in the divisome derive from genetic approaches involving the inactivation of one of the components, which permits the identification of proteins acting upstream and downstream of the inactivated one. These studies led to the proposal that the second phase of divisome assembly follows a linear hierarchical pathway (Figure 8A) (Attaibi and Den Blaauwen, 2022). However, the operation of a sequential assembly is currently under disscusion. Some groups have shown that forced premature incorporation of some late proteins promotes the recruitment of earlier components, a

phenomenon known as *back recruiting*, which speaks of a more complex pathway (Goehring and Beckwith, 2005; Goehring *et al.*, 2005; Du and Lutkenhaus, 2017). The emerging picture is that the divisome assembles following aproximately the proposed linear hierarchical pathway, but with the occurrence of dynamic interactions between some components, which changes during the assembly process. In addition, some proteins can fulfill different functions at different stages of assembly (see e.g. FtsA or FtsEX below) (Du and Lutkenhaus, 2017; Barrows and Goley, 2021).

A brief description of the components of the *E. coli* divisome is shown in Table 2. FtsA is an actin-like protein with ATPase activity, linked to the PM by a C-terminal amphipatic helix (Pichoff and Lutkenhaus, 2005; Pichoff *et al.*, 2012; Szwedziak *et al.*, 2012), and ZipA is a bitopic protein with a large cytoplasmic domain. Both, FtsA and ZipA, bind to the CTP domain of FtsZ to anchor the FtsZ protofilaments to the PM. Both proteins are necessary for the recruitment of downstream proteins, but FtsA has a broader role, being also responsible for regulation of the divisome activity (Liu *et al.*, 2015; Tsang and Bernhardt, 2015; Du and Lutkenhaus, 2017). FtsA can be found in two conformational states, but only in its monomeric state it is active for downstream protein recruitment (Du and Lutkenhaus, 2017). FtsE and FtsX form a FtsEX subcomplex homologous to ABC transporter components, where FtsE is an ATPase-like protein and FtsX a transmembrane protein. This subcomplex fulfils at least two functions: regulation of FtsA polymerization and activation of PG amidases (see below) to separate daugher cells (Arends *et al.*, 2009; Du *et al.*, 2016; Attaibi and Den Blaauwen, 2022). FtsK is a DNA translocase that pumps DNA from the septal zone (Chen and Beckwith, 2001; Männik *et al.*, 2017). FtsQ, FtsL and FtsB are three bitopic proteins that form a subcomplex whose main function is to recruit the PG synthases FtsW and FtsI (PBP3) (Du and Lutkenhaus, 2017). As mentioned above, FtsW is a glycosyl transferase of the SEDS family and FtsI is its partner bPBP transpeptidase. The last protein to join the divisome is FtsN (SPOR domain), which triggers PG synthesis and septum constriction (Levin and Janakiraman, 2021).

Table 2. Essential components of the *E. coli* divisome.

Protein (complex)	Incorporation timing	Localization	Comments	Role(s)	References
FtsZ	Early	C	Tubulin-like GTPase	1. Cell division initiation 2. Guiding septal PG synthesis	Bisson-Filho *et al.*, (2017) Levin and Janakiraman, (2021)
FtsA	Early	C	Actin-like	1. Membrane anchor 2. Recruitment of downstream proteins 3. Regulation of PG synthesis activity	Pichoff *et al.*, (2012) Du and Lutkenhaus, (2017)
ZipA	Early	PM / C		1. Membrane anchor	Levin and Janakiraman, (2021)
FtsEX	Mid time	PM / C	ABC transporter-like ATPase and membrane subunits	1. FtsA oligomerization regulation 2. Septal cell wall hydrolysis control. 3. EnvC regulation	Arends *et al.*, (2009) Du *et al.*, (2016)
FtsK	Late	PM / C	DNA translocase	1. Exclusion of DNA from the division site 2. Linkage of downstream proteins to the Z-ring	Chen and Beckwith, (2001) Männik *et al.*, (2017)
FtsQLB	Late	PM / P		1. FtsW and FtsI regulation	Du and Lutkenhaus, (2017)
FtsW	Late	PM	Glycosyl transferase	1. PG synthase	Levin and Janakiraman, (2021)
FtsI	Late	PM / P	Transpeptidase	1. PG synthase	Levin and Janakiraman, (2021)
FtsN	Late	PM / P	C- terminal SPOR domain	1. PG synthesis regulation	Du and Lutkenhaus, (2017)

PM, plasma membrane; C, cytoplasmic; P, periplasmic.

4.3. Divisome activation and function

In diderm bacteria, the constriction of the septum initiates once the last essential divisome protein, FtsN, is recruited. PG remodelling involves coupled synthesis of new PG close to the PM and degradation of the outermost layer by PG hydrolases to allow OM invagination. At this step, PG degradation and new synthesis are tightly coordinated, which is necessary to prevent deleterious events.

Among the PG hydrolases, the amidases AmiA and AmiB, which break the stem peptides of the glycan chains of the PG, have main roles in septal PG splitting (Figures 8B and 8C). These amidases are strictly regulated by the divisome factor EnvC. EnvC is anchored to the periplasmic side of the PM and its C-terminal domain, which is involved in amidase activation, contains the so-called restraining arm. This part is subjected to an autoinhibitory mechanism that is released upon interaction of the EnvC N-terminal coiled-coil domain with the periplasmic domain of FtsX (Cook *et al.*, 2020). Such interaction is fostered by the ATPase activity of FtsE in the cytoplasm, which promotes a conformational change in the periplasmic side of FtsX (Yang *et al.*, 2011; Tsang *et al.*, 2017; Cook *et al.*, 2020; Shaku *et al.*, 2020), with the FtsE ATPase activity being in turn regulated by FtsX (Heidrich *et al.*, 2001; Bernhardt and de Boer, 2004; Uehara *et al.*, 2009; Yang *et al.*, 2011). The amidase activity produces denuded glycans (PG strands stripped of the peptide

stems), which are recognized by the periplasmic SPOR domain of FtsN, which then promotes the FtsQLB subcomplex to be in an ON state able to activate the PG synthases FtsW and FtsI. In this way, it is ensured that new PG can be added at the points of hydrolysis.

4.4. Constriction mechanism

During constriction, simultaneous and coordinated events occur in the three layers of the cell envelope, as the PM undergoes constriction while PG is remodelled in the periplasm and the OM invaginates at the septal site (Du and Lutkenhaus, 2017; Levin and Janakiraman, 2021; Navarro *et al.*, 2022). Coordination is achieved in several ways. For instance, while the AmiA and AmiB amidases are regulated by the divisome from the PM, the activity of a third amidase, AmiC, is regulated by the OM protein NlpD (Tsang *et al.*, 2017). Besides, the Tol-Pal system, a large complex that traverses the cell wall connecting the OM to the PM, activates PG remodelling enzymes (Figure 8D) and provides a physical linkage that couples invagination of the OM to the PM constriction (Petiti *et al.*, 2019; Szczepaniak *et al.*, 2020; Yakhnina and Bernhardt, 2020).

Traditionally it has been thought that the constriction force was provided by FtsZ dynamics, but recent data have shown that in *B. subtilis* and *S. aureus* FtsZ disassembles before the separation of the daughter cells, so at least the last stages of constriction appear not to be dependent on FtsZ (Söderström *et al.*, 2014; Whitley *et al.*, 2021). However, early dissasembly of FtsZ does not seem to occur in all species (Lamanna and Maurelli, 2022). In some cases, the driving force for constriction is provided by PG synthesis in the septal zone, which pushes the PM towards the cell center (Coltharp *et al.*, 2016; Monteiro *et al.*, 2018). Once cytokinesis is completed, the divisome disassembles following approximately the reverse pathway of that followed for assembly, except that FtsN remains in place after cytokinesis has completed (Söderström *et al.*, 2016).

5. MULTICELLULARITY IN BACTERIA

Classically, bacteria have been considered and studied as unicellular organisms, but multicellularity has emerged during evolution in all three Domains of life (Figure 9A), even with losses and secondary gains of this character (Shapiro, 1988; Bonner, 1998; Carroll, 2001; Grosberg and Strathmann, 2007). Multicellularity is a form of social organization whereby cells cooperate to favor survival of the ensemble instead of the individual cells. This relies on a coordinated behavior of cells within the multicellular entity, which is based on cell-cell adhesion, intercellular communication and, in some cases, cell differentiation that allows a division of labor between different cell types (Flores and Herrero, 2010; Lyons and Kolter, 2015). Multicellularity can be achieved in two ways: by aggregation of individual cells or by incomplete cell division that give rise to cell chains or to the formation of other types of aggregates (Bonner,

1998; Claessen *et al.*, 2014; Flemming *et al.*, 2016). In some cases, the increase in size of the ensemble with respect to the individual cell confers a competitive and adaptive advantage, for instance against predation (Carroll, 2001; Bonner, 2003; Grosberg and Strathmann, 2007). Other advantages of the multicellular entity are an improved acquisition of resources, the displacement of competitors or the widening of metabolic capacities by addition of the metabolic functions of the different cell types (Grosberg and Strathmann, 2007; Claessen *et al.*, 2014).
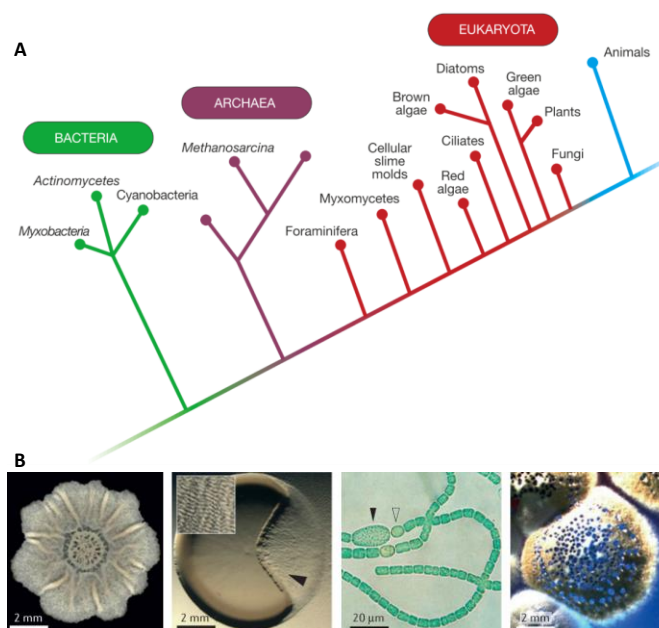
Figure 9. Bacterial multicellularity and its evolution. (A) Schematic of the evolution of multicellularity in all domains of life. (B) Some bacterial species that show multicellularity; from left to right: *B. subtilis* biofilm, *Myxococcus xanthus* swarm (rigth side) predating a colony of *E. coli*, *Anabaena cylindrica* filaments with cells differentiated into heterocysts (open arrowhead) and akinete (solid arrowhead), and *Streptomyces coelicolor* fruiting body. (A) from Carroll, (2001); (B) from Claessen *et al*., (2014).

In the Bacteria domain, multicellular forms (Figure 9B) are found in diverse genera. In Actinobacteria, representatives of the genus *Streptomyces* grow as branching hyphae, forming a vegetative mycelium, and disperse by spores formed in aerial hyphae (Flärdh and Buttner, 2009; Bush *et al.*, 2015). In Myxobacteria, the best studied species, *Myxococcus xanthus*, develops multicellular mounds and spore-producing fruiting bodies reproducing the complex behavior of macroscopic social organisms (Zusman *et al.*, 2007; Muñoz-Dorado *et al.*, 2016). In Cyanobacteria the multicellular character evolved early, about $2.4\text{-}2.7\text{x}10^9$ years ago, and has reverted several times during the evolution of this monophyletic group (Schirrmeister *et al.*, 2011; 2013; 2015). Recent studies have shown that some cyanobacterial strains can display facultative multicellularity (Urrejola *et al.*, 2020; Tang *et al.*, 2023). In multicellular cyanobacteria, the intercellular exchange of nutrients and regulatory components is an essential feature (Flores and Herrero, 2014; Herrero *et al.*, 2016) (see below).

6. THE PHYLUM CYANOBACTERIA

Cyanobacteria, formerly known as blue-green algae, constitute a phylum of diverse and widely distributed prokaryotes included in the Bacteria Domain of life (Woese, 1987), within the Terrabacteria group (Coleman *et al.*, 2021) (see Figure 4). Cyanobacteria are diderm bacteria. The trait that defines this phylum is the capacity to perform oxygenic photosynthesis, which is unique among bacteria. A photosynthetic apparatus similar to, and indeed the precursor of, that of eukaryotic chloroplasts accomplishes this task.

6.1. History, classification and diversity of cyanobacteria

6.1.1. Impact of cyanobacteria on the evolution of life on Earth

The date for the origin of cyanobacteria is a controverted issue. Studies on this matter focus on three directions: (i) the origin of oxygenic photosynthesis, (ii) molecular clock estimations on the origin of the phylum and (iii) the study of the geobiological record (micro-fossils). The difficulty for an accurate estimation of the origin of cyanobacteria is evidenced by the wide variation, in the range of hundreds of million years, offered by the different studies (Schopf, 2011; Schirrmeister *et al.*, 2016; Cardona, 2018; Garcia-Pichel *et al.*, 2019). We may still be far from an accurate determination of when the last cyanobacterial common ancestor appeared on Earth. However, most studies coincide in the notion that the origin of cyanobacteria predates the "Great Oxygenation Event" (GOE), an increase in the oxygen levels of the atmosphere that occurred during the Proterozoic period, about 2.2-2.4 billion years ago, for which cyanobacteria are considered responsible (Tomitani *et al.*, 2006; Schirrmeister *et al.*, 2011; Luo *et al.*, 2016). Ancient cyanobacteria evolved the capacity to use solar energy to split the water molecule and use it as a source of electrons for photosynthesis, producing oxygen, a side product of the reaction. Most of the oxygen produced by the biological activity of cyanobacteria was initially absorbed by the oceans and the surface rocks. However, in the long term, the accumulation of oxygen in the atmosphere determined a dramatic switch from a primitive biosphere, mostly dominated by anaerobic life forms, that were henceforth subjected to a strong selective preasure for tolerance to a highly toxic molecule, O_2. Eventually, this trend led to the evolution of O_2-dependent organisms.

Another crucial event in which cyanobacteria were mayor players in life history is the origin of algae and land plants as water-splitting photosynthetic organisms. The widely accepted endosymbiotic origin of plastids, according to which algae and land plant plastids originated form a prokaryote that established as a symbiont in an eukaryotic host cell, was first proposed by Mereschkowsky in 1905, and later re-formulated in more precise terms by Lynn Margullis, who identified cyanobacteria as the putative ancestor of plastids (Sagan, 1967; Martin and

Kowallik, 1999, Annotated English translation of Merescholowsky's 1905 paper; Gray, 2017). This hypothesis was an object of controversy for decades, but the absence of biological entities apart from cyanobacteria and chloroplasts able to carry out oxygenic photosynthesis suggested that this process appeared only once in evolution. Besides, the present-day abundance of genomic sequence data has abrogated any skepticism about the concept of cyanobacteria as the origin of plastids (Martin *et al.*, 2002; Raven and Allen, 2003). There is much interest in the identification of the founder cyanobacteria that was the ancestor of chloroplasts of the green algae and land plant lineage. However, despite intensive efforts this issue is still under debate (Dagan *et al.*, 2013; Ochoa de Alda *et al.*, 2014; Ponce-Toledo *et al.*, 2017; Lawrence *et al.*, 2019).

6.1.2. Classification of cyanobacteria: classic taxonomy and sequence-based phylogeny

A longstanding classification of cyanobacteria based on morphology, structure and cell differentiation capacity divided the phylum into five sections (Rippka *et al.*, 1979) (Figure 10A): Section I (Chroococcales) includes unicellular forms that divide by binary fission or by budding (genera *Synechococcus* or *Synechocystis*); Section II (Pleurocapsales) is composed of unicellular organisms that divide by multiple fission producing small cells (called baeocytes) or by multiple and binary fission (genera *Dermocarpa* or *Pleurocapsa*); Section III (Oscillatoriales) includes filamentous non-heterocysts-forming cyanobacteria that divide in one plane (genera *Oscillatoria* or *Spirulina*); Section IV (Nostocales) comprises filamentous heterocyst-forming strains that divide in one plane (genera *Anabaena* or *Nostoc*); Section V (Stigonematales) is composed of filamentous heterocyst-forming cyanobacteria that can divide in more than one plane, resulting in branched filaments (genera *Fischerella* and *Mastigocladus*). However, recent studies indicate that this classification does not always reflect phylogenetic relationships (see Schirrmeister *et al.*, 2013; Shih *et al.*, 2013). Indeed, only sections IV and V are phylogenetically coherent, and they have been suggested to constitute a single monophyletic group (Figure 10B) (Tomitani *et al.*, 2006; Schirrmeister *et al.*, 2015). Recent studies have renamed the Cyanobacteria as *Oxyphotobacteria* and have classified them alongside two bacterial groups, named *Melainabacteria* and *Sericytochromatia*, respectively, that lack genes for phototrophy and carbon fixation. It has been proposed that the common ancestor of these groups was a non-photosynthetic organism and that *Oxyphotobacteria* acquired photosynthetic ability through horizontal gene transfer after diverging from *Melainabacteria* (Soo *et al.*, 2017).

A

I
Synechocys)s sp.

II
Chroococcidiopsis sp.

III
Oscillatoria sp.

IV
Anabaena sp.

V
Fischerella sp.

B
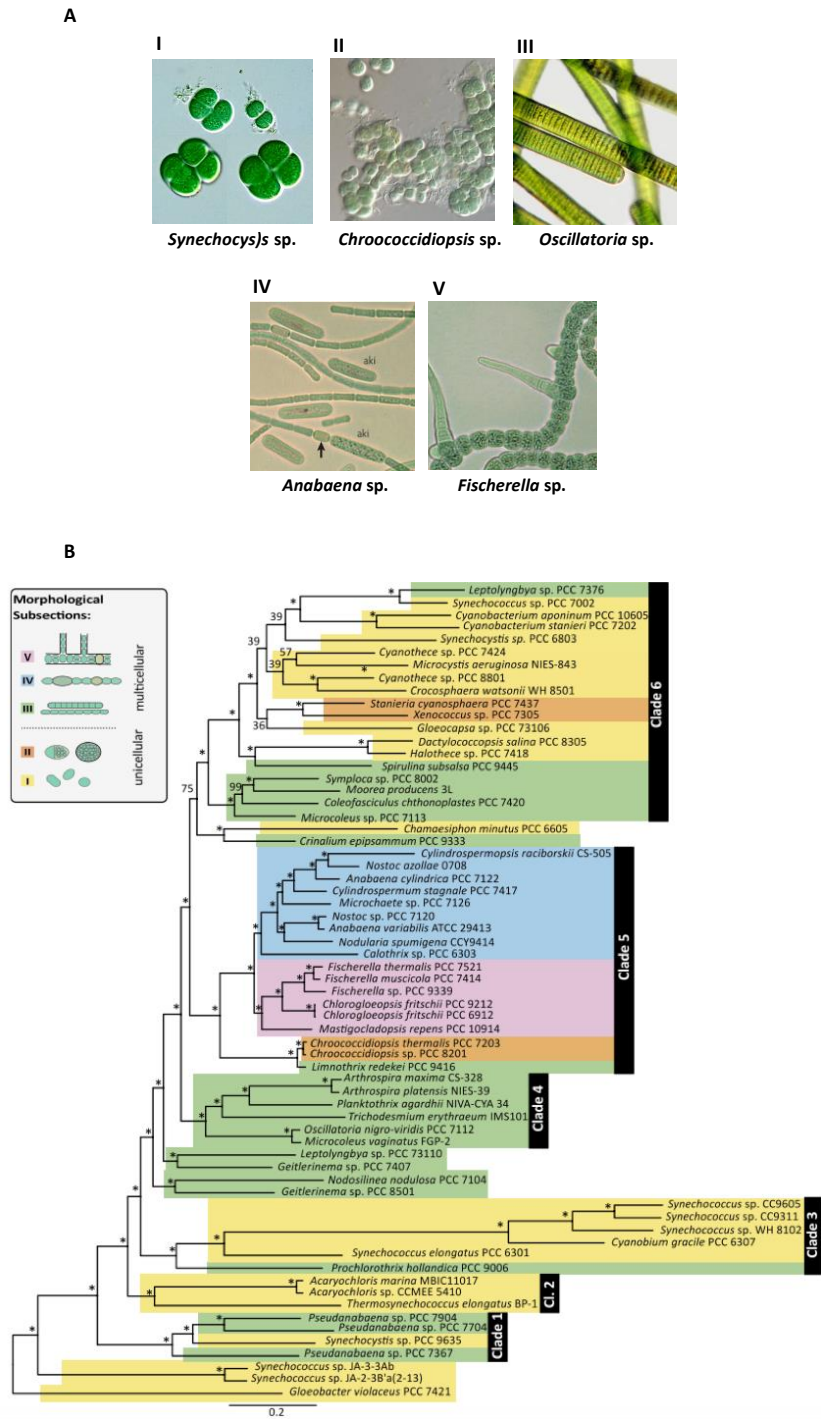
Figure 10. Morphological and phylogenetic classification of cyanobacteria. (A) Images of representative strains of each Section of Rippka's classification (Rippka *et al*., 1979). Images of representatives of Sections I, II and III are from http://alchetron.com. Images of representatives of Sections IV and V are from Flores and Herrero, (2010). (B) Phylogenetic tree of cyanobacteria from Schirrmeister *et al*., (2015). Colors indicate the Section of the Rippka's classification for each strain.

6.2. Current role of cyanobacteria in nature

The importance of cyanobacteria for life on Earth is not restricted to historical past events. At present, cyanobacteria are abundant at a planetary scale and can be found in a wide variety of habitats including freshwater, marine, terrestrial and even extreme environments. *Prochlorococcus* is one of the most abundant cyanobacteria in the oceans, and indeed it is claimed to represent the most abundant organism on Earth (Partensky *et al.*, 1999). Their profusion, widespread distribution and biological activity make present-day cyanobacteria major players in the global biogeochemical cycles of carbon, oxygen and nitrogen. For instance, about 50% of the global primary productivity on Earth (net C fixation into organic matter) is estimated to occur in the oceans, with cyanobacteria contributing importantly to this process (Field *et al.*, 1998). The highest contribution to the cyanobacterial primary production is estimated to occur in the oligotrophic sub-tropical areas dominated by strains of the genera *Synechococcus* and *Prochlorococcus* (Liu *et al.*, 1997). Therefore, present-day cyanobacteria play a major role at removing CO_2, one of the principal greenhouse gases, from the Earth's atmosphere and releasing to it stoichiometric quantities of oxygen. Besides, the cyanobacterial phylum includes a number of genera that fix atmospheric nitrogen, an ability restricted to few bacteria in nature. The ability to fix nitrogen is found in distant bacterial species, indicating that this feature might have arisen early in the evolution of bacteria (Fay, 1992). Cyanobacterial N_2-fixation is considered one of the major ways of nitrogen replenishment in the biosphere (Zehr and Capone, 2020). Marine cyanobacteria are thought to be responsible for 25–50% of the global natural N_2 fixation, corresponding to ca. $4.5\text{-}9\text{x}10^{12}$ mol per year, representing the major input of nitrogen to the oceans (Gruber, 2004; Mahaffey *et al.*, 2005; Gruber and Galloway, 2008; Canfield *et al.*, 2010; Zehr, 2011).

Cyanobacteria are also able to establish symbiotic associations with various organisms, being of note the relationship between nitrogen-fixing cyanobacteria and fungi or plants (Meeks and Elhai, 2002). Cyanobacteria also associate in symbiosis with diatoms, importantly contributing to nitrogen fixation in the oceans (Karl *et al.*, 2012; Hilton *et al.*, 2013). Finally, due to their metabolic versatility, there is a wide range of biotechnological applications of cyanobacteria, such as its use as source of bioactive compounds, in bioremediation protocols, or as biofertilizers (Abed *et al.*, 2009).

6.3. Cyanobacterial physiology

6.3.1. Photosynthesis

Cyanobacterial physiology rely mainly on the process of oxygenic photosynthesis. It has been argued that anoxygenic photosynthesis was first to evolve on Earth, setting the basis for the

development of the more complex oxygenic photosynthesis, with the two processes coexisting for millions of years (Nowicka and Kruk, 2016). Cyanobacteria were the first organisms to use two photosystems (PSI and PSII) and water as an electron donor to release O_2 and generate ATP and reducing power as reduced ferredoxin and NADPH (Hohmann-Marriott and Blankenship, 2011; Cardona, 2018). The process of oxygenic photosynthesis carried out by cyanobacteria is similar to that nowadays found in vascular plants and algae. However, cyanobacteria contain a different light-harvesting complex formed by phycobilisomes (PBSs) (Bailey and Grossman, 2008). PBSs are multiprotein complexes constituted by distinct pigmented phycobiliproteins and linker peptides that capture excitation energy and transfer it to the reaction centers. The plasticity of phycobilisomes allows the organism to adapt to variable ecophysiological conditions (Liu *et al.*, 2013). Some species can modify the pigment composition of the phycobilisomes, and also the photosystem chlorophylls, as a function of the quality of the incident light, a phenomenon known as chromatic acclimation that allows the optimization of light absorbance in nature (Gutu and Kehoe, 2012; Montgomery, 2016). The photosynthetic life style of cyanobacteria also impinges on their ultrastructure, since the photosynthetic apparatus is harbored in a system of internal membrane sacculi, named thylakoids, which in general occupy the periphery of the cytoplasm.

6.3.2. Carbon assimilation

Cyanobacteria fix CO_2 principally through the pentose phosphate, or Calvin-Bassham-Benson, cycle. This pathway is used by all photosynthetic organisms, from bacteria to higher plants, to fix carbon (Kroth, 2015). The enzyme that carries out CO_2 fixation is ribulose-1,5-bisphosphate carboxylase/oxygenase (RuBisCO). This enzyme has a low affinity for CO_2, and in addition it can also accept O_2 as a substrate. These limitations likely have favored the selection of a system known as the CO_2 concentrating mechanism (CCM), which include CO_2/HCO_3^- transporters, carbonic anhydrases and the carboxysome, a protein-coated organelle where RuBisCo is confined and concentrated (Cameron *et al.*, 2013). CCM promote the accumulation of CO_2 at high concentrations around RuBisCO, which improves the photosynthetic yield under natural conditions and the survival of the organism under conditions of carbon limitation (Kaplan and Reinhold, 1999; Giordano *et al.*, 2005; Price *et al.*, 2008). According to the protein composition, carboxysomes are classified into alpha carboxysomes and beta carboxysomes, the latter being more closely related in evolutionary terms to the microcompartments of heterotrophic bacteria (Kerfeld and Melnicki, 2016).

Although cyanobacteria are photoautotrophic organisms, some strains can also assimilate reduced carbon sources and grow heterotrophically, such as *Anabaena variabilis* (Rippka, 1972; Wolk and Shaffer, 1976). Other strains, such as *Synechocystis* sp. PCC 6803, show light-activated heterotrophic growth (Anderson and McIntosh, 1991). One of the main primary producers, *Prochlorococcus marinus* SS120, is able to take up glucose (Muñoz-Marín *et al.*, 2013). Indeed,

the uptake of sugars such as glucose by cyanobacteria could not only have a nutritional role but be also important for the establishment of symbiosis with plants, as described for *Nostoc punctiforme* (Ekman *et al.*, 2013; Picossi *et al.*, 2013).

6.3.3. Nitrogen assimilation

Nitrogen constitutes 5-10% of the dry weight of the cyanobacterial cells, which preferably use inorganic nitrogen, as ammonium or nitrate, and can also use nitrite, urea, cyanate and some amino acids as nitrogen sources (Stanier and Cohen-Bazire, 1977; Fay, 1992; Flores and Herrero, 1994; Herrero *et al.*, 2001). In addition, some cyanobacteria of different taxonomic groups can perform N_2 fixation (Rippka and Waterbury, 1977; Bergman *et al.*, 1997). Nitrogen fixation is a costly process in terms of energy and resources and it is easily inactivated by low concentrations of oxygen (Fay, 1992). Therefore, different cyanobacterial strains have developed different strategies to segregate nitrogen fixation from the oxygen produced by photosynthesis, as will be detailed below (see 6.4.2.1).

The diversity of nitrogen sources that cyanobacteria can assimilate are metabolized to generate intracellular ammonium, which is incorporated into carbon skeletons by the glutamine synthethase-glutamate synthase (GS-GOGAT) cycle (Figure 11) (Stanier and Cohen-Bazire, 1977; Fay, 1992). 2-OG is the molecule that connects the pathways for nitrogen and carbon assimilation. Its intracellular levels depend on the available nitrogen and carbon sources, being highest in the absence of ammonium and the presence of abundant carbon. Indeed, the 2-OG levels signal the C-to-N balance of the cell (Muro-Pastor *et al.*, 2001; Vázquez-Bermúdez *et al.*, 2003). In cyanobacteria, the assimilation of nitrogen is tightly regulated. For most strains, ammonium is the preferred nitrogen source and, when available, it provokes a negative regulation of the pathways for the assimilation of other nitrogen sources. NtcA is a global transcriptional regulator, of the Crp/CAP (catabolite gene activator protein) family, of universal distribution in cyanobacteria. It regulates the expression of multiple genes involved in nitrogen assimilation and other cellular functions, acting as an activator or as a repressor depending on the position of its DNA binding site relative to the regulated genes (Herrero *et al.*, 2001; 2004; Picossi *et* al., 2014; Giner-Lamia *et al.*, 2017). NtcA binds 2-OG, which is indeed required for NtcA-dependent transcription activation (Valladares *et al.*, 2008; Zhao *et al.*, 2010). The PII protein also has an important role in nitrogen regulation in cyanobacteria (Flores *et al.*, 2005). It is a widespread protein that senses the C-to-N balance, also binds 2-OG, and the energetic status of the cell (see Herrero *et al.*, 2019). In *Synechococcus* sp. PCC 7942, PII sequesters PipX, another protein involved in nitrogen regulation, which interacts with NtcA stimulating its activity (Burillo *et al.*, 2004; Forchhammer and Selim, 2019). However, PII interacts with PipX only in its 2-OG-free form. Thus, PII and PipX modulate the NtcA activity in a 2-OG-dependent manner (Espinosa *et al.*, 2006; Llácer *et al.*, 2010). In *Anabaena,* PipX plays a specific role in the activation

of NtcA-dependent promoters activated during the differentiation of the heterocysts (Valladares *et al*., 2011).
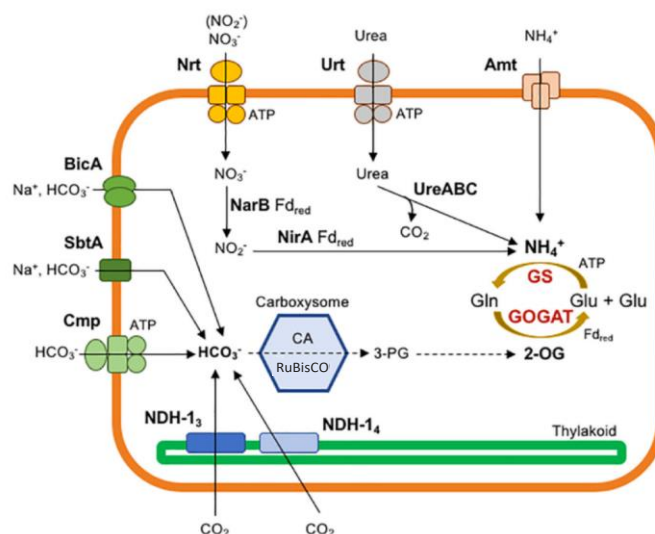

Figure 11. Schematic of the pathways for nitrogen and carbon assimilation in *Anabaena* sp. PCC 7120. Uptake of nitrogenous compounds by Nrt, Urt and Amt transporters, and of inorganic carbon by the NDH-1 systems, in the thylakoid membrane, and BicA, SbtA and Cmp is represented. Intracellular nitrate reduction depends on reduced ferredoxin and is catalyzed by nitrate reductase (NarB) and nitrite reductase (NirA). Urea reduction is mediated by the urease (UreABC) complex. Ammonium is incorporated to the GS/GOGAT pathway, which also incorporates 2-oxoglutarate (2-OG). In the carboxysome, bicarbonate is converted to CO_2 by carbonic anhydrase (CA) and incorporated into organic compounds by RuBisCO, producing 3-phospho-glycerate (3-PG) that is catabolized with the production of 2-OG. The orange line represents the plasma membrane. Figure adapted from Herrero and Flores, (2019).

6.4. Multicellularity in cyanobacteria

6.4.1. Intercellular communication

As mentioned above, multicellularity relies on cell aggregation and intercellular communication. In filamentous cyanobacteria, the cells are held together by a continuous outer membrane, and PG sacculus, and by septal proteins that bind contiguous cells in the filament (Mariscal *et al.*, 2007; Mullineaux *et al.*, 2008). The continuity of the OM conforms a continuous filament periplasm, which is also functionally continuous and allows the movement through it of molecules of between 25 and 50 kDa in size (Mariscal *et al.*, 2007; Haselkorn, 2008; Zhang *et al.*, 2008; Flores and Herrero, 2010). Intercellular exchange though this compartment requires the export and import of molecules involving PM transporters (Picossi *et al.*, 2005; López-Igual *et al.*, 2010; Pernil *et al.*, 2010; Nieves-Morión *et al.*, 2017). In order for the periplasm to be a conduit for efficient intercellular exchange, the OM should represent an efficient permeability barrier, to avoid leakage of molecules to the extracellular milieu. In *Anabaena*, this property has been demonstrated for the molecules glutamate and sucrose (Nicolaisen *et al.*, 2009b).

A second path for intercellular communication is represented by structures known as septal junctions (SJs), which are proteinaceous complexes that traverse the septum between neighboring cells in the filament connecting their cytoplasms (Figure 12). Although these connections were already observed decades ago, their structure has been resolved recently (Kieninger and Maldener, 2021). Molecular exchange between cells have been evidenced mainly through the monitorization of low MW fluorescent tracers such as calcein, 5-carboxyfluorescein or esculin. A number of proteins including SepJ, FraC, FraD and FraE have been identified to localize at the intercellular septa and to be involved in cell-cell adhesion and intercellular molecular exchange (Mullineaux *et al.*, 2008; Flores and Herrero, 2010; Merino-Puerto *et al.*, 2010; Merino-Puerto *et al.*, 2011; Nürnberg *et al.*, 2015). However, only FraD and SepN have been demonstrated to be structural constituents of SJs (Weiss *et al.*, 2019; Kieninger *et al.*, 2022). Communication through SJs occurs by diffusion and is regulated by gating (Weiss *et al.*, 2019; Arévalo *et al.*, 2021).
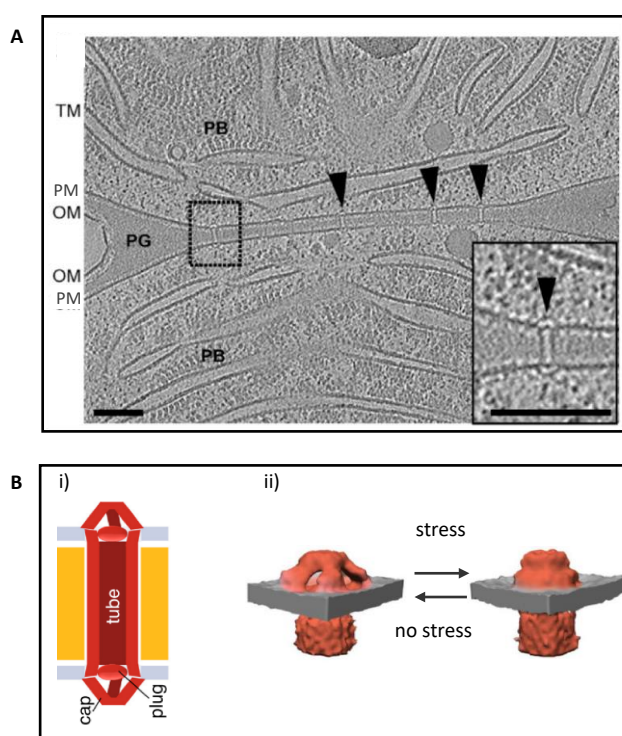
Figure 12. Structure of septal junctions (SJs). (A) Cryotomography of the septum between two *Anabaena* cells. Arrows indicate SJs crossing the septum. Plasma membrane (PM), outer membrane (OM), thylakoid membrane (TM), phycobilisome (PB), peptidoglycan (PG). (B) Schematic of SJs. i) Modules of the complex: tube, plug and cap; ii) 3D representation of open (left) and closed (right) conformations. (A) adapted from Weiss *et al*., (2019); (B) adapted from Kieninger and Maldener, (2021).

6.4.2. Cell differentiation: the heterocyst

When confronted with conditions of nitrogen scarcity, cyanobacteria of sections IV and V of Rippka's classification can differentiate heterocysts, which are cells specialized for the fixation of atmospheric nitrogen in oxic environments (Rippka *et al.*, 1979; Murry and Wolk, 1989;

Corrales-Guerrero *et al.*, 2013). Some of those cyanobacteria can also differentiate other specialized cells like resistance spores, known as akinetes, or hormogonia, short motile filaments involved in the dispersal in natural environments and in host colonization for the establishment of symbiotic associations (Flores and Herrero, 2010).

6.4.2.1. Heterocyst structure and function

Heterocysts allow the spatial separation of the incompatible processes of oxygenic photosynthesis and N_2 fixation, which is catalyzed by the enzyme nitrogenase, a large metalloenzymatic complex highly sensitive to oxygen. The structure and metabolism of the heterocyst present remarkable differences in comparison to the original cell from which it differentiates, aimed to maintain intracellular microoxic conditions and generate the higher input of ATP and reductants required by the nitrogenase activity (see e.g., Kumar *et al.*, 2010; Zeng and Zhang, 2022).

Heterocysts are easily recognizable by their larger size and elongated shape and the presence of refringent granules at the cell poles (Wildon and Mercer, 1963) (Figure 13A). Active PG synthesis allows cell elongation and enlargement during differentiation (Zhang *et al.*, 2018). The poles of the heterocysts are differentiated structures, known as the heterocyst "neck", which reduces the contact surface with the adjacent vegetative cell, and hence intercellular exchanges. Indeed N_2 enters the heterocyst mainly through the neck (Walsby, 2007). The polar granules are made of cyanophycin, a polymer of arginine and aspartic acid resulting from the nitrogen fixation activity (Lang *et al.*, 1972; Flores and Herrero, 2010). Other structural characteristics of heterocysts are the absence of carboxysomes and the reorganization of the thylakoid membranes, which convolute and accumulate around the cell poles forming the so-called "honeycomb" membranes (Valladares *et al.*, 2007; Flores and Herrero, 2010).

During heterocyst differentiation, additional layers of the cell envelope are deposited, which restrict the entrance of gasses, O_2 but also N_2, into the cell cytoplasm (Murry and Wolk, 1989; Fay, 1992). These include an inner laminated layer of glycolipids (HGL), which functions as a gas permeability barrier, and a thicker and more homogeneous outer layer of polysaccharides (HEP), which protects the HGL from physical damage (Cardemil and Wolk, 1979; Kumar *et al.*, 2010; Flores and Herrero, 2010). Both HGL and HEP are engrossed around the cell poles (Nicolaisen *et al.*, 2009a; Herrero *et al.*, 2016).

Regarding metabolic differentiation, the endogenous production of oxygen is abrogated by the loss of PSII, photosynthesis being restricted to cyclic electron flow through PSI (Magnuson and Cardona, 2016). Honeycomb membranes show a high respiratory activity, due to the presence of specific cytochrome oxidases, that readily consume free oxygen that may enter the heterocyst from neighboring vegetative cells (Valladares *et al.*, 2007; Walsby, 2007). Heterocysts have lost the ability to fix CO_2 due to the loss of the RuBisCO enzyme and carboxysomes. This adaptation

creates the necessity of receiving fixed carbon from adjacent vegetative cells, which transfer to the heterocyst glutamate, alanine and sucrose (Winkenbach and Wolk, 1973; Valladares *et al.*, 2007; Flores and Herrero, 2010; Herrero *et al.*, 2016). The GOGAT enzyme is also absent in heterocysts. Hence, glutamine produced by GS is exported to vegetative cells (Wolk *et al.*, 1976; Thomas *et al.*, 1977; Martín-Figueroa *et al.*, 2000). Heterocysts also transfer to the adjacent cells β-aspartyl-arginine dipeptide, which derives from the hydrolysis of cyanophycin (Burnat *et al.*, 2014).

Given the metabolic compartmentalization, molecular exchange between heterocysts and vegetative cells is an absolute requirement for the operation and survival of the diazotrophic filament. Net transfer of carbon compounds from vegetative cells to heterocysts, and of nitrogen compounds in the opposite direction, ensures the correct nutrition of all cells in the filament. NanoSIMS (nanometer-scale secondary ion mass spectrometry) technology has recently helped to monitor this exchange, showing that vegetative cells are progressively more nitrogen limited as the distance from the nearest heterocysts increases (Popa *et al.*, 2007; Kumar *et al.*, 2010; Herrero *et al.*, 2016; Nieves-Morión *et al.*, 2021). Molecular transfer between heterocysts and vegetative cells take place through SJs (see 6.4.1), although the flow rate is slower than that between two vegetative cells, and the SJ array also differ (Nicolaisen *et al.*, 2009a; Arévalo and Flores, 2021) (see section 7 below). The presence of the cyanophycin granules located at the poles of the heterocysts appears to represent a factor limiting transfer (Mullineaux *et al.*, 2008).
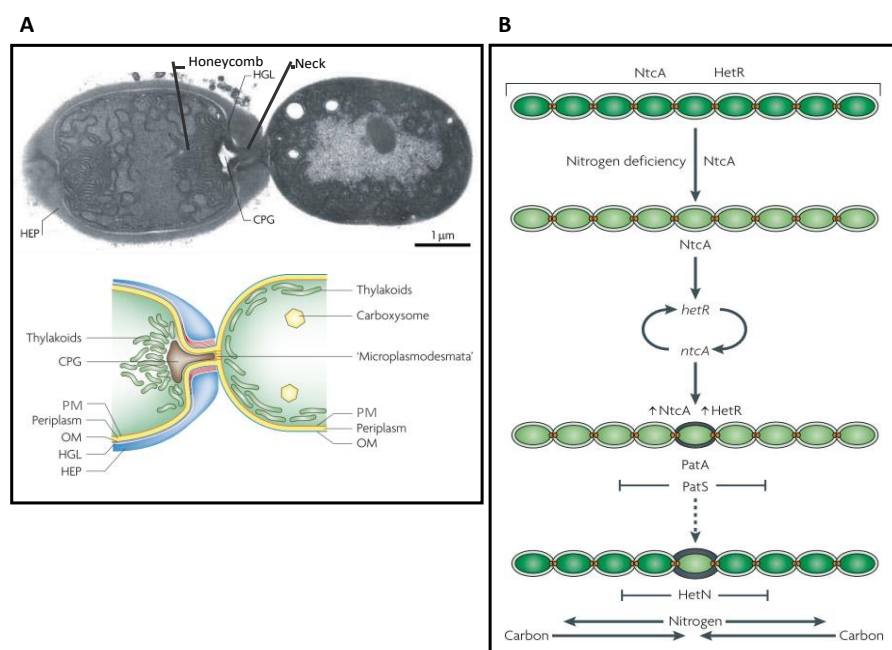
Figure 13. Heterocyst ultrastructure and regulatory circuit for heterocyst differentiation. (A) Transmission electron microscopy image and schematic of a heterocyst (left) and a vegetative cell (right). The main structures of the heterocyst are indicated: cyanophycin granule polypeptide (CGP), glycolipid (HGL) and polysaccharide (HEP) layers of the cell envelope. (B) Sequence of regulatory events during heterocyst differentiation indicating the the participation of the transcription factors NtcA and HetR, and their mutual activation. The inhibitory signaling peptides derived from PatS and HetN, produced in the differentiating cells and mature heterocysts, respectively, are transferred to inhibit differentiation of adjacent cells. PatA is a positive regulator of differentiation. Transfer of carbon compounds from vegetative cells to the heterocyst and of nitrogen compounds in the opposite direction is also indicated. Adapted from Flores and Herrero, (2010).

6.4.2.2. Heterocyst differentiation

The process of heterocyst differentiation is triggered by the perception of nitrogen scarcity. In different strains the pattern of heterocysts distribution along the filament can differ, with some species showing heterocysts only at the filament ends and others showing both terminal and intercalary heterocysts. The regulatory mechanisms controlling heterocyst differentiation has been particularly well characterized in *Anabaena*, whereby heterocysts are separated by tracts of ca. 10-12 vegetative cells (Flores and Herrero, 2010) (Figure 13B). Differentiation involves the sequential activation and repression of multiple genes directed by two wide-range transcription factors: NtcA, the global nitrogen regulator, and the heterocyst-differentiation factor HetR. In addition, other regulators, including sRNAs, participate in specific steps (Buikema and Haselkorn, 1991; Flores and Herrero, 2010; Flaherty *et al.*, 2014; Herrero *et al.*, 2016; Brenes-Álvarez *et al.*, 2019; Xu *et al.*, 2020; Zeng and Zhang, 2022). Under conditions of low nitrogen availability, intracellular levels of 2-OG increase and activate NtcA, which in turn is required for the expression of the *nrrA* gene. The NrrA factor represents a link between NtcA and HetR and it is required for the full induction of the *hetR* gene (Xu *et al.*, 2008). The expression of NtcA and HetR are mutually activated in a regulatory loop that seems essential for the establishment of differentiation (Muro-Pastor *et al.*, 2002). Although all cells might sense nitrogen deficiency, not all cells in the filament differentiate. The decision on which cells undergo differentiation appears to rely on positive signals in the cell to differentiate and negative signals that would diffuse from it to the neighboring cells, inhibiting their differentiation (Wolk, 1967; Herrero *et* al., 2016, Muñoz-García and Ares, 2016). One positive signal is identified with the induction of *hetR*, whereas negative signals correspond to diffusible peptides of 5-7 amino acids excised from longer peptides, PatS, PatX, HetN, produced in the differentiating cells and processed during export from them (Yoon and Golden, 2001; Corrales-Guerrero *et al*., 2013; 2014; Videau *et al*., 2015; Zhang *et al*., 2017; Elhai and Khudyakov, 2018). Whereas *patS* is expressed together with *patX* at an early stage of differentiation and would participate in the establishment of the heterocyst distribution pattern, *hetN* is expressed at a later stage and would participate in pattern maintenance. In the vegetative cells, the inhibitory peptides would interact with HetR, inhibiting its DNA binding activity and thereby HetR-dependent transcription activation, blocking the differentiation of these cells (Yoon and Golden, 2001; Kim *et al*., 2011).

6.5. Cell Morphology in Cyanobacteria

Cyanobacterial cells display a wide variety of sizes and morphologies. Size ranges between the 0.5 µm diameter of *Prochorococcus* strains to the 69 µm of *Oscillatoria princeps* (Schulz-Vogt *et al.*, 2007). Cell morphologies include coccoidal, elipsoidal, discoidal, rod-shaped or spiral forms, and some species like *Mastigocladus laminosum* or *Fischerella muscicola* are pleomorphic

(Flores and Herrero, 2014) (Figure 10A) (see e.g. https://www-cyanosite.bio.purdue.edu/images/images.html for some images of cyanobacterial species). In addition, some environmental cues can induce changes in cell morphology. For instance, in *Fremyella diplosiphon* the quality of light has been reported to induce the transition from rod-shaped cells (predominant in green light) to more coccoid cells (predominant in red light) (Bordowitz and Montgomery, 2008). In *Anabaena*, the nutritional status as well as the light intensity provoke changes in cell shape and size (this work, Velázquez-Suárez, in preparation). The mechanisms underlying the determination of these cell shapes in different strains are still poorly understood, but they surely involve the PG synthesis complexes. Multicellularity adds an additional layer of complexity, as multicellular strains show unique features of the cell envelope (see below). In addition, morphological changes associated to cell differentiation require remodelling of the cell wall (Singh and Montgomery, 2011).

Knowledge on the mechanisms governing cyanobacterial cell shape and size could also be of interest for biotechnological applications. Recent reports have shown that morphology can be manipulated resulting in advantages for some applications; e.g., making easier cell harvesting from scaled-up cultures (Jordan *et al.*, 2017).

7. THE CELL ENVELOPE OF CYANOBACTERIA

The cyanobacteria are diderm bacteria with a thick PG layer, ranging in thickness from 10 to 35 nm (although in some cases it can be up to 700 nm thick) in the periplasmic space between the PM and the OM (Hoiczyk and Hansel, 2000; Springstein *et al.*, 2020c). Traditionally classified as Gram-negative bacteria, the high degree of crosslinkage and the anomalous thickness of their PG layer, in comparison to model Gram-negative bacteria, led to propose that the cyanobacterial envelope was intermediate between those of canonical Gram-positive and Gram-negative bacteria, showing features specific to each type (see Hahn and Schleiff, 2014 and references therein). The presence in cyanobacterial genomes of cell wall-processing and cell division genes homologous to those of Gram-negative and Gram-positive bacteria was thought to further support this proposal (Hoiczyk and Hansel, 2000; Springstein *et al.*, 2020c). Recent advances in the knowledge on the early evolution of bacterial lineages have helped to understand their current features. Cyanobacteria are clasified in the Terrabacteria group that includes diderm and all known monoderm bacteria (Coleman *et al.*, 2021) (see Figure 4). In this group, the monoderm phenotype arose as a result of multiple independent losses of OM genes. Thus, given the phylogenetic position of Cyanobacteria as a sister clade of monoderm bacteria, it is not surprising to observe genes and features in common to them (Witwinowski *et al.*, 2022).
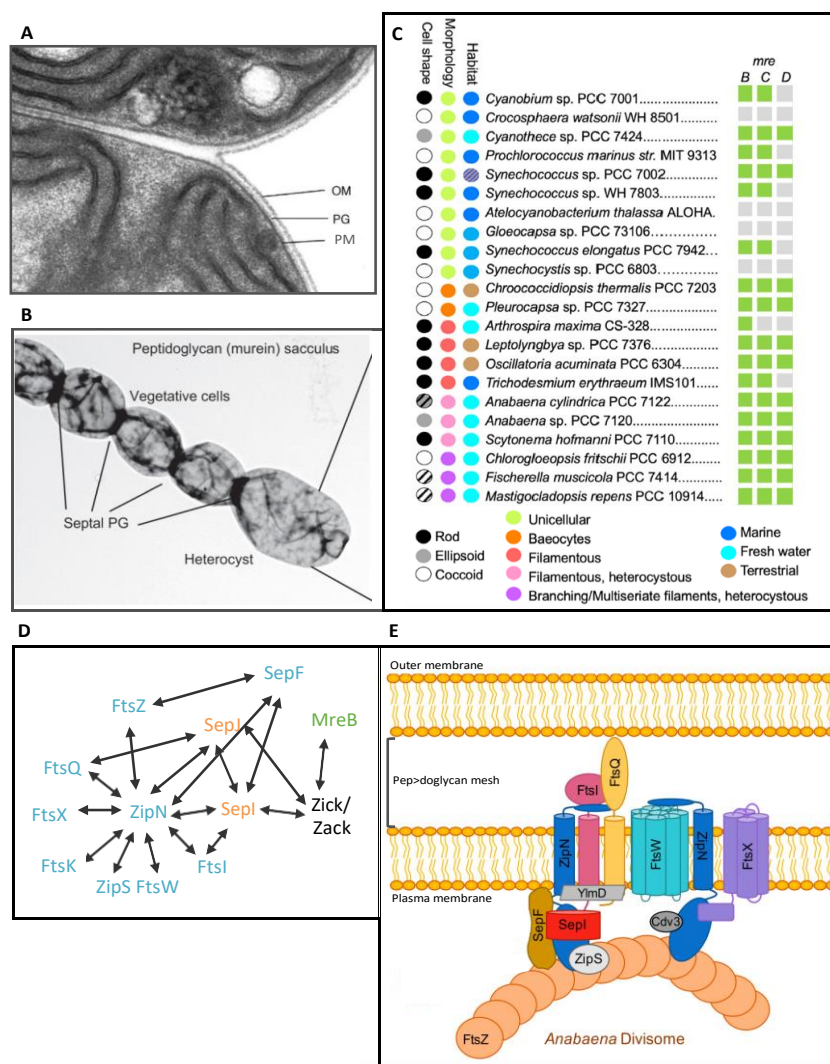
Figure 14. The cyanobacterial cell envelope and divisome components. (A) The cell envelope of *Anabaena* with focus on an intercellular septum: plasma membrane (PM), peptidoglycan layer (PG) and continuous outer membrane (OM). (B) Continuous peptidoglycan sacculus from *Anabaena*. (C) Distribution of *mre* genes in representative strains from different habitats showing different morphologies. (D) Interaction network of proteins of the *Anabaena* divisome (blue), elongasome (green) and septal complexes (orange). (E) The *Anabaena* divisome. (A) Adapted from Flores *et al.*, (2006), (B) from Arévalo *et al.*, (2021); (C) and (D) adapted from Springstein *et al.*, (2020c).

In addition to a thick PG layer, the cyanobacterial cell envelope shows other specific features. For instance, the OM contains carotenoids that are thought to protect the cell from excess radiation (Resch and Gibson, 1983). Besides, the OM proteome of cyanobacteria is mainly composed of beta barrel proteins that show significant differences in the overall structure and pore size with respect to OM proteins of *E. coli* (Huang *et al.*, 2004; Moslavac *et al.*, 2005). Of note, some cyanobacterial strains have an additional outermost proteinaceous S-layer, and some others produce a muscillage capsule that confers protection against desiccation and UV-radiation (Hoiczyk and Hansel, 2000).

As mentioned above, in filamentous cyanobacteria, whereas the PM is individual for each cell, the OM is continuous, enclosing a periplasmic space that is common to all the cells of the filament and constitutes a conduit for molecular exchanges between them (Flores *et al.*, 2006; Mariscal *et al.*, 2007; Wilk *et al.*, 2011) (Figure 14A). The continuity of the OM relies on the lack

of OM invagination and fission during cell division. During cell division the newly synthetized septal PG does not split either, so that the resulting daughter cells are separated by a single PG layer, named septal disk, that is thicker than the lateral PG layer. This makes the PG saculus to be also continuous for the whole filament and, indeed, it can be isolated as an unit (Figure 14B). PG septal disks present an average of ca. 20 nm-wide perforations, termed nanopores, that likely serve to lodge the SJ protein complexes that comunicate the cytoplasms of adjacent cells. Nanopores in septal PG disks are drilled by amidases, whose inactivation provoke complete loss or alterations in the number and size of septal nanopores, and impairment in cell-cell communication (Lehner *et al.*, 2011; Berendt *et al.*, 2012; Bornikoel *et al.*, 2017; Zheng *et al.*, 2017). The number of nanopores and the nanopore diameter are larger in the septa between a vegetative cell and a heterocyst than in septa between two vegetative cells (Nicolaisen *et al.*, 2009a; Arévalo and Flores, 2021).

7.1. PG synthesis in cyanobacteria

The pattern of PG growth has been studied in a variety of cyanobacteria with diverse morphologies by labeling with Van-FL. Van-FL binds to the D-Ala-D-Ala in lipid II, either not incorporated or incorporated in nascent PG chains but not yet involved in cross-linking (Lehner *et al*., 2013; Springstein *et al.*, 2020b). Also, a fluorescent analog of D-alanine, HADA (D-Ala, 7-Hydroxycoumarin-amino-D-alanine), which incorporates in the cell wall has been used (Zhang *et al.*, 2018). Significant differences were observed associated with different morphotypes. Both septal and peripheral labelling were observed in unicellular strains such as the coccoid *Synechocystis* sp. PCC 6803 and the rod-shaped *Synechococcus* sp. PCC 7942. In addition, the coccoid *Microcystis* sp. PCC 7806 showed double staining rings at midcell typical of pre-septal PG growth. Filamentous strains, like *Arthospira* sp. FACHB 792, *Oscillatoria animalis*, *Leptolyngbya* sp. CB006, *Spirulina subsalsa* or *Anabaena*, all showed both peripheral and septal staining, although in the former two labeling was confined to cells at the tip of the filament, indicating that cell elongation and division are restricted to these cells (Zhang *et al.*, 2018). The pleomorfic strain *Fischerella muscicola*, a filamentous branching cyanobacteria, showed Van-FL staining indicative of PG growth at peripheral and septal position throught the filament and at polar position in the apical cells of the branches.

Most bacteria contain a long cluster of genes, named *dcw* (*division and cell wall*), involved in PG synthesis and cell division, which is not observed in cyanobacteria, whereby such genes are commonly found as individual genes or in short clusters (Megrian *et al.*, 2022). Some genes involved in PG synthesis in cyanobacteria, including the intracellular synthesis of PG precursors (Videau *et al.*, 2016; Liu *et al.*, 2021) and the extracellular PG polymerization (Lázaro *et al.*, 2001; Leganés *et al.*, 2005; Marbouty *et al.*, 2009) have been identified and their products characterized. Of note, it was observed that the number of genes encoding PBPs increases with the size of the genome, with a minimum of four in marine unicellular strains and up to 14 in

Nostoc punctiforme. Filamentous strains include a higher number of class A PBPs than unicellular ones, and it was proposed that these enzymes are involved in the differentiation of specific cells such as heterocysts (Leganés *et al.*, 2005).

7.1.1. The elongasome

As mentioned above, the protein MreB is generally present in rod-shaped and absent in coccoid bacteria. In cyanobacteria, some correlation has been observed between the presence of *mre* genes and the cell morphology (Springstein *et al.*, 2020c), but the rules that determine this correlation are not fully understood. In cyanobacteria the *mre* genes generally group in a *mreBCD* cluster, although this cluster in not universally conserved in the phylum. In *Anabaena* this cluster has been shown to constitute an operon (Hu *et al.*, 2007). Genomic analyses have revealed that out of 131 genomes surveyed, only four, corresponding to coccoid bacteria, lacked the three *mreB, mreC* and *mreD* genes (Figure 14C). Some spherical cyanobacteria such as *Prochlorococcus marinus* bear *mreBC* genes, whereas some others, such as the unicellular *Cyanobium* sp. and even the filamentous *Trichodesmium erythraeum*, maintain a rod-shape in the absence of *mreD* or, in the case of *Arthrospira maxima*, of *mreC* and *mreD*. Filamentous cyanobacteria that form heterocysts, including those that also form branched or multiseriated filaments, present a *mreBCD* gene cluster, although *Chlorogloeopsis fritschii* features coccoid cells (Springstein *et al.*, 2020b). The obligate symbiont *Atelocyanobacterium thalassa* (also known as UCYN-A) present coccoid cells and lack not only the *mre* genes, but also *rodA* (Cassier-Chauvat and Chauvat, 2014; Springstein *et al.*, 2020c).

In the unicellular, rod-shaped strain *Synechococcus* sp. PCC 7942, *mreB* is essential, and partially segregated mutants showed a rounder shape, indicating that this gene is involved in the determination of cell morphology (Savage *et al.*, 2010). In *Anabaena* sp. PCC 7120, MreB is not essential but it is also involved in cell morphology and cell wall stability (Hu *et al*., 2007). MreB from *Anabaena* was reported to interact with Zick and Zack, two coiled-coil-rich proteins (CCRPs) that form heteropolymeric filaments, and this interaction was shown to impact the MreB localization (Springstein *et al.*, 2021). In *F. diplosiphon*, the expression of *mreB* is regulated by BolA, a protein that under red light binds to the *mreB* promoter region repressing transcription. This might explain that under red light *F. diplosiphon* cells are rounder than under green light (Singh and Montgomery, 2014). In species that differentiate hormogonia, such as *N. punctiforme*, the *mreBCD* operon is involved in the transition from coccoid vegetative cells to rod-shaped hormogonia (Gonzalez *et al.*, 2019).

Regarding the relationship between elongasome and divisome proteins, interactions have been reported to occur in several species (Springstein *et al.*, 2020b), and in *Synechocystis* it has been suggested that MreB could be, directly or indirectly, negatively regulated by cell division factors

such as ZipN or ZipS (Koksharova *et al.*, 2007). Finally, no relationship was found between MreB and cell division in *Anabaena* (Hu *et al.*, 2007).

Other components of the elongasome have been scarcely investigated in cyanobacteria and there are no systematic analyses of their conservation in the phylum. However, the *Anabaena* genome would encode for all the elongasome components including MreB, MreC, MreD, RodA, PBP2 and RodZ.

8. CELL DIVISION IN CYANOBACTERIA

Although still limited, knowledge on cell division in cyanobacteria is gradually increasing. Bioinformatic analyses have revealed the existence in cyanobacteria of homologues of divisome proteins of diderm bacteria, such as *E. coli*, and of monoderms, such as *B. subtilis* (Table 2). In addition, cyanobacterial-specific components have been identified (Figure 14E) (Cassier-Chauvat and Chauvat, 2014; Springstein *et al.*, 2020c). In cyanobacteria, the role of cell division proteins has been studied mainly by gene mutagenesis or depletion, localization studies (i.e. inmunolocalization or tagging with fluorescent proteins) and analysis of protein-protein interactions (Mazouni *et al.*, 2004; Miyagishima *et al.*, 2005; Marbouty *et al.*, 2009; Ramos-León *et al.*, 2015; Corrales-Guerrero *et al.*, 2018; Camargo *et al.*, 2019; Springstein *et al.*, 2020b). The emerging picture in that in divisome composition and in some mechanistic aspects of cell division cyanobacteria differs from the model unicellular bacteria like *E. coli* and B. *subtilis*. Besides, differences have been reported between different species within this phylum. Differences with model bacteria and between cyanobacterial species may derive from the idiosincrasies of the specific life style; indeed, the photosyntetic nature, multicellularity and cell differentiation are features that impact cell division.

8.1. The cyanobacterial divisome

The protein initiating cell division, FtsZ, is present in all cyanobacteria and chloroplasts. In cyanobacteria, the FtsZ dynamics is similar to that of FtsZ in *E. coli*, although exhibiting a lower GTPase activity, which could be a feature conserved in cyanobacteria and chloroplasts (Springstein *et al.*, 2020b; 2020c; Porter *et al.*, 2023). Based on the capacity to form curled filaments in vitro, FtsZ dynamics has been proposed to contribute constriction force in *Synechocystis* and *Anabaena*, whereas in *Prochorococcus* FtsZ has been proposed to act only as a scaffold for the divisome (Liu *et al.*, 2017; Springstein *et al.*, 2020c). The location of the Z-ring in succesive rounds of division varies in different cyanobacteria, with some strains forming rings parallel (*Anabaena*) or perpendicular (*Synechocystis*) to that of the previous division event.

Unlike in *E. coli*, in cyanobacteria the *ftsZ* gene is not included in *a dcw* operon, but it is commonly found close to the *ftsQ* gene, except in *Procholoroccus* and marine *Synechococcus*, in

which *ftsQ* is absent (Springstein *et al.*, 2020b). *ftsZ* is essential in all species tested and a decrease in gene dosage, or the inhibition of FtsZ polymerization, provokes morphological alterations, i.e. cell elongation in the rod-shaped *Synechococcus* sp. PCC 7942, cell swelling in the coccoid *Synechocystis* sp. PCC 6803 and elongated and swelled cells in *Anabaena* (Sarcina and Mullineaux, 2000; Miyagishima *et al.*, 2005; Ramos-León *et al.*, 2015). Overexpression of FtsZ in several heterocyst-forming cyanobacteria also provoke morphological alterations and reduced viability and induced altered multiplane division (Springstein *et al.*, 2020b). Therefore, FtsZ levels must be precisely regulated for proper cell growth. Mechanisms controlling FtsZ levels are scarcely known, although in *Anabaena* and in branched heterocyst-forming filamentous strains FtsZ appears to be a substrate of Ser-Cys and metalloproteases, respectively (Lopes Pinto *et al.*, 2011; Springstein *et al.*, 2020b). In many cyanobacteria, FtsZ includes a 20-80 amino acid long N-terminal part. In particular, a distinct ca. 55 aa-long N-terminal peptide is highly conserved in FtsZ from heterocyst-forming strains. In *Anabaena*, this N-terminal peptide of FtsZ is essential for viability and for establishing the correct lateral and longitudinal self-interacctions during FtsZ polymerization, as well as for interactions of FtsZ with at least another divisome component, SepF (Corrales-Guerrero *et al.*, 2018).

Regarding FtsZ anchors to the PM, homologs of FtsA and ZipA are absent in cyanobacteria. Instead, the cyanobacterial-specific proteins ZipN and ZipS have been implicated in FtsZ filament estabilization and membrane anchoring. These two proteins localize to the Z-ring in *Synechococcus*, *Synechocystis* and *Anabaena*, and their depletion or inactivation provoke strong morphological alterations, including the formation of elongated or swollen cells in the three strains (Springstein *et al.*, 2020c).

ZipN, also known as Ftn2, is ubiquitous in cyanobacteria, being essential in *Synechocystis* and *Anabaena*. It localizes early at midcell and presumably anchors FtsZ to the PM though a C-terminal transmembrane domain. The level of ZipN must be precisely regulated for the correct positioning of FtsZ and for the interaction with other divisome proteins such as SepF or ZipS, as well as with septal proteins such as SepJ (Marbouty *et al.*, 2009; Camargo *et al.*, 2019; Springstein *et al.*, 2020c). SepF is essential in *Synechocystis* and *Synechococcus*. *Synechocystis* SepF interacts *in vitro* with FtsZ stimulating the assembly of FtsZ filaments (Cassier-Chauvat and Chauvat, 2014; Springstein *et al.*, 2020c). ZipS, also known as Ftn6, is present in all tested cyanobacteria except *A. thalassa* and marine species. In *Synechocystis* ZipS is essential and it arrives at midcell once the Z-ring is already functional. ZipS contains an N-terminal DnaD-like domain, presumably allowing interaction with DNA, leading to the proposal that this protein could coordinate DNA replication and cell division (Cassier-Chauvat and Chauvat, 2014; Springstein *et al.*, 2020c).

Regarding homologs to other components of the *E. coli* divisome, cyanobacteria lack FtsL and FtsB, whereas FtsN has been detected only in *Synechocystis* sp. PCC 6803. FtsK and FtsE are generally present, whereas FtsX has been detected only in *Anabaena* (Cassier-Chauvat and

Chauvat, 2014; Springstein *et al.*, 2020c). Reported interactions between divisome constituents are shown in Figure 14D.

8.2. Adaptations of cell division in cyanobacteria

As photosynthetic organisms, cyanobacteria are highly dependent on light and their physiology is governed by the daily succession of light and dark periods that provoke wide oscillations in gene expression and global cell physiology. The control of this circadian rithmicity is exerted by complex systems out of which the KaiABC proteins constitute the central oscillator (Cohen and Golden, 2015). In *Synechococcus elongatus*, FtsZ expression shows circadian oscillations that peak late in the light phase (Dong *et al.*, 2010). In cyanobacteria, cell division is not strictly linked to the circadian rhythm (i.e. cells do not divide synchronously following the light/dark cycles) but cell division is gated by the circadian control (Yang *et al.*, 2010), involving the central oscillator KaiC protein and the CikA, SasA and RpaB signal transducers. High ATPase activity of KaiC correlates with the inhibition of FtsZ polymerization, favoring cell division during the dark period (Dong *et al.*, 2010).

Whereas in unicellular bacteria amidases mediate the splitting of the PG during cytokynesis, in filamentous muticellular strains, in which citokynesis is incomplete, the amidases have adopted a distinctive role at perforation of nanopores in the septal PG (Lehner *et al.*, 2013). Remarkably, multiple interactions have been reported between divisome and septal junction proteins, which moreover are localized to the divisome during cell division. Thus, recruitment by the divisome appears a way for the localization of SJ components in the intercellular septa, where they remain after cell division is completed (Ramos-León *et al.*, 2015; Camargo *et al.*, 2019; Springstein *et al.*, 2020a). For instance, the septal protein SepJ interacts with FtsQ and ZipN and losses its septal localization in strains depleted of any of them (Ramos-León *et al.*, 2015; Camargo *et al.*, 2019). Thus, specific mechanisms during cell division result in the propagation of structures for cell-cell adhesion and intercellular communication that are key features for multicellularity in these cyanobacteria.

Cell differentiation also impinges on the cell division activity. A connection between differentiation and cell division was deduced from the apparent requirement of a previous division event for the initiation of heterocyst differentiation (Sakr *et al.*, 2006; Risser *et al.*, 2012; Wang *et al.*, 2021). The basis for this dependence is still not understood, but recently a divisome-associated protease, HetF, has been shown to regulate both cell division and heterocyst differentiation. HetF is a membrane protein bound to the divisome by interaction with FtsI. The protein PatU3 is degraded by HetF around the division site, precluding PatU3 interaction with ZipS and its inhibitory action on PG synthesis. The remaining PatU3 in the cytoplasm is sufficient to sequester HetZ, an inducer of heterocyst differentiation, preventing the initiation of the differentiation program (Figure 15) (Li *et al.*, 2021; Xing *et al.*, 2022). Consistently Δ*hetF* mutants

show enlarged cells, impaired cell division and low heterocyst frequency. Conversely, Δ*patU3* mutants show small cells and multiple contiguous heterocysts (Xing *et al.*, 2022).

Also, it has been long known that heterocysts are terminal differentiated cells that do not divide. Consistently, FtsZ and ZipN rings are undetectable in heterocysts, and the genes *zipN* and *ftsZ*
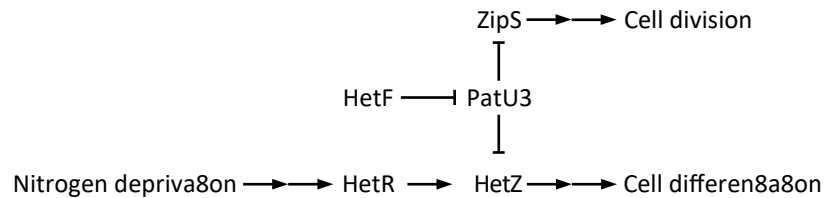
Figure 15. Schematic of a part of the regulatory network connecting cell differentiation and cell division in *Anabaena* (see the text for details).

are repressed early during differentiation and in mature heterocysts, respectively (Zhang *et al.*, 2018; Valladares *et al.*, 2020). It has been proposed that early during differentiation, the protein PatA, which interacts with ZipN and SepF, destabilize the Z-ring but allowing the presence of free FtsZ during intermediate stages (Valladares *et al.*, 2020). The protein PatD, which is expressed early in differentiating cells, has been shown to interact with FtsZ and ZipN altering FtsZ polimerization and also precluding Z-ring formation (Wang *et al.*, 2021). In addition, free FtsZ, at levels limited by PatD, would represent a positive signal for differentiation to proceed (Wang *et al.*, 2021). Together, these studies reveal a link between the inhibition of cell division and the completion of the heterocyst differentiation process.

OBJECTIVES

Objectives

1. To study the influence of the nitrogen and carbon availability on cell size and morphology in *Anabaena* sp. PCC 7120.

2. To investigate the spatiotemporal pattern of PG incorporation and the role of the *mre* genes in filaments of *Anabaena* sp. PCC 7120 growing with combined nitrogen or diazotrophically.

3. To unravel specific interactions between cell growth, PG synthesis and cell division in *Anabaena* sp. PCC 7120.

SUMMARY OF RESULTS

Out of the great diversity of existing bacteria, PG synthesis has mainly been studied in a few model organisms that share an unicellular character. Therefore, expanding our knowledge to other bacteria with different morphologies and life styles appears necessary for a deeper understanding of this essential issue. Towards this goal, we have chosen a representative of the clade of multicellular cyanobacteria, which present a distinct organismal organization. We have addressed the pattern of PG synthesis, including the influence of environmental factors and the relationships with the process of cell division, in *Anabaena* sp. PCC 7120. The work and the results obtained in this thesis have been divided into three chapters, each corresponding to a published research article.

Chapter I: The Inorganic Nutrient Regime and the *mre* Genes Regulate Cell and Filament Size and Morphology in the Phototrophic Multicellular Bacterium *Anabaena*.

Velázquez-Suárez, C, Luque, I, Herrero, A. (2020). *mSphere, 5*(5):e00747-20.

https://doi.org/10.1128/msphere.00747-20

Cell shape and size are inheritable traits that can be modified under certain environmental conditions. The information on PG synthesis in *Anabaena* was scarce and little was known on the influence of the carbon and nitrogen sources and on the role of MreB, MreC and MreD in the determination of cell size and shape, and the filament length, in this cyanobacterium.

Results in this work showed that in *Anabaena* the carbon and nitrogen regime impact the cell size, the filament length and the aspect ratio (the ratio between the length of the cell axis parallel to the filament and the one perpendicular to the filament). When growing with combined nitrogen, these morphological parameters fluctuated throughout the cell cycle. In general, cells growing in the presence of nitrogen compounds, specially with abundant inorganic carbon supply, are larger and longer than vegetative cells from diazotrophic cultures, and filaments are longer in the former conditions.

The *mreB*, *mreC* and *mreD* genes form an operon whose expression is highest in the exponential phase of growth, when the cells were increasing the aspect ratio, and is negatively regulated by NtcA, consistent with the higher aspect ratio observed in cells of an *ntcA* mutant in comparison to the wild type (WT). *mreBCD* expression increases during heterocyst differentiation upon N-stepdown and, transiently, in the differentiating cells. Mutants lacking *mreB*, *mreC* or *mreD* exhibit impaired growth, especially under diazotrophic conditions. Filaments of these mutants are longer than those of the WT, and their cells are bigger and rounder; indeed, in the mutants the cell axis parallel to the filament is shorter than that perpendicular to the filament. Also, heterocysts of the mutants are larger and rounder than the wild-type heterocysts. In addition, intercellular septa along the filament are wider and thicker than in the WT. These results indicate a role of MreB, MreC and MreD in the synthesis of peripheral PG for cell elongation during growth with combined nitrogen or diazotrophically, as well as during differentiation of the heterocysts, affecting also the intercellular PG along the filament.

Chapter II: The Role of Mre Factors and Cell Division in Peptidoglycan Growth in the Multicellular Cyanobacterium *Anabaena*.

Velázquez-Suárez, C, Valladares, A, Luque, I, Herrero, A. (2022). *mBio, 13*(4):e0116522.

https://doi.org/10.1128/mbio.01165-22

PG synthesis is required for cell growth and subsequent division, giving rise to the specific morphology of each bacterial species. PG growth has been studied in depth in model unicellular rod-shaped bacteria. However, the envelope structure of *Anabaena* is peculiar since cytokinesis does not proceed to completion and OM invagination does not occur, which results in a continuous OM, enclosing all cells of the filament, and a continuous periplasm containing the PG sacculus, which is not split during cytokinesis and remains fused in the intercellular septa along the filament.

This work focused on the growth of PG in *Anabaena* and in *mreB*, *mreC* and *mreD* mutants. It permitted to conclude that *Anabaena* presents three modes of PG growth: lateral, divisional and intercellular septal. The intercellular septal synthesis is permanent and represent a distinctive mode that likely is shared by other filamentous multicellular cyanobacteria. In *Anabaena*, the MreB, MreC and MreD proteins are not only localized in the cylindrical part of the cell periphery, but also in the intercellular septa and, notably, in the divisome localization during all the stages of cell division. Continuous septal PG synthesis can contribute to the positioning and remodeling of septal protein complexes for intercellular communication. Besides alterations in the cell morpholgy, the absence of the *mreB*, *mreC* or *mreD* genes provoke alterations in the positioning of the Z-ring and the division septa, resulting in impared orientation of the intercellular septal PG along the filament. Molecular interactions have been detected between MreB or MreD and some divisome components. These results led to the proposal that the elogasome Mre proteins are required for the correct positioning of the divisome. Conversely, mutants affected in the expression of FtsZ or ZipN not only are deficient in cell division, but also present impaired uncheked peripheral PG growth, leading to giant cells prone to lysis. Thus, the divisome appear not only to direct the septal synthesis, but also to regulate the lateral PG growth. These results show unprecedented mutual connections between the elongasome and the divisome, as well as between the different modes of cellular PG growth.

Chapter III: The Role of MreB, MreC and MreD in the Morphology of the Diazotrophic Filament of *Anabaena* sp. PCC 7120.

Velázquez-Suárez, C., Luque, I., & Herrero, A. (2022). *Life*, *12*(9):1437.

https://doi.org/10.3390/life12091437

In *Anabaena*, the absence of nitrogenous compounds in the external medium triggers the differentiation of heterocysts, a process that has been widely studied. However, the role of the elongasome proteins MreB, MreC and MreD during heterocyst differentiation and in the diazotrophic filament was not known. In filamentous multicellular cyanobacteria, intercellular communication through the shared periplasm and the SJs, including the exchange of nutritional compounds and signalling molecules, is pivotal for the organism performance under diazotrophic conditions.

This work evidenced that during heterocyst differentiation there is a transient incorporation of PG in the periphery of the differentiating cells and in the septal regions between heterocys and the adjacent vegetative cells, the latter involved in the remodeling of the cell wall to form the hetrocyst neck. Polar PG incorporation persists in mature heterocysts, likely involved in maintenance of the structure of the septa between both cell types. MreB, MreC and MreD localize to the periphery and the poles of the differentiating cells, but they go away from the periphery of old heterocysts. Inactivation of *mreB*, *mreC* or *mreD* leads to instances of abnormally high and aberrant PG incorporation in the periphery and the poles of the differentiating cells, and the presence of heterocysts with conspicuous morphological alterations, including deformed poles and instances of filament breackage at vegetative cell-heterocyts connections. Moreover, septa devoid of SepJ can be detected in the mutants. These results involve the Mre proteins in the formation of septal communication structures in the heterocyst poles. Also, apparently mature heterocyst still presenting a Z-ring could be detected in the *mre* mutants, consistent with a role of Mre factors in the disassembly of the divisome in the differentiating cells.

CHAPTER I: The inorganic nutrient regime and the mre genes regulate cell and filament size and morphology in the phototrophic multicellular bacterium *Anabaena*

The Inorganic Nutrient Regime and the *mre* Genes Regulate Cell and Filament Size and Morphology in the Phototrophic Multicellular Bacterium *Anabaena*

Cristina Velázquez-Suárez,[a] Ignacio Luque,[a] Antonia Herrero[a]

[a]Instituto de Bioquímica Vegetal y Fotosíntesis, CSIC and Universidad de Sevilla, Seville, Spain

ABSTRACT The model cyanobacterium *Anabaena* sp. PCC 7120 exhibits a phototrophic metabolism relying on oxygenic photosynthesis and a complex morphology. The organismic unit is a filament of communicated cells that may include cells specialized in different nutritional tasks, thus representing a paradigm of multicellular bacteria. In *Anabaena*, the inorganic carbon and nitrogen regime influenced not only growth, but also cell size, cell shape, and filament length, which also varied through the growth cycle. When using combined nitrogen, especially with abundant carbon, cells enlarged and elongated during active growth. When fixing N_2, which imposed lower growth rates, shorter and smaller cells were maintained. In *Anabaena*, gene homologs to *mreB*, *mreC*, and *mreD* form an operon that was expressed at higher levels during the phase of fastest growth. In an *ntcA* mutant, *mre* transcript levels were higher than in the wild type and, consistently, cells were longer. Negative regulation by NtcA can explain that *Anabaena* cells were longer in the presence of combined nitrogen than in diazotrophic cultures, in which the levels of NtcA are higher. *mreB*, *mreC*, and *mreD* mutants could grow with combined nitrogen, but only the latter mutant could grow diazotrophically. Cells were always larger and shorter than wild-type cells, and their orientation in the filament was inverted. Consistent with increased peptidoglycan width and incorporation in the intercellular septa, filaments were longer in the mutants, suggesting a role for MreB, MreC, and MreD in the construction of septal peptidoglycan that could affect intercellular communication required for diazotrophic growth.

IMPORTANCE Most studies on the determination of bacterial cell morphology have been conducted in heterotrophic organisms. Here, we present a study of how the availability of inorganic nitrogen and carbon sources influence cell size and morphology in the context of a phototrophic metabolism, as found in the multicellular cyanobacterium *Anabaena*. In *Anabaena*, the expression of the MreB, MreC, and MreD proteins, which influence cell size and length, are regulated by NtcA, a transcription factor that globally coordinates cellular responses to the C-to-N balance of the cells. Moreover, MreB, MreC, and MreD also influence septal peptidoglycan construction, thus affecting filament length and, possibly, intercellular molecular exchange that is required for diazotrophic growth. Thus, here we identified new roles for Mre proteins in relation to the phototrophic and multicellular character of a cyanobacterium, *Anabaena*.

KEYWORDS bacterial multicellularity, cell size, cell aspect, filament length, NtcA regulation

In bacteria, cell shape and cell size are key determinants of their interactions with the surrounding milieu. They present a rich diversity of cellular morphologies, which are heritable and adaptive (see references 1 and 2). Bacteria range in cell volume over at

least 10 orders of magnitude (see reference 3), and cell size is also a heritable trait that can be modulated within a certain range. Recent data revealed that, at least in some model bacteria, metabolism, growth, and cell cycle progression play main roles in size setting (4).

In *Escherichia coli* and *Bacillus subtilis*, the current prevalent paradigm to explain the homeostasis of cell size is the so-called adder principle, which states that, regardless of the size at birth, a constant cell volume is added at each generation under constant growth conditions (5). Considering the dynamics of cell size variations in response to environmental conditions, at least at the population level, a relationship appears to exist between the growth rate, determined by the availability of nutrients, and cell size, so that the volume added in each generation would depend on nutrient availability. It has been proposed that the ratio between the rates of surface area growth and volume growth is a key parameter in adjusting cell size (6). However, little is known at the molecular level about how cell growth is sensed and how it could impact the initiation of cell division as a determinant of cell size (6, 7). The unicellular cyanobacterium *Synechococcus elongatus* has been observed to follow a sizer-like model, so that the amount of material added depends on environmental conditions and the circadian clock, which modulates growth and constricts the time window of cell division (8). In *E. coli* and *B. subtilis*, the cell size in rich medium can duplicate that in minimal medium, and an effect of carbon availability in the initiation of cell division has been described (9–11).

Regarding the determination of cell morphology, the cell wall, which allows the bacterial cell to cope with the internal osmotic pressure, has a pivotal role (12). Hence, the spatiotemporal dynamics of cell wall synthesis during the cell cycle is a key determinant of cell shape during cell growth and of its maintenance during cell division (13–15). The peptidoglycan (PG) forming the cell wall is made of long glycan strands bridged by short peptides that form a giant polymer, the murein sacculus. Considerable insight has been gained into the spatial dynamics of PG growth in bacteria that exhibit rod shape or variations thereof, such as *E. coli* and *B. subtilis*, in which PG synthesis takes place in the cylindrical part of the cell during growth. The multiprotein complex for lateral PG growth, the elongasome, integrates synthetic enzymes, including penicillin-binding proteins (PBPs), PG hydrolases, and the RodZ, MreB, MreC, and MreD proteins or homologs thereof that contribute to the peripheral localization of the PG processing enzymes (13, 15–17). MreB is an actin structural homolog characteristic of rod-shaped bacteria (18). MreB and MreC have been described as essential proteins in *Caulobacter crescentus* (19). In *B. subtilis*, MreB and MreC, but not MreD, are essential under standard growth conditions, although cells depleted of MreB or MreC can be propagated in the presence of high concentrations of magnesium (20). In *E. coli*, MreB, MreC, and MreD are essential (21), although cells lacking these proteins can propagate as small spheres under conditions of slow growth (22).

Much less is known about the mechanisms of determination of other bacterial cell morphologies (see references 23 and 24). Hence, toward the biological challenge of understanding how the environment influences the strain-specific shape and size of bacteria and their variations, data on different strains with disparate life modes should be accumulated.

Cyanobacteria are phototrophic organisms of ancient origin, in which the process of oxygenic photosynthesis evolved. Hence, these organisms have played a crucial role in the evolution of our planet and life on it. Currently, cyanobacteria are responsible for a large fraction of the oceans' primary productivity at a global scale, thus significantly influencing climate dynamics (e.g., 25). The photoautotrophic mode of life has a global impact on the physiology and anatomy of cyanobacteria, and an example of this is the conspicuous presence of an intracellular membrane system, the thylakoids, where the photosynthetic apparatus is harbored (26). Regarding the assimilation of nitrogen, most cyanobacteria preferentially utilize inorganic nitrogen, and nitrate and ammonium are excellent nitrogen sources for growth. In addition, many strains are able to fix atmospheric nitrogen and, indeed, make a principal contribution to N_2 fixation in the oceans

(27). The cyanobacteria are diderm bacteria classified as Gram-negative bacteria, although their PG sacculus has several layers, which makes cyanobacteria intermediate between model Gram-negative and Gram-positive bacteria (28). Cyanobacteria show a remarkable diversity of cellular sizes and morphologies, and in addition to unicellular forms, strains characterized by the formation of different types of cell aggregates, including linear unbranched or branched filaments, are found (26, 29).

Morphology is a complex character in filamentous cyanobacteria. In genera such as *Anabaena* and *Nostoc*, the organismic unit is a uniseriate filament of cells that have been considered spherical, ovoid, ellipsoid, or cylindrical in shape (29). The cells in the filament are delimited by individual cytoplasmic membranes, and the peptidoglycan sacculus, which surrounds each cell, is thickened and frequently fussed in the intercellular septa. However, the outer membrane is continuous, thus delimiting a continuous periplasm that is shared by all the cells of the filament (30). Besides the periplasmic connection, neighboring cells in the filament are linked by proteinaceous complexes, called septal junctions, that traverse the septal PG and bridge the cytoplasm of contiguous cells, providing cell-to-cell cohesion and intercellular communication functions, as has been studied in the model strain *Anabaena* sp. strain PCC 7120 (here, *Anabaena*) (31). Moreover, depending on external factors, the filament may include different cell types specialized in different functions. Thus, when utilizing combined nitrogen, all the cells of the filament are equivalent. In contrast, under conditions of combined-nitrogen scarcity, *Anabaena* forms heterocysts, which are cells specialized in the fixation of N_2, at semiregular intervals along the filament, resulting in a pattern of heterocysts separated by intervals of ca. 10-to-15 vegetative cells (32). Heterocysts fix N_2 and transfer organic nitrogen-rich compounds to the vegetative cells, which in turn perform photosynthetic CO_2 fixation and transfer organic carbon-rich compounds to the heterocysts. Hence, these organisms represent a unique case of division of labor regarding nutritional function in a pluricellular bacterium (31).

Despite their remarkable features and global significance, studies of the determination of cell morphology in filamentous cyanobacteria, as in cyanobacteria in general, are scarce (see, however, references 33 and 34). Moreover, little is known about the homeostasis of cell size in cyanobacteria, as representatives of bacteria that exhibit a metabolism relying on phototrophy and the photosynthetic assimilation of inorganic nitrogen, in contrast to the better-studied heterotrophic bacteria. We addressed here the study of morphological parameters of *Anabaena* growing under different nutritional contexts and in different regulatory-mutant backgrounds and investigated the role of the *mreB*, *mreC*, and *mreD* genes in morphology determination in this organism.

RESULTS

We addressed the determination of morphological parameters through the different growth phases in batch cultures of *Anabaena* using inorganic combined nitrogen (either nitrate or ammonium) or N_2 as a nitrogen source and two different regimes of inorganic carbon supply, air (low carbon, LC) and air plus a supplement of 10 mM $NaHCO_3$ in the culture medium (high carbon, HC). We also studied mutants lacking a functional *ntcA* gene, which encodes a transcriptional regulator of nitrogen assimilation that is required for growth using nitrate or N_2 (35), or lacking a functional *hetR* gene, which encodes a transcriptional regulator specifically required for diazotrophic growth (see reference 36).

Dynamics of *Anabaena* cell growth in batch cultures. To settle defined conditions for the study of the dynamics of cell size and morphology, the growth of *Anabaena* was followed during 28 days of incubation under each of the nutritional conditions indicated above (Fig. S1). Under these conditions, the fastest exponential growth (FEG) was observed during the first ca. 48 h in the presence of nitrate or ammonium, whereas in the absence of combined nitrogen, a lag of ca. 20 h, a period in which heterocyst differentiation takes place, preceded the exponential growth. Generally, the growth rate decreased after the first week of incubation, and by the fourth week growth ceased in cultures with ammonium or N_2 and LC (stationary phase), whereas in the presence

TABLE 1 Growth rate constants of *Anabaena* and mutants *ntcA*, *hetR*, *mreB*, *mreC* and *mreD*

Strain	Condition	Growth rate constant (day^{-1})^a				
		Phase				
		FEG	Wk 1	Wk 2	Wk 3	Wk 4
PCC 7120 (WT)	N_2 LC	0.35	0.262	0.149	0.065	−0.024
	N_2 HC	0.35	0.274	0.125	0.065	0.029
	NO_3^- LC	0.86	0.605	0.094	0.053	0.031
	NO_3^- HC	0.54	0.466	0.077	0.072	0.055
	NH_4^+ LC	0.90	0.576	0.127	0.026	−0.005
CSE2 (*ntcA*)	NH_4^+ LC	0.497	0.449	0.139	0.022	0.012
CSSC2 (*hetR*)	NO_3^- LC	0.473	0.410	0.146	0.043	0.019
	NO_3^- HC	0.497	0.425	0.101	0.043	0.022
	NH_4^+ LC	0.466	0.427	0.122	0.007	−0.001
CSCV1 (*mreB*)	NO_3^- LC	0.574	0.401	0.142	0.053	0.036
	NO_3^- HC	0.480	0.365	0.108	0.053	0.029
	NH_4^+ LC	0.566	0.389	0.156	0.046	0.019
CSCV4 (*mreC*)	NO_3^- LC	0.499	0.432	0.156	0.062	0.026
	NO_3^- HC	0.370	0.226	0.190	0.091	0.043
	NH_4^+ LC	0.557	0.355	0.134	0.067	−0.038
CSCV2 (*mreD*)	N_2 LC	0.156	0.110	0.18	0.139	0.046
	N_2 HC	0.197	0.067	0.22	0.067	0.019
	NO_3^- LC	0.538	0.422	0.139	0.043	0.026
	NO_3^- HC	0.504	0.336	0.168	0.053	0.041
	NH_4^+ LC	0.581	0.473	0.127	0.041	0.012

^{a}Growth rate constant, μ (day^{-1}), corresponds to ln2/t_d, where t_d is the doubling time, calculated from the increase in the optical density at 750 nm (OD$_{750}$) in each time interval with values from 4 independent cultures of each condition (see growth curves in Fig. S1). FEG (fastest exponential growth) corresponded to growth during the first 48 h for BG11 and BG11$_0$ + NH_4^+ media, and during 24 to 72 h for BG11$_d$ medium. Mann-Whitney tests were performed to assess significance of differences with the mean values calculated from the independent experiments (Data Set S1).

of nitrate, slow growth was maintained. (Table 1 presents the growth rates during each of the 4 weeks of incubation).

When incubated with LC, the FEG rate was similar with nitrate or ammonium and was approximately 0.4-fold under diazotrophic conditions (the significance of comparisons can be found in Data Set S1). Although the assimilation of nitrate, which involves nitrate transport and intracellular reduction to ammonium, is energetically more expensive than the assimilation of ammonium (35), it can be considered that under the illumination conditions used here, reducing power is not limiting for nitrate reduction, which is a process directly linked to photosynthesis (37). Regarding diazotrophic growth, the large investment of cellular resources, energy and reductants, required for heterocyst differentiation and N_2 reduction to ammonium can explain the lower diazotrophic growth rate in comparison to growth with combined nitrogen. Fixing N_2, HC did not affect the FEG, although it had a positive effect on the phases of slowest growth. In the presence of nitrate, the FEG rate with HC was ca. 0.4-fold smaller than the rate observed with LC, although this difference has low statistical significance. Finally, no growth was detected in the presence of ammonium and HC.

Although both the *ntcA* and *hetR* mutants can grow with ammonium, the growth rate was ca. half that in the wild type. In the *hetR* mutant, which in contrast to the *ntcA* mutant can grow with nitrate, the growth rate was similar with LC or HC and about half that in the wild type with LC (Table 1).

Dynamics of cell size during growth using different C and N supplies. We measured the cell area during growth under the conditions described above (Fig. 1; the significance of comparisons can be found in Data Set S1). Generally, the carbon supply had only a small impact on cell area. Cells incubated with combined nitrogen tended to increase area throughout the growth curve until reaching the stationary phase (550.5
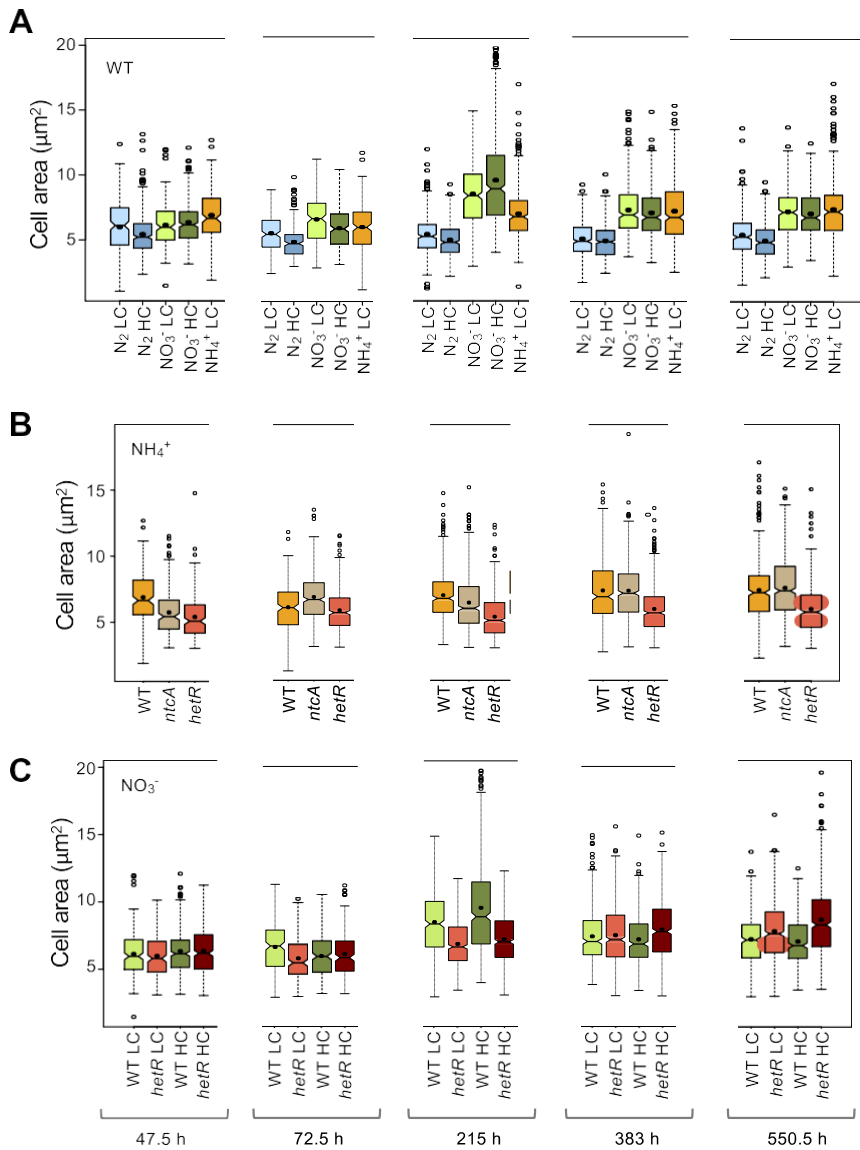
FIG 1 Dynamics of cell area in *Anabaena* and strains CSE2 (*ntcA* mutant) and CSSC2 (*hetR* mutant) grown with different nitrogen and carbon supplies. Cells grown in BG11 medium with low carbon (LC) or high carbon (HC), in $BG11_0$ + NH_4^+ medium with LC, or in $BG11_0$ medium (lacking combined nitrogen) with LC or HC, were used to inoculate, at an initial cell density corresponding to 0.2 μg chlorophyll/ml, flasks containing the same medium, which were incubated under culture conditions. At the indicated times, aliquots of each culture were photographed and used for cell area determination, as described in Materials and Methods. A total of 500 to 700 cells (vegetative cells in the diazotrophic cultures) from three or four different cultures of each time and condition were measured. Notched boxplot representations of the data are shown. The mean values are represented by black dots. Tukey tests were performed to assess significance of differences (Data Set S1). (A) WT; (B) *ntcA* and *hetR* mutants in $BG11_0$ + NH_4^+; (C) *hetR* mutant in BG11.

h in Fig. 1A), so that they appeared smaller when more actively growing. Cells incubated with ammonium or nitrate were similar in size except for a transient peak that, in the transition from more active to slower growth, was repeatedly observed only with nitrate (215 h in Fig. 1A). In contrast, vegetative cells of diazotrophic cultures showed a more homogeneous cell size during growth, being smaller than cells incubated with nitrate or ammonium. Thus, diazotrophy results in not only a slower growth rate and smaller cell size than when using combined nitrogen, but also in a restriction for cell mass increase throughout the growth cycle.

To assess whether any correlation existed between the growth rate and the cell size in *Anabaena*, the growth rate constant was plotted against the mean cell area for the
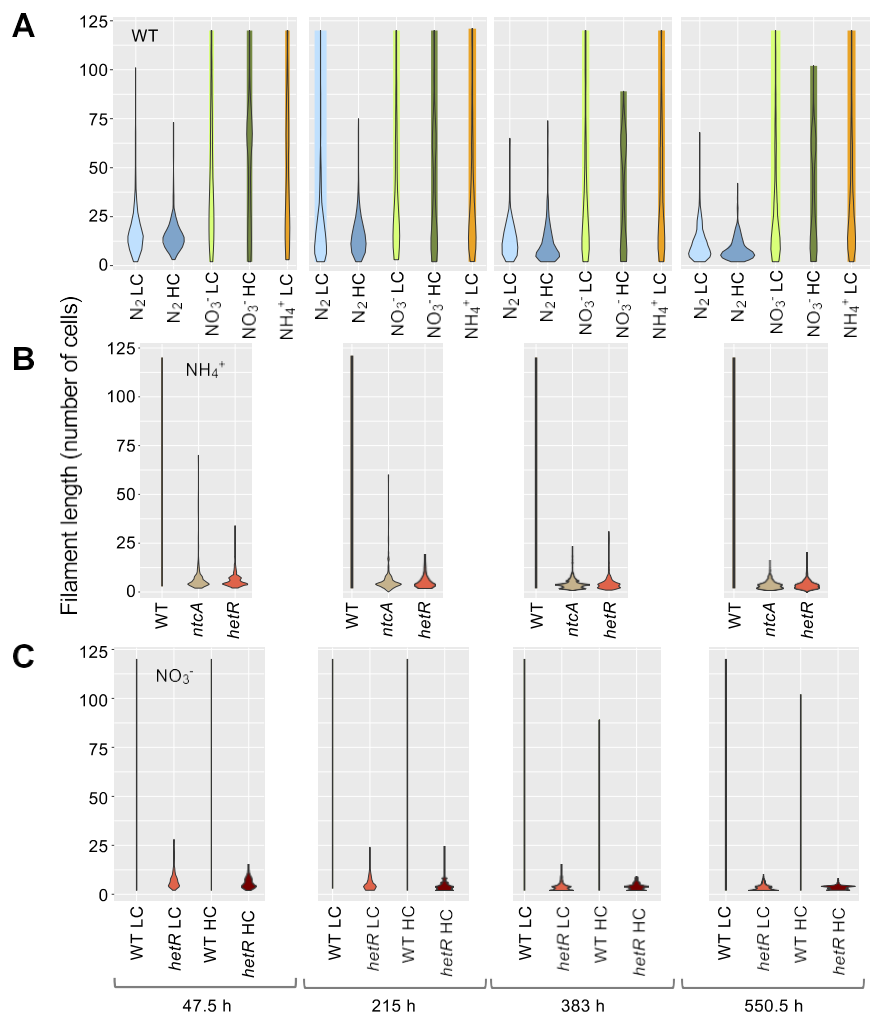
FIG 2 Distribution of filament length in *Anabaena* and strains CSE2 (*ntcA* mutant) and CSSC2 (*hetR* mutant) grown with different nitrogen and carbon supplies. At the indicated times, aliquots of cultures treated as described in the legend to Fig. 1 were taken with care to avoid filament breakage and photographed. Filaments from three independent cultures of each condition were counted. Filaments longer than 120 cells were counted as of 120. Violin-plot representations of the data are shown. Mann-Whitney tests were performed to assess significance of differences with data from filaments up to 119 cells long (214 to 387 filaments) (Data Set S1).

different nutrient conditions in each of the considered growth periods (Fig. S2). *Anabaena* showed a positive correlation during the phases of more active growth (see FEG and first week in Fig. S2), although this correlation was nonlinear. Notably, a linear negative correlation was observed with data corresponding to the 2nd week of growth, which corresponded to the transit to phases of less active growth and, in the case of nitrate-grown cells, of larger cell size.

Regarding the *ntcA* and *hetR* mutants, cells of the former, with ammonium and LC, were generally similar to those of the wild type (Fig. 1B). Under these conditions, cells of the *hetR* mutant were smaller than those of the wild type or the *ntcA* mutant. Also, during fast growth in the presence of nitrate, with LC or HC, cells of the *hetR* mutant were similar or somewhat smaller than those of the wild type (Fig. 1C).

Filament length responds to the C and N nutrition. The number of cells per filament was counted through the growth cycle under the different nutritional conditions described above, and the distribution of filament lengths was analyzed (Fig. 2; the significance of comparisons can be found in Data Set S1). In the wild type, filaments tended to be longer during the phases of more active growth. Perhaps senescence and

death of random intercalary cells, which would be more frequent during less active growth, could contribute to shorten the filaments.

Filaments incubated with nitrate and LC were similar in size to those incubated with ammonium and tended to be shorter than those incubated with nitrate and HC. A larger difference was observed between filaments incubated with nitrate or ammonium and the shorter diazotrophic filaments. Perhaps the septa between vegetative cells and heterocysts are more fragile than the septa between vegetative cells, contributing to shortening of filaments under diazotrophic conditions. Moreover, because heterocysts are terminally differentiated cells, senescence and lysis of old heterocysts would increase filament breakage. This is consistent with the fact that filaments of 5 to 15 cells, roughly coincident with the size of vegetative-cell intervals separating two heterocysts, were the most frequently observed under diazotrophic conditions.

Finally, both in the *ntcA* mutant and in the *hetR* mutant, the filaments were much shorter than in the wild type.

Dynamics of cell morphology during growth using different C and N supplies. The lengths of the longitudinal (parallel to the filament) and the transversal (perpendicular to the filament) axes of the cells were determined in *Anabaena* under the different growth conditions used and, as an indication of cell aspect, the ratio between the two cell axes (aspect ratio) was calculated (Fig. 3; the significance of comparisons can be found in Data Set S1). In nitrate- and ammonium-supplemented medium, with LC, the aspect ratio increased through the phases of more active growth and then decreased more pronouncedly in the presence of ammonium. This same trend was observed for cells incubated under diazotrophic conditions, although in this case the aspect ratio increase was smaller and delayed, consistent with a delayed FEG (see above), compared to growth in combined nitrogen-supplemented medium.

The aspect ratio of cells incubated with nitrate or ammonium reached higher values than in diazotrophic cultures, and HC supplement generally had a positive effect. Because in rod-shaped cells an increase in length would increase the total surface area, it could have larger benefits when growth depends on nutrients taken up from the external medium (see reference 1), such as nitrate, ammonium or bicarbonate, and during phases of faster growth, and could facilitate light adsorption also. In contrast, under diazotrophic conditions, it is assumed that most N_2 enters the heterocysts from the neighboring vegetative cells by intercellular connections (38). Moreover, because elongation is likely more costly than making short rods, the energetic balance would represent another factor favoring *Anabaena* cells being longer when combined nitrogen is available.

Notably, in ammonium-supplemented medium, the aspect ratio of the *ntcA* and *hetR* mutants was considerably higher than that of the wild type (Fig. 3B). In the *hetR* mutant, the aspect ratio was higher in cultures with ammonium than in those with nitrate (see Fig. 3B and C).

The *mre* gene cluster of *Anabaena*. In the *Anabaena* genomic sequence, the *mreB* gene (all0087) and a homologue to *mreC* (all0086) are clustered together, being separated by 95 nucleotides. Downstream of *mreC*, open reading frame (ORF) all0085 is found, which is separated from the putative *mreC* by 114 nucleotides (see Fig. 4A). *Anabaena* MreB has 347 residues with 52% identity to *E. coli* MreB. No transmembrane helix is present in *Anabaena* MreB (checked with TMHMM) although, similar to *E. coli* MreB (39), it may include an amphipathic in-plane membrane anchoring segment (Amphipaseek, NPS@ [Network Protein Sequence Analysis]) for interaction with the cytoplasmic membrane. MreC is a bitopic protein with a transmembrane helix and a large periplasmic part (40). The predicted product of all0086 has 273 amino acids (aa) and 19% identity to *E. coli* MreC (367 aa), bears an N-terminal signal peptide locating almost the whole protein in the periplasm (Phobius), and includes a coiled-coil motif encompassing residues ca. 60 to 90 (Network Protein Sequence Analysis [41]). Finally, all0085 would encode a 170-aa product with 19% identity to *E. coli* MreD (162 aa). However, in spite of the low overall sequence identity, All0085 would include 5 transmembrane helices with a periplasmic N terminus and cytoplasmic C terminus,
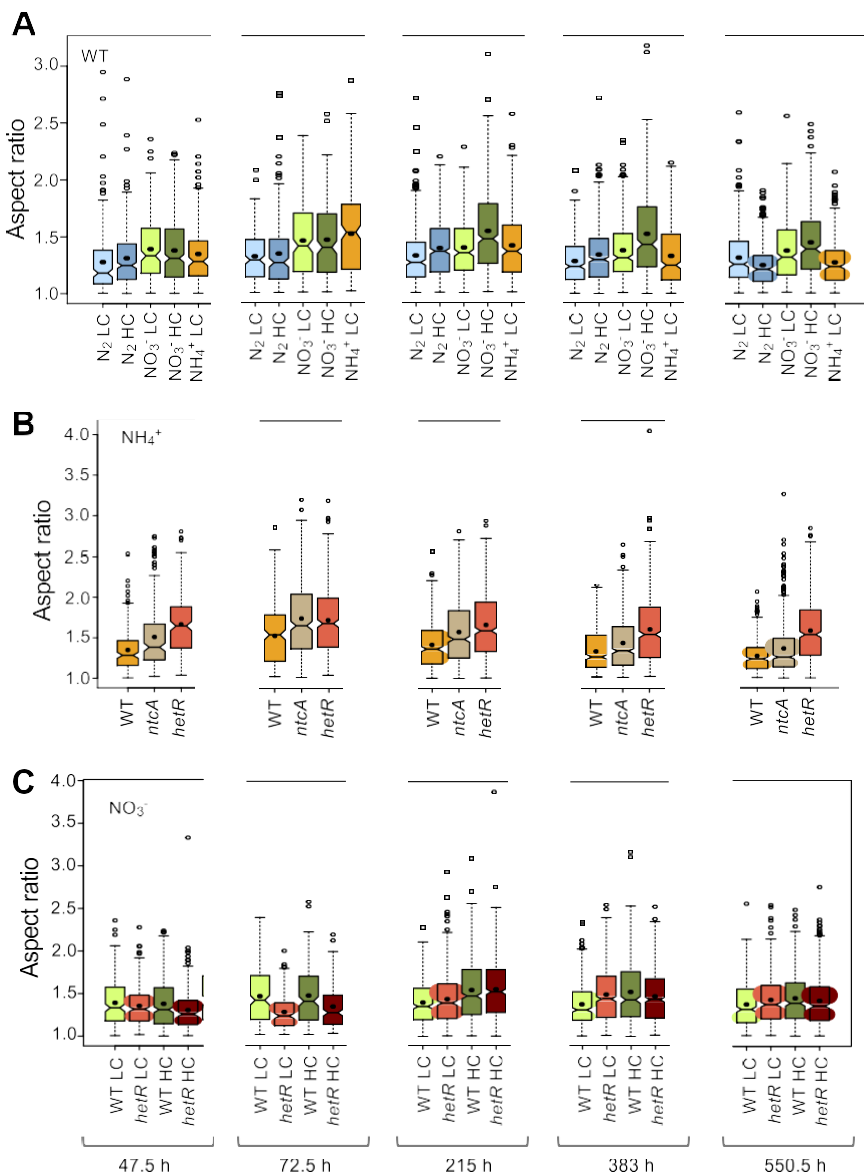
FIG 3 Aspect ratio of cells of *Anabaena* and strains CSE2 (*ntcA* mutant) and CSSC2 (*hetR* mutant) grown with different nitrogen and carbon supplies. In the same cells used in Fig. 1, the lengths of the longitudinal and transversal cell axes were measured as described in Materials and Methods. The aspect ratio is the result of dividing the length of the axis parallel to the filament by the length of the axis perpendicular to the filament. Notched boxplot representations of the data are shown. The mean values are represented by black dots. Tukey tests were performed to assess significance of differences (Data Set S1). (A) WT; (B) *ntcA* and *hetR* mutants in $BG11_0 + NH_4^+$; (C) *hetR* mutant in BG11.

similar to the organization of *E. coli* MreD (Phobius, TMHMM). Thus, we will consider all0085 to be a putative *mreD* gene of *Anabaena*.

Expression of the *Anabaena mre* gene cluster. Expression of the *Anabaena mreBCD* cluster was studied by means of Northern blot analysis. RNA was extracted from filaments of the wild type and the *ntcA* and the *hetR* mutants in the FEG phase (24 h) and in a period of slower growth (360 h) using ammonium or N_2 as the nitrogen source. Consistent with previous results (42), different transcripts hybridized with the probe of each gene. We found transcripts of ca. 3 and 1.3 kb (*mreB*), of ca. 3 and 1.7 kb (*mreC*), and of ca. 3, 1.7 and 1.1 kb (*mreD*) (Fig. 4A). For the different strains and conditions, the levels of *mreB* transcripts were always higher than those of *mreC*, which were higher than those of *mreD* (Table 2). For the different nitrogen sources, total
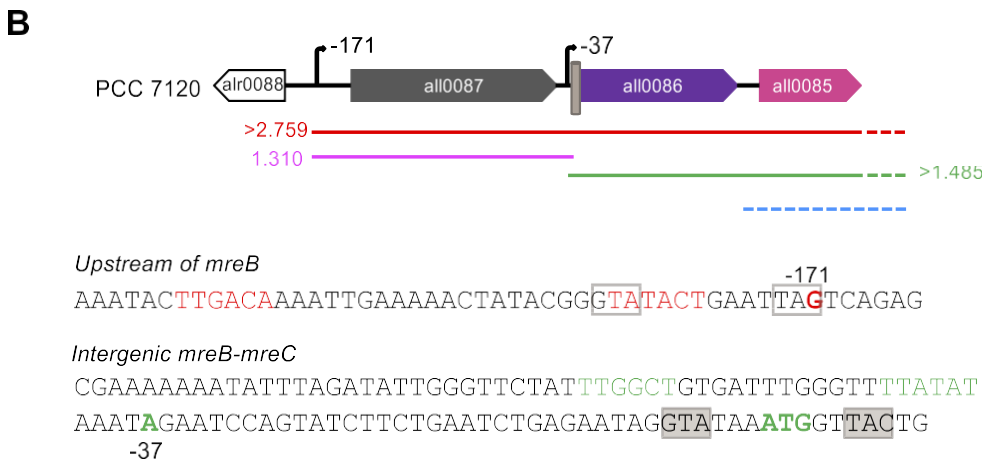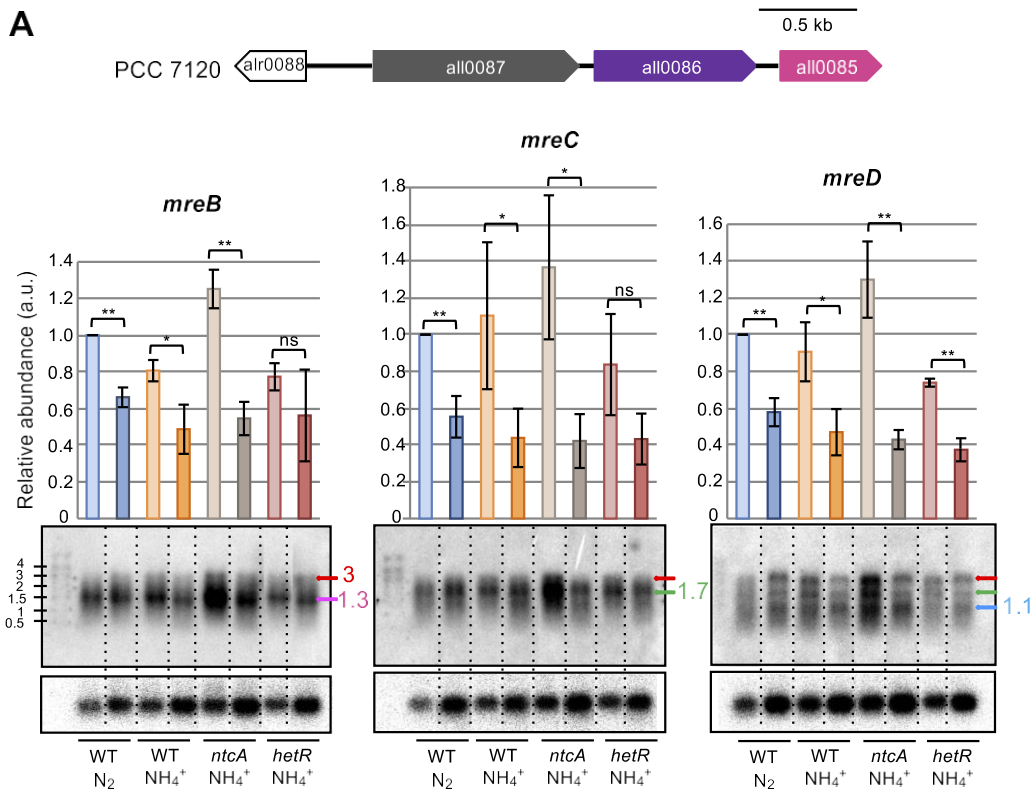
A

B

Upstream of mreB

AAATACTTGACAAAATTGAAAAACTATACGGGTATACTGAATTAGTCAGAG

-171

Intergenic mreB-mreC

CGAAAAAAATATTTAGATATTGGGTTCTATTTGGCTGTGATTTGGGTTTTATAT
AAATAGAATCCAGTATCTTCTGAATCTGAGAATAGGTATAAATGGTTACTG
-37

FIG 4 Expression of the *Anabaena mre* gene cluster. (A) Northern-blot analysis of the expression of the *mreB*, *mreC*, and *mreD* genes (genomic cluster represented in the upper part). RNA was extracted from filaments of the indicated strains grown in $BG11_0$ or $BG11_0 + NH_4^+$ medium, refreshed in the same medium at a cell density of 0.2 µg chlorophyll/ml, and incubated under culture conditions for 24 h (lighter colors) or 360 h (darker colors). Hybridization was performed with probes of the indicated *mre* gene (upper panels) or of *rnpB* used for normalization (lower panels). Three different cultures were used for each strain and condition (one representative filter of each strain and condition is shown). The mean and standard deviation of total transcript abundance, normalized for the *rnpB* signal for each lane, are represented, and significance of differences was assessed with Student's *t* test (**, $P < 0.01$; *, $P < 0.05$; ns, $P > 0.05$). Colored arrows at the right side of each panel point to the main transcripts detected (size in kb indicated). A size standard (RiboRuler High Range, Thermo) is shown at the left. (B) Schematic model of transcription in the *mre* gene cluster. In the upper part, the localization and size of expected transcripts is depicted (dashed segments indicate unprecise localization or transcript end). TSPs located at 171 nucleotides upstream from *mreB* and 37 nucleotides upstream from *mreC* are indicated, and a gray barrel represents a putative NtcA-binding sequence. Nucleotide sequences upstream from *mreB* and in the *mreB-mreC* intergenic region are depicted. Colored sequences denote putative −10 and −35 promoter elements; colored bold, transcription start points and the ATG start of *mreC*. Shadowed GTA and TAC sequences represent a putative NtcA-binding site (consensus sequence $GTAN_8TAC$), and framed GTA and TAG sequences represent an imperfect NtcA-binding site.

TABLE 2 Comparisons of the expression of the *Anabaena mreB*, *mreC*, and *mreD* genes by Northern blot analysis[a]

Strain/condition	Time (h)	Ratio of total transcript levels		
		mreB/mreD	*mreC/mreD*	*mreB/mreC*
PCC7120 (WT)/N_2	24	4.21 ± 1.03	3.52 ± 1.43	1.28 ± 0.26
	360	3.69 ± 0.09	4.21 ± 1.79	1.11 ± 0.56
PCC 7120 (WT)/NH_4^+	24	4.08 ± 0.85	3.44 ± 0.83	1.29 ± 0.46
	360	4.50 ± 1.49	3.77 ± 1.31	1.29 ± 0.40
CSE2 (*ntcA*)/NH_4^+	24	4.91 ± 1.42	3.23 ± 0.96	1.61 ± 0.49
	360	4.85 ± 2.21	3.07 ± 0.98	1.51 ± 0.35
CSSC2 (*hetR*)/NH_4^+	24	5.20 ± 0.40	3.21 ± 1.01	1.76 ± 0.46
	360	5.87 ± 1.32	3.64 ± 0.48	1.59 ± 0.15

[a]RNA was extracted from filaments of the indicated strains grown in $BG11_0$ (N_2) or $BG11_0 + NH_4^+$ (NH_4^+) medium for 24 or 360 h (see Fig. 4A for further details). The figures represent the mean and standard deviation of the ratio of total transcript levels of the corresponding gene pair in three independent cultures of each strain and condition.

transcript levels of any of the three genes were higher in the FEG phase than during slow growth (Fig. 4A; Student's *t* test *P* values between 0.019 and 0.001, except for *mreB* and *mreC* in the *hetR* mutant, which gave *P* values higher than 0.05). No significant differences were detected comparing ammonium-grown and diazotrophic filaments (Student's *t* test *P* > 0.05). In the presence of ammonium, total transcript levels were higher in the *ntcA* mutant than in the wild type (Student's *t* test *P* = 0.003 for comparison of *mreB* transcript levels in the exponential phase; *P* = 0.050 for *mreD*). This result, together with the fact that the longer (ca. 3 kb) transcript was better detected in the *ntcA* mutant than in the wild type (WT), indicates a negative effect of NtcA on the expression of the *mre* genes. No significant effect of the *hetR* mutation was detected.

We also studied the spatial pattern of the activity of the *mreB* promoter along the *Anabaena* filament. In a previous report, a *gfp* gene under the control of the *mreB* promoter introduced in *Anabaena* in a shuttle vector established with several copies per chromosome copy was reported to produce higher fluorescence in heterocysts than in vegetative cells (42). Here, we generated strain CSCV3, an *Anabaena* derivative that includes a *gfp-mut2* gene fused after the 6th codon of the *mreB* sequence, thus preserving the transcription and translation start signals of native *mreB*, in the chromosomal *mreB* locus. In addition, an intact copy of *mreB*, *mreC*, and *mreD* preceded by their native promoter region was preserved (Fig. 5A; see Materials and Methods for details).

Green fluorescent protein (GFP) fluorescence was monitored through the growth cycle in filaments of strain CSCV3 incubated with nitrate or ammonium or in the absence of combined nitrogen. In the latter case, the filaments included vegetative cells and cells in different stages of differentiation into heterocysts. Importantly, growth of strain CSCV3 was not impaired in comparison to the wild type (not shown). In cultures containing nitrate or ammonium, green fluorescence above the background in the wild-type strain was homogenously observed along the filament during active growth (Fig. 5B). Maximum fluorescence was observed during the first 24 to 48 h of incubation. After that time, fluorescence decreased, so that after 168 h, only background fluorescence was detected (Fig. S3). Upon N-stepdown, fluorescence levels increased in differentiating cells, which exhibited higher levels than vegetative cells (see 24 h in Fig. 5B). However, this increase was transitory, so that in mature heterocysts, GFP fluorescence levels were similar to those of vegetative cells (see 24 h in Fig. 5B). Indeed, 48 h after the transfer, mature heterocysts exhibited very low or undetectable GFP fluorescence, lower than that in vegetative cells. (Of note, overexpression of the P_{mreB}-*gfp* reporter utilized previously [42] could have led to maintenance of increased fluorescence for longer than the expression of the promoter activity in the native context.) Meanwhile, increased fluorescence was observed in stretches of vegetative cells that were neighbors to heterocysts, likely those that were most actively growing.
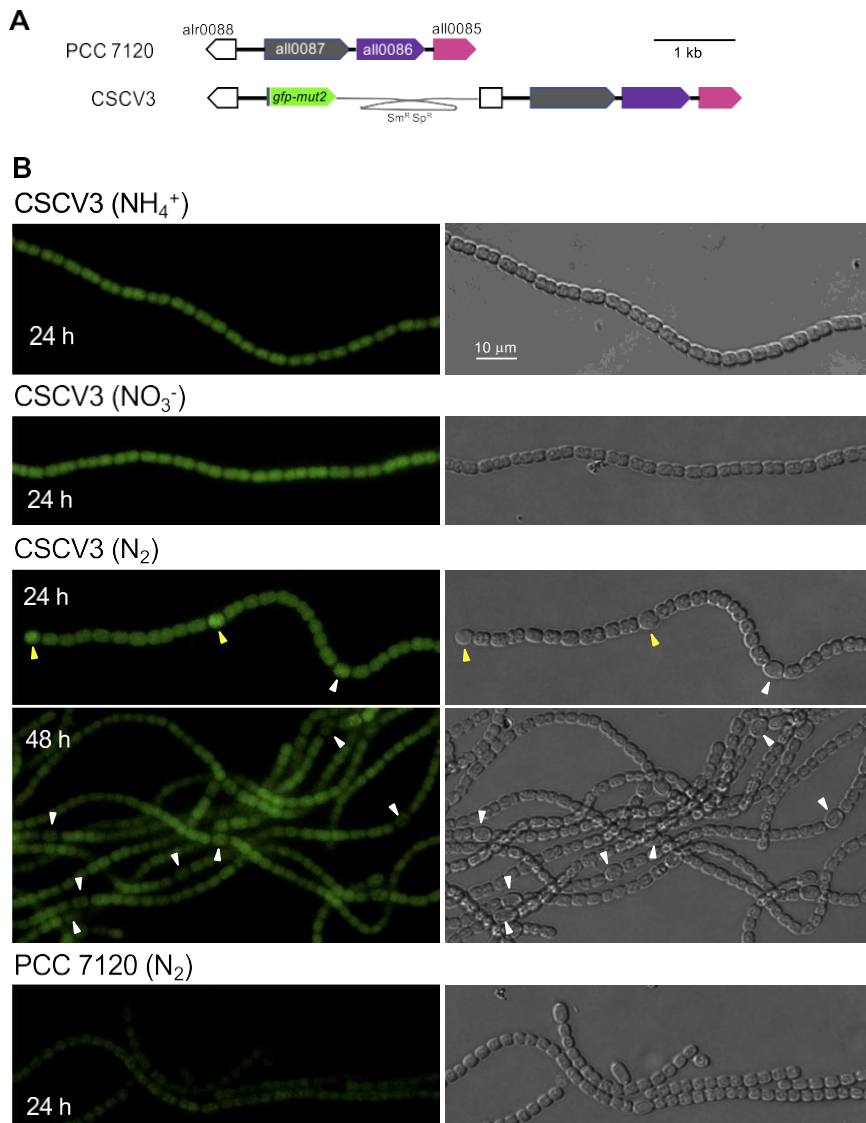
FIG 5 Spatiotemporal expression of the *mreB* gene promoter in *Anabaena*. (A) Genomic structure of strain CSCV3 (expressing [P$_{mreB}$-*gfp*] in comparison to PCC 7120 [WT]). (B) Filaments of strains PCC 7120 and CSCV3 grown in solid BG11 medium were transferred (at a cell density of 0.2 μg chlorophyll/ml) to BG11, BG11$_0$ + NH$_4$$^+$, and BG11$_0$ media and incubated under culture conditions. At 24 h intervals, filaments were observed under a fluorescence microscope and photographed. GFP fluorescence (left) and bright-field (right) images are shown. Arrowheads point to heterocysts: immature heterocysts (yellow); mature heterocysts, exhibiting polar refringent cyanophycin granules (white). Magnification is the same for all micrographs.

After 72 h, the fluorescence in vegetative cells had decreased also (not shown). Thus, activity of the *mreB* promoter is maximum during the FEG phase, and upon N-stepdown expression transiently increases in the cells differentiating into heterocysts.

mre mutants of Anabaena. To investigate the role of *mreB*, *mreC*, and *mreD* genes in *Anabaena*, derivatives carrying inactivated versions of these genes were created. Mutants were generated by substituting parts of each gene by an antibiotic-resistance-encoding gene cassette (Fig. 6A). Gene cassette C.S3 was inserted into the coding sequence of *mreD*. To avoid polar effects, gene cassette C.K1, which includes no transcriptional termination sequence, was inserted into genes *mreB* and *mreC* (see Materials and Methods for details). Strains CSCV1, CSCV4, and CSCV2 bear only deleted versions of *mreB*, *mreC*, and *mreD* genes, respectively (see Fig. S4).

Strains CSCV1, CSCV4, and CSCV2 were characterized in terms of growth rate and morphology. The three mutants grew using either nitrate or ammonium, although growth
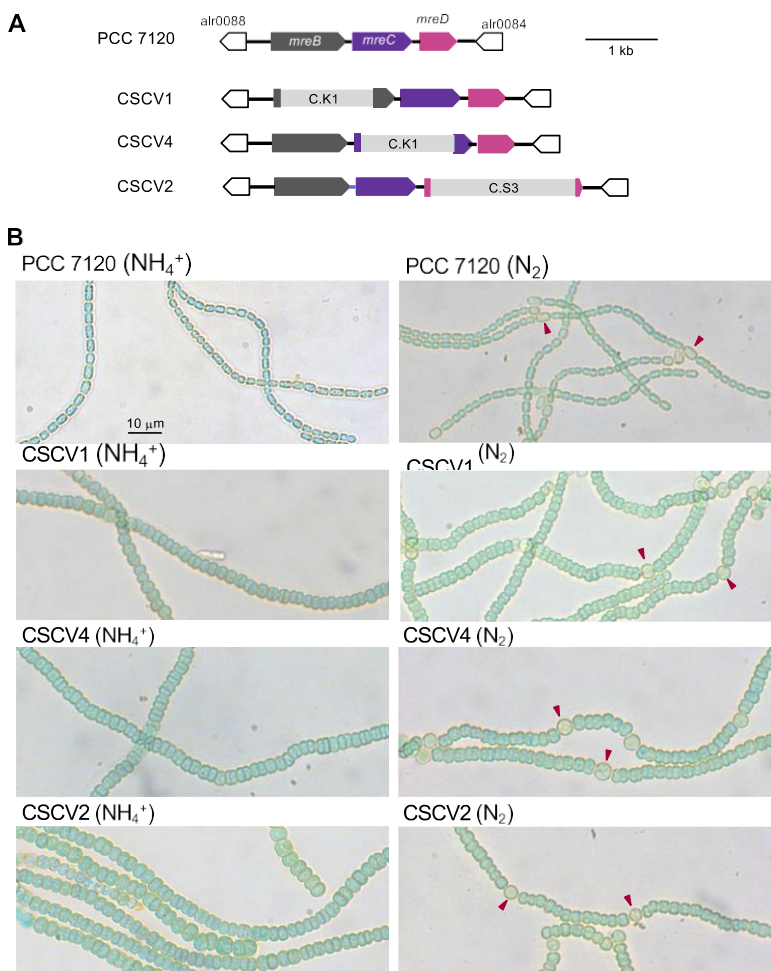
FIG 6 *Anabaena mreB*, *mreC*, and *mreD* mutants. (A) Genomic structure in the *mre* region in strains CSCV1 (*mreB*), CSCV4 (*mreC*), and CSCV2 (*mreD*) in comparison to *Anabaena* (WT). (B) Filaments grown in BG11$_0$ + NH$_4$+ or in BG11$_0$ (lacking combined nitrogen) medium were used to inoculate, at an initial cell density corresponding to 0.2 μg chlorophyll/ml, flasks containing the same medium, which were incubated under culture conditions. After 24 h, aliquots of each culture were taken and filaments photographed. Arrowheads point to heterocysts. Magnification is the same for all micrographs.

was slower than in the wild type, especially with a regime of LC (the growth rate of the mutants was about 60% of that of the corresponding wild-type value) (Table 1). In the absence of combined nitrogen, the three mutants formed heterocysts (Fig. 6B). However, whereas strain CSCV2 was capable of sustained diazotrophic growth, CSCV1 and CSCV4 did not significantly increase mass and, indeed, got lysed after some days of incubation (Fig. 7). The diazotrophic growth rate of CSCV2 under LC was ca. 45% that of the wild type and 56% under HC (Table 1). To seek the cause of the impaired diazotrophic growth, nitrogenase activity was measured (Table 3). Whereas activity levels after 24 h of incubation in the absence of combined nitrogen were considerably lower in the three mutants than in the wild type, after 48 h, only strain CSCV4 was significantly impaired (activity was ca. 36% of the WT activity). Thus, the heterocysts formed in the mutants were largely active.

The three mutants exhibited conspicuous morphological differences compared to the wild type, in both the presence and absence of combined nitrogen (Fig. 6). Figure 8 presents data on the determination of cell area (the significance of comparisons is shown in Data Set S1). Cells of the three mutants had similar sizes in medium supplemented with nitrate (LC or HC). Notably, the mean cell area values of CSCV2 (*mreD*), and especially of CSCV4 (*mreC*), incubated with ammonium were larger than those of nitrate-incubated cells of the same strain and larger than those of ammonium-
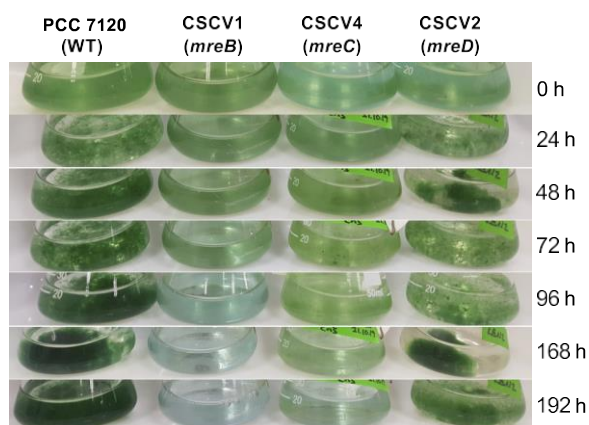
FIG 7 Growth of *Anabaena* and mutant strains CSCV1 (*mreB*), CSCV4 (*mreC*), and CSCV2 (*mreD*). Filaments grown in $BG11_0 + NH_4^+$ medium were used to inoculate, at an initial cell density corresponding to 0.2 µg chlorophyll/ml, flasks containing $BG11_0$ (lacking combined nitrogen) medium, which were incubated under culture conditions and photographed at the indicated times.

incubated cells of CSCV1 (*mreB*). Moreover, cell size appeared heterogeneous in CSCV2, showing filament stretches of larger cells and others of smaller cells (see Fig. 6), which is indicative of the inability to regulate cell size. Under any growth condition, cells of any of the three mutants (vegetative cells for filaments incubated in the absence of combined nitrogen) were larger than those of the wild type (compare Fig. 8 and Fig. 1A). As in the wild type, cells growing diazotrophically (CSCV2) were smaller than those growing with combined nitrogen (Fig. 8).

In filaments incubated in the absence of combined nitrogen, we also measured the size of heterocysts, which in the wild type were larger than vegetative cells and relatively constant during growth (compare Fig. 9A and Fig. 1A). Heterocysts of any of the *mre* mutants were larger than heterocysts of the wild type (Fig. 9A; Data Set S1).

Regarding cell morphology, the aspect ratio of the cells of strains CSCV1, CSCV4, and CSCV2 was closer to 1 than the wild-type values (compare Fig. 10 and Fig. 3A; see Data Set S1), meaning that cells of the mutants are more rounded than cells of the wild type. Indeed, in the mutants, the aspect ratio values were smaller than 1, indicating that the cell axis parallel to the length of the filament is shorter than the axis perpendicular to the filament. Thus, the geometrical orientation of the cells in the filaments of the mutants is inverted compared to the orientation in the wild-type filaments (see Fig. 6B). Also, heterocysts of the three mutants were more rounded, and inverted, compared to the wild-type heterocysts, in which the aspect ratio was higher than in vegetative cells and showed a tendency to increase during the first 72 h of incubation (see Fig. 9B).

Finally, in the three *mre* mutants, the filaments were generally longer than in the wild type (compare Fig. 11 and Fig. 2A; see Data Set S1). Thus, it appears that the intercellular septa of the mutants were more robust than those of the wild type.

TABLE 3 Nitrogenase activity of *mreB*, *mreC*, and *mreD* mutants

Strain	Nitrogenase activity (nmol · mg clorophyll^{-1} · h^{-1})[a]	
	24 h	48 h
PCC 7120 (WT)	7.15	10.66
CSCV1 (*mreB*)	2.54	8.97
CSCV4 (*mreC*)	1.83	3.86
CSCV2 (*mreD*)	2.77	9.12

[a]Nitrogenase activity was assayed in filaments of the indicated strain incubated in $BG11_0$ medium for 24 or 48 h. The figures represent the mean of the activities measured in two independent cultures that yielded similar results.
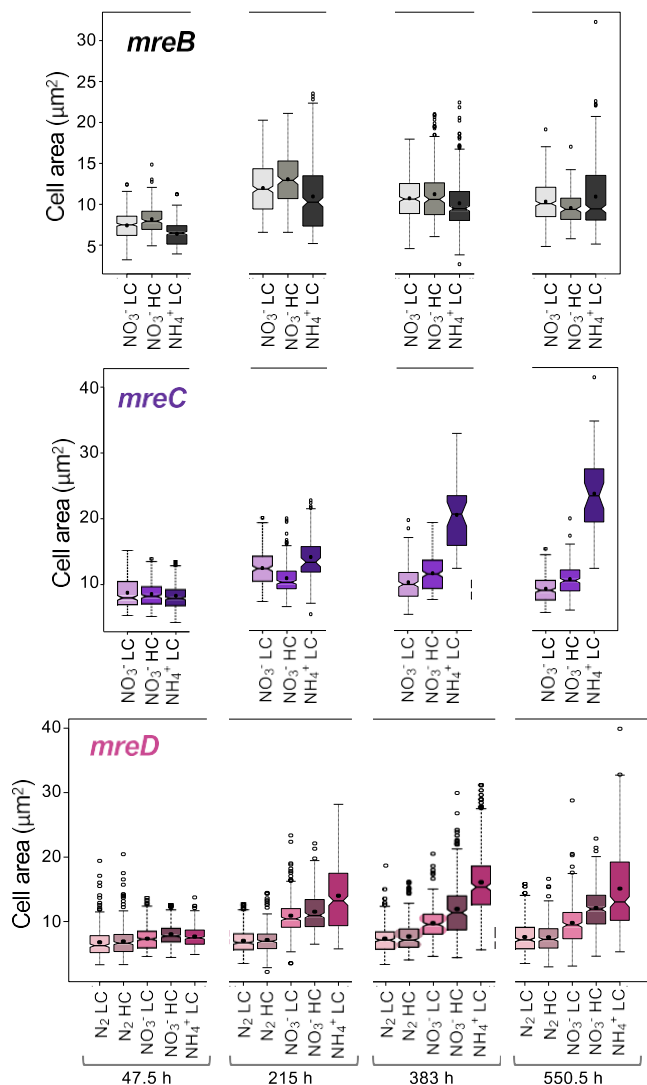
FIG 8 Dynamics of cell area in mutant strains CSCV1 (*mreB*), CSCV4 (*mreC*), and CSCV2 (*mreD*) grown with different nitrogen and carbon supplies. Cells grown in the indicated conditions were used to inoculate, at an initial cell density corresponding to 0.2 µg chlorophyll/ml, cultures under the same conditions. At the indicated incubation times, aliquots of each culture were photographed and used for cell area determination. A total of 200 to 400 cells (vegetative cells in the diazotrophic cultures) from three different cultures of each time and condition were measured. Notched boxplot representations of the data are shown. The mean values are represented by black dots. Tukey tests were performed to assess significance of differences (Data Set S1).

In order to identify possible factors contributing to the observed increased filament robustness in the *mre* mutants, we used Van-FL (fluorescent vancomycin) to estimate the septal width of vegetative cells. Van-FL labels sites of active PG synthesis (43), and in *Anabaena*, significant staining is found in the intercellular septa (e.g., 44). On average, septa were significantly wider in the mutants than in the wild type, and in CSCV1 and CSCV4, were wider than in CSCV2 (Fig. 12). Total Van-FL fluorescence detected at the septa was also higher in CSCV1 and CSCV4 than in CSCV2, which also rendered higher values than the wild type (Fig. 12). Increased septal width in the mutants can contribute to increased cell-to-cell cohesion and, thus, filament length.

DISCUSSION

Although many previous data on the growth of *Anabaena* under various experimental conditions have been reported, here we aimed at setting defined conditions
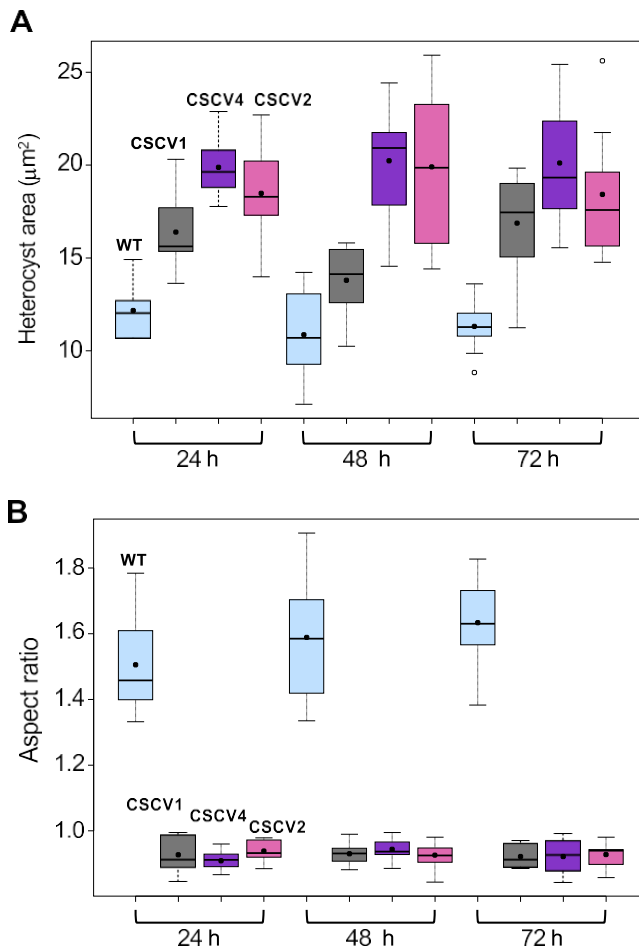
FIG 9 Morphological parameters of heterocysts in *Anabaena* and mutant strains CSCV1 (*mreB*), CSCV4 (*mreC*), and CSCV2 (*mreD*). Cells grown in $BG11_0$ medium and LC were used to inoculate, at an initial cell density corresponding to 0.2 µg chlorophyll/ml, flasks containing the same medium, which were incubated under culture conditions. (A and B) At the indicated times, aliquots of each culture were photographed and used for heterocyst cell area (A) and cell axis length (B) determination. The aspect ratio is the result of dividing the length of the axis parallel to the filament, by the length of the axis perpendicular to the filament. Ten heterocysts of each time and strain were measured. Boxplot representations of the data are shown. Black dots represent the mean values. Tukey tests were performed to assess significance of differences (Data Set S1).

that would permit comparisons between growth rates and morphological features under different nutritional contexts. Indeed, we found that in this phototrophic bacterium, the nitrogen and carbon regime influence not only growth, but also cell size and shape and filament length.

Regarding cell size, during the FEG phase, *Anabaena* using different nitrogen sources and carbon supplies would grossly meet the classical growth law, which entails that cells of rod-shaped bacteria exhibit larger volume when they grow with a nutrient-imposed lower generation time (45), confirmed by recent studies at the population level (5). However, the positive linear correlation that was found between these two parameters in both *E. coli* and the slow-growing bacterium *Sinorhizobium meliloti* (46) could not be observed in *Anabaena* (Fig. S2). Moreover, in *Anabaena*, different relationships between growth and size were established during the growth cycle, resulting in a net cell size increase. These observations suggest that throughout active growth, the rate of cell division would progressively slow down more than the rate of total cell mass increase. In other words, the cell size at division would be increasing. Because *Anabaena* has multiple copies of the chromosome, and chromosome partitioning during cell division appears to be to a good extent aleatory (42), a large size would favor both daughter cells inheriting intact chromosomes during active growth (see reference 47).
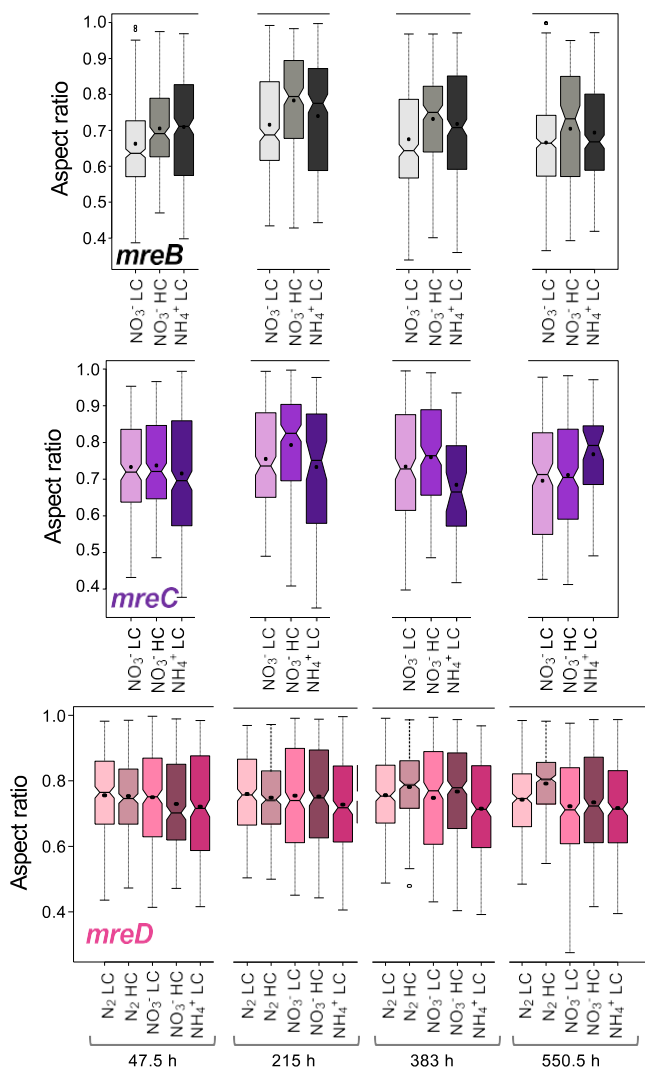
FIG 10 Aspect ratio of cells of *Anabaena* and mutant strains CSCV1 (*mreB*), CSCV4 (*mreC*), and CSCV2 (*mreD*) grown with different nitrogen and carbon supplies. In the same cells used in Fig. 8, the length of the longitudinal and transversal cell axes was measured. The aspect ratio is the result of dividing the length of the axis parallel to the filament, by the length of the axis perpendicular to the filament. Notched boxplot representations of the data are shown. Black dots represent the mean values. Tukey tests were performed to assess significance of differences (Data Set S1).

Regarding cell shape, little has been investigated about the adaptive value of the different bacterial morphologies, but it appears that the actual bacterial shape would be the result of trade-offs between the suitability for different critical physiological tasks (see reference 2). In comparison to other studied bacteria, cell-shape transitions in *Anabaena* might be similar to the situation in the euryarchaeon *Haloferax volcanii* (48) and in some other bacteria, such as *E. coli* (49), in which a transition from rod shape (during exponential growth) to coccus (upon entry into stationary phase) has been described. However, in contrast to *Anabaena* using ammonium, in *E. coli* the morphological transition is concomitant with a decrease in size, which relies on continuing division without mass increase. In other bacteria, such as *C. crescentus*, cells adopt an elongated morphology and increased size during prolonged culture in the stationary phase (50). These contrasting responses stress the influence of the bacterial mode of life on determination of cell morphology.

Regarding the role of NtcA and HetR regulators, it is noteworthy that although both are dispensable for ammonium-dependent growth, the growth rate of the *ntcA* and
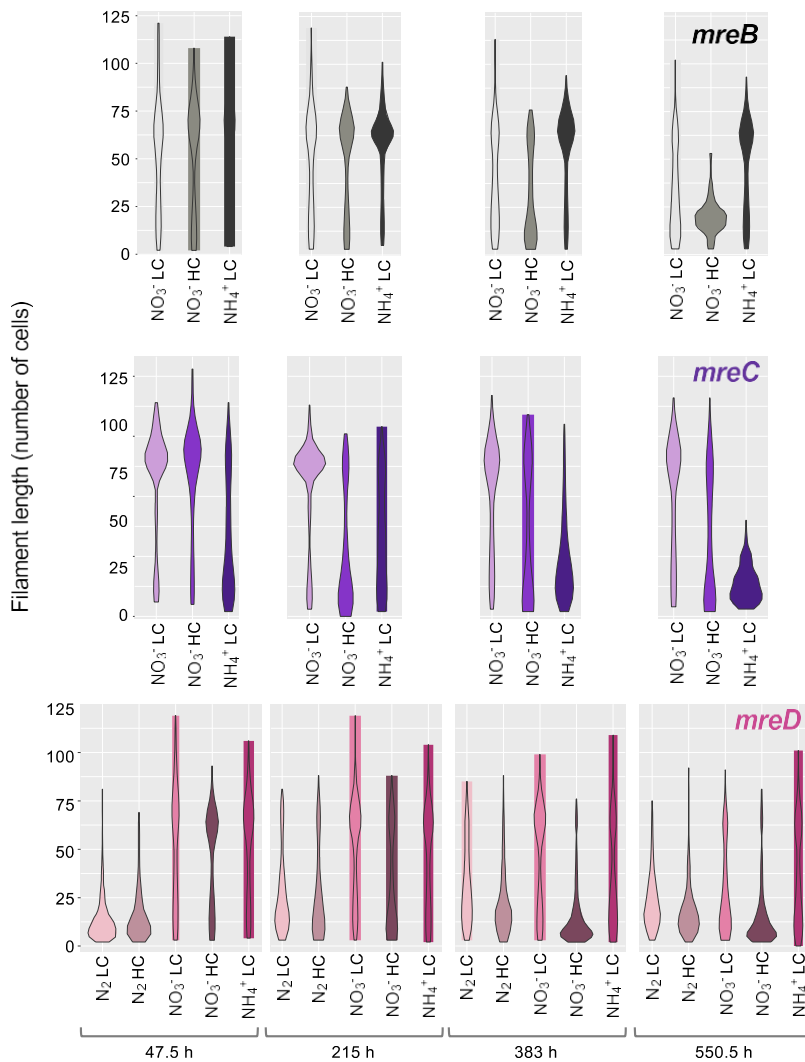
FIG 11 Distribution of filament length in mutant strains CSCV1 (*mreB*), CSCV4 (*mreC*), and CSCV2 (*mreD*) grown with different nitrogen and carbon supplies. At the indicated times, aliquots of cultures treated as described in the legend to Fig. 8 were taken with care to avoid filament breakage and photographed. Filaments from two to three independent cultures of each condition were counted. Filaments longer than 120 cells were counted as of 120. Violin-plot representations of the data are shown. Mann-Whitney tests were performed to assess significance of differences with data from filaments up to 119 cells long (89 to 352 filaments) (Data Set S1).

hetR mutants was slower than that of the wild type. Moreover, during the growth cycle, cell size and aspect ratio in the mutants showed an evolution different from that in the wild type. Also, in the mutants, filaments were much shorter than in the wild type. These results abound in the tenability of HetR (and NtcA) influencing *Anabaena* physiology also in cultures supplemented with ammonium, consistent with the identification of some instances of HetR-promoted repression in the presence of ammonium (e.g., 51). The possible roles of the global regulator NtcA and of HetR in linking cell growth and cell division hint at research subjects of considerable interest.

We have studied here the spatiotemporal pattern of expression of the *Anabaena mre* gene cluster and its role in growth and morphology under different contexts. In contrast to the essential role of MreB and MreC in other studied bacteria, and in some cases of MreD also, we have found that *Anabaena* mutants lacking MreB, MreC, or MreD actively grow in the presence of nitrate or ammonium, although the growth rate was about half of that in the wild type. Our results with strain CSCV1 contrast with a previous report describing that an *Anabaena mreB* mutant was affected in cell size and
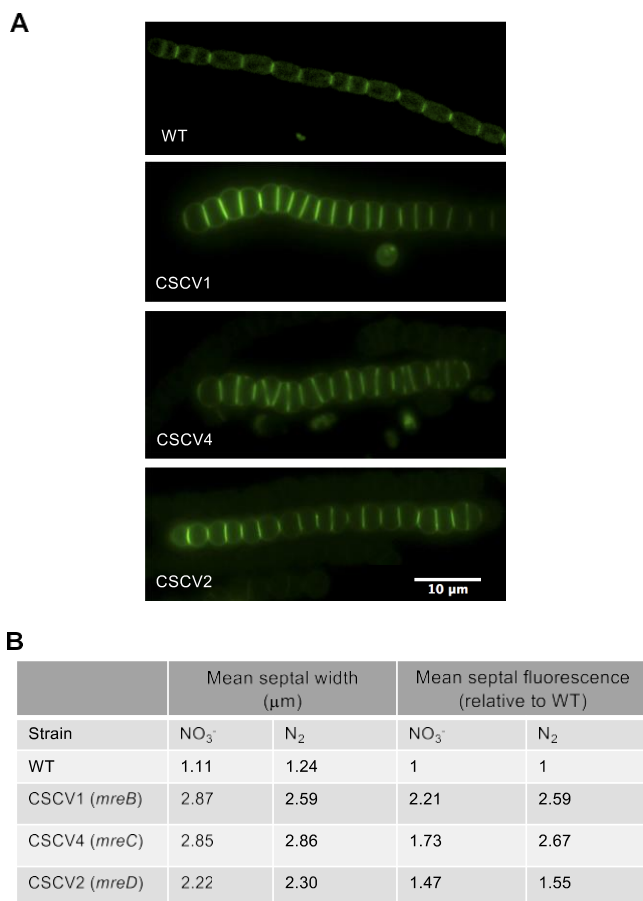
A

B

	Mean septal width (μm)		Mean septal fluorescence (relative to WT)	
Strain	NO_3^-	N_2	NO_3^-	N_2
WT	1.11	1.24	1	1
CSCV1 (mreB)	2.87	2.59	2.21	2.59
CSCV4 (mreC)	2.85	2.86	1.73	2.67
CSCV2 (mreD)	2.22	2.30	1.47	1.55

FIG 12 Septal width and septal Van-FL incorporation in *Anabaena* and CSCV1 (*mreB*), CSCV4 (*mreC*), and CSCV2 (*mreD*) mutants. (A) Representative fluorescence images of filaments incubated in BG11 medium and stained with Van-FL as specified in Materials and Methods. Magnification is the same for all micrographs. (B) The width of the fluorescent signal and total fluorescence detected in septa were estimated in filaments of the indicated strain incubated in BG11 (NO_3^-) or $BG11_0$ (N_2) medium with LC. For each strain and condition, 35 to 38 septa were measured. Student's *t* test was used to assess significance of differences. *P* values were <0.01 for all comparisons except for the septal width of CSAV1 versus CSCV4 in BG11 (*P* = 0.9) and septal fluorescence of CSCV2 versus CSCV4 in BG11 (*P* = 0.136) and of CSCV1 versus CSCV4 in $BG11_0$ (*P* = 0.748).

morphology but unaltered in growth rate or filament length (42), although no detailed counting was provided for the latter parameter. In strains CSCV1, CSCV4, and CSCV2, extensive morphological alterations were observed. Not only were the cells less elongated than in the wild type, but also, the cell geometry with regard to the filament orientation was altered, so that the longer cell axis became perpendicular to the filament, whereas it was parallel to the filament in the wild type. In addition, in the three *Anabaena mre* mutants, especially in *mreC*, the cells were larger than in the wild type. Also, cells of the *mreD* mutant, and especially of the *mreC* mutant, were larger using ammonium than nitrate, which was not the case in the wild type. These observations suggest that in *Anabaena,* MreB, MreC, and MreD affect not only cell shape, but also the coordination between cell growth and cell division dependent on external nutrients. In addition, filaments were longer in the mutants than in the wild type, which suggests that intercellular septa are more robust in the mutants. This is consistent with the observations of increased width and apparent incorporation of septal PG in the mutants and suggests a role of Mre proteins in septal PG construction during cell division.

The variations of cell shape during the growth cycle in *Anabaena* correlate to a good extent with expression levels of the *mreB*, *mreC*, and *mreD* genes. Thus, higher expression was observed in the FEG phase, at the time that cells were increasing the aspect

ratio, than during slower growth. Also, the activity of the P_{mreB} promoter was maximal during FEG, indeed, preceding the time of maximal aspect ratio value (longer rods). Subsequently, promoter activity and gene expression levels decreased, in parallel with the decrease in the value of the aspect ratio.

Combining the results of Northern blot and P_{mreB}-*gfp*-reporter expression analyses, we propose a transcription pattern and regulation of the *Anabaena mre* gene cluster, as depicted in Fig. 4B. The three genes can be expressed together as an operon from a promoter upstream of *mreB* (putative transcription start point [TSP] located at −171 nt [52], which is preceded by −10 and −35 promoter determinants representing a putative consensus u^{70}-type promoter). The whole operon transcript would be at least 2,759 nucleotides long, depending on its 3′ end, and would correspond to the ca. 3-kb transcript detected with the probes of the three *mre* genes. However, elongation of this transcript downstream of *mreB* could be inhibited by binding of NtcA to an NtcA-binding site (consensus sequence $GTAN_8TAC$ [53]), which is found overlapping the ATG start of *mreC*. Transcription halting at this point would produce a ca. 1.3-kb monocistronic *mreB* gene transcript. The observation that not only the ca. 3-kb transcript, but also the ca. 1.3-kb transcript was more abundant in the *ntcA* mutant than in the WT suggests that NtcA also represses transcription from the operon promoter (e.g., by binding to the imperfect site found overlapping the operon TSP). Additionally, joint transcripts of *mreC* and *mreD* (longer than 1,485 kb; possibly the ca. 1.7-kb transcript detected with the *mreC* and *mreD* probes) could be produced from an intergenic promoter (putative TSP located at 37 nucleotides upstream from *mreC* [53]), which could be partially blocked by NtcA also. Finally, the ca. 1.1-kb transcript detected with the *mreD* probe could correspond to a degradation product of the ca. 1.7-kb transcript. In summary, both the transcription pattern of *mreB*, *mreC*, and *mreD* genes and transcript abundance appear to be regulated by NtcA, which responds to the C-to-N balance of the cells influenced by the nitrogen regime. The negative effect of NtcA on transcript abundance is manifest when comparing the wild type and the *ntcA* mutant (Fig. 4A). This regulation could explain the higher aspect ratio observed in the *ntcA* mutant in comparison to the wild type. Also, although at the times studied here no significant differences in *mre* expression were found, the aspect ratio was lower in diazotrophic cultures, when the NtcA levels are higher (54) than in ammonium-supplemented cultures.

In contrast to growth with combined nitrogen, MreB and MreC, but not MreD, appear to be essential for diazotrophic growth of *Anabaena*. Under these conditions, vegetative cells of strain CSCV2 (*mreD*) were larger, less elongated, and inversely oriented compared to cells in wild-type filaments. In spite of the lack of growth of strains CSCV1 (*mreB*) and CSCV4 (*mreC*), the three *mre* mutants were able to form heterocysts that, although larger and altered in shape compared to the wild type, appeared similar in the three mutants. Also, the three mutants exhibited considerable levels of nitrogenase activity, although activity development was retarded compared to the wild type. (It should be noted that, although in CSCV4, nitrogenase activity was about one-third of the wild-type level, in our experience this activity suffices to maintain diazotrophic-growth rates comparable to those of wild-type *Anabaena*.) Moreover, besides CSCV2, at least CSCV1 also bore in the heterocysts cyanophycin polar granules, a polymer of Asp and Arg made after the incorporation of the ammonium resulting from N_2 fixation into amino acids (55) (see Fig. 6). Thus, it appears that the incapacity for diazotrophic growth in the absence of MreB or MreC is not due to altered regulation of differentiation or of synthetic metabolism of the heterocysts. Moreover, the phenotype of strains CSCV1 and CSCV4 incubated in the absence of combined nitrogen is not that of a progressive yellowing, largely maintaining viability, characteristic of *Anabaena* when subjected to nitrogen deficiency. Instead, both strains differentiated heterocysts and then lysed, apparently when they started to resume growth (see Fig. 7). This progression could be the consequence of a defective lateral PG wall unable to maintain cell pressure during diazotrophic growth. In *Anabaena*, different PBPs (44, 56, 57) and cell wall hydrolyzing AmiC-type amidases (58, 59) have been

described as required specifically for diazotrophic growth but not for growth with combined nitrogen. Perhaps, MreB and/or MreC are needed for regulation of enzymes specifically required for PG remodeling in the vegetative cells during diazotrophic growth. In addition, altered molecular transfer between cells in the filament, which is more stringently required under diazotrophic conditions than when combined nitrogen is available, could contribute to the lack of diazotrophic growth in *mreB* and *mreC* mutants. In this regard, a miss-dimensioned septal PG, as observed in the mutants, could interfere with the construction of septal nanopores, which after septum closure during cell division are drilled in the central part of septal PG caps (60) to hold septal junction protein complexes (see reference 31). The specific roles of Mre proteins in septal peptidoglycan construction in the filament of *Anabaena* are issues worthy of future investigation.

In summary, in *Anabaena*, a filamentous phototrophic bacterium, the cell size, filament length, and cell shape are regulated in response to the nitrogen and carbon nutrition and the growth phase, but here, the relationships between growth rate and size only partially follow those established in bacteria with other life styles. *Anabaena* bear homologs to the genes *mreB*, *mreC*, and *mreD*, whose expression is regulated by the growth phase and the transcriptional regulator NtcA, which responds to the C-to-N balance of the cells. As in other rod-shaped bacteria, Mre proteins are required for cell shape determination, but here, they are also required for the regulation of cell size and filament geometry. In addition, in *Anabaena*, at least MreB and MreC are required for the formation of active diazotrophic filaments, which might entail a role in the construction of functional intercellular septa allowing intercellular communication functions that are at the basis of the multicellular character of this bacterium.

MATERIALS AND METHODS

Strains and growth conditions. *Anabaena* sp. PCC 7120 and mutant strains were grown in BG11 medium (containing $NaNO_3$ as a nitrogen source), BG11$_0$ (lacking combined nitrogen) (29), or BG11$_0$ supplemented with 4 mM NH_4Cl and 8 mM TES-NaOH buffer (pH 7.5). For high-carbon (HC) conditions, BG11 and BG11$_0$ media were supplemented with 10 mM $NaHCO_3$. Cultures were incubated at 30°C with illumination (12 μE m^{-2} s^{-1} from LED lamps) in Erlenmeyer flasks with shaking or in plates in medium solidified with 1% Difco agar. For the mutants, media were supplemented with antibiotics as follows: spectinomycin (Sp) and streptomycin (Sm) at 5 μg ml^{-1} each in solid media or 2 μg ml^{-1} each in liquid media (CSE2, CSCV3, CSCV2) or with neomycin (Nm) at 25 μg ml^{-1} in solid media or 5 μg ml^{-1} in liquid media (CSCV1, CSCV4). Strain CSE2 is an *ntcA* mutant (61); strain CSSC2 is a *hetR* mutant (62). The chlorophyll content (Chl) of the cultures was determined after extraction with methanol (63). (In *Anabaena*, 1 μg chlorophyll corresponds to ca. 3.3 X 10^6 cells.)

Strain CSCV3 expresses a fusion of the *mreB* gene promoter to the gene encoding *gfp-mut2*. To generate it, *Anabaena* genomic DNA (isolated as described in reference 64) was used to amplify (with the oligodeoxynucleotide primers alr0088-3/all0087-9; all oligodeoxynucleotide primers are described in Table S1) a ClaI/EcoRV-ended fragment encompassing sequences upstream and the six N-terminal codons of *mreB*. This DNA fragment was cloned upstream and in-frame to the *gfp-mut2* gene in ClaI/EcoRV-digested mobilizable plasmid pCSEL22 (65), generating plasmid pCSCV7, which was transferred to *Anabaena* by conjugation (66) with selection for Sm/Sp (resistance to Sm and Sp is encoded in the vector portion of pCSEL22). One of the clones that had inserted pCSCV7 into the *Anabaena mreB* locus by a single recombination event, keeping an intact version of the gene preceded by its native promoter (analyzed by PCR, not shown), was selected and named strain CSCV3.

Mutant strain CSCV1 carries a version of the *mreB* gene in which codons 14 to 267 were substituted by gene cassette C.K1, encoding Km/Nm resistance. To generate it, two DNA fragments were amplified from *Anabaena* genomic DNA using the primer pairs all0086-2/all0087-6 (encompassing sequences internal and upstream of *mreB*) and all0087-1/alr0088-2 (encompassing sequences internal and downstream of *mreB*), including terminal restriction sites XbaI/BglII and BglII/XbaI, respectively. Both fragments were joined together by overlapping PCR, and the resulting single fragment was cloned into mobilizable vector pCSRO (encoding the gene *sacB* for positive selection [67]). Gene cassette C.K1 was then inserted into the internal BglII site, generating plasmid pCSCV2, which was transferred to *Anabaena* by conjugation.

Mutant strain CSCV2 carries a version of the *mreD* gene in which codons 4 to 163 were substituted by gene cassette C.S3, encoding Sm/Sp resistance. To generate it, a strategy similar to that used for strain CSCV1 described above was used, with oligonucleotide pairs alr0084-2/all0085-6 (encompassing sequences internal and upstream of *mreD*) and all0085-7/all0086-5 (encompassing sequences internal and downstream of *mreD*), including terminal restriction sites XbaI/BamHI and BamHI/XbaI, respectively. The resulting fragment was cloned into plasmid vector pRL271 (encoding the gene *sacB* and a chloramphenicol resistance determinant) (68), and gene cassette C.S3 was inserted into the internal BamHI site rendering plasmid pCSCV6, which was transferred to *Anabaena* by conjugation.

Mutant strain CSCV4 carries a version of the *mreC* gene in which codons 12 to 266 were substituted by gene cassette C.K1. To generate it, two DNA fragments were generated using *Anabaena* genomic DNA

and primer pairs all0085-1/all0086-11 (encompassing sequences internal and upstream of *mreC*) and all0086-12-1/all0087-7 (encompassing sequences internal and downstream of *mreC*), including terminal restriction sites XbaI/EcoRV and EcoRV/XbaI, respectively. Both fragments were joined together by overlapping PCR, and the resulting single fragment was cloned into mobilizable vector pCSRO. Gene cassette C.K1 was then inserted into the internal EcoRV site generating plasmid pCSCV4, which was transferred to *Anabaena* by conjugation.

The presence of the mutagenic gene construct was analyzed by PCR in selected clones resistant to Nm or Sm/Sp and to sucrose (sensitivity to sucrose is encoded in the vector portion of the transferred plasmids), implying that the corresponding inactivating gene construct was inserted in the *mre* locus by double recombination substituting for the corresponding native allele. The presence of chromosomes with the wild-type copy of each gene was also tested (Fig. S4). No wild-type allele was detectable in any case. One clone of each construct was selected and named strain CSCV1 (*mreB*), strain CSCV4 (*mreC*), and strain CSCV2 (*mreD*), respectively.

Analysis of *mreBCD* expression by Northern blotting. Total RNA from *Anabaena* was isolated as described in reference 69, and trace DNA in the samples was removed by treatment with Turbo RNase (Ambion) following the manufacturer's instructions. Northern blot assays were performed as described in reference 70, with 4 μg RNA loaded per lane, and electrophoresed in denaturing 1% agarose formaldehyde gels. DNA probes were internal gene fragments generated by PCR using *Anabaena* genomic DNA and primer pairs all0087-22/all0087-23 (*mreB*), all0086-13/all0086-14 (*mreC*), and all0085-8/all0085-9 (*mreD*). The *rpnB* gene, which was used for normalization, was amplified from plasmid pT7-7120 (71) with the primers Universal and Reverse. Probes were labeled by annealing the PCR-generated fragments to oligonucleotides complementary to the coding strand (all0087-8/all0087-23 for *mreB*, all0086-6/all0086-14 for *mreC*, and all0085-5/all0085-9 for *mreD*) and polymerization catalyzed by the Klenow fragment of DNA polymerase (Thermo Fisher) in the presence of [a-^{32}P]dCTP (Perking-Elmer). Radioactive areas in Northern blot hybridization membranes were visualized and quantified with a Cyclone storage phosphor system (Packard).

Nitrogenase activity determination. Nitrogenase activity was estimated by the acetylene reduction assay carried out under oxic conditions (72) in nitrate-grown filaments incubated in BG11$_0$ medium (at 1 μg chlorophyll/ml, without antibiotics) for 24 or 48 h.

Microscopy. Cell area and cell axis length were determined automatically by processing light-microscopy images with ImageJ software (make images binary/fill holes/watershed/analyze) (https://imagej.nih.gov/ij/index.html). Data were plotted using the open source software RStudio Desktop. For Van-FL staining, filaments incubated for 24 h in solid medium were suspended in liquid medium supplemented with 2 μg/ml Vancomycin-FL (Bodipy-FL conjugate; Invitrogen) and incubated for 1 h in the dark with shaking. Filaments were washed twice with liquid medium and spotted in agar. GFP and Van-FL fluorescence was visualized with a Leica DM6000B fluorescence microscope, and FITCL5 filter (excitation band-pass, 480/40; emission band-pass, 527/30), and photographed with an ORCA-ER camera (Hamamatsu). Septum width and total septal fluorescence were determined with ImageJ processing of fluorescence images of filaments stained with Van-FL, by collecting fluorescence signals in manually defined septal sections.

SUPPLEMENTAL MATERIAL

Supplemental material is available online only.

FIG S1, PDF file, 0.1 MB.

FIG S2, PDF file, 0.1 MB.

FIG S3, PDF file, 0.8 MB.

FIG S4, PDF file, 1 MB.

TABLE S1, PDF file, 0.1 MB.

DATA SET S1, XLSX file, 0.1 MB.

REFERENCES

1. Young KD. 2006. The selective value of bacterial shape. Microbiol Mol Biol Rev 70:660–703. https://doi.org/10.1128/MMBR.00001-06.
2. Schuech R, Hoehfurtner T, Smith DJ, Humphries S. 2019. Motile curved bacteria are pareto-optimal. Proc Natl Acad Sci U S A 116:14440–14447. https://doi.org/10.1073/pnas.1818997116.
3. Schulz HN, Jørgensen BB. 2001. Big bacteria. Annu Rev Microbiol 55:105–137. https://doi.org/10.1146/annurev.micro.55.1.105.
4. Westfall CS, Levin PA. 2017. Bacterial cell size: multifactorial and multifaceted. Annu Rev Microbiol 71:499–517. https://doi.org/10.1146/annurev-micro-090816-093803.
5. Taheri-Araghi S, Bradde S, Sauls JT, Hill NS, Levin P, Paulsson J, Vergassola M, Jun S. 2015. Cell-size control and homeostasis in bacteria. Curr Biol 25:385–391. https://doi.org/10.1016/j.cub.2014.12.009.
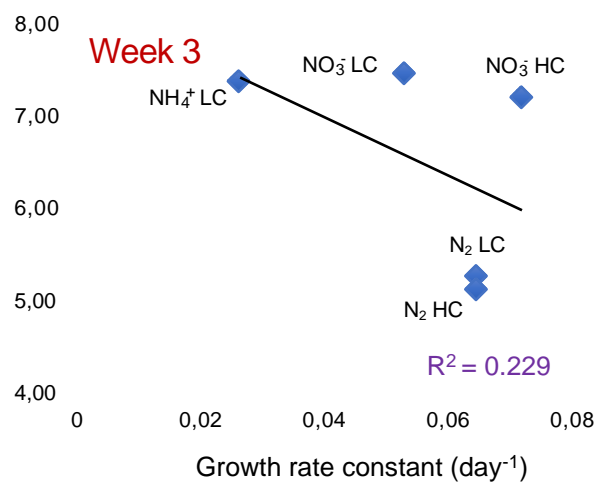6. Harris LK, Theriot JA. 2016. Relative rates of surface and volume synthesis

set bacterial cell size. Cell 165:1479–1492. https://doi.org/10.1016/j.cell.2016.05.045.
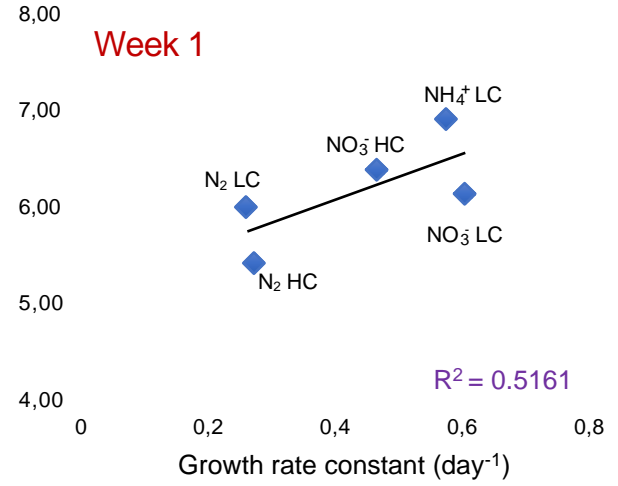
7. Van Teeffelen S, Renner L. 2018. Recent advances in understanding how rod-like bacteria stably maintain their cell shapes. F1000Res 7:241. https://doi.org/10.12688/f1000research.12663.1.

8. Martins BMC, Tooke AK, Thomas P, Locke JCW. 2018. Cell size control driven by the circadian clock and environment in cyanobacteria. Proc Natl Acad Sci U S A 115:E11415–E11424. https://doi.org/10.1073/pnas.1811309115.

9. Chien A, Zareh S, Wang Y, Levin P. 2012. Changes in the oligomerization potential of the division inhibitor UgtP co-ordinate Bacillus subtilis cell size with nutrient availability. Mol Microbiol 86:594–610. https://doi.org/10.1111/mmi.12007.

10. Hill N, Buske P, Shi Y, Levin PA. 2013. A moonlighting enzyme links Escherichia coli cell size with central metabolism. PLoS Genet 9:e1003663. https://doi.org/10.1371/journal.pgen.1003663.

11. Monahan L, Hajduk I, Blaber S, Charles I, Harry E. 2014. Coordinating bacterial cell division with nutrient availability: a role for glycolysis. mBio 5:e00935–14. https://doi.org/10.1128/mBio.00935-14.

12. Randic A, Brun Y. 2015. Molecular mechanisms for the evolution of bacterial morphologies and growth modes. Front Microbiol 6:580. https://doi.org/10.3389/fmicb.2015.00580.

13. Egan AJF, Errington J, Vollmer W. 2020. Regulation of peptidoglycan synthesis and remodeling. Nat Rev Microbiol 18:446–460. https://doi.org/10.1038/s41579-020-0366-3.

14. Cava F, Kuru E, Brun Y, de Pedro MA. 2013. Modes of cell wall growth differentiation in rod-shaped bacteria. Curr Opin Microbiol 16:731–737. https://doi.org/10.1016/j.mib.2013.09.004.

15. Vollmer W, Bertsche U. 2008. Murein (peptidoglycan) structure, architecture and biosynthesis in Escherichia coli. Biochim Biophys Acta 1778:1714–1734. https://doi.org/10.1016/j.bbamem.2007.06.007.

16. Bendezú FO, Hale CA, Bernhardt TG, de Boer PAJ. 2009. RodZ (YfgA) is required for proper assembly of the MreB actin cytoskeleton and cell shape in E. coli. EMBO J 28:193–204. https://doi.org/10.1038/emboj.2008.264.

17. Errington J. 2015. Bacterial morphogenesis and the enigmatic MreB helix. Nat Rev Microbiol 13:241–248. https://doi.org/10.1038/nrmicro3398.

18. Esue O, Cordero M, Wirtz D, Tseng Y. 2005. The assembly of MreB, a prokaryotic homolog of actin. J Biol Chem 280:2628–2635. https://doi.org/10.1074/jbc.M410298200.

19. Dye NA, Pincus Z, Theriot J, Shapiro L, Gitai Z. 2005. Two independent spiral structures control cell shape in Caulobacter. Proc Natl Acad Sci U S A 102:18608–18613. https://doi.org/10.1073/pnas.0507708102.

20. Leaver M, Errington J. 2005. Roles for MreC and MreD proteins in helical growth of the cylindrical cell wall in Bacillus subtilis. Mol Microbiol 57:1196–1209. https://doi.org/10.1111/j.1365-2958.2005.04736.x.

21. Kruse T, Bork-Jensen J, Gerdes K. 2005. The morphogenetic MreBCD proteins of Escherichia coli form an essential membrane-bound complex. Mol Microbiol 55:78–89. https://doi.org/10.1111/j.1365-2958.2004.04367.x.

22. Bendezú FO, de Boer PAJ. 2008. Conditional lethality, division defects, membrane involution, and endocytosis in mre and mrd shape mutants of Escherichia coli. J Bacteriol 190:1792–1811. https://doi.org/10.1128/JB.01322-07.

23. Pinho MG, Kjos M, Veening J-W. 2013. How to get (a)round: mechanisms controlling growth and division of coccoid bacteria. Nat Rev Microbiol 11:601–614. https://doi.org/10.1038/nrmicro3088.

24. Massidda O, Nováková L, Vollmer W. 2013. From models to pathogens: how much have we learned about Streptococcus pneumoniae cell division? Environ Microbiol 15:3133–3157. https://doi.org/10.1111/1462-2920.12189.

25. Ting CS, Rocap G, King J, Chisholm SW. 2002. Cyanobacterial photosynthesis in the oceans: the origins and significance of divergent light-harvesting strategies. Trends Microbiol 10:134–142. https://doi.org/10.1016/s0966-842x(02)02319-3.

26. Flores E, Herrero A. 2014. The cyanobacteria: morphological diversity in a photoautotrophic lifestyle. pip 1:63–72. https://doi.org/10.1127/pip/2014/0008.

27. Zehr J, Capone D. 2020. Changing perspectives in marine nitrogen fixation. Science 368:eaay9514. https://doi.org/10.1126/science.aay9514.

28. Hahn A, Schleiff E. 2014. The cell envelope, p 29–87. In Flores E, Herrero A (ed), The cell biology of cyanobacteria. Caister Academic Press, Norfolk, UK.

29. Rippka R, Deruelles J, Waterbury JB, Herdman M, Stanier RY. 1979. Generic assignments, strain histories and properties of pure cultures

30. Wilk L, Strauss M, Rudolf M, Nicolaisen K, Flores E, Kühlbrandt W, Schleiff E. 2011. Outer membrane continuity and septosome formation between vegetative cells in the filaments of Anabaena sp. PCC 7120. Cell Microbiol 13:1744–1754. https://doi.org/10.1111/j.1462-5822.2011.01655.x.

31. Herrero A, Stavans J, Flores E. 2016. The multicellular nature of filamentous heterocyst-forming cyanobacteria. FEMS Microbiol Rev 40:831–854. https://doi.org/10.1093/femsre/fuw029.

32. Wolk CP, Ernst A, Elhai J. 1994. Heterocyst metabolism and development, p 769–823. In Bryant DA (ed), The molecular biology of cyanobacteria. Kluwer Academic Publishers, The Netherlands.

33. Zhang J-Y, Lin G-M, Xing W-Y, Zhang C-C. 2018. Diversity of growth patterns probed in live cyanobacterial cells using a fluorescent analog of a peptidoglycan precursor. Front Microbiol 9:791. https://doi.org/10.3389/fmicb.2018.00791.

34. Singh SP, Montgomery BL. 2014. Morphogenes bolA and mreB mediate the photoregulation of cellular morphology during complementary chromatic acclimation in Fremyella diplosiphon. Mol Microbiol 93:167–182. https://doi.org/10.1111/mmi.12649.

35. Herrero A, Flores E. 2019. Genetic responses to carbon and nitrogen assimilation in Anabaena. Environ Microbiol 21:1–17. https://doi.org/10.1111/1462-2920.14370.

36. Kim Y, Joachimiak G, Zi Y, Binkowski TA, Zhang R, Gornicki P, Callahan SM, Hess WR, Haselkorn R, Joachimiak A. 2011. Structure of transcription factor HetR required for heterocyst differentiation in cyanobacteria. Proc Natl Acad Sci U S A 108:10109–10114. https://doi.org/10.1073/pnas.1106840108.

37. Flores E, Frías J, Rubio LM, Herrero A. 2005. Photosynthetic nitrate assimilation in cyanobacteria. Photosynth Res 83:117–133. https://doi.org/10.1007/s11120-004-5830-9.

38. Walsby AE. 2007. Cyanobacterial heterocysts: terminal pores proposed as sites of gas exchange. Trends Microbiol 15:340–349. https://doi.org/10.1016/j.tim.2007.06.007.

39. Salje J, van den Ent F, de Boer P, Löwe J. 2011. Direct membrane binding by bacterial actin MreB. Mol Cell 43:478–487. https://doi.org/10.1016/j.molcel.2011.07.008.

40. van den Ent F, Leaver M, Bendezu F, Errington J, de Boer P, Löwe J. 2006. Dimeric structure of the cell shape protein MreC and its functional implications. Mol Microbiol 62:1631–1642. https://doi.org/10.1111/j.1365-2958.2006.05485.x.

41. Combet C, Blanchet C, Geourjon C, Deléage G. 2000. NPS@: Network Protein Sequence Analysis. Computer Corner 25:147–150. https://doi.org/10.1016/S0968-0004(99)01540-6.

42. Hu B, Yang G, Zhao W, Zhang Y, Zhao J. 2007. MreB is important for cell shape but not for chromosome segregation of the filamentous cyanobacterium Anabaena sp. PCC 7120. Mol Microbiol 63:1640–1652. https://doi.org/10.1111/j.1365-2958.2007.05618.x.

43. Daniel RA, Errington J. 2003. Control of cell morphogenesis in bacteria: two distinct ways to make a rod-shaped cell. Cell 113:767–776. https://doi.org/10.1016/s0092-8674(03)00421-5.

44. Burnat M, Schleiff E, Flores E. 2014. Cell envelope components influencing filament length in the heterocyst-forming cyanobacterium Anabaena sp. strain PCC 7120. J Bacteriol 196:4026–4035. https://doi.org/10.1128/JB.02128-14.

45. Schaechter M, Maaloe O, Kjeldgaard NO. 1958. Dependency on medium and temperature of cell size and chemical composition during balanced growth of Salmonella typhimurium. J Gen Microbiol 19:592–606. https://doi.org/10.1099/00221287-19-3-592.

46. Dai X, Shen Z, Wang Y, Zhu M. 2018. Sinorhizobium meliloti, a slow-growing bacterium, exhibits growth rate dependence of cell size under nutrient limitation. mSphere 3:e00567-18. https://doi.org/10.1128/mSphere.00567-18.

47. Männik J, Bailey MW. 2015. Spatial coordination between chromosomes and cell division proteins in Escherichia coli. Front Microbiol 6:306. https://doi.org/10.3389/fmicb.2015.00306.

48. Li Z, Kinosita Y, Rodriguez-Franco M, Nußbaum P, Braun F, Delpech F, Quax TEF, Albers S-V. 2019. Positioning of the motility machinery in halophilic Archaea. mBio 10:e00377-19. https://doi.org/10.1128/mBio.00377-19.

49. Lange R, Hengge-Aronis R. 1991. Growth-phase regulated expression of bolA and morphology of stationary-phase Escherichia coli cells are controlled by the novel sigma factor sigma s. J Bacteriol 173:4474–4481. https://doi.org/10.1128/jb.173.14.4474-4481.1991.

of cyanobacteria. J Gen Microbiol 111:1–61. https://doi.org/10.1099/00221287-111-1-1.

50. Wortinger MA, Quardokus EM, Brun YV. 1998. Morphological adaptation and inhibition of cell division during stationary phase in *Caulobacter crescentus*. Mol Microbiol 29:963–973. https://doi.org/10.1046/j.1365-2958.1998.00959.x.

51. López-Igual R, Flores E, Herrero A. 2010. Inactivation of a heterocyst-specific invertase indicates a principal role of sucrose catabolism in heterocysts of *Anabaena* sp. J Bacteriol 192:5526–5533. https://doi.org/10.1128/JB.00776-10.

52. Mitschke J, Vioque A, Haas F, Hess WR, Muro-Pastor AM. 2011. Dynamics of transcriptional start site selection during nitrogen stress-induced cell differentiation in *Anabaena* sp. PCC7120. Proc Natl Acad Sci U S A 108:20130–20135. https://doi.org/10.1073/pnas.1112724108.

53. Picossi S, Flores E, Herrero A. 2014. ChIP analysis unravels an exceptionally wide distribution of DNA binding sites for the NtcA transcription factor in a heterocyst-forming cyanobacterium. BMC Genomics 15:22. https://doi.org/10.1186/1471-2164-15-22.

54. Muro-Pastor AM, Valladares A, Flores E, Herrero A. 2002. Mutual dependence of the expression of the cell differentiation regulatory protein HetR and the global nitrogen regulator NtcA during heterocyst development. Mol Microbiol 44:1377–1385. https://doi.org/10.1046/j.1365-2958.2002.02970.x.

55. Herrero A, Burnat M. 2014. Cyanophycin, a cellular nitrogen reserve material, p 211–219. *In* Flores E, Herrero A (ed), The cell biology of *Cyanobacteria*. Caister Academic Press, Norfolk, UK.

56. Lazaro S, Fernandez-Pinas F, Fernandez-Valiente E, Blanco-Rivero A, Leganes F. 2001. *pbpB*, a gene coding for a putative penicillin-binding protein, is required for aerobic nitrogen fixation in the cyanobacterium *Anabaena* sp. strain PCC7120. J Bacteriol 183:628–636. https://doi.org/10.1128/JB.183.2.628-636.2001.

57. Leganés F, Blanco-Rivero A, Fernández-Piñas F, Redondo M, Fernández-Valiente E, Fan Q, Lechno-Yossef S, Wolk PC. 2005. Wide variation in the cyanobacterial complement of presumptive penicillin-binding proteins. Arch Microbiol 184:234–248. https://doi.org/10.1007/s00203-005-0046-8.

58. Berendt S, Lehner J, Zhang YV, Rasse TM, Forchhammer K, Maldener I. 2012. Cell wall amidase AmiC1 is required for cellular communication and heterocyst development in the cyanobacterium *Anabaena* PCC7120 but not for filament integrity. J Bacteriol 194:5218–5227. https://doi.org/10.1128/JB.00912-12.

59. Zheng Z, Omairi-Nasser A, Li X, Dong C, Lin Y, Haselkorn R, Zhao J. 2017. An amidase is required for proper intercellular communication in the filamentous cyanobacterium *Anabaena* sp. PCC 7120. Proc Natl Acad Sci U S A 114:E1405–E1412. https://doi.org/10.1073/pnas.1621424114.

60. Bornikoel J, Staiger J, Madlung J, Forchhammer K, Maldener I. 2018. LytM factor Alr3353 affects filament morphology and cell–cell communication in the multicellular cyanobacterium *Anabaena* sp. PCC 7120. Mol Microbiol 108:187–203. https://doi.org/10.1111/mmi.13929.

61. Frías JE, Flores E, Herrero A. 1994. Requirement of the regulatory protein NtcA for the expression of nitrogen assimilation and heterocyst development genes in the cyanobacterium *Anabaena* sp. PCC7120. Mol Microbiol 14:823–832. https://doi.org/10.1111/j.1365-2958.1994.tb01318.x.

62. Camargo S, Valladares A, Flores E, Herrero A. 2012. Transcription activation by NtcA in the absence of consensus NtcA-binding sites in an *Anabaena* heterocyst differentiation gene promoter. J Bacteriol 194:2939–2948. https://doi.org/10.1128/JB.05994-11.

63. Mackinney G. 1941. Absorption of light by chlorophyll solutions. J Biol Chem 140:109–112.

64. Cai Y, Wolk CP. 1990. Use of a conditionally lethal gene in *Anabaena* sp. strain PCC 7120 to select for double recombinants and to entrap insertion sequences. J Bacteriol 172:3138–3145. https://doi.org/10.1128/jb.172.6.3138-3145.1990.

65. Olmedo-Verd E, Muro-Pastor AM, Flores E, Herrero A. 2006. Localized induction of the *ntcA* regulatory gene in developing heterocysts of *Anabaena* sp. strain PCC 7120. J Bacteriol 188:6694–6699. https://doi.org/10.1128/JB.00509-06.

66. Elhai J, Wolk CP. 1988. A versatile class of positive-selection vectors based on the nonviability of palindrome-containing plasmids that allows cloning into long polylinkers. Gene 68:119–138. https://doi.org/10.1016/0378-1119(88)90605-1.

67. Merino-Puerto V, Herrero A, Flores E. 2013. Cluster of genes that encode positive and negative elements influencing filament length in a heterocyst-forming cyanobacterium. J Bacteriol 195:3957–3966. https://doi.org/10.1128/JB.00181-13.

68. Black TA, Cai YP, Wolk CP. 1993. Spatial expression and autoregulation of *hetR*, a gene involved in the control of heterocyst development in *Anabaena*. Mol Microbiol 9:77–84. https://doi.org/10.1111/j.1365-2958.1993.tb01670.x.

69. Mohamed A, Jansson C. 1989. Influence of light on accumulation of photosynthesis-specific transcripts in the cyanobacterium *Synechocystis* 6803. Plant Mol Biol 13:693–700. https://doi.org/10.1007/BF00016024.

70. Paz-Yepes J, Herrero A, Flores E. 2007. The NtcA-regulated *amtB* gene is necessary for full methylammonium uptake activity in the cyanobacterium *Synechococcus elongatus*. J Bacteriol 189:7791–7798. https://doi.org/10.1128/JB.00404-07.

71. Vioque A. 1997. The RNase P RNA from cyanobacteria: short tandemly repeated repetitive (STRR) sequences are present within the RNase P RNA gene in heterocyst-forming cyanobacteria. Nucleic Acids Res 25:3471–3477. https://doi.org/10.1093/nar/25.17.3471.

72. Valladares A, Maldener I, Muro-Pastor AM, Flores E, Herrero A. 2007. Heterocyst development and diazotrophic metabolism in terminal respiratory oxidase mutants of the cyanobacterium *Anabaena* sp. strain PCC 7120. J Bacteriol 189:4425–4430. https://doi.org/10.1128/JB.00220-07.

Velázquez-Suárez *et al.*, Fig. S1

Velázquez-Suárez *et al.*, Fig. S2
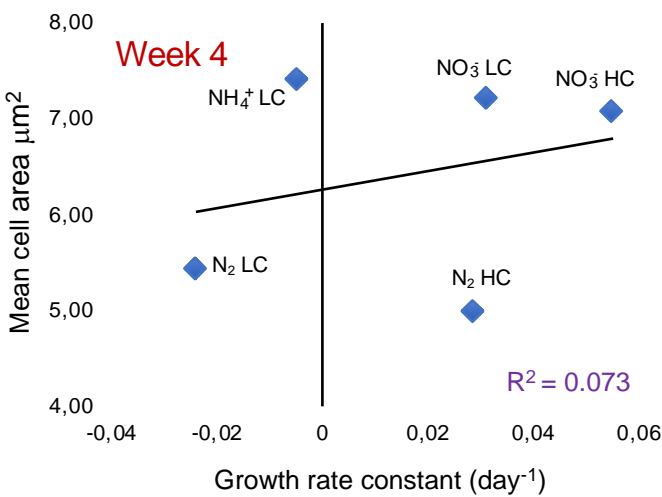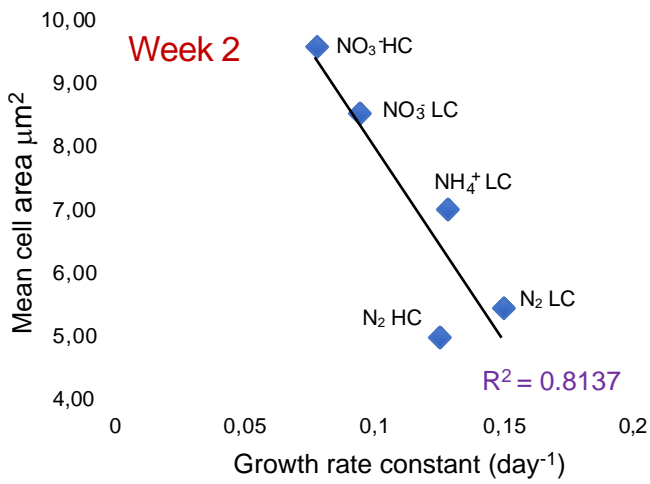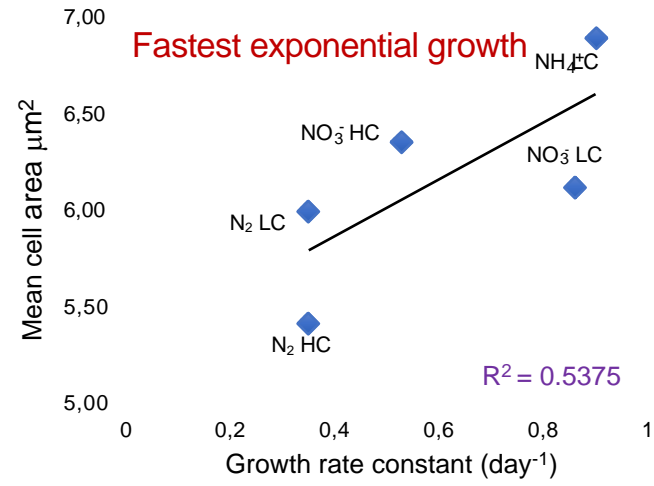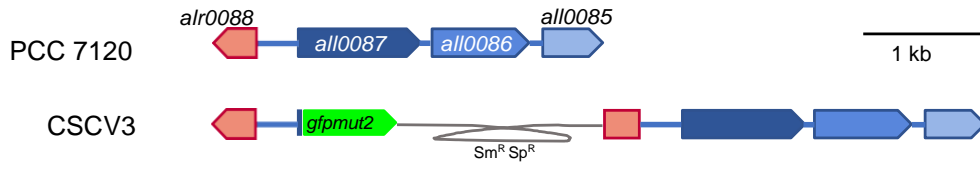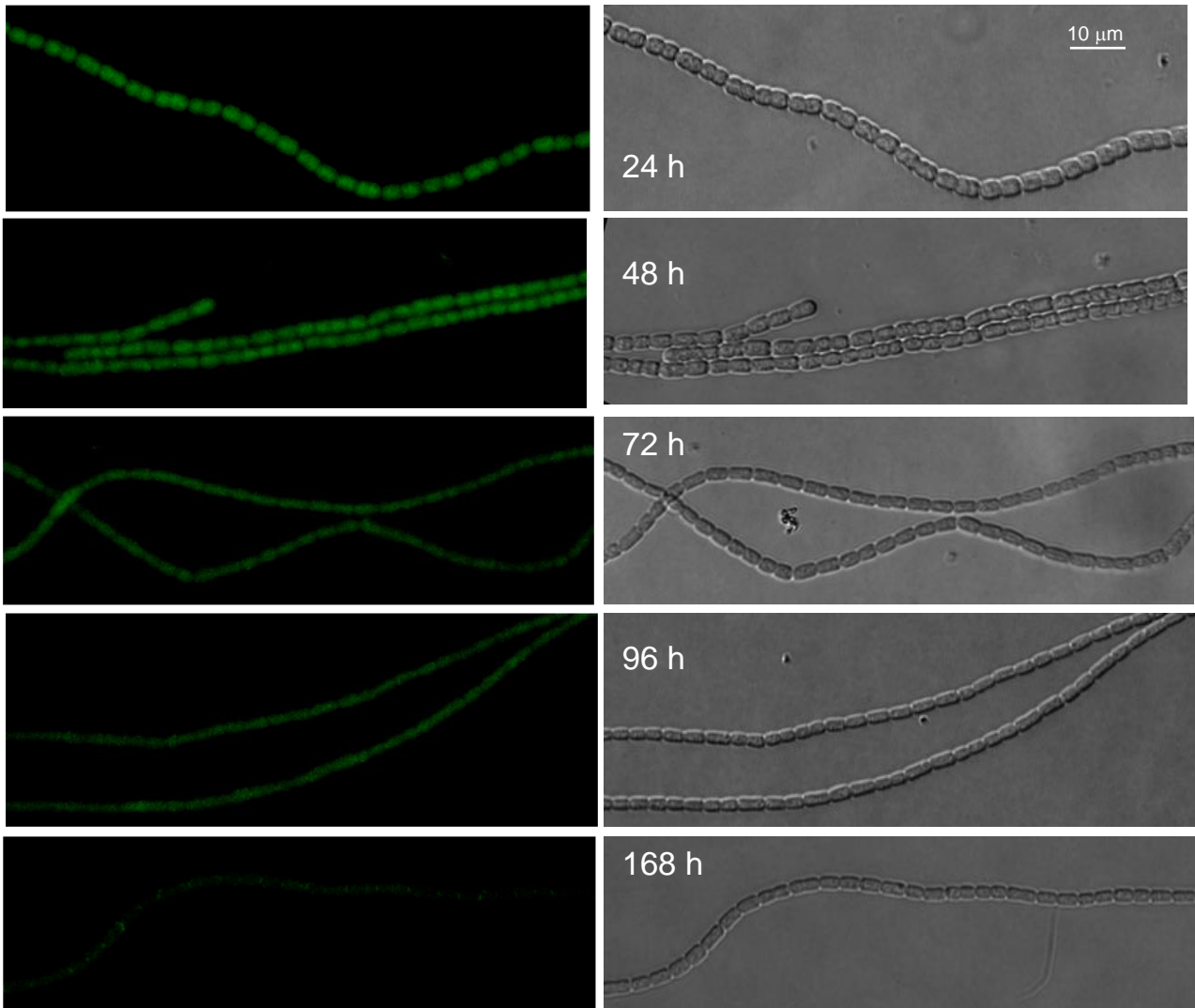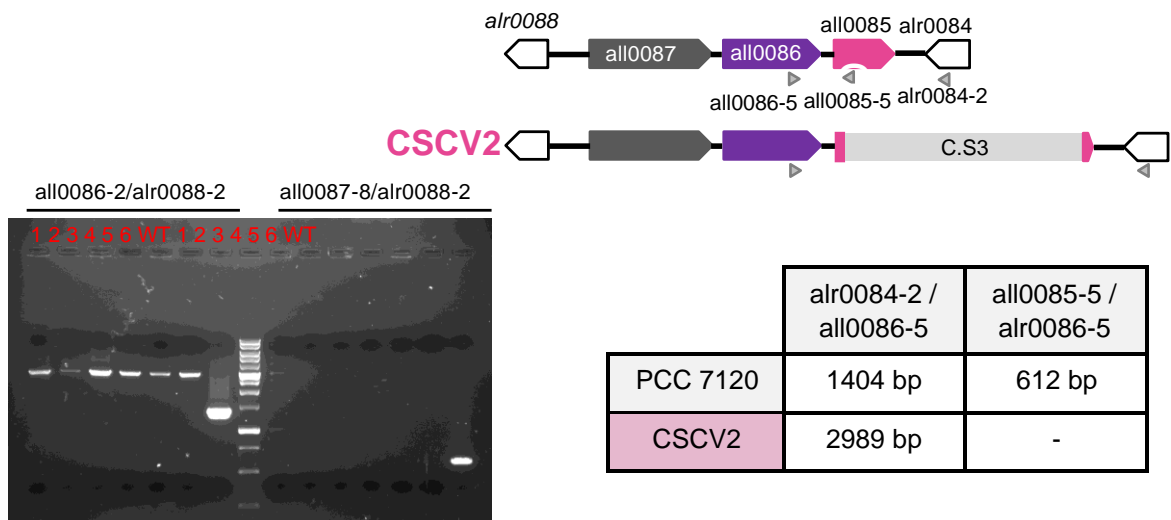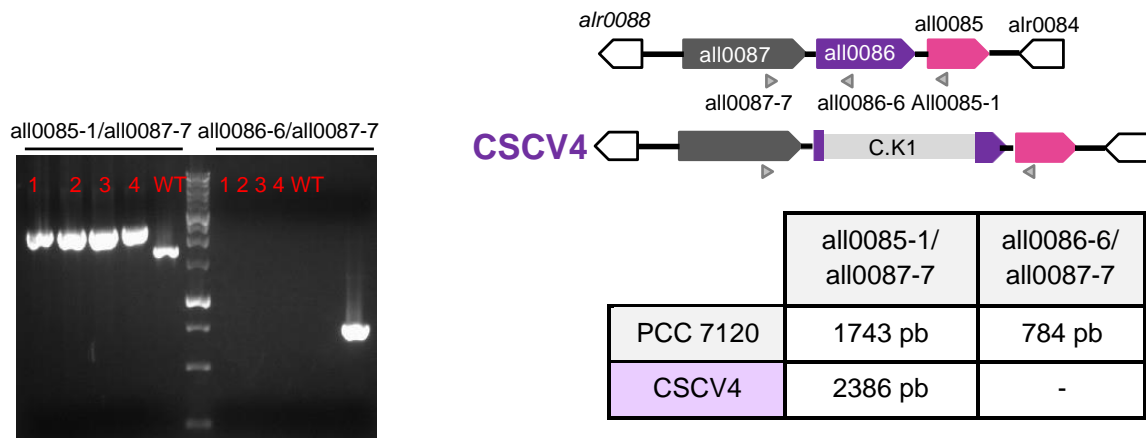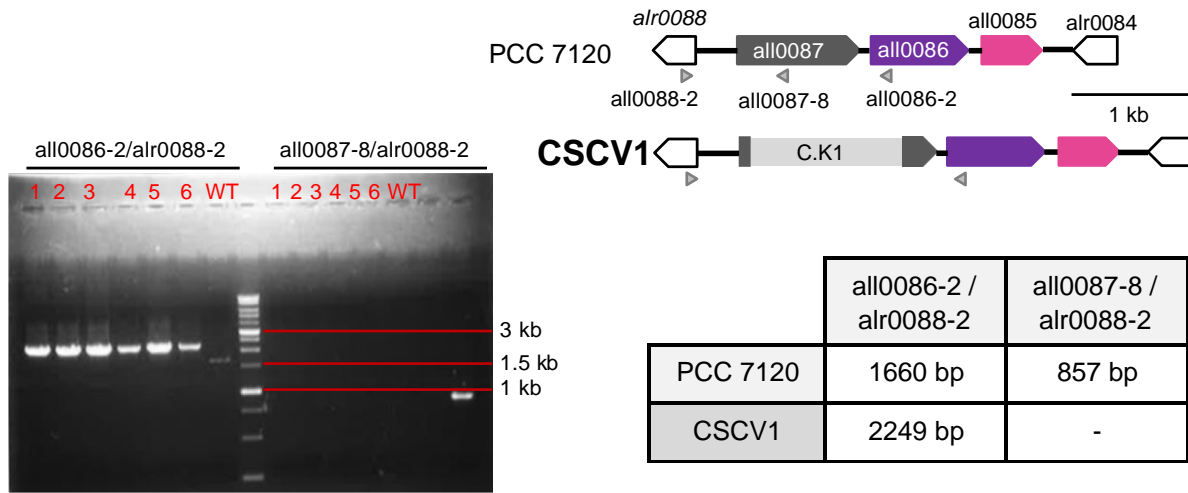
CSCV3 (NH$_4^+$)

	all0086-2 / alr0088-2	all0087-8 / alr0088-2
PCC 7120	1660 bp	857 bp
CSCV1	2249 bp	-

	all0085-1/ all0087-7	all0086-6/ all0087-7
PCC 7120	1743 pb	784 pb
CSCV4	2386 pb	-

	alr0084-2 / all0086-5	all0085-5 / alr0086-5
PCC 7120	1404 bp	612 bp
CSCV2	2989 bp	-

CHAPTER II: The role of Mre factors and cell division in peptidoglycan growth in the multicellular cyanobacterium *Anabaena*

The Role of Mre Factors and Cell Division in Peptidoglycan Growth in the Multicellular Cyanobacterium *Anabaena*

Cristina Velázquez-Suárez,[a] Ana Valladares,[a] Ignacio Luque,[a] Antonia Herrero[a]

[a]Instituto de Bioquímica Vegetal y Fotosíntesis, CSIC and Universidad de Seville, Seville, Spain

ABSTRACT Bacteria in general serve two main tasks: cell growth and division. Both processes include peptidoglycan extension to allow cell expansion and to form the poles of the daughter cells, respectively. The cyanobacterium *Anabaena* forms filaments of communicated cells in which the outer membrane and the peptidoglycan sacculus, which is engrossed in the intercellular regions between contiguous cells, are continuous along the filament. During the growth of *Anabaena*, peptidoglycan incorporation was weak at the cell periphery. During cell division, midcell peptidoglycan incorporation matched the localization of the divisome, and incorporation persisted in the intercellular septa, even after the division was completed. MreB, MreC, and MreD were located throughout the cell periphery and, in contrast to other bacteria, also to the divisome all along midcell peptidoglycan growth. In *Anabaena* mutants bearing inactivated *mreB, mreC*, or *mreD* genes, which showed conspicuous alterations in the filament morphology, consecutive septal bands of peptidoglycan growth were frequently not parallel to each other and were irregularly spaced along the filament, reproducing the disposition of the Z-ring. Both lateral and septal growth was impaired in strains down-expressing Z-ring components, and MreB and MreD appeared to directly interact with some divisome components. We propose that, in *Anabaena*, association with the divisome is a way for localization of MreB, MreC, and MreD at the cell poles, where they regulate lateral, midcell, and septal peptidoglycan growth with the latter being involved in localization and maintenance of the intercellular septal-junction protein structures that mediate cell-cell communication along the filament.

IMPORTANCE Peptidoglycan surrounds the bacterial cell, being essential for the determination of the bacterium-specific morphology and survival. Peptidoglycan growth has been thoroughly investigated in some model rod-shaped bacteria, and more recently some representatives with disparate morphologies became into focus, revealing that patterns of peptidoglycan growth are much more diverse than previously anticipated. *Anabaena* forms filaments of communicated cells exhibiting features of multicellular organisms, such as the production of morphogens and coupled circadian oscillations. Here, we showed that *Anabaena* presented a distinct pattern of peptidoglycan growth characterized by continuous incorporation of material at the polar intercellular regions, contributing to assembling and maintaining the protein complexes that expand the septal peptidoglycan mediating intercellular molecular exchange in the filament.

KEYWORDS cell growth, *Anabaena* filaments, intercellular septa, lateral peptidoglycan growth, septal peptidoglycan growth

Bacterial activity ultimately serves two main tasks: cell growth and division. Bacterial cells are encircled by distinct envelopes that compartmentalize the intracellular milieu and protect it from external insults while also permitting exchanges with the surrounding environment. Both cell growth and cell division processes must include an extension of the cell envelope to allow cell enlargement and daughter cell separation,

respectively. A component of the bacterial cell envelope is the murein, an elastic sacculus that surrounds the cell outside the cytoplasmic membrane, allowing it to cope with osmotic challenges and playing a pivotal role in the determination of the strain-specific morphology.

The murein is a giant peptidoglycan (PG) molecule made of long glycan strands of alternating *N*-acetylglucosamine and *N*-acetylmuramic acid units cross-linked by short peptides. It occurs as a single monolayer in common Gram-negative bacteria, in which the PG is placed in the periplasm between the cytoplasmic and outer membranes and is multilayered in Gram-positive bacteria. The synthesis of PG involves cytoplasmic and inner membrane-linked steps to form the lipid-anchored disaccharide pentapeptide (lipid II), the building block for PG synthesis, which is thereafter flipped to the outer leaflet of the plasma membrane. Outside of the cell (in the periplasm in Gram-negative bacteria), the lipid II precursor is polymerized into a PG growing strand by membrane-bound glycosyl transferases (which catalyze the bonding of precursor units to the glycosidic backbone with the release of the lipid moiety) and transpeptidases that cross-link the peptide units in adjacent PG strands (1, 2).

The spatiotemporal pattern of PG synthesis is tightly regulated according to the growth cycle and the environment, and this can be achieved by the organization of PG-processing enzymes in multiprotein complexes that are directed by cytoplasmic cytoskeletal proteins to specific subcellular localizations. Thus, at the initiation of cell division, the tubulin structural homolog FtsZ is bound to the inner membrane by interaction with diverse membrane-associated proteins and polymerizes to form a dynamic ring of short filaments that contract and move circumferentially at the future site of division by a head-to-tail treadmilling mechanism that drives the movement of the PG-processing machinery directing midcell PG incorporation to form the new poles of the daughter cells (2–5). In addition, in most rod-shaped bacteria, the actin structural homolog MreB ini- tiates the assembly of the elongasome, which directs a dispersed incorporation of PG in the cylindrical part of the cell wall allowing the growth of newly divided cells (2, 6).

The subcellular organization and localization of the MreB macromolecular complexes have been debated, being proposed to form cell-spanning helical structures or discrete patches of filaments with variable lengths (see reference (7)). In any case, the movement of MreB filaments, together with the integral membrane protein MreD and the periplasmic MreC, which also forms patches or short filaments (MreC from *Pseudomonas aeruginosa* has been recently shown to form tubular filaments *in vitro*; (7)), would guide the spatial localization of both the cytoplasmic enzymatic complex for PG precursor synthesis and the periplasmic PG-processing enzymes to insert new PG circumferentially, which in turn would contribute to the motion of MreB filaments, resulting in cell elongation (e.g., (8–11)).

In both *Escherichia coli* (12) and *Caulobacter crescentus* (13), in addition to septal and lateral growth, a midcell-localized PG synthesis takes place at the initiation of cell division leading to ring-like cell elongation at prospective division sites. In both bacteria, preseptal PG growth requires FtsZ, and, in *E. coli*, ZipA (a secondary FtsZ membrane tether) (13, 14). Mre proteins have been observed to form rings adjacent to the FtsZ ring at the initiation of cell division (15–21).

In addition, studies on other bacteria with different cell morphologies, such as the spherical *Staphylococcus aureus* (22) and the ovococcus *Streptococcus pneumoniae*, (23, 24), or even the rod-shaped *Corynebacterium glutamicum* (25), have revealed an ample diversity in the spatial and temporal pattern of localization of PG growth.

Filamentous heterocyst-forming cyanobacteria, such as those in the *Anabaena* genus, represent paradigmatic cases of bacterial multicellularity, in which the organismic unit was shifted from the individual cells to the filament (26, 27). The *Anabaena* filament is composed of tens to hundreds of cylindrical cells, which may include different cell types, that communicate by two paths allowing intercellular molecular exchange throughout the filament: a shared periplasm, which is established by continuity of the outer membrane, and proteinaceous septal channels that traverse the cell envelope at

the septa of contiguous cells (26). In *Anabaena*, the PG sacculus appears to be continuous along the filament, surrounding each cell and is engrossed at the intercellular septa between the cytoplasmic membranes of the daughter cells resulting from intercalary cell division (28). Indeed, PG sacculi fragments encompassing several cells can be readily isolated (e.g., (28)). Notably, the PG intercellular septal caps are perforated by nanopores, which have been proposed to hold the septal junction proteins that communicate the contiguous cells (28, 29). Despite the distinct structural features of *Anabaena*, relatively little is known about the mechanisms of cell elongation and cell division that operate to produce adjoined and communicated cells in comparison to the available detailed knowledge of these processes in unicellular bacteria.

Regarding elongasome components, *Anabaena* possesses homologs to MreB, MreC, and MreD factors, and mutants with inactivated *mre* genes present cells bigger than those of the wild-type and, especially in the case of the *mreC* mutant, stretches of filaments with cells of different sizes, indicating a role of MreB, MreC, and MreD in cell size control (30). The cells of the three mutants are more rounded than those of the wild-type and, contrary to the latter, in the mutant cells, the axis parallel to the filament is shorter than the axis perpendicular to the filament (30, 31). Cell enlargement and inversion of cell axes in the filament were also reported for an *Anabaena* derivative with inactivated ORF alr5045 encoding a PG transpeptidase, thus suggesting its involvement in cell elongation (32).

Regarding cell division proteins, *Anabaena* presents homologs of some of the widespread bacterial divisome components, together with specific cyanobacterial components. As in most other bacteria, cell division initiates by the polymerization of a Z-ring. However, *Anabaena* FtsZ has an N-terminal peptide specific to filamentous heterocyst-forming strains that is essential for cell division and appears to determine a distinct FtsZ polymerization mode (33). On the other hand, the cyanobacterium-specific protein ZipN represents the main FtsZ tether to the cytoplasmic membrane and the main organizer of the *Anabaena* divisome (34). Otherwise, little has been investigated on further divisome functions, except the recruitment of septal proteins involved in intercellular communication by specific interactions with divisome components during cell division (34–36), and the involvement of AmiC amidases in building the septal PG nanopore arrays (37–39).

In this work, we aimed at getting advance on the knowledge of the modes of PG growth operating in *Anabaena*, including the influence on these processes of the MreB, MreC, MreD, FtsZ, and ZipN proteins, and their involvement in cell growth and the determination of the cell morphology and the structure of the filament.

RESULTS

Topology of PG growth in *Anabaena*. Van-FL is a derivative of the antibiotic vancomycin that binds to the terminal $_D$-Ala-$_D$-Ala of PG precursor lipid II once externalized, either bound or not to the sacculus, but not involved in cross-linking, thus providing a probe for nascent PG synthesis (25). Some previous reports that included Van-FL-staining of *Anabaena* filaments are available (e.g., (32)). Here, we aimed to compare the patterns of PG growth in different growth phases in *Anabaena* and mutants impaired in cell division or elongasome factors. Fig. 1A shows images of *Anabaena* filaments stained with Van-FL. Quantitative determination of the labeling at lateral and septal locations is presented in Fig. 1B Under exponential growth (Fig. 1A, 24 and 48 h; see Fig. 1E), Van-FL staining produced weak, mostly homogenous fluorescence at the cell periphery and conspicuous labeling as bands at the intercellular septa between contiguous cells in the filaments. Additionally, labeling was observed at the midcell, matching the nascent septum in dividing cells. Average septal fluorescence intensity was about 3-fold that of the peripheral fluorescence (Fig. 1B). Notably, fluorescence intensity was higher in alternating older (narrower) septa than in the more recently constructed (wider) septa along the filament (Fig. 1A; a continuous recording in a stretch of a 24-h filament is shown in Fig. 1C, and an estimation of total fluorescence in alternating narrow and wide septa in Fig. 1D). This suggested that septal PG synthesis continues in *Anabaena* after daughter cells start new rounds of cell division, contributing to PG thickening in the intercellular
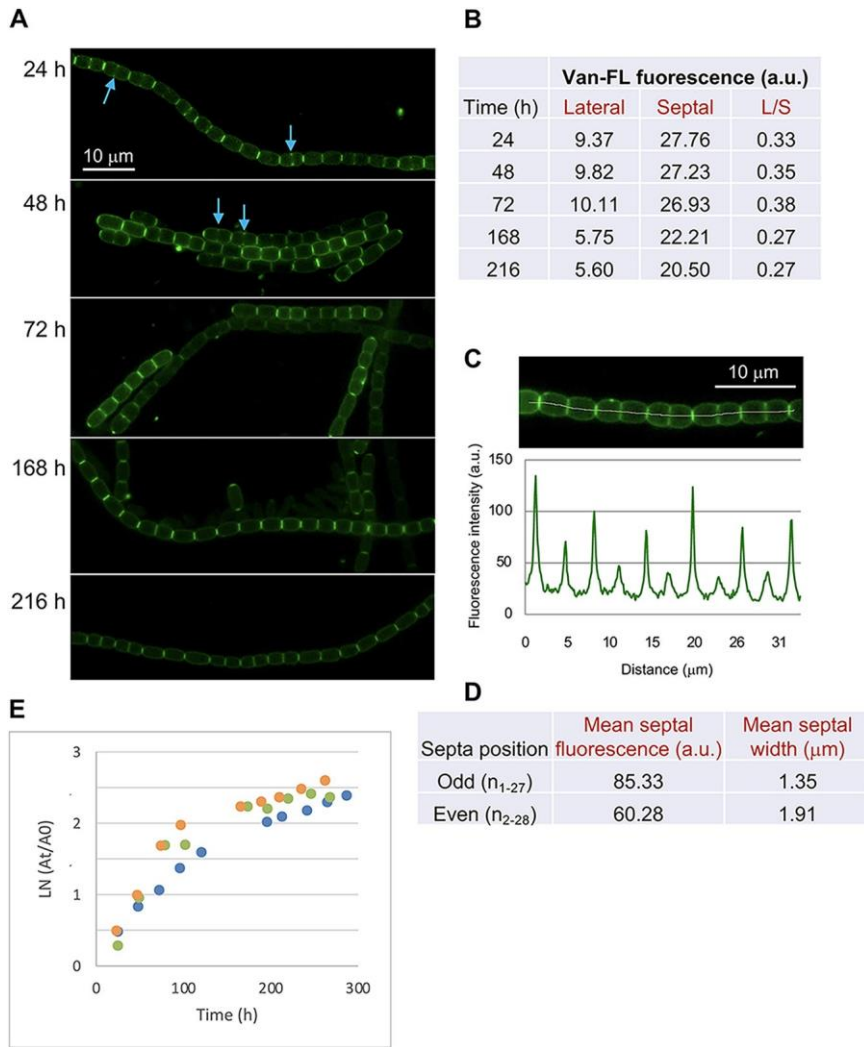
FIG 1 Van-FL staining of *Anabaena*. Exponential cultures were set as specified in Materials and Methods. At the indicated times, samples were labeled with Van-FL and observed under a fluorescence microscope. (A) Filaments were photographed. Arrows indicate fluorescence matching divisome localization. Magnification is the same for all micrographs. (B) Lateral and septal fluorescence was quantified as described in Materials and Methods. Student's *t* test was used to assess the significance of differences. For lateral labeling, $P <$ 0.01 for comparisons of 24 h, 48 h, or 72 h with 168 h or 216 h. For septal labeling, $P <$ 0.01 for 24 h or 72 h in comparison to 168 h or 216 h and $P <$ 0.05 for comparisons of 48 h with 168 h or 216 h. For the ratio lateral/septal (L/S), $P <$ 0.01 for comparisons of 24 h, 48 h, or 72 h with 168 h or 216 h, and $P <$ 0.05 for 24 h against 72 h (Data Set S1). (C) Fluorescence was recorded (lower panel) along a representative stretch of a 24 h-incubated filament (upper panel) in the area covered by the manually defined white line. (D) In the same filament used in (C), total septal fluorescence and septal width were measured in 28 consecutive septa, and the mean fluorescence and mean width were calculated for septa occupying the 14 odd and the 14 even positions. $P = 0.00022$ and $P <$ 0.00001 for comparisons of total septal fluorescence and septal width, respectively, between the two classes of septa. (E) Increase in the absorbance at 750 nm (A_{750}) of cultures incubated under the same conditions as those used in (A to D) (data from three independent cultures, denoted by different colors are presented). At, absorbance at the corresponding time; A0, absorbance at the start of culture.

regions. In the phases of nonexponential growth (Fig. 1A, 168 and 216 h), peripheral fluorescence decreased (Fig. 1B), likely reflecting a lower activity of cell growth. Septal labeling along the filament, although also decreased, was still readily detected (Fig. 1A and B), suggesting persistence of septal PG incorporation, and it was more homogeneous than during exponential growth (Fig. 1A), likely reflecting a lower frequency of cell division. This pattern results in a decrease in the average ratio of lateral versus septal labeling in comparison to the phases of exponential growth.
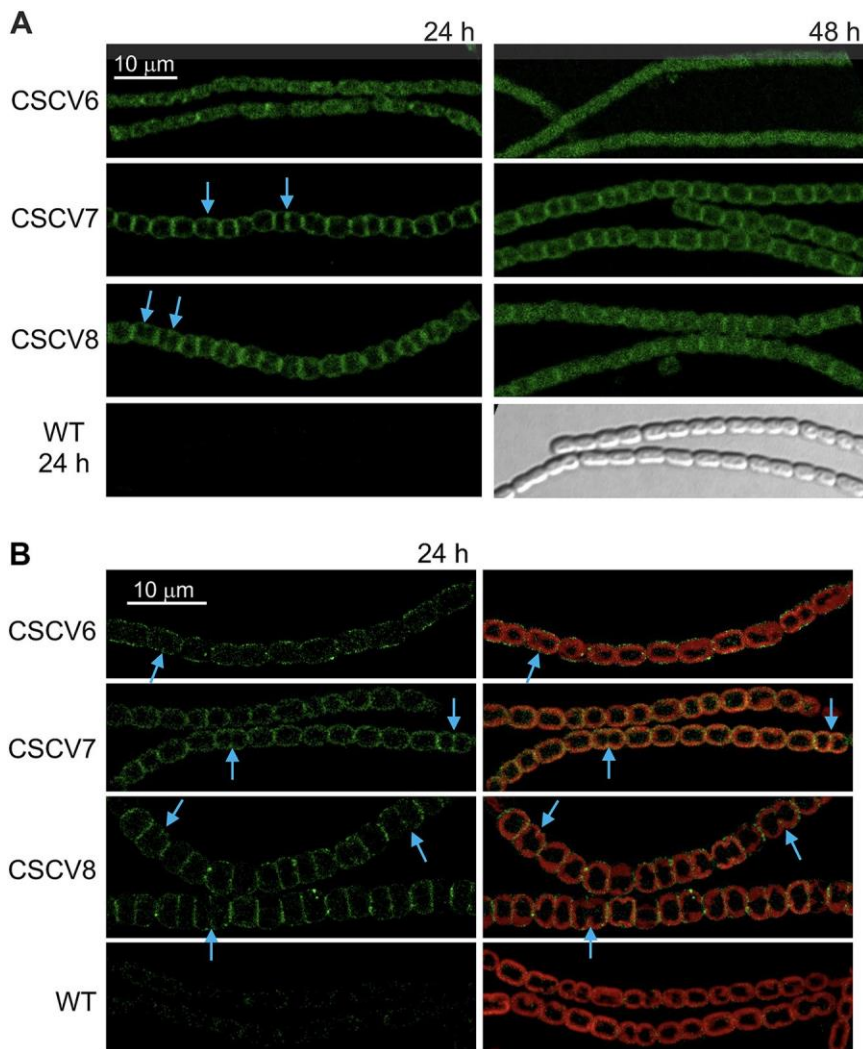
FIG 2 Localization of MreB, MreC and MreD in *Anabaena*. Exponential cultures of strains PCC 7120 (WT) and their derivatives CSCV6 (sfGFP-MreB), CSCV7 (sfGFP-MreC), and CSCV8 (sfGFP-MreD) were set, and, at the indicated times, filaments were visualized by confocal microscopy with a TCS (A) or FLUOVIEW (B) equipment. GFP fluorescence (green), bright-field images, and merged GFP and cyanobacterial autofluorescence (red) are shown. Arrows point to GFP fluorescence matching divisome localization. Magnification is the same for all micrographs in A or B.

Localization of MreB, MreC and MreD in *Anabaena*. The localization of MreB, MreC, and MreD in filaments of *Anabaena* was studied using protein fusions to green fluorescence protein (GFP). For that, we generated strains CSCV6, CSCV7, and CSCV8 that bear the genes *sfgfp-mreB*, *sfgfp-mreC*, or *sfgfp-mreD* (encoding the superfolder GFP fused to MreB, MreC or MreD, respectively) preceded by the native promoter of the *mreBCD* operon, located on an ectopic chromosomal locus (see Materials and Methods; cyanobacterial strains used in this work are listed in Table S1). Besides, these strains carry the intact *mreBCD* operon in its native location. GFP fluorescence was monitored in filaments of CSCV6, CSCV7, and CSCV8. In the phases of faster growth (Fig. 2, 24 h), strain CSCV6 presented weak fluorescence through the cell periphery (see especially high-resolution images in Fig. 2B) and in some discrete patches in the intercellular septal regions (Fig. 2A). Strains CSCV7 and CSCV8 exhibited high fluorescence around the cell periphery. In Fig. 2A, fluorescence appeared most intense in the septal regions between neighboring cells, an effect to which the superposition of two membrane units in these regions could contribute. In addition, in CSCV7 and CSCV8 (and in CSCV6, although less conspicuously due to weakness of signals) midcell fluorescent signals progressing inwards from the cell periphery, likely matching the progressing septa under

FIG 3 Van-FL staining of *Anabaena mreB*, *mreC*, and *mreD* mutants. Cultures of strains CSCV1 (*mreB*), CSCV4 (*mreC*), and CSCV2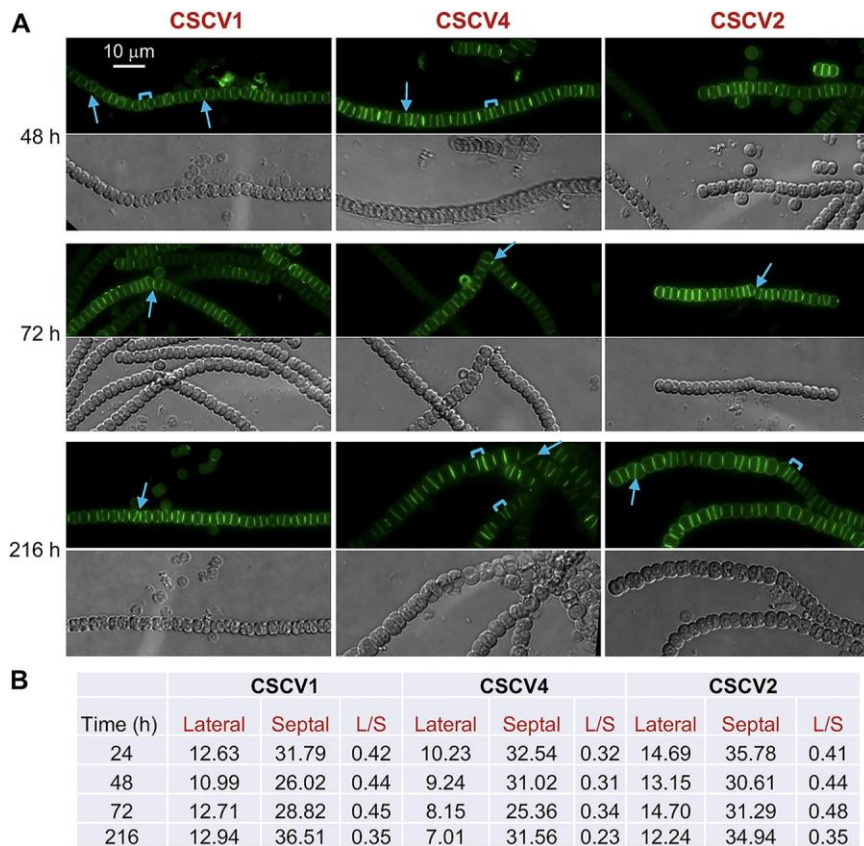 (*mreD*) were set and, at the indicated times, samples were stained with Van-FL and observed under a fluorescence microscope. (A) Filaments were photographed. Van-FL fluorescence (green) and bright-field images are shown. Arrows point to tilted fluorescent bands and brackets to cell compartments of disparate sizes. (B) Lateral and septal fluorescence was quantified and compared to the values obtained for the wild-type (presented in Fig. 1B). For the ratio L/S, P values were ˌ0.01 for comparisons of the WT with CSCV1 or CSCV2 at any time, and with CSCV4 at 216 h, and P value was ˌ0.05 between the WT and CSCV4 at 48 h (Data Set S1). Magnification is the same for all micrographs.

construction in the dividing cells, could be detected. It is worth noting that some cultures, especially of CSCV8 after 24 h of incubation, presented cells bigger and rounder than the wild-type cells. This could indicate that GFP-MreD might interfere with MreD function. Nonetheless, the specificity of the GFP fluorescence localization in CSCV8 and its consistency with the signals produced by GFP-MreB (in CSCV6) and GFP-MreC (in CSCV7) support that GFP-MreD is reporting the physiological localization of MreD. In the three strains, the peripheral fluorescence became more diffuse after 48 h of incubation, and the septal signal also diminished (Fig. 2A). In summary, during active growth, MreB, MreC, and MreD localize throughout the cell periphery. Notably, they also localize to the septa that are under construction during cell division, remaining localized in the intercellular septal regions after compartmentalization of the resulting daughter cells.

Influence of MreB, MreC, and MreD on PG growth. Van-FL staining was also performed in filaments of strains containing only inactivated versions of *mreB* (CSCV1), *mreC* (CSCV4), or *mreD* (CSCV2), previously generated (30). Despite conspicuous alterations in filament and cell size and morphology (30), strong septal bands of alternating intensity that resemble the septal labeling pattern in the WT, could be observed in filaments of the three mutants (Fig. 3A and Fig. S1). Indeed, the average septal fluorescence intensity in the mutants was somewhat higher than in the wild type (compare Fig. 3B and Fig. 1B). As in the wild type, fluorescence matching the progression of septum formation during cell division could be detected in some cells. However, in the mutants, the septal
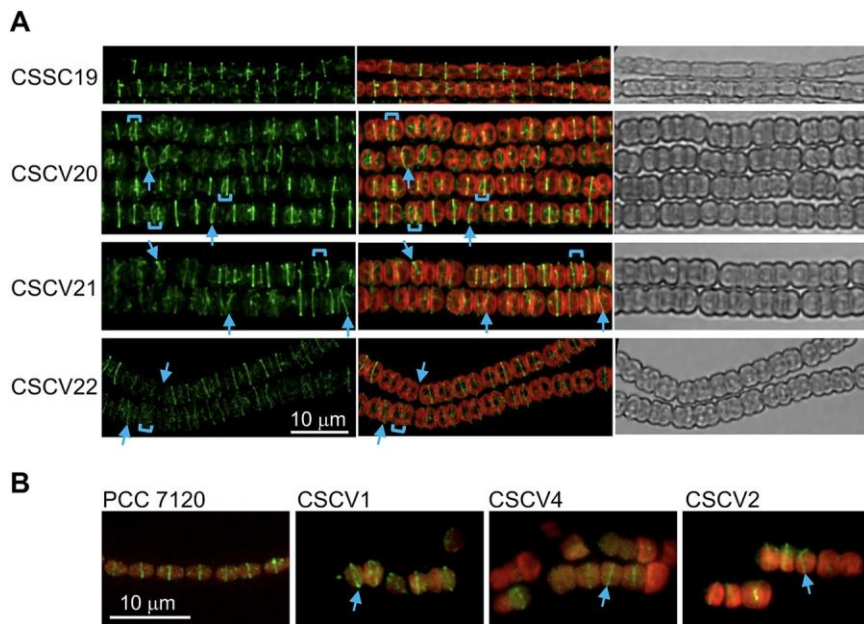
FIG 4 Localization of FtsZ in *Anabaena mreB*, *mreC,* and *mreD* mutants. (A) Cultures of strains CSSC19 (*ftsZ-gfp-mut2* in WT background), CSCV20 (*ftsZ-gfp-mut2* in *mreB* background), CSCV21 (*ftsZ-gfp-mut2* in *mreC* background) and CSCV22 (*ftsZ-gfp-mut2* in *mreD* background) were set and, after 48 h, filaments were visualized by confocal microscopy and photographed. GFP fluorescence (green), merged GFP and cyanobacterial autofluorescence (red), and bright-field images are shown. To improve visibility, contrast is higher for the green image of CSCV22. (B) Immunolocalization with antibodies against *Anabaena* FtsZ in the wild-type and strains CSCV1 (*mreB*), CSCV4 (*mreC*), and CSCV2 (*mreD*) incubated for 48 h in liquid BG11 medium (initial cell density, 1 *m*g chlorophyll/mL). Arrows point to tilted fluorescence bands and brackets to cell compartments of disparate sizes. Magnification is the same for all micrographs in (A or B).

bands frequently appeared tilted or separating compartments of different sizes. These alterations could explain the observed local deviations in the filament plane and hetero-geneity of cell size in the mutants (30) (Fig. 3A and Fig. S1). Thus, MreB, MreC, and MreD are not needed for septal PG synthesis during cell division, but they appear to be needed for the correct positioning of the septal PG growth-plane. On the other hand, peripheral labeling of the mutant round cells was also detected in strains CSCV1, CSCV2, and CSCV4 (Fig. 3 and Fig. S1).

Localization of FtsZ and ZipN in *mre* mutants. Given the observed instances of misplacement of the medial and septal bands of Van-FL staining in the *mre* mutants, we asked whether the absence of Mre proteins affected the localization of the cell division plane. We then studied the localization of FtsZ-rings and ZipN in the absence of MreB, MreC, or MreD. To study FtsZ, a gene construct, including an *ftsZ-gfp* reporter expressed from the P$_{ftsz}$ promoter was transferred to strains CSCV1 (*mreB*), CSCV4 (*mreC*), and CSCV2 (*mreD*), generating strains CSCV20, CSCV21, and CSCV22, respectively. Strain CSSC19 expresses the *ftsZ-gfp* reporter in the WT background (33). As in CSSC19, fluores-cent FtsZ-rings were readily detected in strains CSCV20, CSCV21, and CSCV22. However, in the mutant backgrounds some rings were not parallel to those of neighboring cells, and the distance between two consecutive Z-rings was irregular (Fig. 4A). In addition, FtsZ was detected by immunolocalization with antibodies against *Anabaena* FtsZ in the mutants CSCV1, CSCV4, and CSCV2 in comparison to the wild type. Consistent with the results obtained with GFP fusions, some aberrantly located rings could be detected in the mutants (Fig. 4B).

To study the localization of ZipN in the absence of MreB, MreC, or MreD, an *sfgfp-zipN* reporter gene expressed from the P$_{zipN}$ promoter was transferred to strains CSCV1, CSCV4, and CSCV2, generating strains CSCV14, CSCV15 and CSCV16, respectively. In fil-aments of strain CSAV39 (*sfgfp-zipN* in the wild-type background, (40)), fluorescence
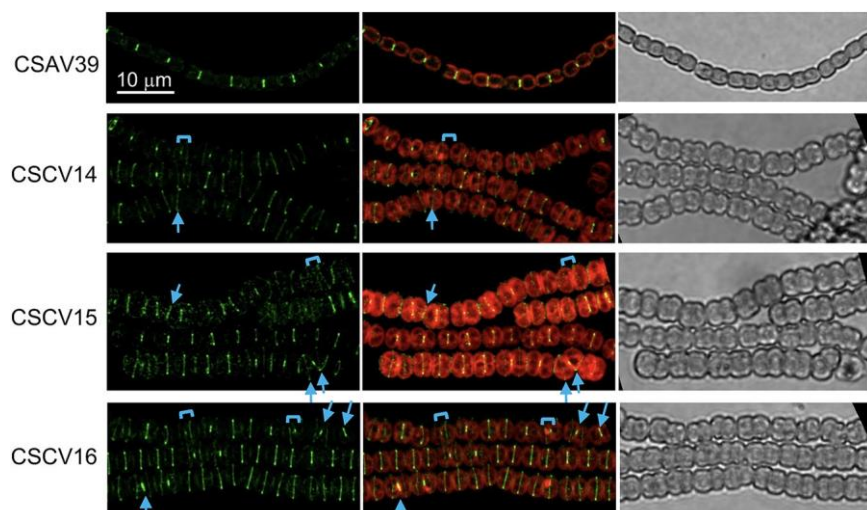
FIG 5 Localization of ZipN in *Anabaena mreB*, *mreC* and *mreD* mutants. Cultures of strains CSAV39 (*sfgfp-zipN* in WT background), CSCV14 (*sfgfp-zipN* in *mreB* background), CSCV15 (*sfgfp-zipN* in *mreC* background) and CSCV16 (*sfgfp-zipN* in *mreD* background) were set and, after 24 h, filaments were visualized by confocal microscopy and photographed. GFP fluorescence (green), merged GFP and cyanobacterial autofluorescence (red), and bright-field images are shown. Arrows point to tilted fluorescence bands and brackets to cell compartments of disparate sizes. Magnification is the same for all micrographs.

was detected in midcell bands and as bands or spots in recently matured septa. In fresh cultures of strains CSCV14, CSCV15, and CSCV16, midcell and septal fluorescent bands or spots could be detected frequently. However, especially in CSCV15, cells exhibiting diffuse fluorescence over the cell periphery were also found (Fig. 5). As with FtsZ-GFP, some neighboring cells exhibited tilted GFP-ZipN bands, and at some places, the distances between consecutive bands in the filament varied.

These results suggest that the misplaced Van-FL-labeled septal bands observed in the *mre* mutants corresponded to places where cell division took place at a plane tilted with regard to that of the previous division or deviated from the midcell position.

PG growth in *Anabaena* mutants was impaired in FtsZ or ZipN. We have previously described *Anabaena* derivatives that conditionally down-express *ftsZ* (strain CSFR18; (35)) or *zipN* (strain CSL109; (34)) from P_{ND}, a synthetic promoter that directs low expression levels in the presence of ammonium. Upon transfer of filaments grown with nitrate (permissive conditions for P_{ND}-*ftsZ* or P_{ND}-*zipN* expression) to a medium with ammonium (restrictive conditions), strains CSFR18 and CSL109 underwent drastic alterations in cell morphology and extensive cell lysis (see representative images in Fig. 6 and 7, respectively). In the two mutants, morphological alterations preceding cell lysis included cell elongation, bulging of the central cell region, and drastic cell swelling. In CSFR18, long bulged cells could be observed, initially forming filaments, and later as single cells (which likely results from lysis of accompanying cells in the filament). Strain CSL109 presented giant spherical-like cells or ellipsoidal cells in which the axis perpendicular to the filament is longer than that parallel to the filament. These and previous observations (33–35) show that in *Anabaena* impairment of cell division leads to unchecked cell enlargement with restricted elongation producing giant cells with aberrant shapes.

Van-FL staining was performed in strains CSFR18 and CSL109. In filaments incubated with nitrate (permissive conditions), Van-FL staining produced weak peripheral, and strong septal fluorescence signals similar to those observed in the WT (not shown). Upon transfer of strain CSFR18 to medium with ammonium (restrictive conditions for P_{ND}-*ftsZ* expression), it showed weak peripheral labeling in the still slightly enlarged cells, and strong dispersed peripheral fluorescence, including occasional discrete spots, in the aberrantly more enlarged cells, which were increasingly abounding (see some
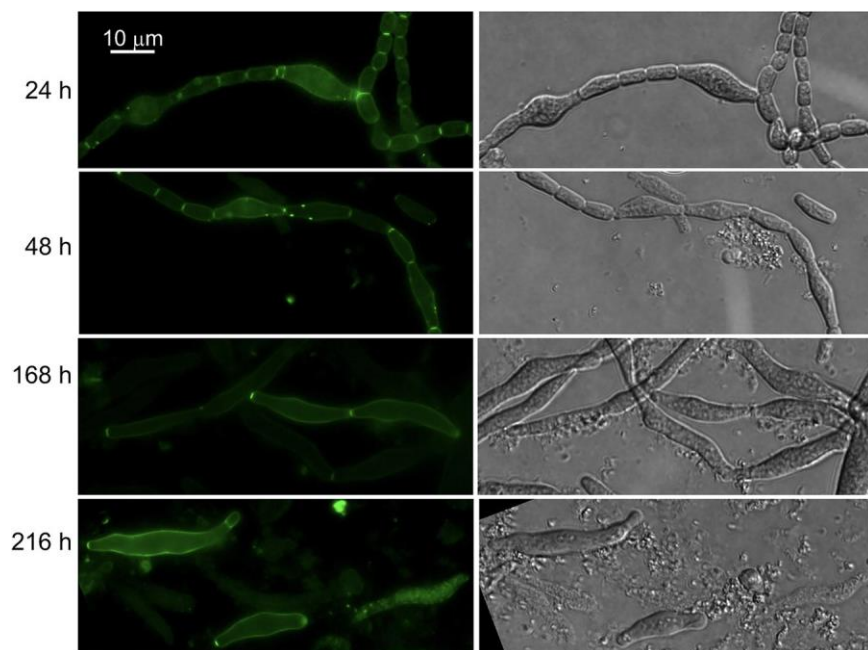
FIG 6 Van-FL staining of strain CSFR18 impaired in FtsZ expression. Filaments of strain CSFR18 (P_{ND}-*ftsZ*) (see the text for details) grown in BG11 medium (permissive conditions) were transferred to $BG11_0$ 1 NH_4[1] medium (restrictive conditions for *ftsZ* expression) and incubated under culture conditions. At the indicated times, samples were stained with Van-FL, observed under a fluorescence microscope, and photographed. Van-FL fluorescence (green) and bright-field images are shown. Magnification is the same for all micrographs.

examples in Fig. 6). After prolonged incubation under these conditions, most of the remaining cells appeared very deformed and had lost fluorescence, although some very aberrant, mostly isolated cells with conspicuous peripheral fluorescence could also be observed (Fig. 6). In strain CSL109 transferred to ammonium-containing medium (restrictive conditions for P_{ND}-*zipN* expression), some cells that began to adopt aberrant engrossed shapes exhibited strong peripheral labeling. However, upon prolonged incubation, most cells showed very weak, progressively fading labeling (Fig. 7).

Regarding midcell staining, no Van-FL labeling was detected in the enlarged cells of CSFR18 or CSL109. Regarding septal labeling, Van-FL bands could be initially detected in the intercellular regions of slightly elongated cells, but they did not increase in width in parallel to the observed increase in cell volume (note enlarged cells connected by tiny septal fluorescent spots in Fig. 6, 48 and 168 h, and in Fig. 7, 168 and 216 h). In CSL109, septal fluorescence was promptly lost, and in CSFR18 many aberrant cells appeared also devoid of septal fluorescence. Thus, the observed septal Van-FL signals appear to correspond to cell division events initiated before restrictive conditions for *ftsZ*, or *zipN* expression were imposed. In summary, in the two strains, the transfer to restrictive conditions leads to the cessation of divisome-associated midcell PG incorporation, but also decreased PG incorporation at the septa and the cell periphery, although a phase of strong peripheral PG incorporation concomitant with severe morphological alterations took place.

BACTH analysis of protein interactions. Given the alterations of Z-ring localization in *mreB*, *mreC,* and *mreD* mutants, and the localization of Mre proteins also to division rings in dividing cells, we tested direct interactions between Mre and cell division proteins. We used a bacterial two-hybrid (BACTH) assay with MreB, MreC, MreD, and the divisome proteins FtsZ, ZipN, ZipS (a cyanobacterium-specific cell division factor, (41)), Alr0487 (putative SepF), Alr1706 (putative FtsE), All1757 (putative FtsX), FtsQ, All7666 (putative FtsK), Alr0718 (putative divisome transpeptidase FtsI), and All0154 (putative divisome glycosyl-transferase FtsW). Besides MreB self-interactions, fully significant, although weak, positive interactions were detected with the pairs: T18-MreB/T25-FtsQ and MreD-T18/T25-FtsI (Student's *t* tests ⌐0.02 for comparisons with all the three
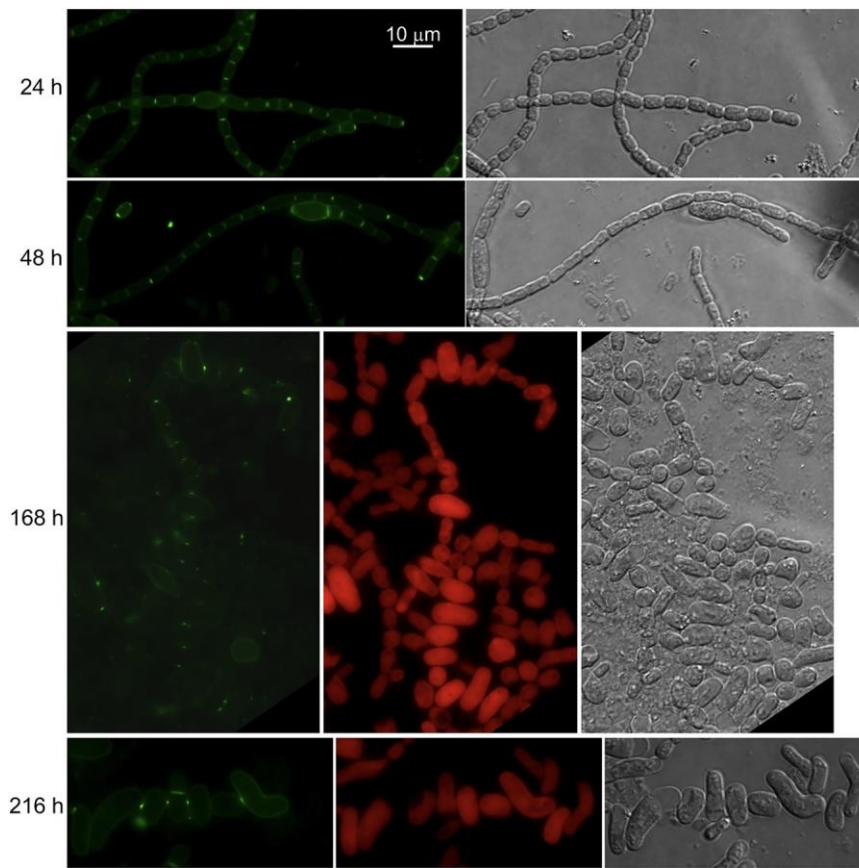
FIG 7 Van-FL staining of strain CSL109 impaired ZipN expression. Filaments of strain CSL109 (P_{ND}-*zipN*) (see the text for details) grown in BG11 medium (permissive conditions) were transferred to BG11$_0$ 1 NH$_4$^{1} medium (restrictive conditions for *zipN* expression) and incubated under culture conditions. At the indicated times, samples were stained with Van-FL, observed under a fluorescence microscope, and photographed. Van-FL fluorescence (green), cyanobacterial autofluorescence (red), and bright-field images are shown. Magnification is the same for all micrographs.

controls). In addition, the results obtained suggested interactions between MreD-T18/T25-FtsW; and MreD-T18/T25-FtsQ (Fig. 8A).

DISCUSSION

In the rod-shaped cells of *Anabaena* sp. strain PCC 7120, Van-FL staining produced weak continuous peripheral fluorescence in the cylindrical part of the cells (Fig. 1; see also reference (32)). This pattern differs from that of weak tilted bands and strong peripheral dots detected in other rod-shaped bacteria such as *Bacillus subtilis* (25) or *C. crescentus* (9), which is indicative of a disperse mode of PG incorporation in the cylindrical part of the cell. In *B. subtilis*, this peripheral PG incorporation is independent of MreB but dependent on Mbl (a MreB homolog), MreC, and MreD (42). Both MreB (8) and Mbl (43) form filaments that rotate around the cell's long axis, and MreC and MreD localize in a similar banded pattern (42). In *E. coli*, MreB also forms peripheral filaments, whereas MreC and MreD were uniformly localized through the cell periphery (44). In *C. crescentus*, MreB and MreC form nonoverlapping periplasmic spirals along the perimeter of the cell and, in contrast to predivisional MreB localization at midcell, MreC is not present at the division site (45). Here, we show that in *Anabaena*, MreB, MreC, and MreD localize throughout the cell periphery (Fig. 2). In the presence of combined nitrogen none of the three *mre* genes is essential (30), but mutants lacking any of them form rounded cells or even cells in which the longer axis is perpendicular to the filament. These results indicate an involvement of MreB, MreC, and MreD in cell

A

	Mean	SD	p	pᵃ	pᵇ	n
T18/T25	13,156	2,345				9
MreB-MreB						
T25-MreB/MreB-T18	109,980	63,264	0,000	0,054	0,052	3
MreB-T25/T18-MreB	40,513	8,868	0,000	0,007	0,003	3
pKT25/MreB-T18	11,265	0,923				3
pUT18/T25-MreB	9,867	2,651				3
pKNT25/T18-MreB	13,830	1,997				3
pUT18C/MreB-T25	7,733	1,791				3
MreB-FtsQ						
T18-MreB/T25-FtsQ	17,070	2,411	0,004	0,001	0,017	8
pKT25/T18-MreB	10,175	0,413				3
pUT18C/T25-FtsQ	12,625	2,850				4
MreD-FtsW						
MreD-T18/T25-FtsW	19,171	3,406	0,001	0,269	0,009	8
pKT25/MreD-T18	16,697	1,677				3
pUT18/T25-FtsW	12,073	2,080				3
MreD-FtsI						
MreD-T18/T25-FtsI	24,61	2,53	0,000	0,008	0,008	8
pUT18/T25-FtsI	14,83	0,21				2
pKT25/MreD-T18	16,70	1,68				3
MreD-FtsQ						
MreD-T18/T25-FtsQ	17,037	2,231	0,003	0,003	0,818	8
pUT18/T25-FtsQ	11,738	2,262				4
pKT25/MreD-T18	16,697	1,677				3

B

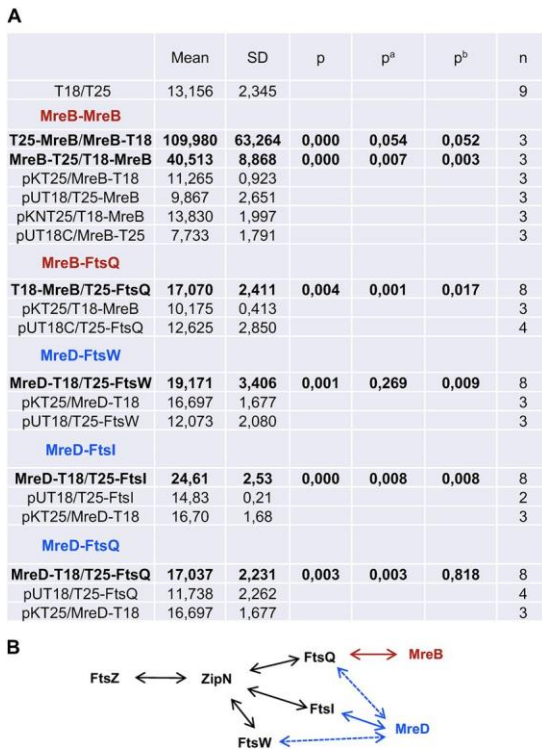FtsZ ↔ ZipN → FtsQ ↔ MreB
ZipN → FtsI ⇠ MreD
FtsW ⇠

FIG 8 BACTH assay of interactions of Mre and divisome proteins. (A) Interactions of protein pairs produced in *E. coli* were assayed by measurements of *b*-galactosidase activity in liquid cultures incubated at 30°C. The topology of each fusion is indicated by the order of components (T18-protein and T25-protein denote the corresponding adenylate cyclase domain fused to the N terminus of the tested protein, whereas protein-T18 and protein-T25 denote fusions to the C terminus). Data are the mean and standard deviation of the indicated number of determinations of the activity (nmol ONP min⁻¹ mg protein⁻¹) with the indicated protein fused to T25 (or the empty vectors pKNT25 or pKT25) and the indicated protein fused to T18 (or the empty vectors pUT18C or pUT18). Significance of differences was assessed by Student's *t* tests: p refers to the test against the strain containing both empty vectors; pᵃ and pᵇ denote tests against the strains expressing each fused protein and the complementary empty vector. (B) Schematic of the positive interactions detected: colored solid lines denote interactions with p, pᵃ, and pᵇ ⌐0.02, and dashed lines denote interactions with p and either pᵃ or pᵇ ⌐ 0.02. Previously deduced interactions between divisome proteins (33, 34) are depicted in black.

elongation ((30); Fig. 3). However, the detection of Van-FL peripheral labeling in the round cells of the mutants suggests that some PG incorporation, likely serving maintenance functions, can take place in them. It is worth noting that the pattern of Van-FL staining shown here for *Anabaena*, with weak peripheral and strong septal labeling, is similar to that observed with the fluorescent amino acid HADA that can be incorporated into PG (46), thus precluding that our observations were due to poor access of Van-FL to the *Anabaena* periplasm or Van-FL staining artifacts.

Anabaena also showed Van-FL staining in the progressing septum under construction during cell division, and intense bands in the intercellular regions along the filament, even under phases of slow growth (Fig. 1), suggesting that septal growth is maintained during the cell cycle. In addition, the observed alternance of septal Van-FL band intensities (stronger in the older septa and weaker in the more recent ones) is indicative of the persistence of septal PG growth or remodeling after cell division has been completed. During the phases of less active growth, the intensity of fluorescence in septal bands homogenize through the filament and remains strong, also suggesting septal PG growth/remodeling after cell division. This contrasts with the pattern in *Bacillus* in which little polar Van-FL staining is observed in mature cells (25), which is consistent with a narrow period of septal PG growth after which the cell poles remain inert during most of the cell cycle.

In *E. coli*, preseptal elongation from the midcell is observed only at the initiation of

cell division (12), and after completion, the cell poles are inert for PG synthesis (47). In *C. crescentus* zonal PG synthesis near the midcell takes place between a period of dispersed lateral growth and cell constriction (13). In *S. pneumoniae*, PG synthesis is halted after completion of cell division and the resulting cell poles become inert (25). In contrast, in the case of *C. glutamicum*, PG growth directed by the divisome remains active after cell division has completed, so that growth continues at the cell poles leading to a rod-like shape (25). These models differ from the situation in *Anabaena*, in which the persistent and strong septal labeling appears restricted to the intercellular regions of the filament, consistent with the thickening of the PG layer observed in these regions.

In *Anabaena*, our observations with strain CSCV6 (*sfgfp-mreB*) suggest the localization of MreB throughout the cell periphery, including the septal regions as well as in the divisome (Fig. 2). These observations could be compared with two previous reports: one with a *gfp-mreBCD* construct overexpressed from a heterologous promoter in a replicative plasmid, which gave conspicuous fluorescent spots at the cell poles (31), and another with *gfp-mreB* expressed from P$_{mreB}$ in a replicative plasmid, which showed filaments dispersed through the cell without any directional preference (48). On the other hand, strains CSCV7 (*sfgfp-mreC*) and CSCV8 (*sfgfp-mreD*) allowed the localization of MreC and MreD, respectively, at midcell matching the growing septum in dividing cells, even at advanced stages of septum formation, and in the intercellular regions between adjacent cells in the filament after septum closure as well as in nondividing cells (Fig. 2). Indeed, in *mreB*, *mreC* and *mreD* mutants, intercellular septa are wider and septal Van-FL labeling signal is stronger than in the wild type, likely contributing to increase filament length and rigidity (compare Fig. 1 and 3; (30)). These results suggest that, although MreB, MreC, and MreD are not required for septal PG synthesis, they participate in septum constriction and intercellular PG maintenance at all stages of the cell cycle.

In contrast to the wild type, in which the new septa localize at midcell in parallel to that of the previous division and perpendicular to the filament long axis, in a *mreB*, *mreC*, or *mreD* mutant septal PG bands are frequently found tilted with regard to those of previous divisions, a disposition never observed in the wild type, or separating compartments with different sizes (Fig. 3). These alterations appear to cause the observed variability of cell size and distortions in the filament plane, even leading to apparent branches, in the mutants (30) (Fig. 3 and Fig. S1). Furthermore, we have shown here that during cell division, whereas in the wild-type the proteins FtsZ and ZipN localized to parallel Z-rings in consecutive cells, in the *mreB*, *mreC*, and *mreD* mutants some tilted and diverted FtsZ (Fig. 4) and ZipN (Fig. 5) rings are observed. Also, especially in the *mreC* mutant, fluorescence from GFP-ZipN appeared somewhat dispersed (Fig. 5). Thus, in the mutants the alterations in the localization of the septal PG incorporation likely originate from misplacement of the Z-ring. Therefore, although MreB, MreC, and MreD are not required for divisome-associated PG growth, they are needed for its correct geometric localization. The altered localization of the division plane might result, at least in part, from the increased cell volume and rounded cell morphology of the *mre* mutants. However, a more direct effect of the Mre proteins localized at the division site is possible, as supported also by our BACTH results suggesting direct interactions involving MreB and MreD and the divisome components FtsQ, FtsW, and FtsI (Fig. 8).

In *Anabaena*, the morphological alterations observed when the initial steps of cell division are inhibited differ from those reported for other bacteria. Hence, in *E. coli* FtsZ depletion (49) or mutation (50) leads to the formation of long filaments; in *B. subtilis*, FtsZ depletion leads to cell elongation but does not affect growth rate (25), and in *C. crescentus* FtsZ depletion leads to cell elongation by a disperse mode of PG synthesis over the sidewalls (13). Thus, in *E. coli*, *B. subtilis*, and *C. crescentus*, lateral PG growth to elongate the cells can be maintained in the absence of cell division. In contrast, *Anabaena* derivatives that conditionally down-express FtsZ or ZipN show strong deformations of the rod-shape morphology normally exhibited by the wild type, or by the mutants under permissive conditions, forming enlarged cells with irregular width (larger in the central region than in the polar regions), more abundant under FtsZ

shortage, and giant cells with inverted polarity in the filaments that progress to lysis under ZipN shortage (34, 35) (Fig. 6 and 7). Upon transfer to repressive conditions, Van-FL staining of strains CSFR18 (P_{ND}-*ftsZ*) and CSL109 (P_{ND}-*zipN*) revealed a phase of strong abnormal PG incorporation through the periphery of aberrant cells, apparently followed by cessation of PG incorporation. Interestingly, it has been previously described that treatment of *Anabaena* with aztreonam (an inhibitor of FtsI) leads, in the short term, to strong peripheral HADA incorporation (46). Moreover, PG-growth in intercellular septa also ceased leading to the presence of minuscule septa, in compari-son to the increased cell volume, joining the aberrant enlarged cells. In summary, in *Anabaena*, inhibition of the initial steps of cell division also inhibits the incorporation of PG at mature filament septa that are observed in the wild type and affects the pe-ripheral PG growth preventing sustained cell elongation without widening.

All present and previous results are consistent with a model in which three modes of PG growth operate in *Anabaena*, namely, peripheral, divisional, and intercellular septal. The peripheral mode requires MreB, MreC, and MreD. The divisional and septal PG growth could proceed in the absence of MreB, MreC, and MreD, although these factors have a role in the correct localization of divisional PG growth at midcell and the correct septal PG dimensions. As was the case for many septal proteins of *Anabaena*, we propose that the localization of Mre proteins to division rings serves to place them in the mature intercellular septa, where the proteins remain after cell division has completed. Septal Mre proteins might represent a topological determinant and regulate the extent of peripheral PG growth. Finally, continuous activity of PG growth and remodeling in the mature intercellular septa could contribute to the maintenance of the inserted septal junction arrays that mediate intercellular communication.

MATERIALS AND METHODS

Strains and growth conditions. *Anabaena* sp. Strain PCC 7120 and mutant strains were grown in a BG11 medium (containing NaNO$_3$ as a nitrogen source) (51). Cultures were incubated at 30°C with illumination (12 mE m^{22} s^{21} white light emitted from Osram LED lamps 16.4 W/4000K) in Erlenmeyer flasks with shaking or in plates of medium solidified with 1% Difco agar. For the mutants, media were supplemented with antibiotics: spectinomycin dihydrochloride pentahydrate (Sp) and streptomycin sulfate (Sm) at 5 mg mL^{21} each in solid medium or 2.5 mg mL^{21} each in liquid medium (CSCV2, CSCV6, CSCV7, CSCV8, CSFR18, CSSC19, CSL109, CSAV39), with neomycin sulfate (Nm) at 25 mg mL^{21} in solid medium or 5 mg mL^{21} in liquid medium (CSCV1, CSCV4), or with Sm, Sp, and Nm (CSCV14, CSCV15, CSCV16, CSCV20, CSCV21, CSCV22). Unless otherwise specified, for the experiments described in this work BG11-grown filaments of the indicated strains were transferred to (at a cell density of 0.5 mg chlorophyll/mL) and incubated in a BG11-based medium lacking NaNO$_3$ and supplemented with 4 mM NH$_4$Cl and 8 mM TES-NaOH buffer, pH 7.5. It should be noted that, except for experiments with strains CSFR18 and CSL109, similar results were obtained with filaments incubated with nitrate instead of ammonium (unpublished data). The growth of cultures was monitored by measuring the absorbance at 750 nm in aliquots withdrawn at the indicated times. The chlorophyll content of the cultures was determined after extraction with methanol (52). In *Anabaena*, 1 mg chlorophyll corresponds to ca. 3 ✗ 10^6 cells (53).

Plasmid and strain constructions. Strains CSCV6, CSCV7, and CSCV8 bear an *sfgfp-mreB*, *sfgfp-mreC*, or *sfgfp-mreD* fusion gene, respectively, expressed from the native *mreBCD* operon promoter (P_{mreB}), in a heterologous genomic locus, *thrS2*, which is dispensable under normal growth conditions (54). These strains were generated in two steps. In a first step, the construct P_{mreB}-*sfgfp* was introduced into the coding sequence of *thrS2*, generating strain CSCV5. For that, the sequence of P_{mreB} was amplified from *Anabaena* genomic DNA with primers all0087-20/all0087-21 (all oligodeoxynucleotide primers used in this work are listed in Table S2), and the *sfgfp* from plasmid pCSAL39 (55) with primers SF-GFP-F2/SF-GFP-R2 (plasmids used in this work are listed in Table S1). Both DNA fragments were joined together by overlapping PCR and introduced into previously cloned *thrS2* sequence in plasmid pMBLT (Canvas), generating plasmid pCSCV9. (To generate a site for introducing the P_{mreB}-*sfgfp* construct, the plasmid containing *thrS2* was amplified with primers all4723-3/all4723-4, both corresponding to internal *thrS2* sequences and ending with NsiI restriction sites.) The insert of pCSCV9 was transferred to the conjugative vector pRL277 including genes for Sm^R/Sp^R and *sacB*, encoding susceptibility to sucrose for positive selection (56), generating plasmid pCSCV10. Finally, pCSCV10 was transferred to *Anabaena* by conjugation selecting first for resistance against Sm and Sp, and later for sensitivity to sucrose. One clone that bore the P_{mreB}-*sfgfp* construct inserted on *thrS2* by double crossover (verified by PCR) was selected (strain CSCV5). In a second step, a DNA fragment encoding *sfgfp* lacking the stop codon (amplified with primers SF-GFP-F/SF-GFP-R) was fused by overlapping PCR to fragments encoding *mreB* (amplified with all0087-22/all0087-23), *mreC* (all0086-13/all0086-14) or *mreD* (all0085-8/all0085-9), preceded by a 5-Gly encoding sequence. The resulting fusions were cloned into the conjugative vector pCSV3 including determinants for Sm^R/Sp^R (57), generating plasmids pCSCV11, pCSCV12, and pCSCV13, which were transferred to strain

CSCV5. Clones bearing plasmids pCSCV11, pCSCV12, or pCSCV13 inserted by single crossover into *thrS2* were selected and verified by PCR.

Strains CSCV14, CSCV15, and CSCV16 bear the fusion *sfgfp-zipN* expressed from the P_{zipN} promoter, together with a native copy of P_{zipN}-*zipN*, in a CSCV1, CSCV4, or CSCV2 background, respectively. To generate them, the pCSV3-based plasmid pCSAV285, which includes the P_{zipN}-*sfgfp-zipN* construct (40), was transferred to strains CSCV1 and CSCV4 with selection for Sm^R/Sp^R. On the other hand, the insert of pCSAV285 was cloned into the KpnI site of pRL424 (58) generating plasmid pCSCV37, which was transferred to strain CSCV2 with selection for Nm^R. One clone resulting from each conjugation that had inserted the transferred plasmid by a single crossover into the *zipN* locus leaving an intact P_{zipN}-*zipN* gene (verified by PCR) was selected.

Strains CSCV20, CSCV21, and CSCV22 bear the fusion *ftsZ-gfpmut2* expressed from the P_{ftsZ} promoter, together with a native copy of P_{ftsZ}-*ftsZ*, in a CSCV1, CSCV4, or CSCV2 background, respectively. To generate them, the pRL277-based plasmid pCSSC39, which includes the P_{ftsZ}-*ftsZ-mut2gfp* construct (33) was transferred to strains CSCV1 and CSCV4 with selection for Sm^R/Sp^R. On the other hand, the insert of pCSSC39 was cloned into the SacI/XhoI sites of pRL278 (59) generating plasmid pCSCV39, which was transferred to strain CSCV2 with selection for Nm^R. One clone resulting from each conjugation that had inserted the transferred plasmid by a single crossover into the *ftsZ* locus leaving an intact P_{ftsZ}-*ftsZ* (verified by PCR) was selected.

Van-FL staining and quantification. For Van-FL staining, filaments were suspended in a liquid medium supplemented with 2 *m*g/mL Vancomycin-FL (Bodipy-FL conjugate, Invitrogen) and incubated for 1 h in the dark with shaking at 30°C. Filaments were washed twice with liquid medium and spotted in agar. Lateral and septal fluorescence was quantified with ImageJ (60) processing of fluorescence images by collecting total fluorescence in manually defined equal square sections (0.41 *m*m in length) at the periphery and the intercellular septa of each counted cell. For each cell, lateral fluorescence was calculated as the mean of the values of four sections, and septal fluorescence as the mean of two sections, one at each cell pole. Twenty to thirty cells were counted for each strain and condition, and the average values were calculated. ImageJ was used also for recording fluorescence along determined filament areas (Fig. 1C) and for quantification of septal width and total septal fluorescence using manually defined sections including the whole septa (Fig. 1D).

BACTH analysis. BACTH assays based on the reconstitution of adenylate cyclase from *Bordetella pertussis* (61) were performed. Genes were amplified by PCR using *Anabaena* DNA as the template and oligonucleotide pairs: all0087-10/all0087-11 (T25-MreB), all0087-12/all0087-11 (T18-MreB), all0087-12/all0087-13 (MreB-T25, MreB-T18), all0086-17/all0086-18 (T25-MreC), all0086-19/all0086-18 (T18-MreC), all0085-12/all0085-13 (MreD-T25, MreD-T18), all0154-11b/all0154-13 (FtsW-T18), all1616-4/all1616-5 (T25-ZipS, T18-ZipS), all7666-3/all7666-2 (T18-FtsK) and all7666-3/all7666-4 (FtsK-T25, FtsK-T18), alr1706-4/alr1706-2 (FtsE-T18). The resulting PCR products, which were flanked by PstI/EcoRI ends, were cloned in pUT18, pUT18C, pKNT25 or pKT25 digested with the same enzymes, producing fusions to the 59 or 39 ends of the genes encoding the adenylate cyclase T18 and T25 fragments. All the resulting plasmids were verified by sequencing. The fusions encoding MreC-T18, MreC-T25, T18-MreD, and T25-MreD could not be cloned. Other fusions to the genes *ftsZ*, *zipN*, *sepF*, *zipS*, *ftsX*, *ftsI*, *ftsQ*, *ftsW*, and *ftsE* were as previously described (33–35). Plasmids were transformed into *E. coli* XL1-Blue for amplification. Isolated plasmids were cotransformed into strain BTH101 (*cya*-99), and the transformants were plated on a solid LB medium containing selective antibiotics and 1% glucose. Cotransformants were grown in a liquid medium in the presence of IPTG plus antibiotics supplemented with *o*-nitrophenol-*b*-galactoside. The *o*-nitrophenol produced per mg of protein versus time was represented, and the *b*-galactosidase activity was deduced from the slope of the linear function.

Microscopy. Van-FL fluorescence was visualized with a Leica DM6000B fluorescence microscope and a FITCL5 filter (excitation band-pass, 480/40; emission band-pass, 527/30), and photographed with an ORCA-ER camera (Hamamatsu). For immunolocalization with antibodies against *Anabaena* FtsZ (35), filaments were treated as specified in reference (34) and visualized by fluorescence microscopy as above. GFP fluorescence was monitored with an Olympus TCS SP2 confocal laser-scanning microscope equipped with an HCX PLAN-APO 63✗.4 NA oil immersion objective (excitation, 488-nm; collection, 500 to 540 nm for GFP or 630 to 700 nm for cyanobacterial autofluorescence) or with an Olympus FLUOVIEW FV3000 (hyper-resolution) confocal laser-scanning microscope equipped with a UPlanApo 60✗.5 NA oil immersion objective (excitation, 488-nm; collection 500 to 540 nm for GFP or excitation, 640 nm; collection, 650 to 750 nm for cyanobacterial autofluorescence).

SUPPLEMENTAL MATERIAL

Supplemental material is available online only.

DATA SET S1, XLSX file, 0.02 MB.

FIG S1, PDF file, 0.2 MB.

TABLE S1, DOCX file, 0.02 MB.

TABLE S2, DOCX file, 0.02 MB.

ACKNOWLEDGMENTS

REFERENCES

1. Lovering AL, Safadi SS, Strynadka NCJ. 2012. Structural perspective of peptidoglycan biosynthesis and assembly. Annu Rev Biochem 81:451–478. https://doi.org/10.1146/annurev-biochem-061809-112742.

2. Egan AJF, Errington J, Vollmer W. 2020. Regulation of peptidoglycan synthesis and remodelling. Nat Rev Microbiol 18:446–460. https://doi.org/10.1038/s41579-020-0366-3.

3. Bisson-Filho A, Hsu Y, Squyres G, Kuru E, Wu F, Jukes C, Sun Y, Dekker C, Holden S, VanNieuwenhze MS, Brun YV, Garner EC. 2017. Treadmilling by FtsZ filaments drives peptidoglycan synthesis and bacterial cell division. Science 355:739–743. https://doi.org/10.1126/science.aak9973.

4. Yang X, Lyu Z, Miguel A, McQuillen R, Huang KC, Xiao J. 2017. GTPase activity–coupled treadmilling of the bacterial tubulin FtsZ organizes septal cell wall synthesis. Science 355:744–747. https://doi.org/10.1126/science.aak9995.

5. Whitley KD, Jukes C, Tregidgo N, Karinou E, Almada P, Cesbron Y, Henriques R, Dekker C, Holden S. 2021. FtsZ treadmilling is essential for Z-ring condensation and septal constriction initiation in *Bacillus subtilis* cell division. Nat Commun 12:2448. https://doi.org/10.1038/s41467-021-22526-0.

6. Sun Y-J, Bai F, Luo A-C, Zhuang X-Y, Lin T-S, Sung Y-C, Shih Y-L, Lo C-J. 2021. Probing bacterial cell wall growth by tracing wall-anchored protein complexes. Nat Commun 12:2160. https://doi.org/10.1038/s41467-021-22483-8.

7. Martins A, Contreras-Martel C, Janet-Maitre M, Miyachiro MM, Estrozi LF, Trindade DM, Malospirito CC, Rodrigues-Costa F, Imbert L, Job V, Schoehn G, Attrée I, Dessen A. 2021. Self-association of MreC as a regulatory signal in bacterial cell wall elongation. Nat Commun 12:2987. https://doi.org/10.1038/s41467-021-22957-9.

8. Errington J. 2015. Bacterial morphogenesis and the enigmatic MreB helix. Nat Rev Microbiol 13:241–248. https://doi.org/10.1038/nrmicro3398.

9. Divakaruni AV, Baida C, White CL, Gober JW. 2007. The cell shape proteins MreB and MreC control cell morphogenesis by positioning cell wall synthetic complexes. Mol Microbiol 66:174–188. https://doi.org/10.1111/j.1365-2958.2007.05910.x.

10. Hussain S, Wivagg CN, Szwedziak P, Wong F, Schaefer K, Izoré T, Renner LD, Holmes MJ, Sun Y, Bisson-Filho AW, Walker S, Amir A, Löwe J, Garner EC. 2018. MreB filaments align along greatest principal membrane curvature to orient cell wall synthesis. Elife 7:e32471. https://doi.org/10.7554/eLife.32471.

11. Laddomada F, Miyachiro MM, Dessen A. 2016. Structural insights into protein-protein interactions involved in bacterial cell wall biogenesis. Antibiotics 5:14. https://doi.org/10.3390/antibiotics5020014.

12. de Pedro MA, Quintela J, Höltje J, Schwarz H. 1997. Murein segregation in *Escherichia coli*. J Bacteriol 179:2823–2834. https://doi.org/10.1128/jb.179.9.2823-2834.1997.

13. Aaron M, Charbon G, Lam H, Schwarz H, Vollmer W, Jacobs-Wagner C. 2007. The tubulin homologue FtsZ contributes to cell elongation by guiding cell wall precursor synthesis in *Caulobacter crescentus*. Mol Microbiol 64:938–952. https://doi.org/10.1111/j.1365-2958.2007.05720.x.

14. Pazos M, Peters K, Casanova M, Palacios P, VanNieuwenhze M, Breukink E, Vicente M, Vollmer W. 2018. Z-ring membrane anchors associate with cell wall synthases to initiate bacterial cell division. Nat Commun 9:5090. https://doi.org/10.1038/s41467-018-07559-2.

15. Figge RM, Divakaruni AV, Gober JW. 2004. MreB the cell shape determining bacterial actin homologue coordinates cell wall morphogenesis in *Caulobacter crescentus*. Mol Microbiol 51:1321–1332. https://doi.org/10.1111/j.1365-2958.2003.03936.x.

16. Vats P, Rothfield L. 2007. Duplication and segregation of the actin (MreB) cytoskeleton during the prokaryotic cell cycle. Proc Natl Acad Sci U S A 104:17795–17800. https://doi.org/10.1073/pnas.0708739104.

17. R van der P, Verheul J, Vischer NO, Alexeeva S, Hoogendoorn E, Postma M, Banzhaf M, Vollmer W, den Blaauwen T. 2013. Colocalization and interaction between elongasome and divisome during a preparative cell division phase in *Escherichia coli*. Mol Microbiol 87:1074–1087. https://doi.org/10.1111/mmi.12150.

18. Vats P, Shih Y-L, Rothfield L. 2009. Assembly of the MreB-associated cytoskeletal ring of *Escherichia coli*. Mol Microbiol 72:170–182. https://doi.org/10.1111/j.1365-2958.2009.06632.x.

19. Fenton AK, Gerdes K. 2013. Direct interaction of FtsZ and MreB is required for septum synthesis and cell division in *Escherichia coli*. EMBO J 32: 1953–1965. https://doi.org/10.1038/emboj.2013.129.

20. Yoshii Y, Niki H, Shiomi D. 2019. Division-site localization of RodZ is required for efficient Z ring formation in *Escherichia coli*. Mol Microbiol 111:1229–1244. https://doi.org/10.1111/mmi.14217.

21. van Teeseling MCF. 2021. Elongation at midcell in preparation of cell division requires FtsZ, but not MreB nor PBP2 in *Caulobacter crescentus*. Front Microbiol 12:732031. https://doi.org/10.3389/fmicb.2021.732031.

22. Monteiro JM, Fernandes PB, Vaz F, Pereira AR, Tavares AC, Ferreira MT, Pereira PM, Veiga H, Kuru E, VanNieuwenhze MS, Brun YV, Filipe SR, Pinho MG. 2015. Cell shape dynamics during the staphylococcal cell cycle. Nat Commun 6:8055. https://doi.org/10.1038/ncomms9055.

23. Pinho M, Kjos M, Veening J-W. 2013. How to get (a)round: mechanisms controlling growth and division of coccoid bacteria. Nat Rev Microbiol 11: 601–614. https://doi.org/10.1038/nrmicro3088.

24. Massidda O, Nováková L, Vollmer W. 2013. From models to pathogens: how much have we learned about *Streptococcus pneumoniae* cell division? Environ Microbiol 15:3133–3157. https://doi.org/10.1111/1462-2920.12189.

25. Daniel RA, Errington J. 2003. Control of cell morphogenesis in bacteria: two distinct ways to make a rod-shaped cell. Cell 113:767–776. https://doi.org/10.1016/s0092-8674(03)00421-5.

26. Herrero A, Stavans J, Flores E. 2016. The multicellular nature of filamentous heterocyst-forming cyanobacteria. FEMS Microbiol Rev 40:831–854. https://doi.org/10.1093/femsre/fuw029.

27. Arbel-Goren R, Buonfiglio V, Di Patti F, Camargo S, Zhitnitsky A, Valladares A, Flores E, Herrero A, Fanelli D, Stavans J. 2021. Robust, coherent, and synchronized circadian clock-controlled oscillations along *Anabaena* filaments. Elife 10:e64348. https://doi.org/10.7554/eLife.64348.

28. Arévalo S, Nenninger A, Nieves-Morión M, Herrero A, Mullineaux CV, Flores E. 2021. Coexistence of communicating and noncommunicating cells in the filamentous cyanobacterium *Anabaena*. mSphere 6:e01091-20. https://doi.org/10.1128/mSphere.01091-20.

29. Lehner J, Berendt S, Dörsam B, Pérez R, Forchhammer K, Maldener I. 2013. Prokaryotic multicellularity: a nanopore array for bacterial cell communication. FASEB J 27:2293–2300. https://doi.org/10.1096/fj.12-225854.

30. Velázquez-Suárez C, Luque I, Herrero A. 2020. The inorganic nutrient regime and the *mre* genes regulate cell and filament size and morphology in the phototrophic multicellular bacterium *Anabaena*. mSphere 5:e00747-20. https://doi.org/10.1128/mSphere.00747-20.

31. Hu B, Yang G, Zhao W, Zhang Y, Zhao J. 2007. MreB is important for cell shape but not for chromosome segregation of the filamentous cyanobacterium *Anabaena* sp. PCC 7120. Mol Microbiol 63:1640–1652. https://doi.org/10.1111/j.1365-2958.2007.05618.x.

32. Burnat M, Schleiff E, Flores E. 2014. Cell envelope components influencing filament length in the heterocyst-forming cyanobacterium *Anabaena* sp. Strain PCC 7120. J Bacteriol 196:4026–4035. https://doi.org/10.1128/JB.02128-14.

33. Corrales-Guerrero L, Camargo S, Valladares A, Picossi S, Luque I, Ochoa de Alda JAG, Herrero A. 2018. FtsZ of filamentous, heterocyst-forming cyanobacteria has a conserved N-terminal peptide required for normal FtsZ polymerization and cell division. Frontiers Microbiol 9:2260. https://doi.org/10.3389/fmicb.2018.02260.

34. Camargo S, Picossi S, Corrales-Guerrero L, Valladares A, Arévalo S, Herrero A. 2019. ZipN is an essential FtsZ membrane tether and contributes to the septal localization of SepJ in the filamentous cyanobacterium. *Anabaena* Sci Rep 9:2744. https://doi.org/10.1038/s41598-019-39336-6.

35. Ramos-León F, Mariscal V, Frías JE, Flores E, Herrero A. 2015. Divisome-dependent subcellular localization of cell-cell joining protein SepJ in the

filamentous cyanobacterium *Anabaena*. Mol Microbiol 96:566–580. https://doi.org/10.1111/mmi.12956.

36. Springstein BL, Arévalo S, Helbig AO, Herrero A, Stucken K, Flores E, Dagan T. 2020. A novel septal protein of multicellular heterocystous cyanobacteria is associated with the divisome. Mol Microbiol 113:1140–1154. https://doi.org/10.1111/mmi.14483.

37. Berendt S, Lehner J, Zhang YV, Rasse TM, Forchhammer K, Maldener I. 2012. Cell wall amidase AmiC1 is required for cellular communication and heterocyst development in the cyanobacterium *Anabaena* PCC 7120 but not for filament integrity. J Bacteriol 194:5218–5227. https://doi.org/10.1128/JB.00912-12.

38. Bornikoel J, Carrión A, Fan Q, Flores E, Forchhammer K, Mariscal V, Mullineaux CW, Perez R, Silber N, Wolk PC, Maldener I. 2017. Role of two cell wall amidases in septal junction and nanopore formation in the multicellular cyanobacterium *Anabaena* sp. PCC 7120. Frontiers Cell Infection Microbiol 7:386. https://doi.org/10.3389/fcimb.2017.00386.

39. Zheng Z, Omairi-Nasser A, Li X, Dong C, Lin Y, Haselkorn R, Zhao J. 2017. An amidase is required for proper intercellular communication in the filamentous cyanobacterium *Anabaena* sp. PCC 7120. Proc Nat Acad Sci U S A 114:201621424. https://doi.org/10.1073/pnas.1621424114.

40. Valladares A, Velázquez-Suárez C, Herrero A. 2020. Interactions of PatA with the divisome during heterocyst differentiation. mSphere 5 Issue 5:e00188-20. https://doi.org/10.1128/mSphere.00188-20.

41. Koksharova OA, Wolk CP. 2002. A novel gene that bears a DnaJ motif influences cyanobacterial cell division. J Bacteriol 184:5524–5528. https://doi.org/10.1128/JB.184.19.5524-5528.2002.

42. Leaver M, Errington J. 2005. Roles for MreC and MreD proteins in helical growth of the cylindrical cell wall in *Bacillus subtilis*. Mol Microbiol 57:1196–1209. https://doi.org/10.1111/j.1365-2958.2005.04736.x.

43. Carballido-López R, Errington J. 2003. The bacterial cytoskeleton: in vivo dynamics of the actin-like protein Mbl of *Bacillus subtilis*. Dev Cell 4:19–28. https://doi.org/10.1016/S1534-5807(02)00403-3.

44. Kruse T, Bork-Jensen J, Gerdes K. 2005. The morphogenetic MreBCD proteins of *Escherichia coli* form an essential membrane-bound complex. Mol Microbiol 55:78–89. https://doi.org/10.1111/j.1365-2958.2004.04367.x.

45. Dye N, Pincus Z, Theriot JA, Shapiro L, Gitai Z. 2005. Two independent spiral structures control cell shape in *Caulobacter*. Proc Natl Acad Sci U S A 102:18608–18613. https://doi.org/10.1073/pnas.0507708102.

46. Zhang J-Y, Lin G-M, Xing W-Y, Zhang C-C. 2018. Diversity of growth patterns probed in live cyanobacterial cells using a fluorescent analog of a peptidoglycan precursor. Front Microbiol 9:791. https://doi.org/10.3389/fmicb.2018.00791.

47. Kawazura T, Matsumoto K, Kojima K, Kato F, Kanai T, Niki H, Shiomi D. 2017. Exclusion of assembled MreB by anionic phospholipids at cell poles confers cell polarity for bidirectional growth. Mol Microbiol 104:472–486. https://doi.org/10.1111/mmi.13639.

48. Springstein BL, Weissenbach J, Koch R, Stücker F, Stucken K. 2020. The role of the cytoskeletal proteins MreB and FtsZ in multicellular cyanobacteria. FEBS Open Bio 10:2510–2531. https://doi.org/10.1002/2211-5463.13016.

49. Dai K, Lutkenhaus J. 1991. *ftsZ* is an essential cell division gene in *Escherichia coli*. J Bacteriol 173:3500–3506. https://doi.org/10.1128/jb.173.11.3500-3506.1991.

50. Redick SD, Stricker J, Briscoe G, Erickson HP. 2005. Mutants of FtsZ targeting the protofilament interface: effects on cell division and GTPase activity. J Bacteriol 187:2727–2736. https://doi.org/10.1128/JB.187.8.2727-2736.2005.

51. Rippka R, Deruelles J, Waterbury JB, Herdman M, Stanier RY. 1979. Generic assignments, strain histories and properties of pure cultures of cyanobacteria. J Gen Microbiol 111:1–61. https://doi.org/10.1099/00221287-111-1-1.

52. Mackinney G. 1941. Absorption of light by chlorophyll solutions. J Biol Chem 140:109–112.

53. Flores E, Wolk CP. 1985. Identification of facultatively heterotrophic, N_2-fixing cyanobacteria able to receive plasmid vectors from *Escherichia coli* by conjugation. J Bacteriol 162:1339–1341. https://doi.org/10.1128/jb.162.3.1339-1341.1985.

54. Rubio MA, Napolitano M, Ochoa de Alda JAG, Santamaría-Gómez J, Patterson CJ, Foster AW, Bru-Martínez R, Robinson NJ, Luque I. 2015. Trans-oligomerization of duplicated aminoacyl-tRNA synthetases maintains the genetic code fidelity under stress. Nucleic Acids Res 43:9905–9917. https://doi.org/10.1093/nar/gkv1020.

55. Corrales-Guerrero L, Flores E, Herrero A. 2014. Relationships between the ABC-exporter HetC and peptides that regulate the spatiotemporal pattern of heterocyst distribution in *Anabaena*. PLoS One 9:e104571. https://doi.org/10.1371/journal.pone.0104571.

56. Black TA, Cai Y, Wolk CP. 1993. Spatial expression and autoregulation of *hetR*, a gene involved in the control of heterocyst development in *Anabaena*. Mol Microbiol 9:77–84. https://doi.org/10.1111/j.1365-2958.1993.tb01670.x.

57. Valladares A, Rodríguez V, Camargo S, Martínez-Noël GMA, Herrero A, Luque I. 2011. Specific role of the cyanobacterial PipX factor in heterocysts of *Anabaena* sp. strain PCC 7120. J Bacteriol 193:1172–1182. https://doi.org/10.1128/JB.01202-10.

58. Elhai J, Wolk CP. 1988. A versatile class of positive-selection vectors based on the nonviability of palindrome-containing plasmids that allows cloning into long polylinkers. Gene 68:119–138. https://doi.org/10.1016/0378-1119(88)90605-1.

59. Cai YP, Wolk CP. 1990. Use of a conditionally lethal gene in *Anabaena* sp. strain PCC 7120 to select for double recombinants and to entrap insertion sequences. J Bacteriol 172:3138–3145. https://doi.org/10.1128/jb.172.6.3138-3145.1990.

60. Schneider CA, Rasband WS, Eliceiri KW. 2012. NIH Image to ImageJ: 25 years of image analysis. Nat Methods 9:671–675. https://doi.org/10.1038/nmeth.2089.

61. Karimova G, Dautin N, Ladant D. 2005. Interaction network among *Escherichia coli* membrane proteins involved in cell division as revealed by bacterial two-hybrid analysis. J Bacteriol 187:2233–2243. https://doi.org/10.1128/JB.187.7.2233-2243.2005.

Supplemental Material

Dataset S1 (Excel file) is available at https://journals.asm.org/doi/10.1128/mbio.01165-22
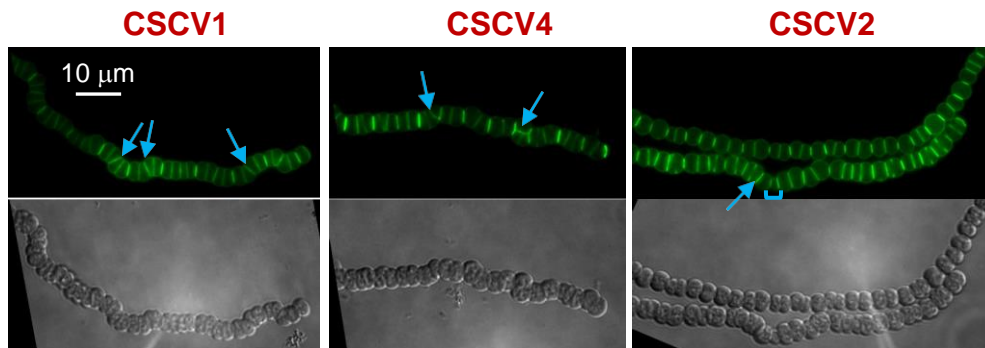
FIG S1 Van-FL staining of *Anabaena mreB, mreC* and *mreD* mutants. Filaments of strains CSCV1 (*mreB*), CSCV4 (*mreC*) and CSCV2 (*mreD*) grown in solid BG11 medium were stained with Van-FL and observed under a fluorescence microscope and photographed. Van-FL fluorescence (green) and bright-field images are shown. Arrows point to tilted fluorescent bands, and brackets to cell compartments with disparate sizes. Magnification is the same for all micrographs.

Table S1. Cyanobacterial strains and plasmids used in this work

Strain	Genotype	Resistance	Source
Anabaena sp. PCC 7120	WT		Pasteur Culture Collection
CSCV1	*mreB*::C.K1	Nm	30
CSCV2	*mreD*::C.S3	Sm, Sp	30
CSCV4	*mreC*::C.K1	Nm	30
CSCV5	*thrS2*::P$_{mreB}$-*sfgfp*		This study
CSCV6	*thrS2*::P$_{mreB}$-*sfgfp-mreB*	Sm, Sp	This study
CSCV7	*thrS2*::P$_{mreB}$-*sfgfp-mreC*	Sm, Sp	This study
CSCV8	*thrS2*::P$_{mreB}$-*sfgfp-mreD*	Sm, Sp	This study
CSSC19	P$_{ftsZ}$-*ftsZ-gfpmut2*	Sm, Sp	33
CSCV20	P$_{ftsZ}$-*ftsZ-gfpmut2*, *mreB*	Nm, Sm, Sp	This study
CSCV21	P$_{ftsZ}$-*ftsZ-gfpmut2*, *mreC*	Nm, Sm, Sp	This study
CSCV22	P$_{ftsZ}$-*ftsZ-gfpmut2*, *mreD*	Nm, Sm, Sp	This study
CSAV39	P$_{zipN}$-*sfgfp-zipN*	Sm, Sp	40
CSCV14	P$_{zipN}$-*sfgfp-zipN*, *mreB*	Nm, Sm, Sp	This study
CSCV15	P$_{zipN}$-*sfgfp-zipN*, *mreC*	Nm, Sm, Sp	This study
CSCV16	P$_{zipN}$-*sfgfp-zipN*, *mreD*	Nm, Sm, Sp	This study
CSFR18	P$_{ND}$-*ftsZ*	Sm, Sp	35
CSL109	P$_{ND}$-*zipN*	Sm, Sp	34

Plasmid	Description	Resistance marker	Source
pCSAV285	pCSV3 carrying P$_{zipN}$-*sfgfp-zipN*)	Sm, Sp	30
pCSCV10	pRL277 carrying *thrS2*::P$_{mreB}$-*sfgfp*	Sm, Sp	This study
pCSCV11	pCSV3 carrying *thrS2*::P$_{mreB}$-*sfgfp-mreB*	Sm, Sp	This study
pCSCV12	pCSV3 carrying *thrS2*::P$_{mreB}$-*sfgfp-mreC*	Sm, Sp	This study
pCSCV13	pCSV3 carrying *thrS2*::P$_{mreB}$-*sfgfp-mreD*	Sm, Sp	This study
pCSCV37	pRL424 carrying P$_{zipN}$-*sfgfp-zipN*	Km, Nm	This study
pCSCV39	pRL278 carrying P$_{ftsZ}$-*ftsZ-mut2gfp*	Km, Nm	This study
pCSSC39	pRL277 carrying P$_{ftsZ}$-*ftsZ-mut2gfp*	Sm, Sp	33

TABLE S2. Oligodeoxynucleotide primes used in this work

Name	Sequence (5'-3')
all0085-8	GGTGGAGGTGGAGGTATGCCTTTGTCGCGTTGG
all0085-9	GAGCTGGATCCCTAACTTTCCAACATCTTC[a]
all0085-12	TCCGCTGCAGACCTTTGTCGCGTTGGCATC
all0085-13	GCTTGAATTCATACTTTCCAACATCTTCATTC
all0086-13	GGTGGAGGTGGAGGTATGGTTACTGTACGTCGTTG
all0086-14	TTCCGGATCCTCTAGTTGGACTTTTGTTGC
all0086-17	ATAGGTCTGCAGGGTTACTGTACGTCGTTG
all0086-18	AGATTTGAATTCAATCTAGTTGGACTTTTG
all0086-19	AATAGGCTGCAGTGGTTACTGTACGTCGTT
all0087-10	ATATACCTGCAGGGCTTTTTAGGAACTTTCGC
all0087-11	CTGCGAGAATTCCTACATATTTCGAGATCGTC
all0087-12	ACTCAGCTGCAGGGGGGCTTTTTAGGAACTTTCG
all0087-13	CGCCGTGAATTCATATTTCGAGATCGTCC
all0087-20	TCTGATGCATCCTTTAGTACATAAG
all0087-21	CTTTGCTCATGCGTCTCTATGCCCCCTATT
all0087-22	GGTGGAGGTGGAGGTGTGGGGCTTTTTAGGAAC
all0087-23	ATTTGGATCCCTACATATTTCGAGATCGTC
all0154-11b	GTAATGCTGCAGGAAGCTACGCAGCCTAATTCC
all0154-13	ACTGTTGAATTCTTAAACATCCGCCGACGTTG
alr0653-1	CAACTCCTGCAGGGTTATTAAAACGATCGCTTC
alr0653-2	GATGACGAATTCTAGTGGTTGGTGGTCAGT
alr0653-3	CAAAACTGCAGCTTATTAAAACGATCGCTTC
alr0653-4	GAAAGTGAATTCGTAAAATAATATTTCTGTCGTTGTC
all1616-4	GCTAGGCTGCAGGCGATGGGTCGATGATTC
all1616-5	CTTCTGGAATTCATCATTAGGAATTTTCGT
alr1706-2	ATCCCTGAATTCTTACGATATAATCTACCATC
alr1706-4	TACCAGCTGCAGGGTGCAGTTAAATGG
all4723-3	TAGTATGCATGAGGAAGCTGGCGGTGG
all4723-4	ATAAATGCATTGTAGTTGGGGCTTGC
alr5045-7	TTTAAGCTGCAGGGCTTTACTGCAACCATC
alr5045-8	TATTTAGAATTCATATTATCTGCTTTTTGC
alr5045-9	CTTTAACTGCAGTGGCTTTACTGCAACCAT
all7666-2	AAAGGCGAATTCAGTTCAAATATCATCTTCAC
all7666-3	GAGAAACTGCAGATTAGAAATGTATATTAATAACAAC
all7666-4	GCATGGGAATTCCGAATATCATCTTCACC
SF-GFP-F	ACGTAGATCTATGAGCAAAGGAGAAGAACTTTTC
SF-GFP-R	ACCTCCACCTCCACCTTTGTAGAGCTCATCCATGCC
SF-GFP-F2	ATAGAGACGCATGAGCAAAGGAGAAGAACT
SF-GFP-R2	ACGTATGCATTTATTTGTAGAGCTCATCCATG

[a]The underlined letters indicated a restriction site.

CHAPTER III: The role of MreB, MreC and MreD in the morphology of the diazotrophic filament of *Anabaena* sp. PCC 7120

The Role of MreB, MreC and MreD in the Morphology of the Diazotrophic Filament of *Anabaena* sp. PCC 7120

Cristina Velázquez-Suárez, Ignacio Luque [ID] and Antonia Herrero *

Instituto de Bioquímica Vegetal y Fotosíntesis, CSIC and Universidad de Sevilla, 41092 Seville, Spain
* Correspondence: herrero@ibvf.csic.es

Abstract: The cyanobacterium *Anabaena* sp. PCC 7120 forms filaments of communicating cells. Under conditions of nitrogen scarcity, some cells differentiate into heterocysts, allowing the oxygen-sensitive N_2-reduction system to be expressed and operated in oxic environments. The key to diazotrophic growth is the exchange of molecules with nutritional and signaling functions between the two types of cells of the filament. During heterocyst differentiation, the peptidoglycan sacculus grows to allow cell enlargement, and the intercellular septa are rebuilt to narrow the contact surface with neighboring cells and to hold specific transport systems, including the septal junction complexes for intercellular molecular transfer, which traverse the periplasm between heterocysts and neighboring vegetative cells through peptidoglycan nanopores. Here we have followed the spatiotemporal pattern of peptidoglycan incorporation during heterocyst differentiation by Van-FL labeling and the localization and role of proteins MreB, MreC and MreD. We observed strong transitory incorporation of peptidoglycan in the periphery and septa of proheterocysts and a maintained focal activity in the center of mature septa. During differentiation, MreB, MreC and MreD localized throughout the cell periphery and at the cell poles. In *mreB*, *mreC* or *mreD* mutants, instances of strongly increased peripheral and septal peptidoglycan incorporation were detected, as were also heterocysts with aberrant polar morphology, even producing filament breakage, frequently lacking the septal protein SepJ. These results suggest a role of Mre proteins in the regulation of peptidoglycan growth and the formation of the heterocyst neck during differentiation, as well as in the maintenance of polar structures for intercellular communication in the mature heterocyst. Finally, as previously observed in filaments growing with combined nitrogen, in the vegetative cells of diazotrophic filaments, the lack of MreB, MreC or MreD led to altered localization of septal peptidoglycan-growth bands reproducing an altered localization of FtsZ and ZipN rings during cell division.

Keywords: heterocyst differentiation; heterocyst neck; intercellular communication; Mre proteins; peripheral peptidoglycan growth; polar peptidoglycan growth

1. Introduction

Filamentous heterocyst-forming cyanobacteria, such as the model strain *Anabaena* sp. PCC 7120 (hereafter *Anabaena*) represents genuine pluricellular bacteria in which the unit for selection has shifted from the single cell to the filament [1,2]. The *Anabaena* filament is composed of hundreds of cells, each of which is surrounded by an individual cytoplasmic membrane, whereas the outer membrane is continuous along the filament, defining a commonly shared periplasm. Indeed, the continuous periplasm has been considered a path that allows intercellular molecular exchange through the filament [3]. In addition, neighboring cells are communicated through *septal junction* complexes composed of polytopic cytoplasmic-membrane anchored proteins [4,5] that traverse the septal peptidoglycan (PG) by perforations termed nanopores, which are drilled by PG amidases [6–8].

Regarding the PG sacculus, the continuous filament periplasm contains a single molecule that completely encircles each cell and is engrossed in the septal location between contiguous cells [9]. In relation to its multicellular structure, *Anabaena* presents distinct

characteristics in the pattern of PG incorporation. During cell division, septal incorporation occurs in the divisome to build the new septa of the resulting daughter cells. In addition, weak peripheral PG growth elongates the cells during cell growth, and continuous PG incorporation occurs in the intercellular locations along the filament, which persists after the division has been completed [10–12]. In model unicellular rod-shaped bacteria, the proteins MreB, MreC and MreD are involved in the spatial localization and regulation of the enzymatic machinery for lateral PG growth organized in the multiprotein complex termed the elongasome. MreB is an actin structural homolog that forms dynamic polymers associated with the inner face of the cytoplasmic membrane. MreC is a cytoplasmic membrane-anchored protein with most of its extension residing in the periplasm, and MreD is an integral membrane protein [13]. Notably, in *Anabaena*, MreB, MreC and MreD have been localized all around the cell periphery, including the mature intercellular septa, and in the divisome through all stages of cell division, having been implicated in the regulation of peripheral, medial (divisome-associated) and septal PG incorporation [10].

Depending on environmental conditions, the *Anabaena* filament can include different cell types specialized in specific functions. Thus, heterocysts are cells specialized in the fixation of atmospheric nitrogen that differentiates at semi-regular intervals along the filament under nitrogen deprivation conditions. Heterocysts supply vegetative cells with organic nitrogen. Vegetative cells fix CO_2 through oxygenic photosynthesis and provide the heterocysts with organic carbon to be utilized as a source of reductants and as carbon skeletons for the incorporation of the ammonium resulting from N_2 fixation [14,15].

Because the enzymatic machinery for N_2 reduction to ammonium is extremely O_2 sensitive, a main issue in heterocyst performance is the maintenance of a microoxic internal milieu, to which the presence of extra glycolipid and polysaccharide envelope layers, deposited during the differentiation process, contribute (see [16]). However, the entrance of N_2 into the heterocysts is needed. Key to regulating gas exchanges is the differentiation of the heterocyst cell poles to form the specialized structure known as the heterocyst neck, which narrows the contact space between the heterocyst and the adjacent vegetative cells and represents the main path for gas exchange [14,17]. Indeed, intercellular molecular exchange involving heterocysts is thought to take place to a good extent through the heterocyst neck. Thus, although some membrane transporters of different protein families are localized through the heterocyst periphery, some others, such as the ABC-type exporters HetC, possibly involved in the export of morphogens from the heterocyst [18,19], and DevBCD-HgdD, for heterocyst glycolipid export [20], preferentially localize at the heterocyst poles. Additionally, the pentapeptide-repeat protein HglK [21] and the septal-junction associated proteins SepJ [22] and FraCD [23] are localized to the heterocyst-vegetative cell septa. Finally, the ABC-permease protein FraE [24] and the TonB-like protein SjdR [25] have been identified as required for the constriction and arrangement of the heterocyst polar structures.

Besides peripheral PG growth required for cell enlargement, the differentiation of the heterocyst neck also appears to involve PG remodeling/turnover see [11]. Consistent with this, mutations in genes encoding enzymes involved in different steps of PG synthesis lead to impaired heterocyst differentiation [26–29]. Moreover, PG septal disk diameter, nanopore diameter and nanopore number are larger in septa between vegetative cells and heterocysts than in septa between two vegetative cells [24], and mutants deficient in the PG amidases AmiC1 [7] or AmiC3 [8] are unable of diazotrophic growth.

In this work, we have monitored the incorporation of PG and the localization of the MreB, MreC and MreD proteins in *Anabaena* during heterocyst differentiation and in mature diazotrophic filaments. We have also addressed the influence of MreB, MreC and MreD on peripheral, medial and septal PG growth, the filament geometry and the formation of heterocyst-vegetative cell connections.

2. Materials and Methods

2.1. Strains and Growth Conditions

Anabaena sp. strain PCC 7120 and mutant strains (strains and plasmids used in this work are listed in Table S1) were grown in BG11 medium (containing $NaNO_3$ as a nitrogen source) [30] containing ferric citrate instead of ferric-ammonium citrate. Cultures were incubated at 30 °C with illumination (12 $\mu E\ m^{-2}\ s^{-1}$ white light from Osram LED lamps 16.4 W/4000 K), in Erlenmeyer flasks with shaking (100 rpm) or in plates of medium solidified with 1% Difco agar. For the mutants, media were supplemented with antibiotics: spectinomycin dihydrochloride pentahydrate (Sp) and streptomycin sulfate (Sm) at 5 $\mu g\ mL^{-1}$ each in solid medium or 2.5 $\mu g\ mL^{-1}$ each in liquid medium (CSCV2, CSCV6, CSCV7, CSCV8, CSSC19, CSAV39), with neomycin sulfate (Nm) at 25 $\mu g\ mL^{-1}$ in solid medium or 5 $\mu g\ mL^{-1}$ in liquid medium (CSS89, CSCV1, CSCV4), or with Sm, Sp and Nm (CSCV14, CSCV15, CSCV16, CSCV17, CSCV18, CSCV19, CSCV20, CSCV21, CSCV22). For the experiments described in this work, BG11-grown filaments of the indicated strains were transferred to (at a cell density corresponding to 0.5 μg chlorophyll mL^{-1}) and incubated in $BG11_0$ medium [30] lacking $NaNO_3$ and antibiotics. Chlorophyll *a* (Chl) content of the cultures was determined after extraction with methanol [31]. In *Anabaena*, 1 μg Chl corresponds to ca. 3.3×10^6 cells [32].

2.2. Strain Constructions

Strains CSCV17, CSCV18 and CSCV19 bear a *sepJ-gfpmut2* fusion gene in a *mreB*, *mreC* or *mreD* mutant background, respectively. To generate strain CSCV19, the conjugative plasmid pCSVT22 (encoding Nm resistance and including sequences of the 3′ part of *Anabaena sepJ* fused to *gfpmut2*) [23] was transferred to strain CSCV2 (*mreD*) by conjugation, and one clone in which the plasmid was inserted by single cross-over into *sepJ* was selected and verified by PCR. To generate strains CSCV17 and CSCV18, the insert of pCSVT22 was amplified with oligonucleotides alr2338-BamH1 and gfp-BamH1 (listed in Table S1) and cloned in the conjugative vector pCSV3 encoding Sm/Sp resistance [33] generating plasmid pCSCV38, which was transferred to strains CSCV1 (*mreB*) and CSCV4 (*mreC*) by conjugation. Clones in which pCSCV38 was inserted by single cross-over into *sepJ* were selected and verified by PCR.

2.3. Microscopy

For Van-FL labeling and detection, filaments were treated as described [10] and visualized with a Leica DM6000B fluorescence microscope and a FITCL5 filter (excitation band-pass, 480/40; emission band-pass, 527/30), and photographed with an ORCA-ER camera (*Hamamatsu*). GFP fluorescence was monitored with an Olympus TCS SP2 confocal laser-scanning microscope equipped with an HCX PLAN-APO 63x 1.4 NA oil immersion objective (excitation, 488-nm; collection, 500–540 nm for GFP or 630–700 nm for cyanobacterial autofluorescence) or with an Olympus FLUOVIEW FV3000 (hyper-resolution) confocal laser-scanning microscope equipped with a UPlanApo 60x1.5 NA oil immersion objective (excitation, 488-nm; collection 500–540 nm for GFP or excitation, 640 nm; collection, 650–750 nm for cyanobacterial autofluorescence).

3. Results

3.1. PG Growth during Heterocyst Differentiation in Anabaena

Van-FL is a fluorescent derivative of the antibiotic vancomycin that binds to the PG precursor Lipid II in the periplasm, either bound or not to the sacculus but not involved in crosslinking, thus providing a probe for nascent PG synthesis [34]. We used Van-FL to label *Anabaena* filaments during heterocyst differentiation upon transfer of filaments grown in BG11 medium (containing nitrate) to $BG11_0$ medium lacking combined nitrogen. The differentiation process can be followed through a succession of cellular signals that include progressive loss of red fluorescence due to photosynthetic pigment rearrangement, cell elongation and enlargement, deposition of extracellular envelope layers, and finally,

accumulation in refringent polar granules of cyanophycin resulting from N_2 fixation. In the differentiating cells, the localization of Van-FL fluorescence appeared to follow a sequence through the different stages of the differentiation process (Figure 1). Thus, at early stages (cells already enlarged but with no conspicuous change in morphology and still detectable red fluorescence), Van-FL fluorescence was detected as a homogenous peripheral signal and in foci localized in the heterocyst neck. In the neighboring vegetative cells, fluorescence was detected at the pole contiguous to the differentiating heterocyst (see the second row in Figure 1; see also [35]). Afterward, concomitant with morphological reshaping and red-fluorescence loss, the peripheral signal in the differentiating cells appeared more pronounced, especially in the polar regions. Moreover, a strong label was detected in the pole proximal to the heterocyst of the neighboring vegetative cells (see the third row in Figure 1). Later, in mature heterocysts (showing conspicuous polar granules), the peripheral signal faded, and fluorescence was more restricted to foci in the center of the heterocyst poles and the neighboring vegetative cell pole (see the fourth row in Figure 1). These observations suggest that during heterocyst differentiation, a phase of peripheral PG growth occurs at intermediate stages of differentiation (as previously noted [11]), being this a transient event. In addition, continuous activity of PG remodeling appears to be maintained at the poles of heterocysts and neighboring vegetative cell poles.
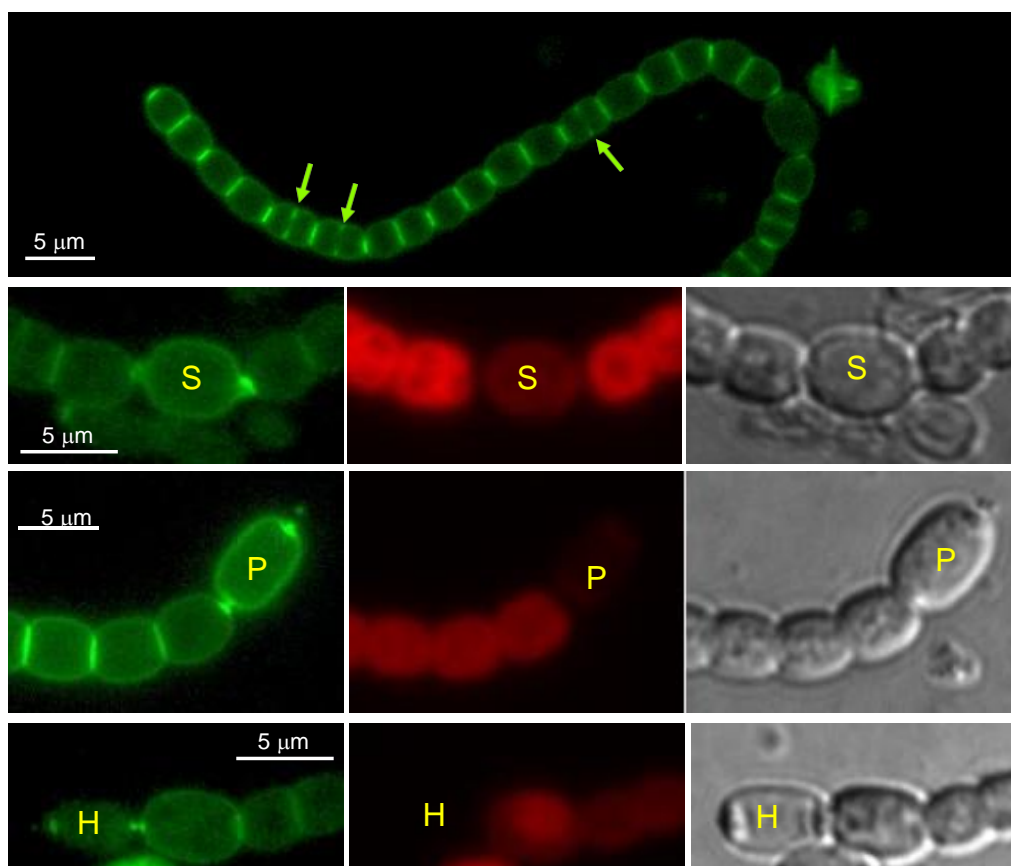
Figure 1. Van-FL staining of filaments of *Anabaena* sp. strain PCC 7120 during heterocyst differentiation. Filaments grown in BG11 medium were transferred to $BG11_0$ (lacking combined nitrogen) medium and incubated under culture conditions. After 24 (row 2) or 48 h (rows 1, 3 and 4), samples were stained with Van-FL and observed under a fluorescence microscope and photographed. Van-FL fluorescence (green), cyanobacterial autofluorescence (red), and bright-field images are shown. Cells in early stages of differentiation (S), immature heterocysts (P) and mature heterocysts exhibiting polar refringent cyanophycin granules (H) (see the text for details) are indicated. Green arrows in row 1 point to fluorescence matching the divisome complex.

Regarding the vegetative cells of filaments incubated in BG11$_0$ medium, continuous peripheral Van-FL fluorescence and strong fluorescence bands in the intercellular regions, reminiscent of the pattern found in filaments growing with combined nitrogen [10], were observed (first row in Figure 1). As in the latter, in actively-growing diazotrophic filaments, the septal bands alternate in intensity, with the intensity detected in the recently formed septa being lower than in the older septa. Additionally, midcell fluorescence progressing inwards from the cell surface, matching the progressing septum under construction, could be detected in dividing cells.

3.2. Localization of MreB, MreC and MreD during Heterocyst Differentiation

We studied the localization of MreB, MreC and MreD in filaments of *Anabaena* subjected to N-stepdown using protein fusions to GFP. For that, we used the previously generated strains CSCV6, CSCV7 and CSCV8 that express the genes *sfgfp-mreB*, *sfgfp-mreC* or *sfgfp-mreD* (encoding superfolder GFP fused to MreB, MreC or MreD, respectively) preceded by the native promoter of the *mreBCD* operon, located on an ectopic chromosomal locus, keeping an intact *mreBCD* operon in its native genomic location [10]. GFP fluorescence was monitored in filaments of CSCV6, CSCV7 and CSCV8 grown with nitrate and transferred to a medium lacking combined nitrogen. In the three strains, fluorescence was localized over the periphery of cells in the early stages of differentiation, as well as of immature and mature heterocysts (exhibiting complete loss of red fluorescence and conspicuous polar granules) (Figure 2), and tended to become more diffuse in older heterocysts (not shown). GFP fluorescence could also be detected frequently as foci in the heterocyst poles (Figure 2A; see CSCV8 in Figure 2B).
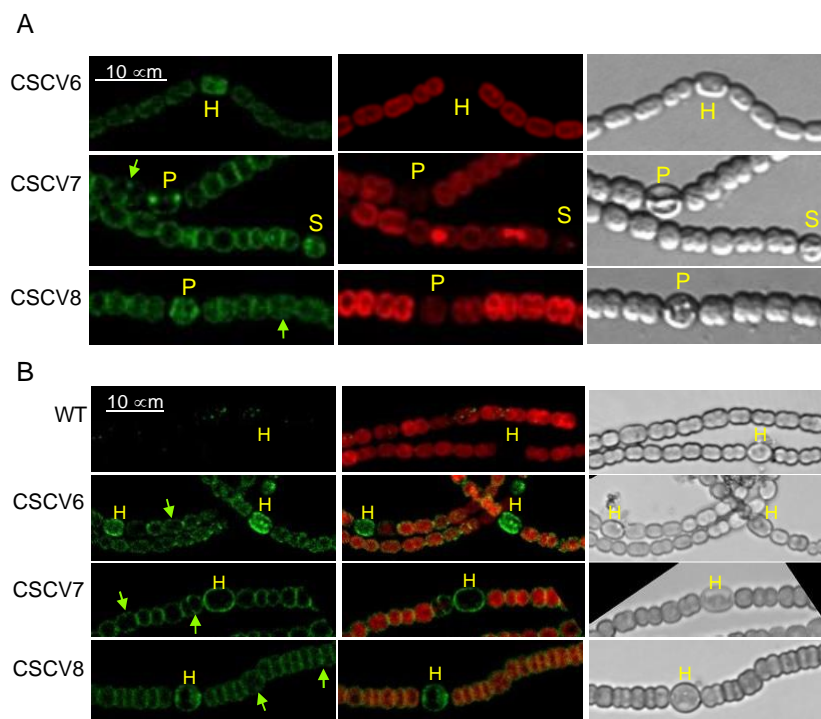
Figure 2. Localization of MreB, MreC and MreD in *Anabaena*. Strain PCC 7120 and their derivatives CSCV6 (sfGFP-MreB), CSCV7 (sfGFP-MreC) and CSCV8 (sf-GFP-MreD) were grown in BG11 medium, transferred to BG11$_0$ medium and incubated under culture conditions. After 24 h, filaments were visualized by confocal microscopy with TCS (**A**) or FLUOVIEW (**B**) equipment. GFP fluorescence (green), cyanobacterial autofluorescence (red), merged GFP and cyanobacterial autofluorescence, and bright-field images are shown. Cells in early stages of differentiation (S), immature heterocysts (P) and mature heterocysts (H) are indicated. Green arrows point to GFP fluorescence matching divisome complexes. Magnification is the same for all micrographs in (**A**) or (**B**).

In the vegetative cells of strains CSCV6, CSCV7 and CSCV8, GFP fluorescence could also be detected in the cell periphery during active growth, and at midcell in signals progressing inwards from the periphery in the dividing cells (Figure 2). As previously noted [10], especially cells of CSCV7 and CSCV8 appeared bigger and rounder than those of the wild type. This could indicate some interference of the fusion proteins with the function of the corresponding native proteins. Nonetheless, the GFP fluorescence localization's specificity and consistency with the signals produced by GFP-MreB (in CSCV6) support that GFP-MreC and GFP-MreD are reporting the physiological localization of MreC and MreD, respectively.

3.3. Influence of MreB, MreC and MreD in PG Growth during Heterocyst Differentiation

Strains CSCV1, CSCV4 and CSCV2 contain only inactivated versions of *mreB*, *mreC*, or *mreD*, respectively. These mutants show strong morphological alterations, forming cells, including heterocysts, that are larger and rounder than wild-type cells [36]. Van-FL staining was performed in filaments of strains CSCV1, CSCV4 and CSCV2 grown with nitrate and incubated in the absence of combined nitrogen. Fluorescence localization was compared to the wild-type (shown in Figure 1). Regarding fluorescence distribution in differentiating cells, some heterocysts with peripheral fluorescence and septal foci could be detected in CSCV1 (see the second row in Figure 3), CSCV4 (see first and the second row in Figure 4) and CSCV2 (see the second row in Figure 5). However, instances of deformed septal fluorescence distribution or aberrantly increased labeling were also found (see the third row in Figure 3, for CSCV1, and the third row in Figure 5, for CSCV2). In the three mutants, but especially in CSCV4, few mature heterocysts with conspicuous polar granules were detected after 48 h of incubation in the absence of combined nitrogen, consistent with the previous description of retarded expression of nitrogenase activity [36]. Frequently, heterocysts with conspicuous peripheral labeling could still be detected at 48 h (see the fourth row in Figure 3 for CSCV1 and Figure 5 for CSCV2).
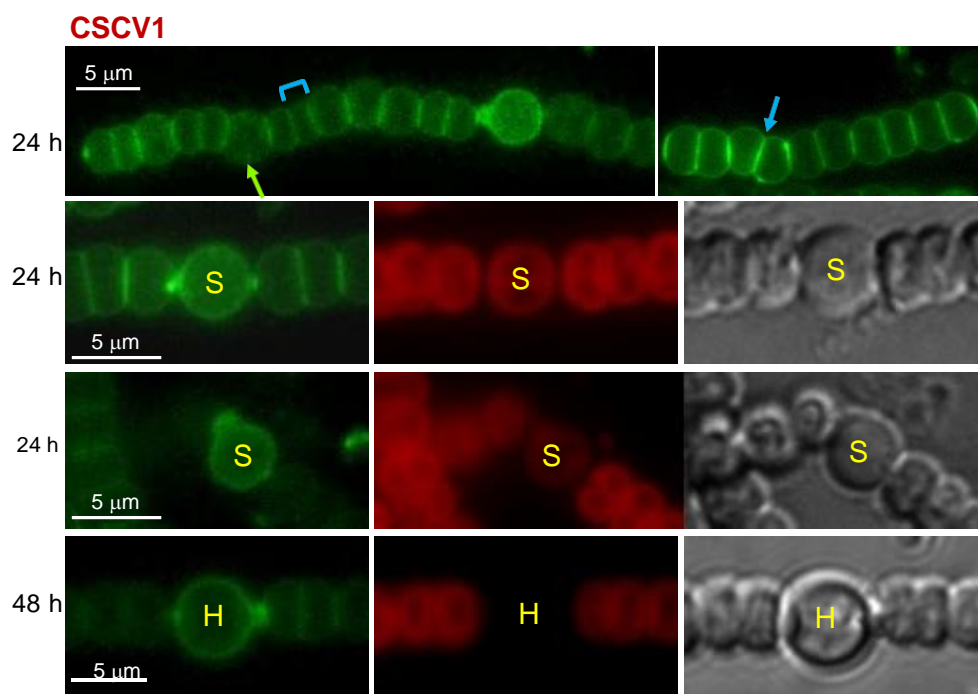
Figure 3. Van-FL staining of *Anabaena mreB* mutant. Strain CSCV1 (*mreB*) was treated under the same conditions described for the WT (PCC 7120) in Figure 1. Van-FL fluorescence (green), cyanobacterial autofluorescence (red) and bright-field images are shown. To improve visibility, contrast/brightness is different for the image at left in row 1. The bracket indicates a cell compartment with disparate size; the blue arrow points to a tilted fluorescent band and the green arrow to fluorescence matching the divisome. Cells in the early stages of differentiation (S) and mature heterocysts (H) are indicated.
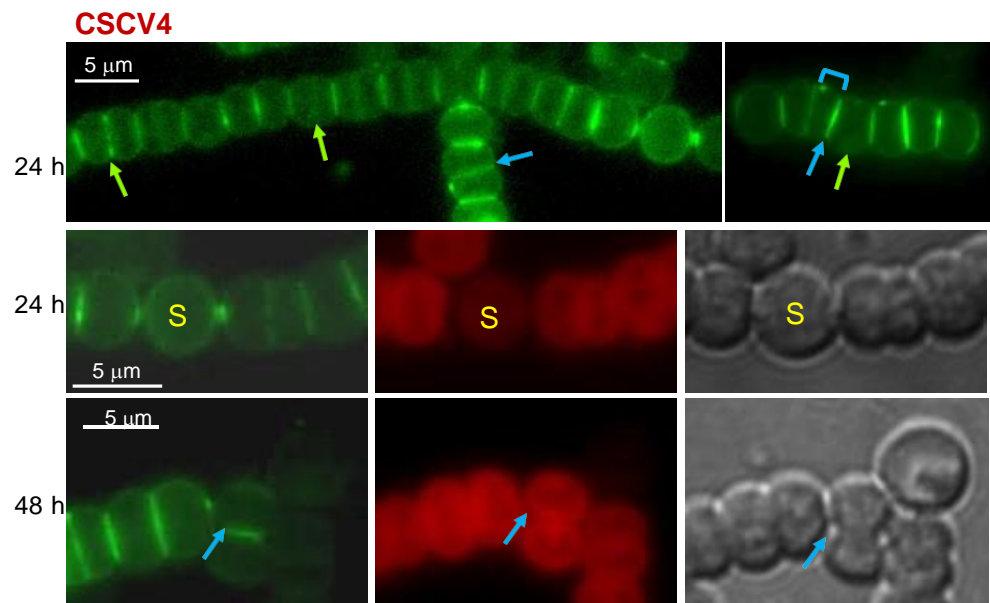
CSCV4

Figure 4. Van-FL staining of *Anabaena mreC* mutant strain CSCV4. See the legend in Figure 3 for details. To improve visibility, contrast/brightness is different for the image at left in row 1.
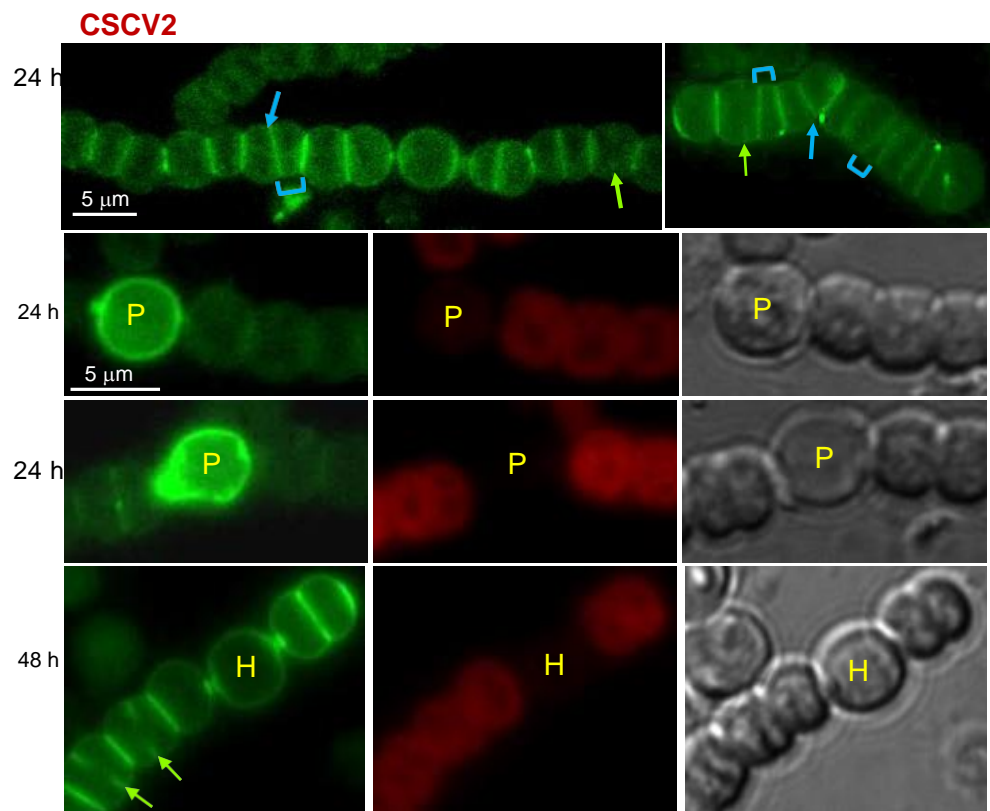
CSCV2

Figure 5. Van-FL staining of *Anabaena mreD* mutant strain CSCV2. See the legend in Figure 3 for details. Immature heterocysts (P) and mature heterocysts (H) are indicated. To improve visibility, contrast/brightness differs for the images in row 1.

In vegetative cells (see the first row in Figures 3–5), the three mutants showed peripheral, septal and midcell Van-FL labeling. However, the consecutive septal bands appeared frequently tilted with regard to each other or at irregular distances from each other (compare first rows in Figures 1 and 3–5). Inspection of 100 to 120 septal bands of each PCC 7120, CSCV1, CSCV4 and CSCV2 incubated for 24 and 48 h in $BG11_0$ medium showed

that, in the mutants, 29–40% septal bands appeared conspicuously tilted with regard to a consecutive band. In the wild type, 95–98% appeared parallel to its consecutive band (Mann–Whitney tests indicated fully significant differences, $p < 0.001$, for any comparison between a mutant and the WT, and no significant differences between the mutants). CSCV4 even showed some instances where the division plane appeared inverted (see row 3 in Figure 4). In addition, abundant cell debris from cell lysis was observed especially in CSCV1 and CSCV4.

3.4. Localization of FtsZ and ZipN in Mre Mutants

Because heterocyst differentiation is linked to inhibition of cell division (see [15]) and because, as shown above, MreB, MreC and MreD are also localized to the divisome, we asked whether the Mre proteins affected the localization of FtsZ and ZipN during the differentiation process. FtsZ initiates the polymerization of the division ring (see [37]), and ZipN is the main tether for binding FtsZ to the cytoplasmic membrane and organizer of the divisome in *Anabaena* [38]. We monitored FtsZ localization using strains that express an *ftsZ-gfp* reporter from the P*ftsZ* promoter in the WT background (strain CSSC19 [37]) and in the *mreB* (strain CSCV20), *mreC* (strain CSCV21) and *mreD* (strain CSCV22) mutant backgrounds [10].

Upon N-stepdown, fluorescent FtsZ-rings could be detected in vegetative cells of filaments of all strains (Figure 6). However, in the mutant backgrounds, some rings were tilted compared to those of neighboring cells, and in some places, the distance between two consecutive Z-rings was irregular. In the differentiating cells described for strain CSSC19 (39), Z-rings were detected during differentiation but not in mature heterocysts. CSSC19 mostly exhibited mature heterocysts 48 h after N-stepdown, whereas in CSCV20, CSCV21 and CSCV22, cells exhibiting fluorescent rings were still abundant at that time, consistent with retardation of heterocyst differentiation. Of note is the observation of some aberrant events in CSCV20, such as the differentiation of consecutive cells (see third and fourth rows in Figure 6), which is very rare in the wild type, or the presence of a Z-ring (see the seventh row in Figure 6) or apparent septation (see the third row in Figure 6) in mature heterocysts.

The effect of the lack of MreB, MreC or MreD on the localization of ZipN was studied in strains that express an *sfgfp-zipN* reporter gene from the P*zipN* promoter in the WT background (strain CSAV39 [39]) and the *mreB* (strain CSCV14), *mreC* (strain CSCV15) and *mreD* (strain CSCV16) mutant backgrounds [10].

Upon N-stepdown, strain CSAV39 presented midcell fluorescent bands in vegetative cells, and this signal was progressively lost in the differentiating cells, being absent in mature heterocysts (Figure 7; [39]). In CSCV14, CSCV15 and CSCV16, the midcell GFP-ZipN fluorescence was also lost in most mature heterocysts, although in some of them, some signals could still be detected (see the heterocyst in the seventh row in Figure 7 for CSCV16). In the three mutant backgrounds, but especially in CSCV15, fluorescence appeared more dispersed than in the wild-type background (strain CSAV39). Of note is the observation that in the three mutant backgrounds some heterocysts deviated from the filament longitudinal plane. Moreover, in CSCV14 and CSCV16, heterocysts with aberrant polar morphology even provoking filament breakage were observed (Figure 7).
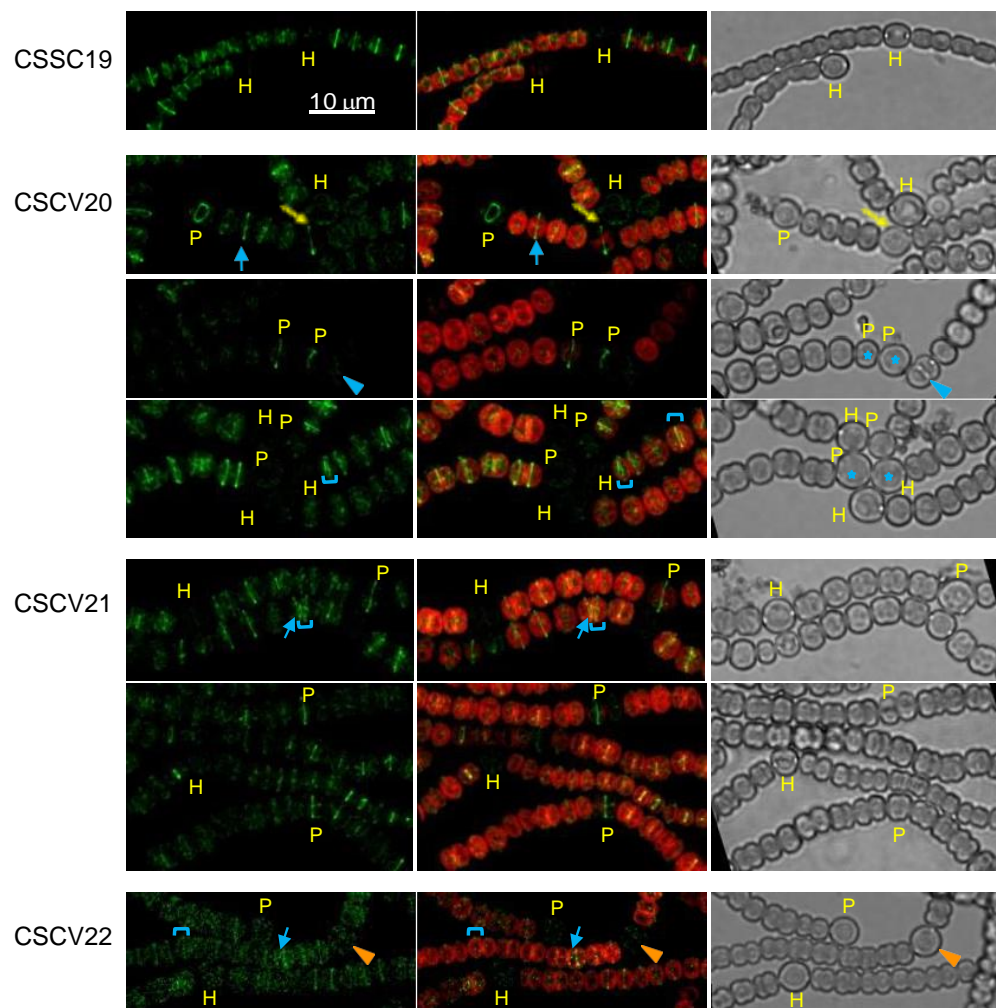
Figure 6. Localization of FtsZ in *mreB*, *mreC* and *mreD* mutants. Strains CSSC19 (*ftsZ-gfpmut2* in WT background), CSCV20 (*ftsZ-gfpmut2* in CSCV1 background), CSCV21 (*ftsZ-gfpmut2* in CSCV4 background) and CSCV22 (*ftsZ-gfpmut2* in CSCV2 background) were treated as above described for Figure 2. After 48 h, filaments were visualized by confocal microscopy with FLUOVIEW equipment. GFP fluorescence (green), merged GFP and cyanobacterial autofluorescence (red), and bright-field images are shown. To improve visibility, contrast is higher for the green image of CSCV22. Blue arrows point to tilted fluorescence bands, and blue brackets to cell compartments with disparate sizes. Immature (P) and mature heterocysts (H) are indicated. Blue arrowheads point to an apparent instance of septation in mature heterocysts; orange arrowheads to a mature heterocyst with Z-ring fluorescence; and blue asterisks to contiguous heterocysts. Magnification is the same for all micrographs.
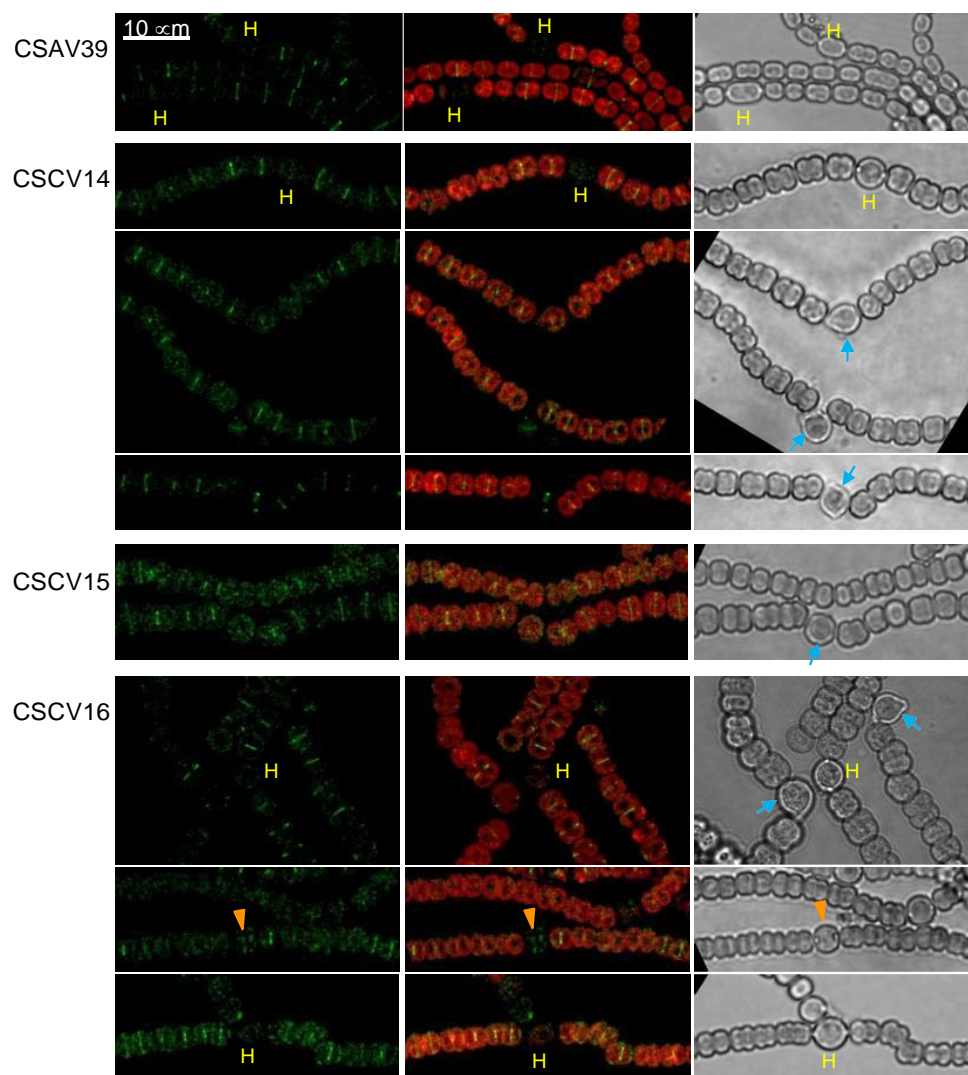
Figure 7. Localization of ZipN in *Anabaena mreB*, *mreC* and *mreD* mutants. Strains CSAV39 (*sfgfp-zipN* in WT background), CSCV14 (*sfgfp-zipN* in CSCV1 background), CSCV15 (*sfgfp-zipN* in CSCV4 background) and CSCV16 (*sfgfp-zipN* in CSCV2 background) were treated as described above for Figure 2, and after 24 h (48 h for rows 7 and 8), filaments were visualized by confocal microscopy with FLUOVIEW equipment. GFP fluorescence (green), merged GFP and cyanobacterial autofluorescence (red), and bright-field images are shown. Mature heterocysts (H) are indicated. Orange arrowheads point to an instance of midcell GFP-ZipN in a mature heterocyst. Blue arrows point to heterocysts deviated from the filament longitudinal plane or with aberrant polar morphology. Magnification is the same for all micrographs.

3.5. Localization of SepJ in Mre Mutants

Because the *mreB*, *mreC* and *mreD* mutants are impaired in diazotrophic growth [36], and because, as shown above, MreB, MreC and MreD are also localized to the heterocyst poles and the neighboring vegetative cell poles, we asked whether Mre proteins had any influence on the localization of the septal protein SepJ. To study that, we generated strains CSCV17, CSCV18 and CSCV19, which express a SepJ-GFP reporter from the native *sepJ* gene promoter as the only SepJ version (see [22]), in *mreB*, *mreC* or *mreD* background, respectively. Strain CSS89 expresses the same reporter in the wild-type background [38].

In strain CSS89, GFP fluorescence appeared as conspicuous focused central spots in the vegetative cell and heterocyst poles (Figure 8; see also [22]). In CSCV17, CSCV18 and CSCV19, a similar fluorescence distribution could be observed, although mature heterocysts with very weak or undetectable fluorescence were also observed (Figure 8). Notably, some

heterocysts in which the cyanophycin polar granules were displaced from the cell equator were detected in strain CSCV17 (see the third row in Figure 8). Additionally, in the three mutant backgrounds, heterocysts with aberrant polar morphology were frequently observed, as well as some points of filament bending, eventually leading to filament breakage, at a heterocyst-vegetative cell connection, sometimes involving a heterocyst pole devoid of SepJ (Figure 8).
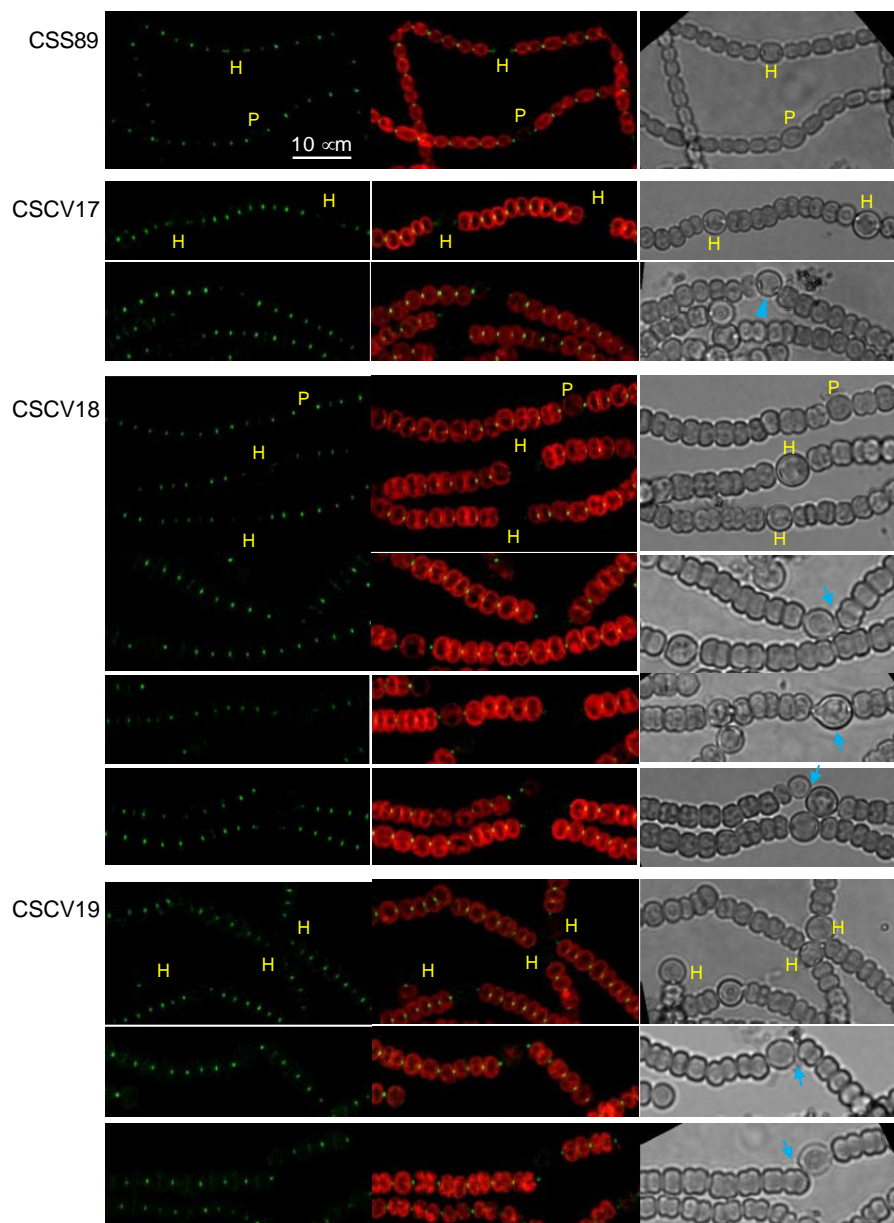
Figure 8. Localization of SepJ in *Anabaena mreB*, *mreC* and *mreD* mutants. Strains CSS89 (*sepJ-gfpmut2* in WT background), CSCV17 (*sepJ-gfpmut2* in CSCV1 background), CSCV18 (*sepJ-gfpmut2* in CSCV4 background) and CSCV19 (*sepJ-gfpmut2* in CSCV2 background) were treated as described above for Figure 2. After 24 h (rows 5, 9 and 10) or 48 h (rows 1–4 and 6–8), filaments were visualized by confocal microscopy with FLUOVIEW equipment. GFP fluorescence (green), merged GFP and cyanobacterial autofluorescence (red), and bright-field images are shown. Immature (P) and mature heterocysts (H) are indicated. Blue arrows point to heterocysts deviated from the filament longitudinal plane or with aberrant polar morphology. The blue arrowhead points to a heterocyst with polar granules deviated from the cell equator. Magnification is the same for all micrographs.

4. Discussion

Under conditions of nitrogen scarcity, the *Anabaena* filament develops into a diazotrophic filament that includes cells specialized for the fixation of atmospheric nitrogen called heterocysts. The differentiation of vegetative cells into heterocysts includes multiple morphological, structural and metabolic changes to permit the efficient operation of the N$_2$ fixation machinery. Heterocysts are larger in size and longer in cell aspect than their mother cells, either of filaments that had grown with combined nitrogen or vegetative cells of diazotrophic filaments [36]. We have shown here conspicuous peripheral labeling with Van-FL of cells in early stages of differentiation, indicating incorporation of PG that would allow for envelope expansion during cell enlargement. Consistent with these results, fluorescent HADA, which incorporates into PG, has been found to label proheterocysts at a stage in which they were also labeled with Alcian blue, which indicates that at least the polysaccharide envelope layer had already been deposited [11]. However, the low turnover of the HADA signal may make Van-FL labeling more adequate for studying the dynamics of PG incorporation. Consequently, we have observed that the peripheral Van-FL labeling decreased in mature heterocysts, suggesting that lateral PG growth is transitory.

Previous observations support the involvement of the MreB, MreC and MreD proteins in PG incorporation during heterocyst differentiation. Thus, the expression of the *mreBCD* operon transiently increases in differentiating cells, returning to a level similar to that of vegetative cells in mature heterocysts, and even decreasing thereafter [36]. Moreover, the *mreB*, *mreC* or *mreD* mutants' heterocysts are no longer rod-shaped. Instead, the axis parallel to the filament is shorter than that perpendicular to the filament [36]. In addition, we have shown here that MreB, MreC and MreD localize to the periphery and the cell poles of differentiating cells and heterocysts (Figure 2). Nonetheless, we have detected peripheral PG incorporation in the rounded differentiating cells of the *mreB*, *mreC* and *mreD* mutants (Figures 3–5). These results indicate that whereas the Mre proteins are not strictly required for PG incorporation in the differentiating cells, they are necessary for a checked peripheral PG growth leading to cell elongation. Consistent with this notion, we have detected instances of aberrantly strong peripheral incorporation of Van-FL, at least in the case of the *mreD* mutant (Figure 5). Although we cannot rule out that this effect results from easier access of Van-FL to the periplasm due to an alteration of the outer membrane, it could also indicate deregulated PG growth in the mutants.

The polar regions of heterocysts represent differentiated structures that allow for controlled intercellular communication with the neighboring cells in the filament. Differentiation of the heterocyst neck includes polar localization of specific membrane transporters and the septal junction complexes traversing the septal PG through nanopores. In addition to peripheral growth, intense activity of PG incorporation at the poles of differentiating heterocysts was detected using HADA [11]. We have observed conspicuous Van-FL labeling in the differentiating cell poles covering the heterocyst neck at the early stages of differentiation (Figure 1), as well as the progression of the wide signals observed early into focal polar labeling, similar to those detected in the vegetative cell poles contiguous to a heterocyst (Figure 1). These observations indicate a strong PG incorporation during the formation of the heterocyst neck that leads to persistent, more focused incorporation at the mature heterocyst poles, likely serving in the formation and maintenance of septal communication arrays.

MreB, MreC and MreD are present in the heterocyst poles (Figure 2). This, together with the instances of increased or aberrant Van-FL distribution found in the poles of the heterocysts of the *mre* mutants (Figures 3–5), suggest the involvement of the Mre proteins in reshaping of septal PG during heterocyst polar differentiation and maintenance. In support of this notion, we have observed that in the *mreB*, *mreC* and *mreD* mutants, heterocysts frequently lack SepJ-GFP fluorescence spots (Figure 8), which suggests an influence of the Mre proteins in the localization of septal structures. Moreover, in those mutants, heterocysts with aberrant polar morphology, including those in which polar granules were displaced from the cell equator and those in which the linearity of the filament was lost at a heterocyst-

vegetative cell connection, even leading to filament breakage at that point, were found. All these polar alterations could provoke impaired intercellular exchange between heterocysts and the neighboring vegetative cells, contributing to the impaired diazotrophic growth exhibited by the *mre* mutants [36].

Finally, the pattern of Van-FL labeling in the vegetative cells of filaments in the process of differentiation and during diazotrophic growth (First row in Figure 1) appeared similar to that previously found in filaments growing with combined nitrogen, with peripheral, septal and midcell labeling (e.g., [10]). Additionally, under diazotrophic conditions, inactivation of *mreB*, *mreC* or *mreD* led to alterations in the pattern of septal bands, which were frequently disposed forming angles or at irregular distances to each other (First row in Figures 3–5), alterations that reproduce those found in the disposition of the FtsZ and ZipN rings (Figures 6 and 7). FtsZ and ZipN rings are dismantled in the cells differentiating into heterocysts at intermediate stages of differentiation [39,40]. This leads to a loss of cell-division capacity, considered to be a crucial step in setting the commitment to terminal differentiation ([41]; see [15]). Indeed, mutations that increase the persistence of division rings in differentiating cells have been considered to inhibit the completion of differentiation [39]. Here, we have observed that 48 h after N-stepdown, some immature heterocysts with conspicuous FtsZ rings were still present in the *mreB*, *mreC* and *mreD* mutant backgrounds but not in the wild-type background (Figure 6). Even some apparently mature heterocysts exhibiting an FtsZ ring (Figure 6) or a ZipN ring (Figure 7) were detected in the *mreD* mutant. These observations are also indicative of retardation of differentiation in the *mre* mutants. Whether, in addition to influencing the division-ring topology, MreB, MreC or MreD also have a role in the inhibition of Z-ring establishment during heterocyst differentiation is an issue worth future investigation.

Author Contributions: Conceptualization, A.H.; methodology, C.V.-S., I.L. and A.H.; software, C.V.-S.; validation, C.V.-S., I.L. and A.H.; formal analysis, C.V.-S., I.L. and A.H.; investigation, C.V.-S.; resources, I.L. and A.H.; data curation, C.V.-S., I.L. and A.H.; writing—original draft preparation, A.H.; writing—review and editing, C.V.-S., I.L. and A.H.; visualization, C.V.-S., I.L. and A.H.; supervision, A.H. and I.L.; project administration, A.H. and I.L.; funding acquisition, A.H. and I.L. All authors have read and agreed to the published version of the manuscript.

References

1. Herrero, A.; Stavans, J.; Flores, E. The multicellular nature of filamentous heterocyst-forming cyanobacteria. *FEMS Microbiol. Rev.* **2016**, *40*, 831–854. [CrossRef]
2. Arbel-Goren, R.; Buonfiglio, V.; Di Patti, F.; Camargo, S.; Zhitnitsky, A.; Valladares, A.; Flores, E.; Herrero, A.; Fanelli, D.; Stavans, J. Robust, coherent, and synchronized circadian clock-controlled oscillations along *Anabaena* filaments. *eLife* **2021**, *10*, e64348. [CrossRef]
3. Mariscal, V.; Herrero, A.; Flores, E. Continuous periplasm in a filamentous, heterocyst-forming cyanobacterium. *Mol. Microbiol.* **2016**, *65*, 1139–1145. [CrossRef]
4. Flores, E.; Herrero, A.; Forchhammer, K.; Maldener, I. Septal junctions in filamentous heterocyst-forming cyanobacteria. *Trends Microbiol.* **2016**, *24*, 79–82. [CrossRef]

5. Weiss, G.; Kieninger, A.-K.; Maldener, I.; Forchhammer, K.; Pilhofer, M. Structure and function of a bacterial gap junction analog. *Cell* **2019**, *178*, 374–384. [CrossRef]

6. Berendt, S.; Lehner, J.; Zhang, Y.V.; Rasse, T.M.; Forchhammer, K.; Maldener, I. Cell wall amidase AmiC1 is required for cellular communication and heterocyst development in the cyanobacterium *Anabaena* PCC 7120 but not for filament integrity. *J. Bacteriol.* **2012**, *194*, 5218–5227. [CrossRef]

7. Bornikoel, J.; Carrión, A.; Fan, Q.; Flores, E.; Forchhammer, K.; Mariscal, V.; Mullineaux, C.W.; Perez, R.; Silber, N.; Wolk, C.P.; et al. Role of two cell wall amidases in septal junction and nanopore formation in the multicellular cyanobacterium *Anabaena* sp. PCC 7120. *Front. Cell Infect. Microbiol.* **2017**, *7*, 386. [CrossRef]

8. Zheng, Z.; Omairi-Nasser, A.; Li, X.; Dong, C.; Lin, Y.; Haselkorn, R.; Zhao, J. An amidase is required for proper intercellular communication in the filamentous cyanobacterium *Anabaena* sp. PCC 7120. *Proc. Nat. Acad. Sci. USA* **2017**, *114*, E1405–E1412. [CrossRef]

9. Arévalo, S.; Nenninger, A.; Nieves-Morión, M.; Herrero, A.; Mullineaux, C.V.; Flores, E. Coexistence of communicating and noncommunicating cells in the filamentous cyanobacterium *Anabaena*. *mSphere* **2021**, *6*, e01091-20. [CrossRef]

10. Velázquez-Suárez, C.; Valladares, A.; Luque, I.; Herrero, A. The role of Mre factors and cell division in peptidoglycan growth in the multicellular cyanobacterium *Anabaena*. *mBio* **2022**, *13*, e01165-22. [CrossRef]

11. Zhang, J.-Y.; Lin, G.-M.; Xing, W.-Y.; Zhang, C.-C. Diversity of growth patterns probed in live cyanobacterial cells using a fluorescent analog of a peptidoglycan precursor. *Front. Microbiol.* **2018**, *9*, 791. [CrossRef]

12. Springstein, B.L.; Wissenbach, J.; Koch, R.; Stücker, F.; Stuken, K. The role of the cytoskeletal proteins MreB and FtsZ in multicellular cyanobacteria. *FEMS Openbio* **2020**, *10*, 2510–2531. [CrossRef]

13. Egan, A.J.F.; Errington, J.; Vollmer, W. Regulation of peptidoglycan synthesis and remodeling. *Nat. Rev. Microbiol.* **2020**, *18*, 446–460. [CrossRef]

14. Flores, E.; Herrero, A. Compartmentalized function through cell differentiation in filamentous cyanobacteria. *Nat. Rev. Microbiol.* **2010**, *8*, 39. [CrossRef]

15. Zeng, X.; Zhang, C.-C. The making of a heterocyst in cyanobacteria. *Ann. Rev. Microbiol.* **2022**, *76*, 597–618. [CrossRef]

16. Flores, E.; Picossi, S.; Valladares, A.; Herrero, A. Transcriptional regulation of development in heterocyst-forming cyanobacteria. *BBA − Gene Regul. Mech.* **2019**, *1862*, 673–684. [CrossRef]

17. Walsby, A.E. Cyanobacterial heterocysts: Terminal pores proposed as sites of gas exchange. *Trends Microbiol.* **2007**, *15*, 340–349. [CrossRef]

18. Corrales-Guerrero, L.; Flores, E.; Herrero, A. Relationships between the ABC-exporter HetC and peptides that regulate the spatiotemporal pattern of heterocyst distribution in *Anabaena*. *PLoS ONE* **2014**, *9*, e104571.

19. Videau, P.; Rivers, O.S.; Higa, K.C.; Callahan, S.M. ABC transporter required for intercellular transfer of developmental signals in a heterocystous cyanobacterium. *J. Bacteriol.* **2015**, *197*, 2685–2693. [CrossRef]

20. Shvarev, D.; Nishi, C.N.; Maldener, I. Glycolipid composition of the heterocyst envelope of *Anabaena* sp. PCC 7120 is crucial for diazotrophic growth and relies on the UDP-galactose 4-epimerase HgdA. *Microbiol.* **2019**, *8*, e811.

21. Arévalo, S.; Flores, E. Pentapeptide-repeat, cytoplasmic-membrane protein HglK influences the septal junctions in the heterocystous cyanobacterium *Anabaena*. *Mol. Microbiol.* **2020**, *113*, 794–806. [CrossRef] [PubMed]

22. Flores, E.; Pernil, R.; Muro-Pastor, A.M.; Mariscal, V.; Maldener, I.; Lechno-Yossef, S.; Fan, Q.; Wolk, C.P.; Herrero, A. Septum-localized protein required for filament integrity and diazotrophy in the heterocyst-forming cyanobacterium *Anabaena* sp. strain PCC 7120. *J. Bacteriol.* **2007**, *189*, 3884–3890. [CrossRef] [PubMed]

23. Merino-Puerto, V.; Mariscal, V.; Mullineaux, C.W.; Herrero, A.; Flores, E. Fra proteins influencing filament integrity, diazotrophy and localization of septal protein SepJ in the heterocyst-forming cyanobacterium *Anabaena* sp. *Mol. Microbiol.* **2010**, *75*, 1159–1170. [CrossRef] [PubMed]

24. Arévalo, S.; Flores, E. Heterocyst septa contain large nanopores that are influenced by the Fra proteins in the filamentous cyanobacterium *Anabaena* sp. strain PCC 7120. *J. Bacteriol.* **2021**, *203*, e00081-21. [CrossRef]

25. Schätzle, H.; Arévalo, S.; Flores, E.; Schleiff, E. A TonB-like protein, SjdR, is involved in the structural definition of the intercellular septa in the heterocyst-forming cyanobacterium *Anabaena*. *mBio* **2021**, *12*, e00483-21. [CrossRef]

26. Videau, P.; Rivers, O.; Ushijima, B.; Oshiro, R. Mutation of the *murC* and *murB* genes impairs heterocyst differentiation in *Anabaena* sp. strain PCC 7120. *J. Bacteriol.* **2016**, *198*, 1196–1206. [CrossRef]

27. Lazaro, S.; Fernandez-Piñas, F.; Fernandez-Valiente, E.; Blanco-Rivero, A.; Leganes, F. *pbpB*, a gene coding for a putative penicillin-binding protein, is required for aerobic nitrogen fixation in the cyanobacterium *Anabaena* sp. strain PCC7120. *J. Bacteriol.* **2001**, *183*, 628–636. [CrossRef]

28. Leganés, F.; Blanco-Rivero, A.; Fernández-Piñas, F.; Redondo, M.; Fernández-Valiente, E.; Fan, Q.; Lechno-Yossef, S.; Wolk, C.P. Wide variation in the cyanobacterial complement of presumptive penicillin-binding proteins. *Arch. Microbiol.* **2005**, *184*, 234–248. [CrossRef]

29. Brenes-Álvarez, M.; Vioque, A.; Muro-Pastor, A.M. The integrity of the cell wall and its remodeling during heterocyst differentiation are regulated by phylogenetically conserved small RNA Yfr1 in *Nostoc* sp. strain PCC 7120. *mBio* **2020**, *11*, e02599-19. [CrossRef]

30. Rippka, R.; Deruelles, J.; Waterbury, J.B.; Herdman, M.; Stanier, R.Y. Generic assignments, strain histories and properties of pure cultures of cyanobacteria. *J. Gen. Microbiol.* **1979**, *111*, 1–61. [CrossRef]

31.   Mackinney, G. Absorption of light by chlorophyll solutions. *J. Biol. Chem.* **1941**, *140*, 109–112. [CrossRef]

32.   Flores, E.; Wolk, C.P. Identification of facultatively heterotrophic, N$_2$-fixing cyanobacteria able to receive plasmid vectors from *Escherichia coli* by conjugation. *J. Bacteriol.* **1985**, *162*, 1339–1341. [CrossRef] [PubMed]

33.   Valladares, A.; Rodríguez, V.; Camargo, S.; Martínez-Noël, G.M.A.; Herrero, A.; Luque, I. Specific role of the cyanobacterial PipX factor in heterocysts of *Anabaena* sp. strain PCC 7120. *J. Bacteriol.* **2011**, *193*, 1172–1182. [CrossRef] [PubMed]

34.   Daniel, R.A.; Errington, J. Control of cell morphogenesis in bacteria: Two distinct ways to make a rod-shaped cell. *Cell* **2003**, *113*, 767–776. [CrossRef]

35.   Mariscal, V.; Nürnberg, D.J.; Herrero, A.; Mullineaux, C.W.; Flores, E. Overexpression of SepJ alters septal morphology and heterocyst pattern regulated by diffusible signals in *Anabaena*. *Mol. Microbiol.* **2016**, *101*, 968–981. [CrossRef] [PubMed]

36.   Velázquez-Suárez, C.; Luque, I.; Herrero, A. The inorganic nutrient regime and the *mre* genes regulate cell and filament size and morphology in the phototrophic multicellular bacterium *Anabaena*. *mSphere* **2020**, *5*, e00747-20. [CrossRef]

37.   Corrales-Guerrero, L.; Camargo, S.; Valladares, A.; Picossi, S.; Luque, I.; Ochoa de Alda, J.A.G.; Herrero, A. FtsZ of filamentous, heterocyst-forming cyanobacteria has a conserved N-terminal peptide required for normal FtsZ polymerization and cell division. *Front. Microbiol.* **2018**, *9*, 2260. [CrossRef]

38.   Camargo, S.; Picossi, S.; Corrales-Guerrero, L.; Valladares, A.; Arévalo, S.; Herrero, A. ZipN is an essential FtsZ membrane tether and contributes to the septal localization of SepJ in the filamentous cyanobacterium *Anabaena*. *Sci. Rep.* **2019**, *9*, 2744. [CrossRef]

39.   Valladares, A.; Velázquez-Suárez, C.; Herrero, A. Interactions of PatA with the divisome during heterocyst differentiation in *Anabaena*. *mSphere* **2020**, *5*, e00188-20. [CrossRef]

40.   Wang, L.; Niu, T.-C.; Valladares, A.; Lin, G.-M.; Zhang, J.-Y.; Herrero, A.; Chen, W.-L.; Zhang, C.-C. The developmental regulator PatD modulates assembly of the cell-division protein FtsZ in the cyanobacterium *Anabaena* sp. PCC 7120. *Environ. Microbiol.* **2021**, *23*, 4823–4837. [CrossRef]

41.   Videau, P.; Rivers, O.S.; Hurd, K.; Ushijima, B.; Oshiro, R.T.; Ende, R.J.; O'Hanlon, S.M.; Cozy, L.M. The heterocyst regulatory protein HetP and its homologs modulate heterocyst commitment in *Anabaena* sp. strain PCC 7120. *Proc. Nat. Acad. Sci. USA* **2016**, *113*, E6984–E6992. [CrossRef] [PubMed]

Table S1. Cyanobacterial strains, plasmids and oligonucleotides used in this work

Strain	Genotype	Resistance	Source
Anabaena sp. PCC 7120	WT		Pasteur Culture Collection
CSCV1	*mreB*::C.K1	Nm	36
CSCV2	*mreD*::C.S3	Sm, Sp	36
CSCV4	*mreC*::C.K1	Nm	36
CSCV6	*thrS2*::P$_{mreB}$-*sfgfp-mreB*	Sm, Sp	10
CSCV7	*thrS2*::P$_{mreB}$-*sfgfp-mreC*	Sm, Sp	10
CSCV8	*thrS2*::P$_{mreB}$-*sfgfp-mreD*	Sm, Sp	10
CSSC19	P$_{ftsZ}$-*ftsZ-gfpmut2*	Sm, Sp	37
CSCV20	P$_{ftsZ}$-*ftsZ-gfpmut2, mreB*	Nm, Sm, Sp	10
CSCV21	P$_{ftsZ}$-*ftsZ-gfpmut2, mreC*	Nm, Sm, Sp	10
CSCV22	P$_{ftsZ}$-*ftsZ-gfpmut2, mreD*	Nm, Sm, Sp	10
CSAV39	P$_{zipN}$-*sfgfp-zipN*	Sm, Sp	39
CSCV14	P$_{zipN}$-*sfgfp-zipN, mreB*	Nm, Sm, Sp	10
CSCV15	P$_{zipN}$-*sfgfp-zipN, mreC*	Nm, Sm, Sp	10
CSCV16	P$_{zipN}$-*sfgfp-zipN, mreD*	Nm, Sm, Sp	10
CSS89	*sepJ-gfpmut2*	Nm	38
CSCV17	*sepJ-gfpmut2, mreB*	Nm, Sm, Sp	This study
CSCV18	*sepJ-gfpmut2, mreC*	Nm, Sm, Sp	This study
CSCV19	*sepJ-gfpmut2, mreD*	Nm, Sm, Sp	This study

Plasmid	Description	Resistance marker	Source
pCSCV38	pCSV3 carrying *sepJ-gfpmut2*	Sm, Sp	This study
pCSVT22	pRL424 carrying *sepJ-gfpmut2*	Nm	23

Oligodeoxynucleotide primers[1]	Sequence (5′-3′)
alr2338-BamHI	CGTG<u>GGATCC</u>TTTTCTGTGGTGAGGTGC
gfp-BamHI	AAGC<u>GGATCC</u>TTATTTGTATAGTTCATCCATGCC

[1]The underlined letters indicate a restriction site.

GENERAL DISCUSSION

The influence of the environment in the *Anabaena* morphology

The results of this work showed that environmental conditions, like the carbon and nitrogen availability, influence cell size and shape and filament length in *Anabaena*. In diverse bacteria, cell morphology has been reported to be important for interaction with the environment and for survival (Young, 2006; van Teeseling *et al.*, 2017). For instance, the spiral morphology of *H. pylori* and the curved shape of *V. cholerae* allow these strains to colonize the gastric and intestinal epithelia, respectively, and favor their movement through the mucus, which facilitates infection (Young, 2006; van Teeseling *et al.*, 2017). Other pathogens like *M. tuberculosis* and uropathogen *E. coli* adopt an elongated morphology that helps them to avoid phagocytosis by macrophages (Young, 2006). In some other cases, environmental conditions impact the morphology of different bacteria although the possible advantage of this effect is not evident. This is the case of *Ancalomicrobium*, which in poor environments undergo filamentation and branching, or the cyanobacterium *F. diplosiphon* that changes morphology in response to the quality of light (Young, 2006; Singh and Montgomery, 2011).

Regarding cell size, in *Anabaena* we have observed differences according to the nutritional regime of carbon and nitrogen and the intensity of the incident light (Velázquez-Suárez *et al.*, in preparation). Also, different relationships were found between the growth rate and cell size through the growth cycle, especially in the presence of combined nitrogen (nitrate or ammonium). In the phase of fastest growth, *Anabaena* cells were larger in the presence of combined nitrogen than in diazotrophic cultures, an effect that would meet the classical growth law entailing that cells are larger when growing with a nutrient-imposed lower generation time (Schaechter *et al.,* 1958; reviewed in Morcinek-Orlowska *et al.*, 2019). Larger cell size during active growth would facilitate chromosome inheritance by a random mechanism, as proposed for *Anabaena* (Hu *et al.*, 2007), during cell division. In the absence of combined nitrogen, a small cell size could facilitate intercellular molecular exchanges through the filament, which take place by diffusion and are more stringently required under these diazotrophic conditions. In any case, differences in cell size report on differences in the balance between cell growth and division through the cell cycle, with an impact of the environment. Recent reports have shown that in *Anabaena*, the level of the signal molecule c-di-GMP plays a role in determining cell size. Cell size control is dependent on the interaction of the CdgR protein with the DevH transcription factor, an interaction that only occurs when CdgR is not bound to c-di-GMP (Zeng *et al.*, 2023). It would be worth to investigate whether c-di-GMP is involved in cell size determination in response to the availability of carbon and nitrogen.

Regarding cell shape, in the presence of combined nitrogen, *Anabaena* cells appeared to elongate through the phases of active growth, and to decrease in length thereafter. Cells of cultures supplemented with nitrate or ammonium were longer than cells of diazotrophic cultures, in which cell morphology appeared to be less variable. In the presence of nitrate, a high C supply also had a positive effect on cell elongation. In rod-shaped cells in general, an increase in length will increase the total surface area, which represents an advantage when nutrients

(nitrate, ammonium, bicarbonate) are to be taken from the external medium. In contrast, under diazotrophic conditions, nitrogen nutrients are exchanged between vegetative cells and heterocysts mainly by septal connections, thus making less clear the advantage of increasing the cell surface. Finally, in *ntcA* and *hetR* mutants growing with ammonium, cells were longer than in the wild type, also supporting an impact of the C-to-N balance on cell morphology (see below). Regarding the length of the filaments (i.e., the number of cells they contain), diazotrophic filaments showed a shorter length than those in cultures supplemented with combined nitrogen, which can be related to the assumption that the septa between heterocysts and vegetative cells are weaker than those between two vetative cells.
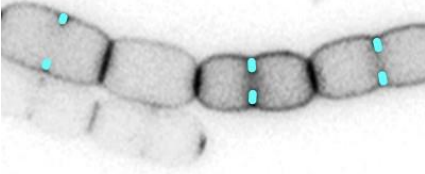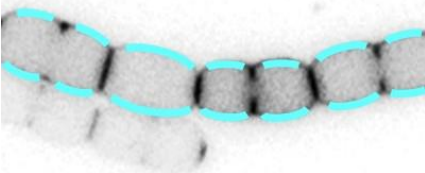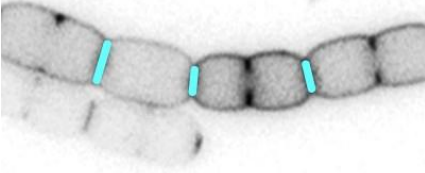
PG growth and the role of MreB, MreC and MreD in *Anabaena*

In model unicellular rod-shaped bacteria, the elongasome directs a disperse mode of PG synthesis in the cylindrical part of the cell, whereas during cell division the divisome directs septal PG synthesis to form the new poles of the daughter cells. In *Anabaena*, both Van-FL (this work) and HADA (Zhang *et al.*, 2018), produces a homogeneous, although rather weak, labeling in the cell periphery. Consistently, in this work GFP fusions to MreB, MreC and MreD were localized through the cell periphery. These observations, together with the round shape of the *Anabaena mreB*, *mreC* and *mreD* mutans, which is similar to the phenotype observed upon Mre depletion in *E. coli* and *B. subtilis* (Dye *et al.*, 2005; Kruse *et al.*, 2005; Leaver and Errington, 2005), indicate that lateral PG growth dependent on Mre factors also take place in *Anabaena* enabling cell elongation. Consistently also, expression of the *mreBCD* operon is higher during the phases of stronger growth, when cells are longer, and is negatively regulated by NtcA, which occurs at higher levels in diazotrophic filaments, where the cells are shorter. Instead of occurring with a patchy distribution excluding the cell poles, like e.g., in *B. subtilis* (Daniel and Errington, 2003), in *Anabaena* peripheral PG growth appears to take place all around the cell surface, an issue worth of further study.

Van-FL staining in *Anabaena* also indicated that PG synthesis linked to the divisome and, remarkably, in the mature intercellular septa takes place (see Table 3). This distinct labeling is indicative of a permanent growth or remodeling of the intercellular septal PG during the phases of active growth, in contrast to the situation in common model rod-shaped unicellular bacteria, like *E. coli*, *B. subtilis* and *C. crescentus*, where the cell poles become inert for PG synthesis once division is completed (Daniel and Errington, 2003; Aaron *et al.*, 2007; Kawazura *et al.*, 2017). These results are consistent with those obtained by pulse-chase experiments with HADA in *Anabaena*, which show a fast turnover of this analog in mature septa (Zhang *et al.*, 2018). It is possible that septal PG remodeling in *Anabaena* were required for the assembly or maintenance of the SJ complexes that expand the intercellular septa through PG nanopores. Indeed, MreB, MreC and MreD were observed also in the intercellular septa and, although inactivation of *mre* genes did not preclude PG incorporation at such location, in the mutants the intercellular septa were wider and more robust than in the WT. Thus, Mre proteins are not required for PG

incorporation at mature intercellular septa, but they appear required for the formation of dimensioned septa. It has been described that under conditions of rapid growth, limitation for PG precursors in *E. coli* could lead to a competition between the incorporation of PG at the lateral and midcell locations. Also, increased or decreased incorporation of PG at the division site provokes the inverse effect at the cell periphery (Navarro *et al.*, 2022). In *Anabaena*, increased PG incorporation at the intercellular septa in the absence of elongation in *mre* mutants could suggest that a competition between septal and peripheral PG incorporation could also operate.

Table 3. Modes of PG incorporation in *Anabaena*.

Mode of PG incorporation		Role of Mre proteins
Divisional		Topologycal regulation
Lateral		Elongasome dependent
Intercellular septal		Septal dimension regulation

Interactions between the elongasome and the divisome in *Anabaena*

In *Anabaena*, MreB, MreC and MreD match the localization of the divisome during all stages of the cell division process. Also, by BACTH tests, we have identified interactions between MreB or MreD and some divisome components, suggesting contacts between the divisome and the elongasome during cell division. This is consistent with the observation of a direct interaction between MreB and FtsZ in other filamentous cyanobacteria (Springstein *et al.*, 2020b). In *E. coli,* MreB was shown to interact and co-localize with FtsZ in Z-rings at the initiation of cell division, leading to the proposal that MreB guides some components of the elongasome PG synthesis

machinery be passed on to the divisome (Fenton and Gerdes, 2013). We cannot rule out that in *Anabaena* Mre factors do play a similar role, but our observations are indicative of additional functions connected to the divisome. In this work we have observed that in *mreB*, *mreC* or *mreD* mutants midcell PG growth bands along the filament, as well as, FtsZ and ZipN rings were frequently non-equidistant and not parallel in consecutive cells and, in many cases, tilted with respect to the filament long axis. This suggests a role of MreB, MreC and MreD in the correct localization of the divisome, which is unprecedented in the literature. The work presented here evidences that the multicellular character of *Anabaena* makes this organism a good model for the study of septa positioning in successive generations of cells.

Evidence for an interplay between the divisome and the elongasome in *Anabaena* also derive from the morphological alterations observed in strains depleted of FtsZ or ZipN (Corrales-Guerrero *et al.*, 2018; Camargo *et al.*, 2019). Model rod-shaped unicellular bacteria depleted of FtsZ maintain PG growth over the sidewalls leading to the classical filamentation phenotype (Dai and Lutkenhaus, 1991; Daniel and Errington, 2003; Redick *et al.*, 2005; Aaron *et al.*, 2007). However, depletion of FtsZ or ZipN in *Anabaena* led to a very aberrant cell and filament morphology, including giant cells with irregular width, or exhibiting central bulged areas, connected by minuscule septa in comparison to the increased cell volume. Also frequent were events of cell detachment from the filament and cell lysis, all this indicative of unchecked cell enlargement with restricted elongation. Van-FL staining revealed either very strong, frequently patched, or very weak, progressively fading, peripheral signals in the aberrant cells. Septal signal did not increase in width during cell enlargement, and frequently was undetected. Thus, lowering the expression of Z-ring components not only impair divisional, but also peripheral and septal PG growth.

PG growth during heterocyst differentiation

In *Anabaena* none of the *mre* genes are essential, although their mutants were impaired in growth, more drastically under diazotrophic conditions. Diazotrophic growth in *Anabaena* depends on heterocyst differentiation to establish a filament with two cell types: the vegetative cells, which fix CO_2 and transfer carbon compounds, and the heterocysts, which fix N_2 and donate nitrogen-rich compounds to the vegetative cells. Heterocysts differentiate from certain vegetative cells of the filament under conditions of nitrogen deficiency. The differentiation process involve extensive morphological changes, including increase in cell size, elongation, remodeling of the cell envelope and remodeling of the cell poles, all involving PG synthesis (Nicolaisen *et al.*, 2009a; Zeng and Zhang, 2022).

Van-FL labeling has revealed different events of PG incorporation during differentiation. Regarding peripheral labeling, strong signals were detected at intermediate stages of differentiation, which became weaker in mature heterocysts. Ours and others' (e.g., Zhang *et al.*, 2018) studies are indicative of the occurrence of transient lateral PG growth effecting cell enlargement and elongation. The involvement of MreB, MreC and MreD in this transient

peripheral PG incorporation is supported by the expression of *mreB*, *mreC* and *mreD* in the differentiating cells and the localization of these proteins to the cell periphery, as well as by the morphological alterations in heterocysts from *mre* mutants that showed increased size, in comparison to the wild-type heterocysts, and a rounder shape.

The heterocyst polar neck represents a differentiated structure for intercellular communication with the neighboring vegetative cell. Indeed, differences in the array of PG nanopores holding septal junction complexes have been detected between vegetative cell-vegetative cell and vegetative cell-heterocyst connections (Arévalo *et al.*, 2021), indicative of remodeling of septal communication structures during differentiation. Van-FL and HADA labeling revealed strong PG incorporation in the heterocyst neck and the pole of the neighboring vegetative cell during heterocyst differentiation. In *mreB*, *mreC* and *mreD* mutants, alterations in the heterocyst polar morphology, including events of displacement of the heterocyst with regard to the filament plane, filament breakage at heterocyst-vegetative cell connections and lack of SepJ at some heterocyst poles were detected. MreB, MreC and MreD were conspicuously detected at the cell poles in differentiating and mature heterocysts. These results involve MreB, MreC and MreD in the remodeling of PG during differentiation and maintenance of the heterocyst septal structures. In future, it would be interesting to further investigate the septal structures in *mre* mutants, including the features of the nanopore array and the activity of molecular exchanges with neighboring vegetative cells.

Heterocysts are terminally differentiated cells that have lost the capacity for cell division, an important step in setting the commitment to differentiation. Indeed, the Z-ring is dismantled early, and *ftsZ* and *zipN* expression is arrested during differentiation (e.g., Valladares *et al.*, 2020). Two factors, PatA (Valladares *et al.*, 2020) and PatD (Wang *et al.*, 2021), whose expression increases transiently in the differentiating cells, have been proposed to participate in the destabilization of the Z-ring during differentiation through a direct interaction with divisome components. An important observation of this work was that proheterocysts of *mreB*, *mreC* and *mreD* mutants frequently showed midcell FtsZ and ZipN rings at times when they are already absent in the wild type. It is tempting to speculate that the Mre proteins could play a role in the inhibition of Z-ring formation during heterocyst differentiation, a proposal consistent also with our observation of MreB and MreD interactions with divisome components. It is worth noting that although Z-rings were visible in some proheterocysts of *mre* mutants, midcell PG incorporation was never observed. This suggests that a functional divisome is not assembled, which is consistent with the existence of additional inhibitory mechanisms, as described above (see section 8.2).

In summary, this work has shown the importance of environmental parameters, such as the carbon and nitrogen sources, and the growth phase in the determination of cell size and morphology in the filamentous cyanobacterium *Anabaena*. In this cyanobacterium, the expression of the *mreB*, *mreC* and *mreD* genes is regulated by the growth phase and the environment through the transcriptional regulator NtcA that responds to the C-to-N balance. *Anabaena* presents three main modes of PG incorporation: a peripheral synthesis that elongate the cells during growth; a midcell synthesis dependent on the divisome that forms the poles of the daughter cells during cell division and a persistent incorporation in the mature intercellular septa along the filament. Peripheral PG growth requires MreB, MreC and MreD. Although divisional and septal PG incorporation do not require MreB, MreC and MreD, these factors are needed for the correct positioning of the divisome and the correct geometry and dimensions of the intercellular septa. Similarly, in the differentiating heterocysts, MreB, MreC and MreD are localized to the cell periphery and the cell poles, regulating the dimensions and shape of the PG wall. MreB, MreC and MreD are also localized to the divisome, which can represent a way for their localization at mature septa once division has completed. During cell division and in the mature septa, as well as in the heterocyst neck, MreB, MreC and MreD could contribute to establishment and maintenance of septal structures involved in intercellular communication. Thus, this work has uncovered unprecedented roles for MreB, MreC and MreD in relation to the multicellular character of *Anabaena*, underscoring the importance of studying basic bacterial mechanisms outside of a few classical models.

CONCLUSIONS

1. In *Anabaena*, the nutritional regime impacts the size and shape of the cells as well as the length of the filaments.

2. *Anabaena* exhibits three modes of peptidoglycan growth: peripheral, for cell elongation during active growth, divisional, to form the poles of the cells resulting from cell division, and intercellular septal, which might be related to the maintenance of intercellular communication structures.

3. The *mreB*, *mreC* and *mreD* genes form an operon that is expressed at higher levels under conditions determining a higher growth rate and longer cells, and is negatively regulated by the global transcription factor NtcA that responds to the C-to-N balance.

4. In *Anabaena*, MreB, MreC and MreD are localized to the whole cell periphery, the divisome, during all stages of cell division, and the mature intercellular septa.

5. Both, in cells of filaments growing in the presence of combined nitrogen and in vegetative cells of diazotrophic cultures, cell elongation and peripheral PG growth depend on MreB, MreC and MreD.

6. Mre proteins interact with divisome components and are required for the correct positioning of the divisome in consecutive parallel and equidistant planes along the filament, and for the correct geometry and dimensions of the intercellular PG disks.

7. In the diazotrophic filament, MreB, MreC and MreD are required for the enlargement and elongation of the cells differentiating into heterocysts and for the correct formation of the heterocyst neck, and might affect the differentiation of septal structures for intercellular communication, which are at the basis of the multicellular character of this bacterium.

8. *Anabaena* features distinct relationships between the elongasome and the divisome, with the latter not only directing divisional PG synthesis but also influencing peripheral and septal PG incorporation.

Appendix I:

Cyanobacterial strains used in this work

Strain	Genotype	Antibiotic resistance	Source
Anabaena sp. PCC 7120	WT		Pasteur culture collection of cyanobacteria (PCC)
CSCV1	Δ*mreB*::C.K1	Nm	Velázquez-Suárez *et al.*, (2020)
CSCV2	Δ*mreD*::C.S3	Sm, Sp	Velázquez-Suárez *et al.*, (2020)
CSCV4	Δ*mreC*::C.K1	Nm	Velázquez-Suárez *et al.*, (2020)
CSCV5	*thrS2*::P$_{mreB}$-*sfgfp*		Velázquez-Suárez *et al.*, (2022a)
CSCV6	*thrS2*::P$_{mreB}$-*sfgfp-mreB*	Sm, Sp	Velázquez-Suárez *et al.*, (2022a)
CSCV7	*thrS2*::P$_{mreB}$-*sfgfp-mreB*	Sm, Sp	Velázquez-Suárez *et al.*, (2022a)
CSCV8	*thrS2*::P$_{mreB}$-*sfgfp-mreB*	Sm, Sp	Velázquez-Suárez *et al.*, (2022a)
CSAV39	P$_{zipN}$-*sfgfp-zipN* in WT background	Sm, Sp	Valladares *et al.*, (2020)
CSCV14	P$_{zipN}$-*sfgfp-zipN* in *mreB* background	Nm, Sm, Sp	Velázquez-Suárez *et al.*, (2022a)
CSCV15	P$_{zipN}$-*sfgfp-zipN* in *mreC* background	Nm, Sm, Sp	Velázquez-Suárez *et al.*, (2022a)
CSCV16	P$_{zipN}$-*sfgfp-zipN* in *mreD* background	Nm, Sm, Sp	Velázquez-Suárez *et al.*, (2022a)
CSS89	*sepJ-gfpmut2* in WT	Nm	Camargo *et al.*, (2019)
CSCV17	*sepJ-gfpmut2,* in *mreB* background	Nm, Sm, Sp	Velázquez-Suárez *et al.*, (2022b)
CSCV18	*sepJ-gfpmut2,* in *mreC* background	Nm, Sm, Sp	Velázquez-Suárez *et al.*, (2022b)
CSCV19	*sepJ-gfpmut2,* in *mreD* background	Nm, Sm, Sp	Velázquez-Suárez *et al.*, (2022b)
CSSC19	P$_{ftsZ}$-*ftsZ-gfpmut2* in WT background	Sm, Sp	Corrales-Guerrero *et al.*, (2018)
CSCV20	P$_{ftsZ}$-*ftsZ-gfpmut2* in *mreB* background	Nm, Sm, Sp	Velázquez-Suárez *et al.*, (2022a)
CSCV21	P$_{ftsZ}$-*ftsZ-gfpmut2* in *mreC* background	Nm, Sm, Sp	Velázquez-Suárez *et al.*, (2022a)
CSCV22	P$_{ftsZ}$-*ftsZ-gfpmut2* in *mreD* background	Nm, Sm, Sp	Velázquez-Suárez *et al.*, (2022a)
CSFR18	P$_{ND}$-ftsZ	Sm, Sp	Ramos-León *et al.*, (2015)
CSL109	P$_{ND}$-zipN	Sm, Sp	Camargo *et al.*, (2019)
CSCV19	*sepJ-gfpmut2,* in *mreD* background	Nm, Sm, Sp	Velázquez-Suárez *et al.*, (2022b)

Other articles published or in preparation during this Ph.D. Thesis time period

Interactions of PatA with the Divisome during Heterocyst Differentiation in *Anabaena*

Interactions of PatA with the Divisome during Heterocyst Differentiation in *Anabaena*

Ana Valladares,[a,b] Cristina Velázquez-Suárez,[a,b] Antonia Herrero[a,b]

[a]Instituto de Bioquímica Vegetal y Fotosíntesis, CSIC, Seville, Spain
[b]Universidad de Sevilla, Seville, Spain

ABSTRACT The *Anabaena* organismic unit is a filament of communicating cells. Under conditions of nitrogen scarcity, some cells along the filament differentiate into heterocysts, which are specialized in the fixation of atmospheric N_2 and provide the vegetative cells with N_2 fixation products. At a certain stage, the differentiation process becomes irreversible, so that even when nitrogen is replenished, no return to the vegetative cell state takes place, possibly as a consequence of loss of cell division capacity. Upon N-stepdown, midcell FtsZ-rings were detected in vegetative cells, but not in differentiating cells, and this was also the case for ZipN, an essential protein that participates in FtsZ tethering to the cytoplasmic membrane and divisome organization. Later, expression of *ftsZ* was arrested in mature heterocysts. PatA is a protein required for the differentiation of intercalary heterocysts in *Anabaena*. The expression level of the *patA* gene was increased in differentiating cells, and a mutant strain lacking PatA exhibited enhanced FtsZ-rings. PatA was capable of direct interactions with ZipN and SepF, another essential component of the *Anabaena* Z-ring. Thus, PatA appears to promote inhibition of cell division in the differentiating cells, allowing progress of the differentiation process. PatA, which in mature heterocysts was detected at the cell poles, could interact also with SepJ, a protein involved in production of the septal junctions that provide cell-cell adhesion and intercellular communication in the filament, hinting at a further role of PatA in the formation or stability of the intercellular structures that are at the basis of the multicellular character of *Anabaena*.

IMPORTANCE *Anabaena* is a cyanobacterial model that represents an ancient and simple form of biological multicellularity. The *Anabaena* organism is a filament of cohesive and communicating cells that can include cells specialized in different tasks. Thus, under conditions of nitrogen scarcity, certain cells of the filament differentiate into heterocysts, which fix atmospheric nitrogen and provide organic nitrogen to the rest of cells, which, in turn, provide heterocysts with organic carbon. Heterocyst differentiation involves extensive morphological, biochemical, and genetic changes, becoming irreversible at a certain stage. We studied the regulation during heterocyst differentiation of several essential components of the *Anabaena* cell division machinery and found that protein PatA, which is required for differentiation and is induced in differentiating cells, interacts with essential cell division factors and destabilizes the cell division complex. This suggests a mechanism for establishment of commitment to differentiation by inhibition of cell division.

KEYWORDS *Cyanobacteria*, bacterial multicellularity, cell differentiation, cell division

*A*nabaena sp. strain PCC 7120 (here referred to as *Anabaena*) is a model of filamentous cyanobacteria able to undertake a developmental program to form a multicellular diazotrophic bacterium. In response to nitrogen shortage, some cells of the filament differentiate into cells specialized in the fixation of atmospheric nitrogen (N_2),

Address correspondence to Antonia Herrero, herrero@ibvf.csic.es.

called heterocysts, which are distributed in a semiregular pattern of two heterocysts separated by an average of ca. 10 vegetative cells along the filament. Thus, the diazotrophic filament is composed of two cell types that exchange nutrients and regulatory molecules: the vegetative cells, which fix CO_2 and transfer C-rich compounds (sugars) to heterocysts, and the heterocysts, which fix N_2 and donate N-rich compounds (amino acids) (1). Additionally, at least one morphogen, PatS, is also transferred from the differentiating cells to inhibit differentiation of its neighbors, thus contributing to the setting of the heterocyst distribution pattern (2, 3). Several septal proteins, including SepJ, FraC, and FraD (4), have been implicated in the formation of the septal junctions that bridge the cytoplasms of neighboring cells and provide cohesion and intercellular communication along the filament.

Vegetative cells and heterocysts differ in multiple morphological and physiological features as the result of largely different gene expression programs that are established in each cell type during the differentiation process, including multiple events of transcriptional *regulation* (the process that has been most extensively studied) but also events of posttranslational *regulation*, which are currently being dissected (5). Two principal transcriptional regulators are required for differentiation: the cAMP receptor protein (CRP)-family type NtcA global factor, which mediates regulatory responses to changes in the C-to-N balance of the cells (6), and HetR, which mediates gene activation in the differentiating cells (7).

Heterocysts are terminally differentiated cells, which implies that beyond a certain point in the differentiation process no reversion to the vegetative cell entity takes place, even when the cue that triggers differentiation, i.e., nitrogen deficiency, is abrogated (8, 9). In the mature diazotrophic filament, old heterocysts are thought to undergo senescence and finally go dead. Irreversibility of heterocyst differentiation can be related to loss of cell division capacity, which is assumed to take place roughly coincidently with the commitment to differentiation. FtsZ has been reported to occur at lower levels in mature heterocysts than in vegetative cells (10, 11). However, the mechanism responsible for an asymmetric distribution of FtsZ in the diazotrophic filament is not known. Other possible regulatory events that may result in inhibition of cell division during heterocyst differentiation are also unknown.

Several genes that are required for heterocyst differentiation have been related to the step of commitment. This is the case with *hetC*, encoding an ABC-type exporter (12) localized in the heterocyst poles that is involved in transferring the PatS morphogen to neighboring cells (13), and with *hetP* and some *hetP* homologs (14). Judging from the morphological effects of their inactivation or overexpression, two other factors that regulate heterocyst differentiation, HetF and PatA, might affect cell division. Thus, inactivation of the *hetF* gene leads to the presence of enlarged and elongated cells, and ectopic overexpression of *hetF* leads to the presence of cells smaller than those of the wild type (WT) throughout the filament (15). The PatA protein of *Anabaena* bears a CheY-like phosphoacceptor domain in its C terminus as well as a so-called PATAN domain of undetermined function (16). Inactivation of *patA* results in a phenotype of a low frequency of heterocysts that, moreover, are mainly found at the filament ends and in consequent poor growth under diazotrophic conditions (17), whereas *patA* overexpression increases the frequency of heterocysts (18).

To gain insight into the mechanism of inhibition of cell division during heterocyst differentiation, we have monitored the expression and localization of initial cell division factors and PatA along the filament during the differentiation process. We have also studied the effects of *patA* deletion on the localization of the FtsZ-ring, as well as possible interactions between PatA and proteins involved in cell division or intercellular communication.

RESULTS

Expression and localization of FtsZ during heterocyst differentiation. To study the expression from the *ftsZ* gene promoter, we generated strain CSAV43, bearing a copy of the *ftsZ* promoter fused to *gfp-mut2* in the native gene locus and keeping an
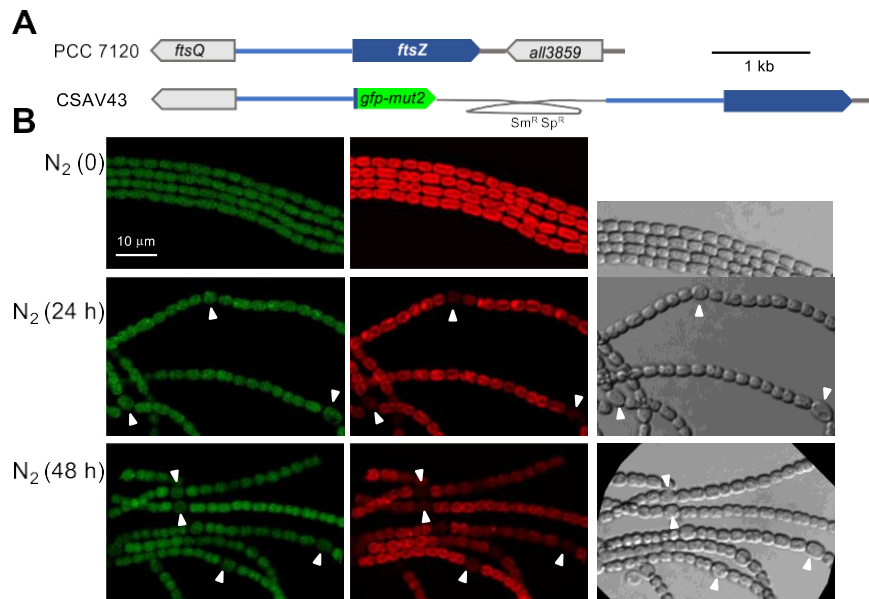
FIG 1 Expression of the *Anabaena ftsZ* gene promoter. (A) Schematic of the genome structure in the *ftsZ* region of strain CSAV43 (P*ftsZ*-*gfp*) in comparison to PCC 7120 (WT). The gray trace represents an inserted plasmid encoding resistance to Sm and Sp (see Materials and Methods for details). (B) Filaments of strain CSAV43 grown in BG11 medium were transferred (at a cell density of 2 µg Chl/ml) to BG11$_0$ (no combined nitrogen) medium (N$_2$) and incubated under culture conditions. After the times indicated, filaments were observed by confocal microscopy and photographed. Time 0 denotes the start of incubation in BG11$_0$. GFP fluorescence (green), cyanobacterial autofluorescence (red), and bright-field images are shown. Arrowheads point to heterocysts. The magnification is the same for all micrographs.

intact copy of the gene expressed from the native promoter (Fig. 1A). The spatiotemporal pattern of expression of P$_{ftsZ}$-*gfp* was monitored in cells of strain CSAV43 grown with nitrate and transferred to medium lacking combined nitrogen, which triggers heterocyst differentiation (Fig. 1B). At the onset of N deprivation, filaments showed similar levels of green fluorescent protein (GFP) fluorescence in all the cells. Then, certain cells along the filament differentiated to heterocysts, so that after 24 h many regularly spaced mature heterocysts, recognized by loss of red fluorescence (due to dismantlement of photosystem II) and by cell morphology (including increased cell size and the presence of refringent polar granules made of cyanophycin, a product of N$_2$ fixation), could be detected. At that time, most heterocysts exhibited GFP fluorescence similar to that in neighboring vegetative cells (the mean level of fluorescence intensity in heterocysts was ca. 1.1 times that in vegetative cells, as counted over 40 heterocysts and 341 vegetative cells). After 48 h, GFP fluorescence in heterocysts became noticeably lower that in vegetative cells (the mean level of fluorescence intensity in heterocysts was ca. 0.7 times that in vegetative cells, as counted over 40 heterocysts and 255 vegetative cells). Thus, the *ftsZ* promoter was downregulated in heterocysts well after the differentiation process has been completed.

We have also studied the localization of FtsZ upon N-stepdown in *Anabaena* strain CSSC19, which expresses a *ftsZ-gfp-mut2* gene fusion placed at the *ftsZ* locus and which keeps an intact copy of *ftsZ* also expressed from the native promoter (19) (Fig. 2A). As shown in Fig. 2B, at 18 h after nitrate removal, GFP fluorescence could be detected in midcell rings in all the cells of the filament, including differentiating cells (the mean level of fluorescence intensity in proheterocysts was ca. 1.2 times that in vegetative cells, as counted over 9 proheterocysts and 126 vegetative cells). By 22 h, proheterocysts still exhibiting high GFP fluorescence, together with immature heterocysts (recognized by a thickened cell envelope) showing low GFP fluorescence, could be detected (the mean levels of fluorescence intensity in proheterocysts and immature
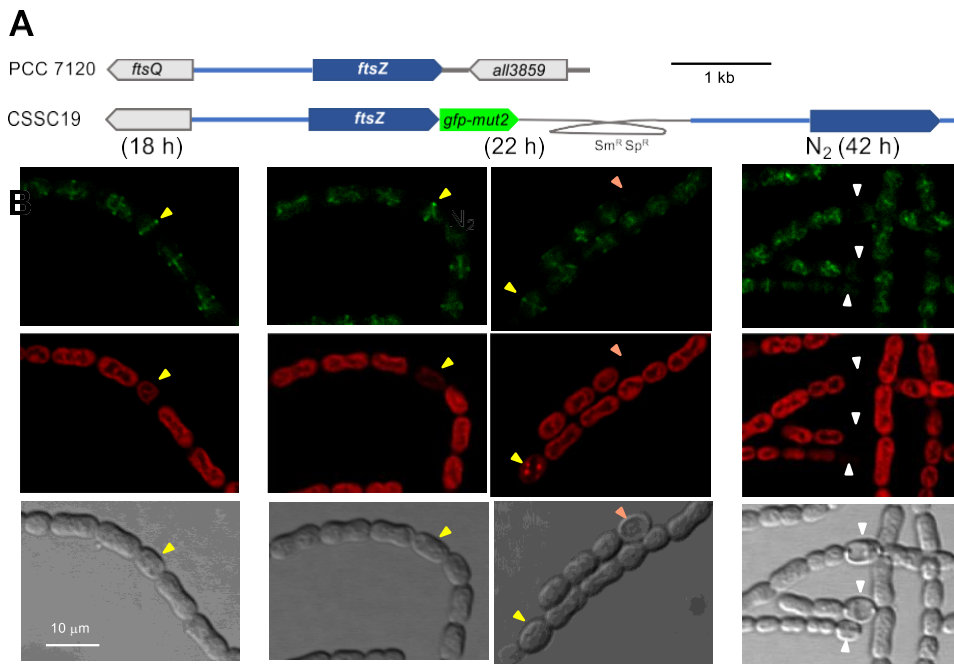
FIG 2 Localization of FtsZ during heterocyst differentiation in *Anabaena*. (A) Schematic of the genome structure of strain CSSC19 (*ftsZ-gfp-mut2*) (19) in comparison to PCC 7120 (WT). The gray trace represents an inserted plasmid encoding resistance to Sm and Sp. (B) Filaments of strain CSSC19 grown in BG11 medium were transferred (at a cell density of 2 µg Chl/ml) to $BG11_0$ medium and incubated under culture conditions. After the times indicated, filaments were observed by confocal microscopy and photographed. GFP fluorescence (green), cyanobacterial autofluorescence (red), and bright-field images are shown. Arrowheads point to proheterocysts (yellow), immature heterocysts (orange), and mature heterocysts, exhibiting polar refringent granules (white). The magnification is the same for all micrographs.

heterocysts were ca. 0.9 and 0.2 times that in vegetative cells, respectively, as counted over 23 proheterocysts, 20 immature heterocysts, and 238 vegetative cells). After 42 h, GFP fluorescence was high in vegetative cells and low in mature heterocysts (which exhibited conspicuous polar granules) (the mean level of fluorescence intensity in heterocysts was ca. 0.2 times that in vegetative cells, as counted over 11 heterocysts and 255 vegetative cells). Thus, Z-rings appear to be lost during the process of heterocyst differentiation.

Downregulation of ZipN during heterocyst differentiation. ZipN is an FtsZ-interacting protein that contributes to FtsZ tethering to the cytoplasmic membrane and is an essential part of the Z-ring in *Anabaena* (20). To study the localization of ZipN during heterocyst differentiation, we generated *Anabaena* strain CSAV39, which bears a version of the *zipN* gene 5= fused to the *sf-gfp* gene (encoding superfolder GFP) in the *zipN* locus (Fig. 3A). Upon nitrate withdrawal, GFP fluorescence localized in midcell rings and in intercellular regions could be detected in vegetative cells but not in either proheterocysts (see 18-h data in Fig. 3B) or heterocysts (see 22-h and 42-h data). This shows that the ZipN protein levels are negatively regulated during heterocyst differentiation.

Morphological features of a *patA* mutant. Strain UHM101, an *Anabaena* mutant in which the coding region of the *patA* gene was deleted, forms predominantly terminal heterocysts (21) (see Fig. 4A). Here, we studied cell and filament size in strain UHM101 in comparison to wild-type *Anabaena*. Cell area was significantly larger in the *patA* mutant than in the wild type, both after incubation with nitrate (mean cell area, 8.47 μm^2 for the wild type [WT] and 10.65 μm^2 for the *patA* mutant) and, in particular, after incubation in the absence of combined nitrogen (mean vegetative cell area after 4 days
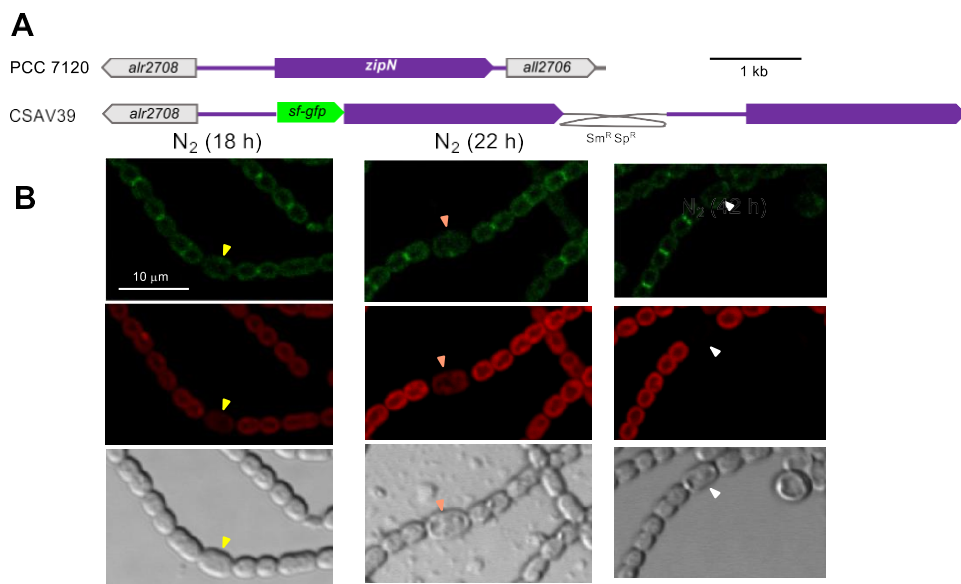
FIG 3 Localization of ZipN during heterocyst differentiation in *Anabaena*. (A) Schematic of the genome structure of strain CSAV39 (*sf-gfp-zipN*) in comparison to PCC 7120 (WT). (B) Filaments of strain CSAV39 were treated as described in the legend for Fig. 2, observed by confocal microscopy, and photographed. Arrowheads point to proheterocysts (yellow), immature heterocysts (orange), and mature heterocysts that exhibit polar refringent granules (white). The magnification is the same for all micrographs.

under diazotrophic conditions, 6.69 μm^2 WT and 9.76 μm^2 *patA* mutant; mean vegetative cell area after 9 days, 6.74 μm^2 WT and 9.64 μm^2 *patA* mutant) (Fig. 4A and B). In addition, filaments were considerably longer in the mutant than in the wild type (Fig. 4C).

Expression and localization of PatA. The expression of the *patA* gene has been described as increasing upon N-stepdown, but always taking place at low levels (17, 22). To study the spatiotemporal pattern of *patA* expression during differentiation, we generated *Anabaena* strain CSAV45, which expresses a fusion of the *patA* gene promoter to *gfp-mut2* in the *patA* locus (Fig. 5A). Fluorescence was monitored in filaments of strain CSAV45 grown with nitrate and incubated during different times after removal of nitrate (Fig. 5B). Only low levels of GFP fluorescence were detected in strain CSAV45, although even at time zero (nitrate growth), the level of fluorescence was noticeably higher than in wild-type *Anabaena* (not bearing the *gfp* gene). Upon N-stepdown, GFP fluorescence increase was detected after 24 h, in cells that still resemble proheterocysts and immature heterocysts. By 48 h, GFP fluorescence in mature heterocysts had decreased to basal levels. Thus, activation of *patA* expression during heterocyst differentiation seems to be transitory. (Given the low expression level, we cannot rule out the possibility that the *patA* gene was activated earlier than the time at which accumulation of GFP was detected.)

To study the localization of PatA, we generated two strains bearing *patA* fusions to *sf-gfp* inserted in the native *patA* locus and maintaining an intact *patA* gene: strain CSAV35 bears a *patA* gene 3= fused to *sf-gfp* and strain CSAV41 a *patA* gene 5= fused to *sf-gfp* (Fig. 6A). In media supplemented with nitrate, both strains, CSAV35 and CSAV41, grew well, and their filament morphology was similar to that of the wild type (Fig. 6C). In the absence of combined nitrogen, both strains were able to grow, although growth was somewhat impaired in comparison to that seen with the wild type (Fig. 6B). Strains CSAV35 and CSAV41 were able to differentiate terminal and intercalary heterocysts (Fig. 6C), although, with regard to the wild type, differentiation was somewhat delayed, and the frequency of intercalary heterocysts was lower in

A

B

C
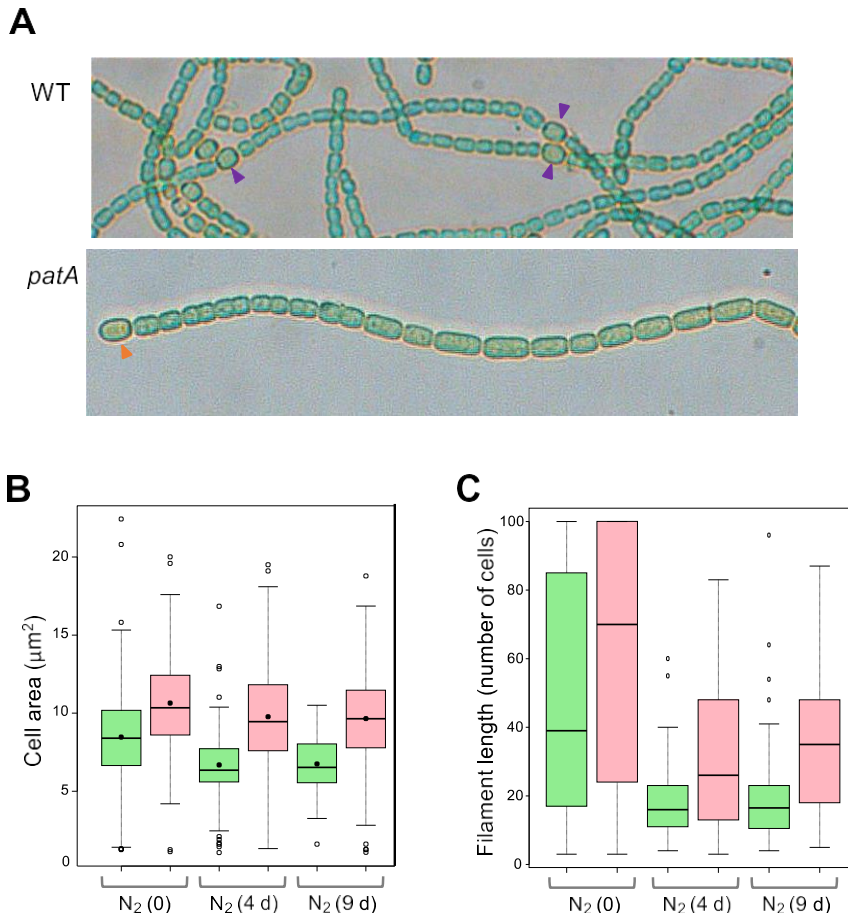
FIG 4 Cell and filament size in a *patA* mutant. Strains PCC 7120 (WT) and UHM101 (*patA* mutant) grown in BG11 medium (NO_3^-) were transferred to BG11$_0$ medium (N$_2$) and incubated under culture conditions. At time zero and after 4 and 9 days on incubation in BG11$_0$ medium, filaments were observed with a bright-field microscope and photographed. (A) Filaments after 4 days of incubation in BG11$_0$. Purple arrowheads indicate intercalary heterocysts and orange arrowheads terminal heterocysts. (B) Photographs were used for determination of cell area (vegetative cell area in the case of N$_2$ cultures) as described in Materials and Methods. A total of 200 to 250 cells of each strain were measured under each condition. A box plot representation of the data is shown. Mean values are represented by black dots. (C) Filament length was counted as the number of cells per filament over 50 to 60 filaments for each strain and condition. Filaments with more than 100 cells were counted as representing 100 cells. WT, green; *patA* mutant, pink.

CSAV35 than in CSAV41 or the wild type. In both the CSAV35 and CSAV41 mutant strains, occasional aberrant cells could be observed, and those cells were more notice-able under conditions of rapid growth (see Fig. 6C). This suggests some degree of interference with cell division, which might have resulted from the presence of two *patA* copies.

GFP fluorescence was monitored in strains CSAV35 and CSAV41. Only occasional weak signals were detected, and, in both strains, they were seen as condensed spots in the polar regions of heterocysts. These signals were absent from strain PCC 7120 (lacking GFP) (Fig. 7).

Localization of FtsZ in a *patA* mutant background. To test whether the mutation of the *patA* gene had any effect on the conformation of FtsZ-rings, we generated strain CSAV38, which bears in UHM101 (*patA* background) the same *ftsZ-gfp-mut2* gene fusion present in strain CSSC19 (wild-type background; see above) (Fig. 8A). In nitrate-grown filaments, both strain CSSC19 and strain CSAV38 showed GFP fluorescence in midcell rings. Notably, the intensity of GFP fluorescence was stronger in CSAV38 than in CSSC19 (the mean midcell fluorescence intensity in CSAV38 was ca. 1.6 times that in CSSC19, as

A

B
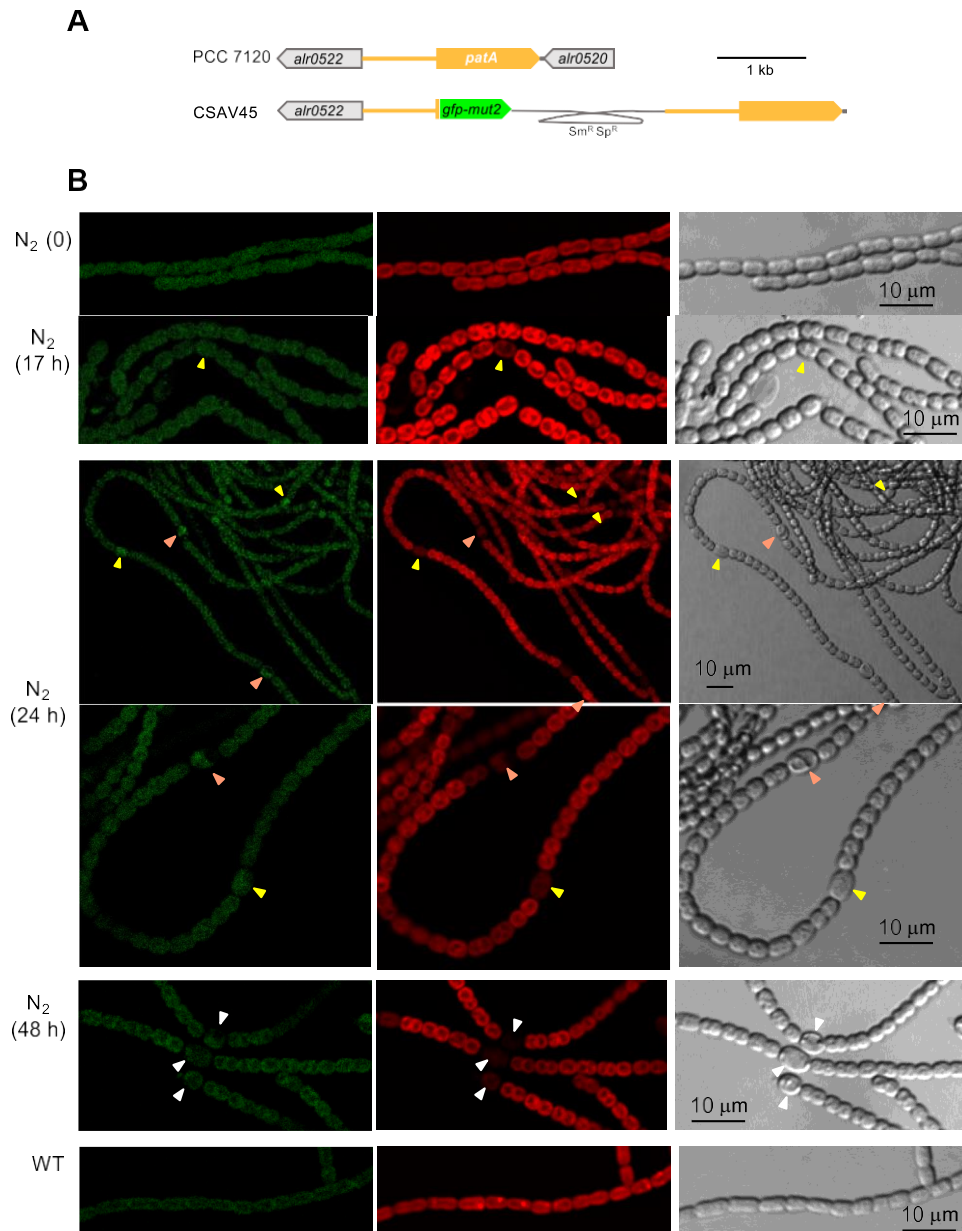
FIG 5 Expression of the *Anabaena patA* gene promoter. (A) Schematic of the genome structure of strain CSAV45 (P_{patA}-*gfp*) in comparison to PCC 7120 (WT). The gray trace represents an inserted plasmid encoding resistance to Sm and Sp (see Materials and Methods for details). (B) Filaments of strain CSAV45 grown in BG11 medium were transferred (at a cell density of 2 µg Chl/ml) to $BG11_0$ medium and incubated under culture conditions. After the times indicated, filaments were observed by confocal microscopy and photographed. Time 0 denotes the start of incubation in $BG11_0$. GFP fluorescence (green), cyanobacterial autofluorescence (red), and bright-field images are shown. Arrowheads point to proheterocysts (yellow), immature heterocysts (orange), and mature heterocysts that exhibit polar refringent granules (white).

counted over 50 cells of CSAV38 and 59 cells of CSSC19; Student's *t* test, $P = 10^{-17}$) (see Fig. 8B for representative images), suggesting that the deletion of *patA* has a positive effect on the formation or stability of the Z-ring. Upon N-stepdown, strain CSAV38, similarly to its parental UHM101 strain, produced mostly terminal heterocysts. After incubation in the absence of combined nitrogen, the levels of fluorescence intensity in vegetative cells of CSSC19 and CSAV38 were similar (the mean midcell fluorescence intensity in CSAV38 was ca. 0.9 times that in CSSC19, as counted over 51 cells of CSAV38 and 55 cells of CSSC19; Student's *t* test, $P = 0.09$). However, a noticeable difference
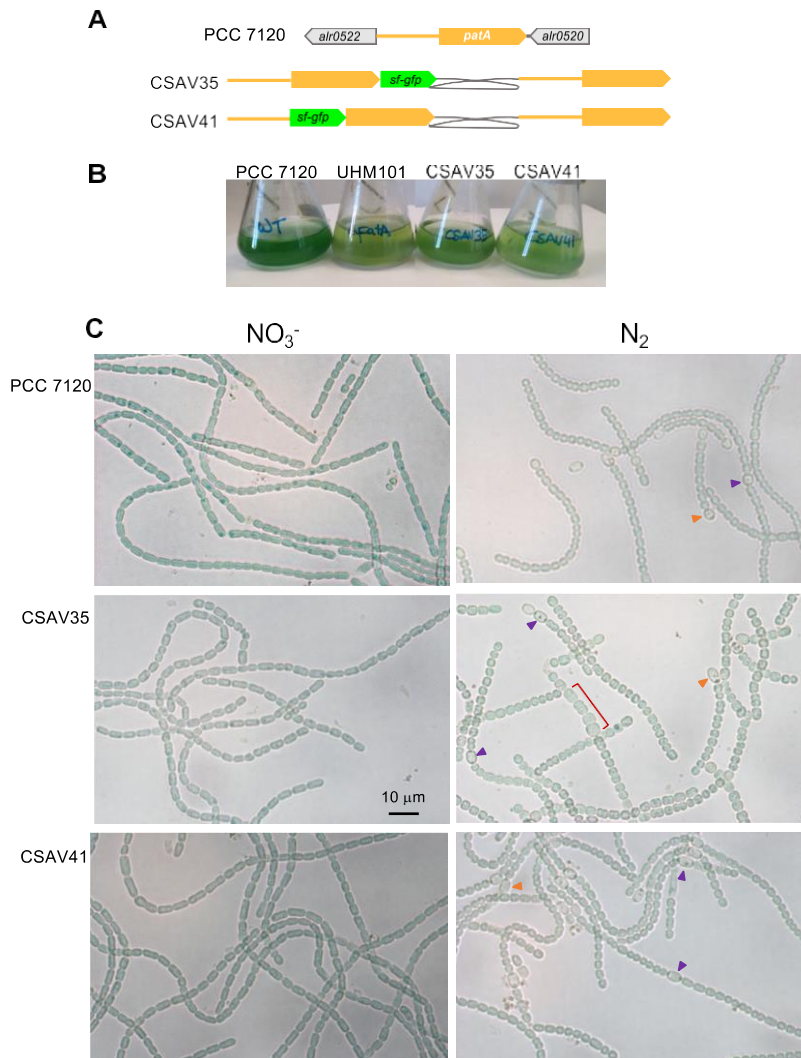
FIG 6 Growth and morphology of strains expressing GFP fusions to PatA. (A) Schematic of the genome structure of strain CSAV35 (*patA-sf-gfp*) and strain CSAV41 (*sf-gfp-patA*) in comparison to PCC 7120 (WT). The gray trace represents an inserted plasmid encoding resistance to Sm and Sp (see Materials and Methods for details). (B) Cultures in BG11 medium (containing NO_3^-) were used to inoculate flasks with $BG11_0$ medium (at a cell density equivalent to 1 µg Chl/ml), which were incubated under culture conditions and photographed after 4 days. Strain UHM101 is a *patA* mutant (see the text). (C) Filaments from flasks inoculated with 0.5 µg Chl/ml and photographed after 43 h. Purple arrowheads indicate intercalary heterocysts, orange arrowheads terminal heterocysts, and red brackets stretches of aberrant cells in the filament. The magnification is the same for all micrographs.

between the two strains was that CSAV38 did not exhibit intercalary cells devoid of GFP fluorescence, as observed in CSSC19 (Fig. 8C; see also Fig. 2).

PatA interactions with *Anabaena* cell division factors. Given the apparent effects of *patA* alterations on cell morphology and detection of the cell division ring, we used bacterial adenylate cyclase two-hybrid system (BACTH) analysis to test possible direct interactions of PatA with identified components of the *Anabaena* Z-ring, namely, the proteins FtsZ, ZipN, Ftn6, and SepF. Also, because of the apparent polar localization of PatA in the heterocysts, we tested interactions with *Anabaena* septal junction proteins SepJ, FraC, and FraD. For that, all four possible versions of PatA (T18-PatA, PatA-T18, T25-PatA, and PatA-T25) were generated. A strong interaction of T18-PatA with T25-ZipN was detected (as already published [20], T25-ZipN was the only ZipN fusion that we were able to clone). A clear interaction was also detected involving T18-PatA and SepF-T25. Finally, a weak but significant interaction was detected between T25-PatA
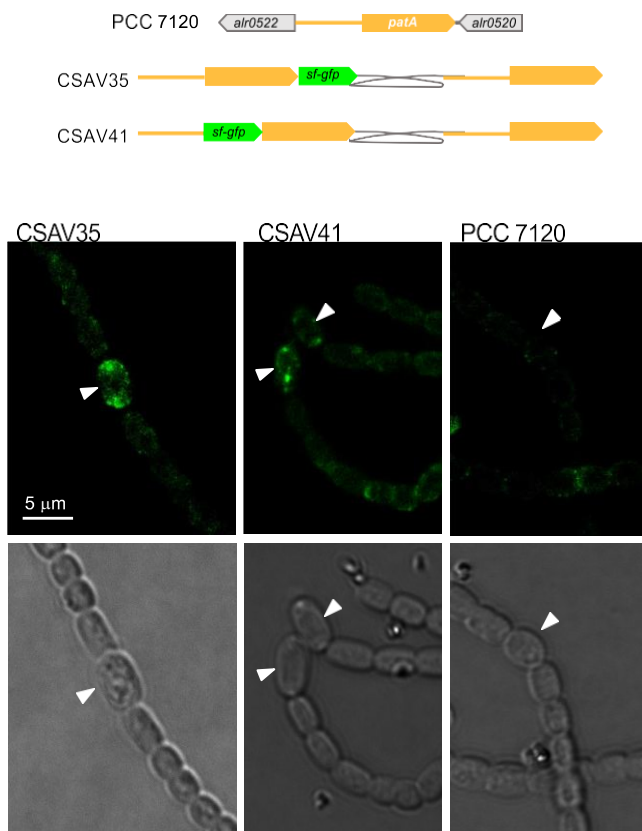
FIG 7 Localization of PatA during heterocyst differentiation. (A) Schematic of the genome structure of strain CSAV35 (*patA-sf-gfp*) and strain CSAV41 (*sf-gfp-patA*) in comparison to PCC 7120 (WT). (B) Filaments of strains PCC7120, CSAV35, and CSAV41 grown in BG11 medium were transferred to BG11$_0$ medium and incubated under culture conditions. After 22 h, filaments were observed under a fluorescence microscope and photographed. GFP fluorescence (green) and bright-field images are shown. Arrowheads point to heterocysts. The magnification is the same for all micrographs.

and SepJ-T18 (Fig. 9). No significant interaction was detected involving C-terminal fusions to PatA (i.e., neither PatA-T18 nor PatA-T25), suggesting that these fusions could lead to the production of PatA versions that are not active for BACTH analysis.

The interaction between PatA and ZipN was also assessed by copurification assays. A version of ZipN that included a 6XHis tag fused to its N-terminal end and a version with PatA N-terminally fused to a Strep-tag were generated. Cell-free extracts of *E. coli* expressing each of these proteins alone or mixed together were incubated and then passed through a His-select column, and the presence of Strep-PatA in the eluted fractions was assessed by immunoblotting with antibodies against the Strep-tag and by matrix-assisted laser desorption ionization–time of flight (MALDI-TOF). As shown in Fig. 10, Strep-PatA, as revealed by immunoblotting, was tightly retained in the column only when it had been previously incubated and loaded together with His-ZipN. In the fractions that, according to Western blotting results, contained His-ZipN and Strep-PatA, MALDI-TOF analysis rendered PatA protein sequence coverage of 34% and a Mascot score of 177 (protein scores greater than 93 were considered significant; $P < 0.05$). For ZipN, sequence coverage of 12% and a Mascot score of 102 were obtained. Taken together, the results of the BACTH and copurification analyses indicate that PatA interacts with ZipN.

DISCUSSION

In the filamentous cyanobacterium *Anabaena*, heterocysts specialized in the fixation of atmospheric nitrogen differentiate in a semiregular spatial pattern under conditions of nitrogen scarcity. Heterocysts are terminally differentiated cells that do not divide or

A

B

C
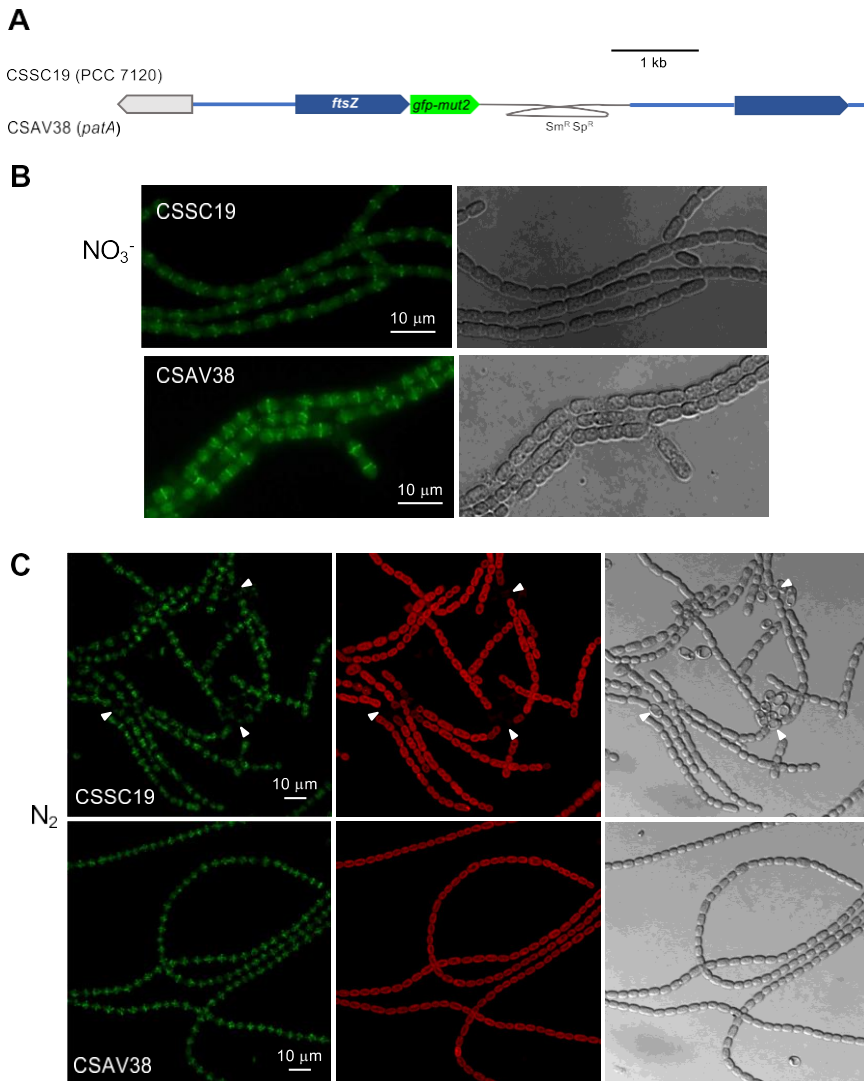
FIG 8 Visualization of FtsZ in a *patA* mutant background. (A) Schematic of the genome structure of strain CSSC19 (*ftsZ-gfp-mut2* in WT background) (19) and strain CSAV38 (*ftsZ-gfp-mut2* in *patA* mutant background) (see Materials and Methods for details). (B) Nitrate-grown filaments were observed under a fluorescence microscope and photographed. (C) Nitrate-grown filaments were incubated for 42 h in BG11$_0$ medium and observed with a confocal microscope and photographed. GFP fluorescence (green), cyanobacterial autofluorescence (red), and bright-field images are shown. Arrowheads point to mature heterocysts.

revert to the vegetative-cell state. At an intermediate stage during differentiation, the process becomes irreversible (8, 9). A question arises concerning whether commitment to differentiation is related to loss of cell division capacity and what the mechanism of inhibition of cell division might be during differentiation.

It has been reported that FtsZ is undetectable, by immunoblotting, in cell extracts from mature heterocysts (10). On the other hand, expression of a GFP reporter directed from the *ftsZ* gene promoter placed in a shuttle plasmid was downregulated in heterocysts (23), and a FtsZ-GFP fusion protein expressed from the heterologous *petE* promoter placed in the same shuttle vector was observed in proheterocysts (12 h after N-stepdown) but not in heterocysts (19 or 24 h after N-stepdown) (24). However, these constructs may not reflect the physiological regulation of the *ftsZ* gene and the FtsZ protein because the shuttle vector used to clone the reporters (pRL25c, based on *Nostoc* plasmid pDU1) is maintained in *Anabaena* with variable copy numbers (25) and, moreover, the P$_{petE}$ promoter itself may be downregulated in heterocysts. Regarding
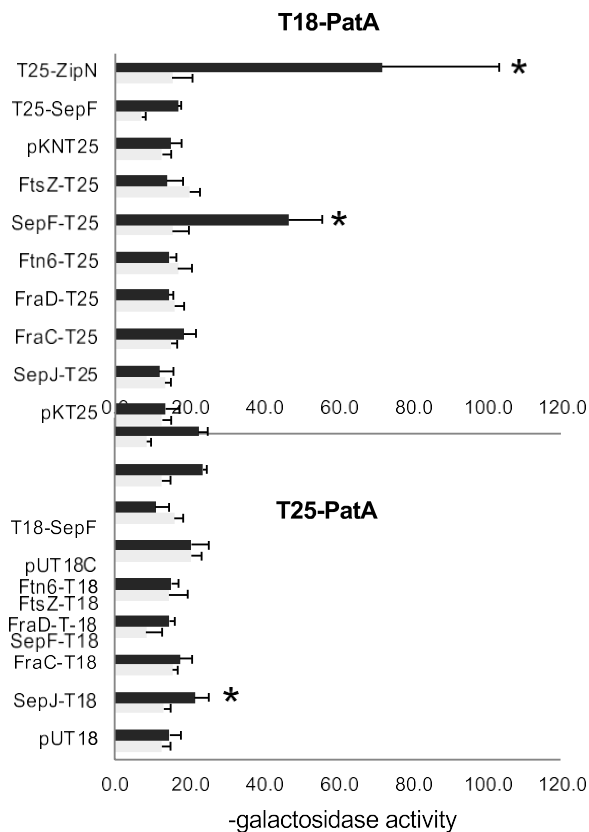
FIG 9 BACTH assays of PatA interactions. Interactions of protein pairs produced in *E. coli* were assayed by measurements of -galactosidase activity (nmol ONP min^{-1} mg $protein^{-1}$) in liquid cultures incubated at 30°C. The topology of each fusion is indicated by the order of components (T18-protein and T25-protein denote the corresponding adenylate cyclase domains fused to the N terminus of the test protein, whereas protein-T18 and protein-T25 denote fusions to the C terminus). Data represent means and standard deviations of 2 to 8 determinations of the activity assayed with the indicated protein fused to T25 (or empty vector pKNT25 or pKT25) and T18-PatA (dark bars) or with the indicated protein fused to T25 (or empty vector pKNT25 or pKT25) and pUT18C (clear bars) (upper part) or with the indicated protein fused to T18 (or empty vector pUT18C or pUT18) and T25-PatA (dark bars) or the indicated protein fused to T18 (or empty vector pUT18C or pUT18) and pKT25 (clear bars) (lower part). The significance of differences was assessed by Student's *t* tests. Asterisks indicate strains expressing a pair of tested proteins that exhibited -galactosidase activity significantly different ($P < 0.01$) from that seen with all three controls: the strain containing both empty vectors and the two strains expressing each fused protein and containing the complementary empty vector.

regulation of *zipN*, we are not aware of any previous report showing the expression of the *zipN* gene or the localization of the ZipN protein during heterocyst differentiation. In this work, we have generated strains in which gene and protein reporters are expressed at levels similar to the physiological levels. Thus, in strain CSAV43, the *gfp* fusion to the *ftsZ* promoter preserves all the promoter and translation initiation signals and is placed in the native genomic locus. In CSSC19 and CSAV39, the genes encoding FtsZ and ZipN protein fusions to GFP, respectively, are also placed in their respective native loci. To minimize possible effects of a lack of an intact copy of the proteins on promoter activity or cell physiology, we chose to keep an intact version of the corresponding gene expressed from its native promoter as well.

We have observed that, upon combined nitrogen deprivation, downregulation of the *ftsZ* promoter was a late event, taking place in mature heterocysts (observed 48 h after N-stepdown; Fig. 1), whereas midcell FtsZ-rings were already downregulated in immature heterocysts (Fig. 2). Regarding ZipN, loss of this protein from differentiating
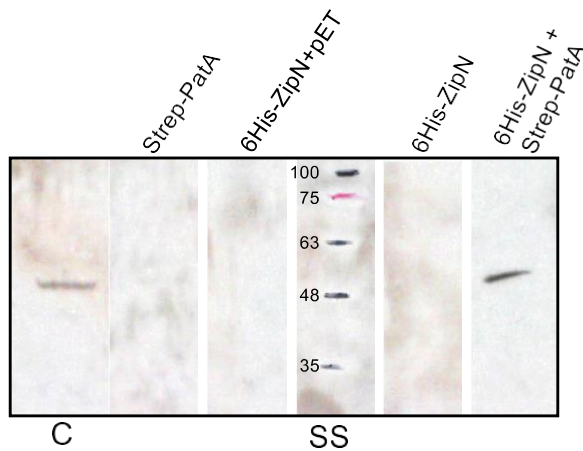
FIG 10 Copurification of PatA and ZipN proteins. Cell-free extracts of *E. coli* expressing 6His-ZipN or Strep-tag-PatA, or including plasmid vector pET28b, were incubated individually, or in various combinations, at 4°C overnight and were passed through a His-Select column (see Materials and Methods). After loading, the column was washed first with buffer A and then with the buffer supplemented with 300 mM imidazole. Finally, tightly bound proteins were eluted with buffer supplemented with 1 M imidazole. Aliquots of the eluents were subjected to Western blotting with antibodies against Strep-tag. C, purified Strep-tag-PatA (45.257 kDa); SS, size standard (kDa).

cells was already observed at early stages, in proheterocysts (Fig. 3). Because ZipN has an essential role in the stability of the Z-ring (20), these observations are consistent with a sequence of regulatory events in which an initial loss of ZipN during differentiation leads to Z-ring destabilization, before downregulation of the *ftsZ* gene, which in turn would result in a permanent incapacity for cell division in the mature heterocyst.

The protein PatA is required for the differentiation of intercalary heterocysts in *Anabaena*. Because terminal cells in the filament contact other cells at only one pole, it can be considered that heterocyst differentiation at the filament ends, such as in *patA* mutants, might be less sensitive to positional information (e.g., information established by intercellularly transferred inhibitors) that impacts the differentiation of intercalary heterocysts (see reference 21). Thus, differentiation at the filament ends could take place even in the absence of some of the regulatory factors required for intercalary differentiation. The *patA* gene is expressed at undetectable levels in the presence of combined nitrogen, and is induced, although always with a low expression level, upon N-stepdown. Some observations suggest that PatA may have a connection to cell division. In a previous report, expression of *patA* from the *petE* promoter determining high overexpression in vegetative cells (construct carried in a plasmid based on pRL444) resulted in enlarged cells with aberrant morphology in both the presence and absence of combined nitrogen, and a PatA-GFP fusion overexpressed equally was concentrated in midcell ring-like structures in dividing cells (18). Although, as recognized by the authors, these effects appear to have been overexpression artifacts, those results might suggest that the PatA protein has an intrinsic capacity of interaction with some component(s) of the *Anabaena* divisome, thus impacting cell division. Under diazotrophic conditions, we have also observed occasional morphological alterations, including an increase in cell size, in strains that express PatA fusions to GFP at physiological levels together with the native PatA (see Fig. 6C), with the alterations being more pronounced under conditions of rapid growth. These observations are consistent with the idea that PatA interferes with cell division.

Previously, GFP directed from a P_{patA}-*gfp* reporter fusion, placed in plasmid pRL25c, was detected in heterocysts 24 h after N-stepdown (22). Using *gfp* fusions to the *patA* gene promoter in the native genomic locus, we have detected that GFP is transiently accumulated upon N-stepdown, being detected in proheterocysts and immature heterocysts and fading thereafter (Fig. 5). The detection of activation of P_{patA} in differentiating cells is consistent with the previous description of upregulated transcription

from one transcription start point located at 614/645 nucleotides upstream of *patA* (18) and with regulation by NtcA (22). Both PatA-sfGFP (PatA-superfolder GFP) (in strain CSAV35) and sfGFP-PatA (in strain CSAV41) protein fusions are observed at the polar regions of the heterocysts (Fig. 7). Given the low level of expression of the PatA protein, the concentration at the heterocyst poles could facilitate visualization in this position. However, this might not be the only localization of PatA. Indeed, the previous hints of PatA localization in cell division complexes are extended by our results showing PatA interactions with the essential components of the *Anabaena* divisome ZipN and SepF. Taking all these results together, it can be suggested that during heterocyst differentiation, PatA might first interact with ZipN (and SepF), with the effect of destabilizing the FtsZ-ring, thus mediating inhibition of cell division. This inhibitory effect is supported by our observation that the levels of FtsZ-GFP in midcell Z-rings are higher in the *patA* mutant than in the wild type (Fig. 8). Upon N-stepdown, the absence of PatA in the mutant would favor persistence of divisional complexes in all the cells of the filament, with the effect of impeding the progression of differentiation. A first interaction of PatA with ZipN is consistent with the strong interaction between these proteins observed in BACTH assays. In summary, we propose that at a certain stage during heterocyst differentiation, PatA inhibits the establishment of the cell division complex to allow completion of differentiation. Later, PatA would localize to the cell poles (as seen in Fig. 7), where it could interact with SepJ, consistent with the significant PatA-SepJ interactions detected in BACTH assays. By acting on SepJ, PatA could affect intercellular communication between heterocysts and its neighboring vegetative cells, an issue worth of further investigation.

MATERIALS AND METHODS

Strains and growth conditions. *Anabaena* sp. strain PCC 7120 and strains UHM101, CSSC19, CSAV35, CSAV38, CSAV39, CSAV41, CSAV43, and CSAV45 were grown in BG11 medium (which includes NaNO$_3$ as a nitrogen source) (26) containing ferric citrate instead of ferric ammonium citrate, or in BG11$_0$ medium, which lacks NaNO$_3$, supplemented with 4 mM NH$_4$Cl and 8 mM TES-NaOH [*N*-tris(hydroxymethyl)methyl-2-aminoethanesulfonic acid-NaOH] buffer (pH 7.5). For incubation in the absence of combined nitrogen, BG11$_0$ medium was used. Cultures were incubated at 30°C in white light (30 µmol photons m^{-2} s^{-1} from LED lamps), in shaken liquid media, or in plates solidified with 1% agar. For strains CSSC19, CSAV35, CSAV38, CSAV39, CSAV41, CSAV43, and CSAV45, the growth medium was supplemented with spectinomycin (Sp) and streptomycin (Sm) at 5 µg ml^{-1} each in solid media and 2 µg ml^{-1} each in liquid media. Chlorophyll content (Chl) of the cultures was determined after extraction with methanol (27). (In *Anabaena*, 1 µg Chl corresponds to ca. 3.3 X 10^6 cells.)

Plasmid and strain constructions. To generate *Anabaena* strains reporting the *ftsZ* (alr3858) or the *patA* (all0521) gene promoter, DNA fragments of 1,037 bp or of 777 bp, encompassing the first six codons and sequences upstream of *ftsZ* or *patA*, respectively, flanked by EcoRV and ClaI sites, were amplified by PCR using *Anabaena* DNA as the template and primers ftsZ-52/ftsZ-53 (all oligodeoxynucleotide primers used are listed in Table 1) (for *ftsZ*) or plasmid pCSAV271 (see below) as the template and primers patA-23/patA-24 (for *patA*). Both fragments were cloned into plasmid pCSEL22 (28), rendering plasmid pCSAV281, which contains a fusion of the *ftsZ* promoter region and sequences encoding the first six amino acids of FtsZ and promoter-less *gfp-mut2*, and plasmid pCSAV280, which contains a fusion of the *patA* promoter and sequences encoding the first six amino acids of PatA and promoter-less *gfp-mut2*. All plasmids used in this work were verified by sequencing. Plasmids pCSAV281 and pCSAV280 were transferred by conjugation (29) to *Anabaena* sp. strain PCC 7120, with selection for Sm and Sp (resistance is encoded in the portion vector of the transferred plasmids), and thus for clones that had the transferred plasmid inserted into the homologous genomic region by a single-crossover event. One clone that included the P$_{ftsZ}$-*gfp-mut2* construct and one that included the P$_{patA}$-*gfp-mut2* construct were selected and named strains CSAV43 and CSAV45, respectively.

For generation of an *Anabaena* derivative expressing a fusion of the FtsZ protein to GFP, plasmid pCSSC39 (containing the *gfp-mut2* gene, preceded by four Gly-encoding codons, fused to the last codon of the *Anabaena ftsZ* sequence) (19) was transferred to strain UHM101 (*patA* mutant [21]) with selection for Sm and Sp, generating strain CSAV38.

For generation of an *Anabaena* strain expressing a fusion of the ZipN protein to sfGFP, a DNA fragment containing the *zipN* promoter sequence and another containing the *sf-gfp* gene were amplified by PCR using *Anabaena* genomic DNA as the template and primers zipN-26/zipN-27 or using plasmid pCSAL39 (which includes the sfGFP-encoding sequence preceded four Gly-encoding codons [13]) and primers sfgfp-14/sfgfp-15, respectively. These fragments were joined together by the use of overlapping PCR with primers sfgfp-14/zipN-26 and cloned into pSpark vector, from which the construct was excised, with PstI ends, and transferred to PstI-digested pCSS192 (which contained the *zipN* open reading frame [ORF] cloned into vector pKT25 [20]), producing plasmid pCSAV284. Finally, the KpnI-ended P$_{zipN}$-*sf-gfp-*

TABLE 1 Oligodeoxynucleotide primers used in this work

Primer name	Primer sequence (5'–3')[a]
patA-7	GCGATCGC<u>CTGCAG</u>AACACTTCCG
patA-8	GTAATAGTTGA<u>GAATTC</u>GTAATGTG
patA-9	GCGATCGC<u>CTGCAG</u>AAACACTTCCG
patA-10	GT<u>GAATTC</u>TTATTACGTAATGTG
patA-11	AAGCAA<u>GGTCTCA</u>CGCCCGTAATGTGTTTAAA
patA-14	ATTATAAA<u>GCGGCCGC</u>CATTAACTTGGACTTTSCCC
patA-17	<u>GCC</u>ATGAAAACACTTCCGATTAC
patA-18	<u>ATCGCTGCAG</u>TTACGTAATGTGTTTAAA
patA-19	<u>AACGGGATCC</u>GGCGATCGCTCTGTTATT
patA-20	<u>TTCGCTGCAG</u>CTTTCAGGTTAATCTTTTv
patA-21	GCAA<u>CATATG</u>AAAACACTTCCGATT
patA-22	CGTT<u>GGATCC</u>TTATTACGTAATGTGTTTAAAAAT
patA-23	ATG<u>GATATC</u>AATCGGAAGTGTTTTCAT
patA-24	GAT<u>ATCGAT</u>GGTTTCTCCTGTACGGTTT
sfgfp-12	TTCG<u>GGATCC</u>ATGGCTAGCAAAGGAGAAGAA
sfgfp-13	<u>GCC</u>TCCACCGCCTTTGTAGAGCTCATC
sfgfp-14	GCACTGCAGGGCCTCCACCGCCTTTGTAGAGCTC
sfgfp-15	ATCATGAGCAAAGGAGAAGAA
ftsZ-52	GTA<u>ATCGAT</u>GTAGTACGTTTCCAGTGGC
ftsZ-53	ATG<u>GATATC</u>GTTATTATCAAGTGTCAT
zipN-24	GCAA<u>CATATG</u>TTGATCACGGTGCAG
zipN-25	CGTT<u>GGATCC</u>TTATTAATTTATAGCGGCTGA
zipN-26	GAA<u>GGTACC</u>GCCCCAAAGTCATGTCTTCG
zipN-27	<u>ATC</u>AATTCACCTAGACCATTCCAG

[a]Underlined letters indicate a restriction site.

zipN construct was transferred to conjugative plasmid pCSV3 (30), producing pCSAV285, which was transferred to *Anabaena* by conjugation with selection for Sm and Sp, generating strain CSAV39.

Two *Anabaena* strains expressing fusions of the PatA protein to sfGFP were generated. For the *patA-sf-gfp* construct, a DNA fragment was amplified using *Anabaena* DNA as the template and primers patA-14/patA-11 and was cloned in plasmid pCSAL39. The KpnI-ended P_{patA}-*patA-sf-gfp* construct was transferred to pCSV3, producing pCSAV255, which was transferred to *Anabaena* by conjugation with selection for Sm and Sp, generating strain CSAV35. For the *sf-gfp-patA* construct, a DNA fragment containing the *patA* gene and another containing the *sf-gfp* gene were amplified by PCR using pCSAV255 as the template and primers patA-17/patA-18 (for *patA*) or plasmid pCSAL39 and primers sfgfp-12/sfgfp-13 (for *sf-gfp*). These fragments were joined together by overlapping PCR with primers sfgfp-12/patA-18 and cloned into pSpark vector, rendering plasmid pCSAV272. A third DNA fragment (which included the *patA* gene promoter) was amplified using *Anabaena* DNA and primers patA-19/patA-20 and cloned in BamHI-digested pCSAV272. Finally, the P_{patA}-*sf-gfp-patA* construct was transferred to conjugative vector pRL277 (31), producing pCSAV271, which was transferred to *Anabaena* by conjugation with selection for Sm and Sp, generating strain CSAV41.

BACTH assays. BACTH assays based on the reconstitution of adenylate cyclase from *Bordetella pertussis* (32) were performed with genes amplified by PCR and cloned in pUT18, pUT18C, pKNT25, or pKT25, producing fusions to the 5' end or 3' end of the adenylate cyclase T18 and T25 fragments. Primer pairs used for amplification of *patA* were as follows: patA-7/patA-8 (T18-PatA, PatA-T18, and PatA-T25) and patA-9/patA-10 (T25-PatA). The resulting plasmids were verified by sequencing and transformed into *E. coli* XL-1-Blue for amplification. Fusions to FtsZ, ZipN, SepF, and Ftn6 (20) and to SepJ (33) were previously described; fusions to FraC and FraD (J. E. Frías and E. Flores, unpublished data) are to be described elsewhere. Isolated plasmids were cotransformed into strain BTH101 (*cya-99*), and the transformants were plated on solid LB medium containing selective antibiotics and 1% glucose. β-Galactosidase activity was measured in liquid cultures incubated at 30°C in the presence of IPTG (isopropyl-β-D-thiogalactopyranoside) and antibiotics, using *o*-nitrophenyl–β-galactoside as the substrate (33). The amount of *o*-nitrophenol (ONP) produced per mg of protein versus time was represented, and β-galactosidase activity was deduced from the slope of the linear function.

Copurification assays. For expression of *Anabaena* ZipN N-terminally fused to 6XHis, the *zipN* gene was amplified by PCR using plasmid pCSS192 and primers zipN-24/zipN-25 and cloned in pET28b (Novagen), producing plasmid pCSAV277. For expression of a version of *Anabaena* PatA N-terminally fused to Strep-tag II, the gene *patA* was amplified by PCR using plasmid pCSAV255 as the template and primers patA-21/patA-22 and cloned in the pCMN28b expression vector, which is based on pET28b and carries the Strep-tag II-encoding sequence instead of 6XHis-encoding sequence (34), producing plasmid pCSAV276. Both pCSAV276 and pCSAV277 were transformed into *E. coli* BL21.

For preparation of cell extracts, *E. coli* cells bearing pCSAV276 or pCSAV277 were incubated for 20 h at 24°C after the addition of 1 mM IPTG. Then, cells were harvested by centrifugation for 10 min at 5,000 rpm. The cell pellets were washed with buffer A (50 mM Tris-HCl [pH 7.5], 150 mM KCl, 10% glycerol) and resuspended in ice-cold buffer A (5 ml g^{-1} of cells) containing protease inhibitor cocktail complete Mini EDTA-free (Roche) and homogenized on ice for 5 min. The cell suspensions were

incubated with 1 mg ml⁻¹ lysozyme for 1 h at 4°C and were subjected to six pulses, 30 s each, of ultrasonication. The lysates were cleared by centrifugation at 15,000 X *g* for 30 min at 4°C. For copurification assays, aliquots of the resulting cell extracts were mixed and incubated overnight at 4°C. As a control, each cell extract alone, or an extract from *E. coli* (including pCSAV277) mixed with an extract from *E. coli* (including pET28b plasmid vector), was incubated overnight at 4°C. Then, extracts were passed through a 1-ml His-Select column (Sigma) following the instructions of the manufacturer, and the material retained was washed and eluted with buffer A supplemented with increasing concentrations of imidazole. Aliquots of the eluted fractions were resolved in 10% SDS-PAGE gels and subjected to Western blotting with a commercial antibody against Strep-tag (Qiagen).

Microscopy. Cell area data were estimated automatically with ImageJ (https://imagej.nih.gov/ij/index.html) processing of light-microscopy images (20), and data were plotted using RStudio Desktop software. GFP fluorescence and *Anabaena* red autofluorescence were visualized with a Leica DM6000B fluorescence microscope equipped with a fluorescein isothiocyanate (FITC) L5 filter (excitation, 480/40 nm; emission, 527/30 nm) for GFP and a Tx2 filter (excitation, 560/40 nm; emission, 645/75 nm) for autofluorescence, and the results were photographed with an Orca-ER camera (Hamamatsu). Alternatively, fluorescence was monitored with a Leica TCS SP2 confocal laser scanning microscope equipped with an HCX PLAN-APO 63X 1.4-numerical aperture (NA) oil immersion lens objective. Samples were excited with 488-nm irradiation from an argon ion laser, and fluorescence was collected across windows of 500 to 540 nm (GFP) and 630 to 700 nm (cyanobacterial autofluorescence). For quantification of GFP fluorescence, ImageJ software was used to compile fluorescence in manually defined areas along filaments.

REFERENCES

1. Flores E, Herrero A. 2010. Compartmentalized function through cell differentiation in filamentous cyanobacteria. Nat Rev Microbiol 8:39–50. https://doi.org/10.1038/nrmicro2242.
2. Yoon HS, Golden JW. 1998. Heterocyst pattern formation controlled by a diffusible peptide. Science 282:935–938. https://doi.org/10.1126/science.282.5390.935.
3. Corrales-Guerrero L, Mariscal V, Flores E, Herrero A. 2013. Functional dissection and evidence for intercellular transfer of the heterocyst-differentiation PatS morphogen. Mol Microbiol 88:1093–1105. https://doi.org/10.1111/mmi.12244.
4. Flores E, Herrero A, Forchhammer K, Maldener I. 2016. Septal junctions in filamentous heterocyst-forming cyanobacteria. Trends Microbiol 24:79–82. https://doi.org/10.1016/j.tim.2015.11.011.
5. Flores E, Picossi S, Valladares A, Herrero A. 2019. Transcriptional regulation of development in heterocyst-forming cyanobacteria. Biochim Biophys Acta Gene Regul Mech 1862:673–684. https://doi.org/10.1016/j.bbagrm.2018.04.006.
6. Picossi S, Flores E, Herrero A. 2014. ChIP analysis unravels an exceptionally wide distribution of DNA binding sites for the NtcA transcription factor in a heterocyst-forming cyanobacterium. BMC Genomics 15:22. https://doi.org/10.1186/1471-2164-15-22.
7. Flaherty BL, Johnson DBF, Golden JW. 2014. Deep sequencing of HetR-bound DNA reveals novel HetR targets in *Anabaena* sp. strain PCC7120. BMC Microbiol 14:255. https://doi.org/10.1186/s12866-014-0255-x.
8. Wilcox M, Mitchison GJ, Smith RJ. 1973. Pattern formation in the blue-green alga, *Anabaena*. I. Basic mechanisms. J Cell Sci 12:707–723.
9. Yoon H-S, Golden J. 2001. PatS and products of nitrogen fixation control heterocyst pattern. J Bacteriol 183:2605–2613. https://doi.org/10.1128/JB.183.8.2605-2613.2001.
10. Kuhn I, Peng L, Bedu S, Zhang CC. 2000. Developmental regulation of the cell division protein FtsZ in *Anabaena* sp. strain PCC 7120, a cyanobacterium capable of terminal differentiation. J Bacteriol 182:4640–4643. https://doi.org/10.1128/jb.182.16.4640-4643.2000.
11. Klint J, Rasmussen U, Bergman B. 2007. FtsZ may have dual roles in the filamentous cyanobacterium *Nostoc/Anabaena* sp. strain PCC 7120. J Plant Physiol 164:11–18. https://doi.org/10.1016/j.jplph.2005.08.021.
12. Xu X, Wolk CP. 2001. Role for *hetC* in the transition to a nondividing state

during heterocyst differentiation in *Anabaena* sp. J Bacteriol 183:393–396. https://doi.org/10.1128/JB.183.1.393-396.2001.
13. Corrales-Guerrero L, Flores E, Herrero A. 2014. Relationships between the ABC-exporter HetC and peptides that regulate the spatiotemporal pattern of heterocyst distribution in *Anabaena*. PLoS One 9:e104571. https://doi.org/10.1371/journal.pone.0104571.
14. Videau P, Rivers OS, Hurd K, Ushijima B, Oshiro RT, Ende RJ, O'Hanlon SM, Cozy LM. 2016. The heterocyst regulatory protein HetP and its homologs modulate heterocyst commitment in *Anabaena* sp. strain PCC 7120. Proc Natl Acad Sci U S A 113:E6984–E6992. https://doi.org/10.1073/pnas.1610533113.
15. Risser DD, Callahan SM. 2008. HetF and PatA control levels of HetR in *Anabaena* sp. strain PCC 7120. J Bacteriol 190:7645–7654. https://doi.org/10.1128/JB.01110-08.
16. Makarova KS, Koonin EV, Haselkorn R, Galperin MY. 2006. Cyanobacterial response regulator PatA contains a conserved N-terminal domain (PATAN) with an alpha-helical insertion. Bioinformatics 22:1297–1301. https://doi.org/10.1093/bioinformatics/btl096.
17. Lian J, Scappino L, Haselkorn R. 1992. The *patA* gene product, which contains a region similar to CheY of *Escherichia coli*, controls heterocyst pattern formation in the cyanobacterium *Anabaena* 7120. Proc Natl Acad Sci U S A 89:5655–5659. https://doi.org/10.1073/pnas.89.12.5655.
18. Young-Robbins SS, Risser DD, Moran JR, Haselkorn R, Callahan SM. 2010. Transcriptional regulation of heterocyst patterning gene *patA* from *Anabaena* sp. strain PCC 7120. J Bacteriol 192:4732–4740. https://doi.org/10.1128/JB.00577-10.
19. Corrales-Guerrero L, Camargo S, Valladares A, Picossi S, Luque I, Ochoa de Alda JAG, Herrero A. 2018. FtsZ of filamentous, heterocyst-forming cyanobacteria has a conserved N-terminal peptide required for normal FtsZ polymerization and cell division. Front Microbiol 9:2260. https://doi.org/10.3389/fmicb.2018.02260.
20. Camargo S, Picossi S, Corrales-Guerrero L, Valladares A, Arévalo S, Herrero A. 2019. ZipN is an essential FtsZ membrane tether and contributes to the septal localization of SepJ in the filamentous cyanobacterium *Anabaena*. Sci Rep 9:2744. https://doi.org/10.1038/s41598-019-39336-6.
21. Orozco CC, Risser DD, Callahan SM. 2006. Epistasis analysis of four genes from *Anabaena* sp. strain PCC 7120 suggests a connection between PatA

and PatS in heterocyst pattern formation. J Bacteriol 188:1808–1816. https://doi.org/10.1128/JB.188.5.1808-1816.2006.

22. Bastet L, Boileau C, Bédu S, Janicki A, Latifi A, Zhang CC. 2010. NtcA regulates *patA* expression in *Anabaena* sp. PCC 7120. J Bacteriol 192:5257–5259. https://doi.org/10.1128/JB.00640-10.

23. Wang Y, Xu X. 2005. Regulation by *hetC* of genes required for heterocyst differentiation and cell division in *Anabaena* sp. strain PCC 7120. J Bacteriol 187:8489–8493. https://doi.org/10.1128/JB.187.24.8489-8493.2005.

24. Sakr S, Thyssen M, Denis M, Zhang C-C. 2006. Relationship among several key cell cycle events in the developmental cyanobacterium *Anabaena* sp. strain PCC 7120. J Bacteriol 188:5958–5965. https://doi.org/10.1128/JB.00524-06.

25. Yang Y, Huang XZ, Wang L, Risoul V, Zhang CC, Chen WL. 2013. Phenotypic variation caused by variation in the relative copy number of pDU1-based plasmids expressing the GAF domain of Pkn41 or Pkn42 in *Anabaena* sp. PCC 7120. Res Microbiol 164:127–135. https://doi.org/10.1016/j.resmic.2012.10.010.

26. Rippka R, Deruelles J, Waterbury JB, Herdman M, Stanier RY. 1979. Generic assignments, strain histories and properties of pure cultures of cyanobacteria. J Gen Microbiol 111:1–61. https://doi.org/10.1099/00221287-111-1-1.

27. Mackinney G. 1941. Absorption of light by chlorophyll solutions. J Biol Chem 140:109–112.

28. Olmedo-Verd E, Muro-Pastor AM, Flores E, Herrero A. 2006. Localized induction of the *ntcA* regulatory gene in developing heterocysts of *Anabaena* sp. strain PCC 7120. J Bacteriol 188:6694–6699. https://doi.org/10.1128/JB.00509-06.

29. Elhai J, Vepritskiy A, Muro-Pastor AM, Flores E, Wolk CP. 1997. Reduction of conjugal transfer efficiency by three restriction activities of *Anabaena* sp. strin PCC 7120. J Bacteriol 179:1998–2005. https://doi.org/10.1128/jb.179.6.1998-2005.1997.

30. Valladares A, Rodríguez V, Camargo S, Martínez-Nöel GMA, Herrero A, Luque I. 2011. Specific role of the cyanobacterial PipX factor in heterocysts of *Anabaena* sp. strain PCC 7120. J Bacteriol 193:1172–1182. https://doi.org/10.1128/JB.01202-10.

31. Black TA, Cai YP, Wolk CP. 1993. Spatial expression and autoregulation of *hetR* a gene involved in the control of heterocyst development in *Anabaena*. Mol Microbiol 9:77–84. https://doi.org/10.1111/j.1365-2958.1993.tb01670.x.

32. Karimova G, Dautin N, Ladant D. 2005. Interaction network among *Escherichia coli* membrane proteins involved in cell division as revealed by bacterial two-hybrid analysis. J Bacteriol 187:2233–2243. https://doi.org/10.1128/JB.187.7.2233-2243.2005.

33. Ramos-León F, Mariscal V, Frías JE, Flores E, Herrero A. 2015. Divisome-dependent subcellular localization of cell-cell joining protein SepJ in the filamentous cyanobacterium *Anabaena*. Mol Microbiol 96:566–580. https://doi.org/10.1111/mmi.12956.

34. Napolitano M, Rubio MA, Camargo S, Luque I. 2013. Regulation of internal promoters in a zinc-responsive operon is influenced by transcription from upstream promoters. J Bacteriol 195:1285–1293. https://doi.org/10.1128/JB.01488-12.

SepT, a novel protein specific to

multicellular cyanobacteria, influences

peptidoglycan growth and septal nanopore

formation in *Anabaena* sp. PCC 7120

SepT, a novel protein specific to multicellular cyanobacteria, influences peptidoglycan growth and septal nanopore formation in *Anabaena* sp. PCC 7120

Cristina Velázquez-Suárez[1,†], Benjamin L. Springstein[2,†], Mercedes Nieves-Morión[1], Andreas O. Helbig[3], Ann-Katrin Kieninger[4], Iris Maldener[4], Dennis J. Nürnberg[5], Karina Stucken[6], Ignacio Luque[1], Tal Dagan[2,*], Antonia Herrero[1,*]

[1] Instituto de Bioquímica Vegetal y Fotosíntesis, CSIC and Universidad de Sevilla, Seville, Spain

[2] Institute of General Microbiology, Kiel University, Kiel, Germany

[3] AG Proteomics & Bioanalytics, Institute for Experimental Medicine, Christian-Albrechts-Universität zu Kiel, Kiel, Germany

[4] Department of Microbiology/Organismic Interactions, University of Tübingen, Tübingen, Germany

[5] Institute of Experimental Physics and Dahlem Centre of Plant Sciences, Free University of Berlin, Berlin, Germany

[6] Department of Food Engineering, Universidad de La Serena, La Serena, Chile.

Current address for BLS: Institute of Science and Technology Austria, Klosterneuburg, Austria

[*] Address for correspondence to Antonia Herrero (herrero@ibvf.csic.es) and Tal Dagan (tdagan@ifam.uni-kiel.de).

[†] These authors contributed equally to this work.

Running Title: SepT, a novel septal protein of *Anabaena*

Key words: Coiled-coil-rich proteins, Divisome-dependent localization, Filamentous cyanobacteria, Septal peptidoglycan nanopores, Septal proteins.

Abstract

Anabaena sp. PCC 7120 grows by forming filaments of communicating cells and is considered a paradigm of bacterial multicellularity. Molecular exchanges between contiguous cells in the filament takes place through multiprotein channels that traverse the septal peptidoglycan through nanopores connecting their cytoplasms. Besides, the septal-junction complexes contribute to strengthen the filament. In search for proteins with coiled-coil domains that could provide for cytoskeletal functions in *Anabaena*, we identified SepT (All2460). SepT is characteristic of the phylogenetic clade of filamentous cyanobacteria with the ability to undergo cell differentiation. SepT-GFP fusions indicate that the protein is located at the cell periphery and, conspicuously, in the intercellular septa. During cell division the protein is found at midcell resembling the position of the divisome. BACTH analysis shows SepT interactions with itself and putative elongasome (MreB, RodA), divisome (FtsW, SepF, ZipN) and septal-junction-related (SepJ) proteins. Thus, SepT appears to rely on the divisome for localization at mature intercellular septa to form part of intercellular protein complexes. Two independently obtained mutants lacking SepT showed alterations in cell size and impaired septal and peripheral peptidoglycan incorporation during cell growth and division. Notably, both mutants showed conspicuous alterations in the array of nanopores present in the intercellular peptidoglycan disks including aberrant nanopore morphology, number and distribution. SepT appears therefore to be involved in the control of peptidoglycan growth and the formation of cell-cell communication structures that are at the basis of the multicellular character of this group of cyanobacteria.

Importance

Multicellular organization is a requirement for the development of complex organisms, and filamentous cyanobacteria such as *Anabaena* represent a paradigmatic case of bacterial multicellularity. The *Anabaena* filament can include hundreds of communicated cells that exchange nutrients and regulators and, depending on environmental conditions, can include different cell types specialized in distinct biological functions. Hence, the specific features of the *Anabaena* filament, and how they are propagated during cell division, represent outstanding biological issues. Here we studied SepT, a novel coiled-coil-rich protein of *Anabaena* that is located in the intercellular septa and influences the formation of these differentiated structures that allow communication between neighboring cells along the filament, a fundamental trait for the performance of *Anabaena* as a multicellular organism.

Introduction

Bacterial multicellularity ranges from transient associations, such as colonies and biofilms, to permanent multicellular forms (1). The basic characteristics of multicellular prokaryotic organisms are mechanisms of cell-cell adhesion and intercellular communication (2).

Additionally, bacterial multicellularity can be reinforced by processes of cell differentiation as in sporulating actinomycetes (3) and cyanobacterial trichomes (4). Cyanobacteria, which are generally classified as Gram-negative bacteria (5), are characterized by a large phenotypic diversity ranging from unicellular species to complex multicellular organisms, and some can undergo irreversible cell differentiation (6). Multicellular cyanobacteria that form trichomes (filaments of cells) and differentiate multiple cell types are considered the peak of prokaryotic complexity (7). Species of the Nostocaceae, including the model strain *Anabaena* sp. PCC 7120 (hereafter *Anabaena*) are characterized by the formation of linear trichomes, where semi-regularly interspaced heterocysts (cells specialized for nitrogen fixation) are produced upon nitrogen starvation in a highly reproducible pattern (7,8). Cells within a trichome are connected through incomplete segregation during cell division, which results in a common outer membrane and a shared periplasm that represents a communication conduit through the filament (9). Nonetheless, each cell is individually enclosed by a cytoplasmic membrane, whereas the septal peptidoglycan (PG) is continuous and engrossed in the intercellular regions (10-13).

In addition, *Anabaena* contains functional analogs to the eukaryotic gap-junctions termed septal junctions, which are proteinaceous complexes located at the intercellular septa that connect the cells and facilitate intercellular communication along the filament (14-17). The septum localized proteins FraC, FraD, SepJ (17-19), SepI (20) and SepN (21) influence septum formation and cell-cell communication, and FraD and SepN could be localized to septal junctions by cryo electron tomography and are likely protein components of them (16,21). The intercellular communication arrangement involves a nanopore array in the septal PG that has been considered to hold the septal-junction protein complexes. The formation of these structures depends on the activities of PG amidases of the AmiC type (22,23) and the PG-binding protein SjcF1 (24). The importance of FraC, FraD, SepJ and SepI for multicellularity in *Anabaena* is highlighted by a defect in trichome integrity and a resulting loss of multicellularity under diazotrophic growth conditions in mutant strains lacking any of the these proteins (18-20). Notably, although diazotrophic growth requires FraC, FraD, SepJ and SepI, heterocyst differentiation only depends on SepJ and SepI and not on FraC or FraD (18-20).

Cytoskeletal proteins are involved in essential tasks such as the determination of cell shape, cell division and the organization of cell components. They all form protein polymers and are divided into three main classes: microtubules (represented by tubulin), microfilaments (represented by actin) and intermediate filaments. Although formerly thought to be specific to eukaryotes, homologs to the three classes of cytoskeletal proteins have also been universally found in bacteria, where they perform different cellular functions, some of which being non-cytoskeletal functions (25). In addition, coiled-coil-rich proteins (CCRPs) in bacteria also may form polymers and exert important structural functions such as the control of cell morphology, motility, cell division and chromosome segregation (see 25).

The bacterial actin homolog MreB is widespread in rod-shaped bacteria, where it is involved in the determination of the cell morphology (26). MreB, together with MreC, MreD and PG synthases, constitutes the protein complex called the elongasome, which is responsible for cell elongation during cell growth (27,28). MreB polymerizes, and it has been proposed that the coupled motion of MreB filaments about the long cell axis coordinates PG-synthetic complexes and orient the circumferential insertion of new PG in the cylindrical part of the cell (see 29). In *Anabaena*, MreB is required for rod-shape determination, but dispensable for cell viability (30,31), although diazotrophic growth is compromised in its absence (31). Distinctly, besides in the cell periphery as in other rod-shaped bacteria, in *Anabaena* MreB, MreC and MreD are localized to the divisome, influencing positioning of the Z-ring and septal PG-growth orientation, as well as in the intercellular mature septa, invoking a role in the formation of septal structures for intercellular communication (32,33).

In most bacteria, the tubulin homolog FtsZ is essential for viability. FtsZ polymerizes into short filaments to form, together with other proteins, a ring at the future site of cell division, the so-called Z-ring. The Z-ring organizes the multiprotein complex termed the divisome, which includes the enzymatic machinery for PG growth to synthesize the new poles of the resulting daughter cells (34). In addition to FtsZ (35,36), *Anabaena* possesses the cyanobacteria-specific essential protein ZipN, identified as a principal tether of FtsZ to the cytoplasmic membrane and divisome organizer (37), as well as homologs for the divisome components FtsE, FtsK, FtsQ, FtsX, FtsI, FtsW and SepF (see 37-39).

In *Anabaena*, the septal-junction related proteins SepJ, which itself contains an N-terminal coiled-coil domain and forms multimers (40,41), FraC (19) and SepI (20) are recruited to the intercellular septa through interactions with the divisome during cell division, thus providing a link between cell division and cell-cell communication. In addition, other cyanobacterial CCRPs were identified more recently to perform cytoskeletal and cytoskeletal-like functions in a diverse set of cyanobacterial species (20,42), including the heteropolymer-forming ZicK and ZacK (43).

In this work we aimed at the characterization of another coiled-coil-rich protein and deciphering its function in *Anabaena* as a model of bacterial multicellularity. We found that All2460, which we have termed SepT, is a new element connecting cell division and PG growth to the formation of the septal structures involved in cell-cell adhesion and intercellular communication through the filament.

Results

All2460 predicted domains and phylogenetic distribution

Initially selected in a screen, using COILS (44), searching for coiled-coil-rich proteins with a putative function in the *Anabaena* multicellularity and morphology (42), All2460 is characterized by three distinct coiled-coil-rich regions as well as two N-terminal transmembrane domains (TMDs, residues 12-50, predicted with TMHMM) (Fig. 1A,B). Using the Conserved Domain Search (CD Search, NCBI), All2460 is predicted to contain a Structural Maintenance of Chromosomes (SMC) and a TerB-C domain, suggesting a metal-dependent function in chromosome biology (Fig. 1A). Predictions of the putative localization of the C-terminal non-TMD parts consistently placed the C-terminus in the cytoplasm (predicted using PSIPRED, PSORTb and Gneg-mPLoc). Using AlphaFold, All2460 is predicted to form a homodimer (Fig. 1C). A further search for All2460 homologs using amino acid sequence similarity shows that all tested filamentous heterocyst-forming cyanobacteria encode a protein homologous to All2460 (Data Set S1; Data Set S2; Fig. 1D). Outside the heterocyst-formers, there are some homologs that using our thresholds are clustered in the same protein family as All2460. These homologs are found in filamentous non-heterocystous cyanobacteria such as *Spirulina*, and closely-related genera to the order Nostocales such as *Gleocapsa*, *Croococcidiopsis* or *Pleurocapsa* (45). Moreover, the protein sequence alignment of SepT homologs (Data Set S2) indicates a high sequence divergence between homologs from the heterocyst-forming and non-heterocystous cyanobacteria, suggesting also functional divergence.

To further study the genomic neighborhood of All2460, we searched for the presence of conserved gene order at the All2460 locus using CSBFinder-S (46). Our results reveal a conserved synteny block that includes two genes next to *all2460*, namely *all2459* and *all2461* (Fig. 1E). Unlike All2460, both All2459 and All2461 are not predicted to contain TMDs but both are predicted to contain P-loop NTPase domains, which are commonly found in MinD, ParA and other DNA partitioning systems (47). All three genes are about 2 fold upregulated 21 h after nitrogen-stepdown (48), suggesting some involvement in diazotrophic growth.

All2460 localization in *Anabaena*

We studied the localization of All2460 in *Anabaena* by means of fusions to GFP. For that, a replicative plasmid encoding All2460 C-terminally fused to GFP, directed by the native promoter sequence, was transferred to *Anabaena* wild type (WT), generating strain CSCV25, and to strain BS1 (Δ*all2460*) (see below), generating strain CSCV26. In both strains, CSCV25 and CSCV26, GFP fluorescence was detected in the cell periphery and, conspicuously, in the intercellular septa between contiguous cells along the filament (Fig. 2). Remarkably, midcell GFP bands were detected in some dividing cells, matching the localization of the progressing new septum. When the N-terminal transmembrane domain of SepT was deleted, the resulting protein fused to GFP

produced fluorescence in patches without any specific localization in the cell (not shown), suggesting that membrane anchorage is essential for the correct localization. These observations suggest that All2460 is a new septal protein of *Anabaena* and, accordingly, we term it SepT.

Analysis of SepT interactions

The apparent localization of SepT to midcell, the intercellular septa and the cell periphery drove us to investigate its possible interactions with known or putative elements of the *Anabaena* divisome, the septal junctions or the elongasome. For this purpose, we used the bacterial adenylate cyclase two-hybrid (BACTH) system. Regarding divisome components, we tested interactions of SepT with FtsZ, ZipN, Alr0487 (putative SepF), All0154 (putative PG glycosyl-transferase, FtsW) and Alr0718 (PG transpeptidase, FtsI). Strong interactions were detected for the pairs SepT-T18/T25-ZipN, SepT-T25/T18-SepF, SepT-T25/T18-FtsW and SepT-T25/FtsW-T18 (Fig. 3A). Regarding septal proteins, we tested FraC, FraD, SepJ and SepI. Significant, although comparatively low, interaction was detected only with SepJ (Fig. 3B). Regarding elongasome components, we tested interactions of SepT with MreB, MreC, MreD, Alr0653 (putative PG glycosyl-transferase, RodA) and Alr5045 (elongasome transpeptidase). Interactions were detected between SepT-T25 and T18-RodA (Fig. 3A), between T25-SepT and MreB-T18, and between T18-SepT and MreB-T25 (Fig. 3B). Finally, SepT was detected to be able of self-interactions (Fig. 3B).

To identify further interaction partners of SepT, we performed co-immunoprecipitations of *Anabaena* WT expressing SepT-GFP and analyzed co-precipitated proteins by LC-MS/MS. With this approach, we were able to verify the interaction of SepT with MreB and SepJ. Additionally, proteins that co-precipitated with SepT included All4981 and All2459, from its own synteny block, and three different penicillin-binding proteins (PBPs): All2981, All2952 and Alr0718 (the full list of interactions identified is supplied in Data Set S3).

Inactivation of *sepT*

To study the function of SepT, we sought the generation of *Anabaena* derivatives lacking a functional *all2460* ORF. Strain CSCV9, generated in the Seville lab, bears gene-cassette C.K1, encoding resistance to kanamycin and neomycin, inserted into *all2460* (Fig. 4A). Growth of this mutant was studied in media supplemented with nitrate or lacking combined nitrogen (Fig. 4B). It was able to grow under the two conditions, exhibiting growth rates similar to those of *Anabaena* WT both in the exponential growth phase and in the phase of slow growth (Fig. 4B). Consistent with these results, strain BS1, which was previously generated in the Kiel lab, bearing gene cassette C.S3 substituting for *all2460* (Fig. 4A), also exhibited growth rates comparable to those of *Anabaena* WT (Fig. 4B). In the absence of combined nitrogen, both CSCV9 and BS1 exhibited mature heterocysts with conspicuous polar granules, as is the case for *Anabaena* WT (Fig. 5A).

The cell area and, as an estimation of the cell morphology, the aspect ratio (the ratio between the cell axis parallel to the filament and the axis perpendicular to the filament), were determined in strains CSCV9 and BS1. Because strains maintained in different labs have frequently been noticed to exhibit some different phenotypic characteristics, each of the two mutants was compared to the respective *Anabaena* WT strain from which they were derived (WT-s: WT from Seville; WT-k: WT from Kiel). While actively-growing cells (48 h) of CSCV9 were smaller than those of its parental strain in the presence and absence of combined nitrogen, (Fig. 5A,B) (Student's *t*-tests indicates significant differences, $p < 0.01$, for comparison of WT and CSCV9 with NO_3^- or N_2 after 48 h of incubation; and non-significant differences, $p > 0.05$, after 216 h), cells of BS1 appeared larger than those of its parental strain (Fig. 5A,B). (Student's *t*-tests indicates significant differences, $p < 0.01$, for comparison of WT and BS1 with NO_3^- or N_2 after 48 h or 216 h of incubation). The alterations in cell size in CSCV9 and BS1 suggests that both strains suffer a certain discoordination between cell growth and division. In contrast to C.K1 introduced in CSCV9, the C.S3 gene cassette introduced in BS1 bears strong transcriptional terminators, which could affect the expression of the downstream ORF *all2459*. This could contribute to explain the differences in the effects of the mutations in CSCV9 and BS1.

Finally, cell aspect ratio determinations indicated that the morphology of strains CSCV9 and BS1 is similar to that of their respective parentals (Fig. 5C). (Student's *t*-tests indicates significant differences, $p = 0.002$, only for comparison of CSCV9 and its WT after 216 h of incubation with NO_3^-).

Localization of PG growth in *sepT* mutants

The interaction of SepT with some proteins involved in lateral or septal PG growth, as suggested by the BACTH assays, led us to check whether the pattern of PG growth was affected by the mutation of *sepT*. For that, we used labeling with fluorescent vancomycin (Van-FL), which highlights the sites of PG incorporation, as done before in *Anabaena* (22; see also 32). Filaments of *Anabaena* WT and strains CSCV9 and BS1 were incubated in BG11 or $BG11_0$ for 48 (exponential growth) and 216 h (slow growth) under the same conditions used for the determination of growth rates, and labeled with Van-FL. In *Anabaena* WT, cells from BG11 cultures, as well as vegetative cells from $BG11_0$ medium, presented weak peripheral and strong septal labeling with alternating intensities (lower in the more recently-formed septa than the older ones), as well as labeling in the septum under construction during cell division (Fig. 6), as previously described (see 32,33). Filaments of CSCV9 and BS1 incubated in BG11 or $BG11_0$ medium showed a labeling pattern similar to that of the WT (Fig. 6A,B). However, quantification of Van-FL fluorescence intensity in the cell periphery (lateral fluorescence) and in the septal regions indicate that after 48 h in BG11 medium, both lateral and septal fluorescence was lower in the mutants than in the WT (Student's *t* tests $p<0.01$), becoming more similar after 216 h (at

216 h only lateral fluorescence in BS1 appeared significantly lower (p<0.01) than in the WT) (see the Table in Fig. 6A). In $BG11_0$ medium, fluorescence intensity in vegetative cells appeared similar in the mutants and the WT (only lateral fluorescence at 216 h was significantly lower ($p<0.01$) in CSCV9 than in the WT) (see the Table in Fig. 6B).

Localization of MreB, MreC and MreD in strain CSCV9

We also studied whether inactivation of *sepT* affected the localization of the elongasome components MreB, MreC and MreD. For that, we transferred gene constructs whereby the *mreBCD* promoter region directs the expression of the fusion proteins sfGFP-MreB, sfGFP-MreC or sfGFP-MreD to strain CSCV9, generating strains CSCV11, CSCV12 and CSCV13, respectively. Strains CSCV6, CSCV7 and CSCV8 express the same fusion proteins, respectively, in the WT background (32). The six reporter strains include, in addition, the intact *mreBCD* operon in its native genomic locus. In the presence of combined nitrogen, strains CSCV11, CSCV12 and CSCV13 exhibited GFP fluorescence localized through the cell periphery including the intercellular septal regions, and at midcell matching the divisome localization in dividing cells (Fig. 7A), a distribution similar to that described for strains, CSCV6, CSCV7 and CSCV8, respectively (32; Fig. 7A). Upon N-stepdown, vegetative cells of CSCV11, CSCV12 and CSCV13 exhibited peripheric, septal and midcell GFP fluorescence, similar to the pattern found in filaments incubated with nitrate. Heterocysts showed peripheric fluorescence and, frequently, fluorescence spots focalized at the cell poles (Fig. 7B). These observations also match the distribution observed in CSCV6, CSCV7, CSCV8, respectively (Fig. 7B; 33), indicating that localization of MreB, MreC and MreD is not noticeably affected in the *sepT* mutant strain.

Morphology of the septal nanopore structures in *sepT* mutants

Given that alterations in the number and morphology of septal nanopores have been described in mutants of other septal proteins in *Anabaena* (e.g., 13), we isolated PG sacculi from the *sepT* mutant strains CSCV9 and BS1 and observed the septal disks by TEM (Fig. 8, Fig. S1). In comparison to the WT, we observed a heterogeneity in the array of septal disk nanopores in the mutants. Septal disks in the WT contain an average of ca. 40 nanopores of about 17 nm in diameter concentrated in the central part of the disk (13; see Fig. 8). In comparison to the WT, septal disks of both CSCV9 and BS1 generally contained fewer nanopores, albeit with a similar size (Fig. 8B). However, although in some cases the mutant disks showed a nanopore distribution that resemble the WT pattern (first line in Fig. 8A), disks with nanopores distributed throughout the whole disk area (second line in Fig. 8A) or including only 2-4, larger than average, nanopores (third line in Fig. 8A) were also observed. In addition, some disks showing pores severely enlarged and of anormal (non-circular) shape, apparently resulting from PG mesh breakage, were also frequently detected in both mutants (fourth line in Fig. 8A). Fig. S1 shows that peptidoglycan isolated from

filaments of BS1 grown on agar plates presented a distribution of septa similar to that found in liquid medium.

Discussion

In this work, we have identified the product of *Anabaena* ORF *all2460*, a cyanobacterial cytoskeletal protein linked to the divisome, elongasome and the septal-junctions, which we have termed SepT. SepT is predicted to be a coiled-coil-rich protein characteristic of filamentous cyanobacteria capable of heterocyst differentiation. Indeed, homologs to SepT have been found encoded in the genomes of all tested heterocyst-forming strains. As in most cases, *Anabaena* SepT is predicted to be an inner membrane-anchored cytoplasmic protein and, as most CCRPs, it appears able of self-interactions (Fig. 3B), with predicted formation of structured dimers (Fig. 1E).

In *Anabaena*, SepT is localized in the cell periphery and the intercellular septa and, in dividing cells, it is also detected at midcell matching the localization of the divisome (Fig. 2). Localization at the cell periphery and the divisome has also been described for the elongasome components MreB, MreC and MreD in *Anabaena* (32). Moreover, we have detected SepT interactions with MreB (Fig. 3B), invoking a role of SepT in the elongasome function. We have not detected any apparent alteration of MreB, MreC or MreD localization in the absence of a functional SepT protein (Fig.7). However, two different *sepT* mutants showed impaired regulation of cell size (Fig. 5B), which might reflect a discoordination between cell growth and division, and altered PG growth, with lower incorporation, specially under conditions of higher growth rate (exponential growth with combined nitrogen) in the mutants (Fig. 6). In addition, we have detected interactions of SepT with putative RodA (Fig. 3A), the elongasome glycosyl-transferase catalyzing PG polymerization, as well as with three putative PBPs (All2981, All2952 and Alr0718) (Fig. 3D). These results suggest a role for SepT in the regulation of PG expansion during cell growth.

The localization of SepT in the intercellular septa and the divisome coincides with that reported for other septal proteins that play important roles in filament maintenance and intercellular communication in *Anabaena*, including SepJ, FraC and SepI. Thus, SepT could have a function related to the specialized structure of the intercellular septa of heterocyst-forming cyanobacteria. Notably, our past and current investigations suggest that interaction with the divisome during cell division is a mechanism for the localization of proteins that remain in the intercellular septa once the division event has concluded. Indeed, SepJ has been shown to interact with the divisome components FtsQ and ZipN (37,40), and also with with SepI, which interacts with FtsI, SepF and ZipN (20). Here we have detected clear interactions of SepT with ZipN, SepF and FtsW. This, together with its localization to the divisome, points to a similar mechanism for SepT localization to the intercellular septa.

The interaction of SepT with putative FtsW (divisome PG glycosyl-transferase) suggests an effect on septal PG growth or remodeling. Indeed, we have observed conspicuous alteration on the nanopore array of the septal PG disks in two different *sepT* mutants, including a lower average nanopore number, altered nanopore distribution, and even very aberrant septal disks with only 2-4 large nanopores or showing apparent tears in the PG mesh (Fig. 8). SepJ, with which SepT also interacts (Fig. 3B), is also a coiled-coil containing protein that influences the septal disk nanopore array in *Anabaena*, although *sepJ* inactivation had milder effects than *sepT* inactivation, leading to reduced nanopore numbers (15). In conclusion, besides influencing lateral PG growth, SepT is a new component of the differentiated septal structure of filamentous heterocyst-forming cyanobacteria directly linked to the cell growth and cell division machinery. It has a role in the processing of the intercellular PG required for the formation of intercellular communication structures that are key feature of multicellular organisms.

Materials and methods

Bacterial strains and growth conditions

Anabaena sp. PCC 7120 and mutant strains were grown photoautotrophically in BG11 medium (containing $NaNO_3$) or in $BG11_0$ (lacking combined nitrogen) (6), or in $BG11_0$ supplemented with 4 mM NH_4Cl and 8 mM TES-NaOH buffer, pH 7.5 at constant illumination of 12-30 photons $m^{-2} s^{-1}$ intensity. Cells were either grown in Erlenmeyer flasks with shaking or on medium solidified with 1 % (w/v) Difco agar. For the mutants, media were supplemented with antibiotics: spectinomycin (Sp) and streptomycin (Sm) at 5 µg ml^{-1} each in solid media or at 2 µg ml^{-1} each in liquid media, or with neomycin (Nm) at 25 µg ml^{-1} in solid media or 5 µg ml^{-1} in liquid media. Chlorophyll content (Chl) of the cultures was determined after extraction with methanol (49). In *Anabaena*, 1 µg chlorophyll corresponds to ca. 3.3 x 10^6 cells (50). (Tables S1, Table S2 list all used cyanobacterial strains, plasmids and oligonucleotides.)

Distribution of homologs in cyanobacteria

Homologs to SepT were detected in completely sequenced genomes publicly available in RefSeq (version 01/2021) by amino acid sequence similarity using stand-alone BLAST (51,52) (v. 2.2.26). Protein sequences that were found as BLAST hits with a threshold of E-value $\leq 1x10^{-5}$ were further compared to SepT by global alignment using needle (53). Hits having ≥30% identical amino acids in the global alignment were considered as homologs. For the phylogenetic analysis, homologs in a set of representative heterocystous species were manually selected and complemented by all homologs in non-heterocystous species. Amino-acid sequences were aligned with MAFFT (v. 7.475) (54). The phylogenetic tree was inferred with IQ-TREE (55) (v. 1.6.12) with restricted automatic model selection to the Le & Gascuel (LG) model (56) and fast

bootstrap with 1000 replicates. The tree was rooted using the MAD approach (57). The phylogenetic tree was visualized with FigTree (http://tree.bio.ed.ac.uk/software/figtree/).

Computational prediction

Coiled-coil-rich regions were predicted using COILS (V. 2.2) (44) and conserved protein domains were predicted using NCBI Conserved Domains Search (58). Prediction of subcellular localization was done using TMHMM (v. 2.0) (59), PSORTb (V. 3.0.2) (60), Gneg-mPLoc (v. 2.0) (61), PSIPRED (v. 4.0) (62) and Phobius (63). The employed putative promoter site for *sepT* (1470 bp upstream of the ORF) was based on promoter and transcription factor binding site predictions by BPROM (64).

Plasmid and Anabaena mutant construction

Mutant strain CSCV9 carries a version of the *sepT* gene in which codons 69-367 have been substituted by gene-cassette C.K1 encoding Km/Nm resistance. To generate it, two DNA fragments were amplified from *Anabaena* genomic DNA using the primer pairs all2459-1/all2460-2 (encompassing sequences internal and upstream of *sepT*) and all2460-1/all2461-1 (encompassing sequences internal and downstream of *sepT*), including terminal restriction sites BamHI and PstI. Both fragments were joined together by overlapping PCR, and the resulting single fragment was cloned into mobilizable vector pRL277 (encoding the gene *sacB* for positive selection; 65). Gene-cassette C.K1 from plasmid pRL161 (66) was then inserted into the internal BamHI site, generating plasmid pCSCV36, which was transferred to *Anabaena* by conjugation (67*)*.

Mutant BS1 carries gene cassette C.S3, encoding Sm/Sp resistance, substituting for the *sepT* gene. To generate it, 1500 bp upstream and downstream of the *sepT* ORF were amplified by PCR from *Anabaena* genomic DNA using primers 842KO_2A/842KO_2B and 842KO_4A/842KO_4B, respectively. The upstream and downstream *sepT* regions flanking the CS.3 cassette (amplified with primers CS.3_Fwd/CS.3_Rev using pCSEL24 (68) as a template) were then inserted into PCR-amplified pRL278, including the gene *sacB* for positive selection (69), using primers pRL271_Fwd/pRL271_Rev, by Gibson assembly, yielding pTHS109, which was transferred to *Anabaena* by conjugation. For both CSCV9 and BS1 mutants, insertion of the mutagenic construct by double cross-over was selected by resistance to sucrose and lack of antibiotic resistance encoded in the vector portion of the transferred plasmid. Both mutants were segregated for the mutant chromosomes, as tested by PCR analysis (not shown).

For the generation of strains CSCV11, CSCV12 and CSCV13, strains expressing a *sfgfp-mreB, sfgfp-mreC* or *sfgfp-mreD* fusion gene, respectively, expressed from the native *mreBCD* operon promoter (P*mreB*), strains CSCV6, CSCV7 and CSCV8, which respectively express the same fusion genes in the WT background, were used as recipient of plasmid pCSCV36. Insertion

of the mutagenic construct and segregation for the mutant chromosomes were verified by PCR analysis as above.

The replicative plasmid pTHS240, used for the localization of SepT-GFP, included a *sepT-gfpmut3.1* fusion gene under the control of the native promoter (predicted by BPROM). To generate it, the *sepT* promoter sequence and ORF were amplified using the primer pair p842_25C_long_A/Nos842_2B; the *gfpmut3.1* sequence was amplified using the primer pair GFP_842_A/GFP_25C_R and both PCR products were cloned into PCR-amplified plasmid pRL25C (70) using primer pair pRL25C_F/pRL25C_R by Gibson assembly.

The replicative plasmid pTHS143, driving the expression of SepT-GFP from P_{petE} used for co-IP analysis, was cloned as follows: the *petE* promoter was amplified using primer pair petE_903_Fwd/ pRL25c_NEB_Rev; *sepT* was amplified using primer pair Nos842_2A/ Nos842_2B and *gfpmut3.1* was amplified using pRL25c_NEB_Fwd/ pRL25c_NEB_Rev and all three PCR products were cloned into PCR-amplified pRL25C using primer pair pRL25c-903_V_F/ pRL25c-903_V_R.

BACTH analysis

BACTH assays were based on the reconstitution of adenylate cyclase from *Bordetella pertussis* (71). Genes were amplified by PCR using *Anabaena* DNA as template and oligonucleotide pairs: MB_25A/MB_25B (SepT-T25), MB_26A/MB_26B (T25-SepT), MB_27A/MB_27B (SepT-T18) or MB_28A/MB_28B (T18-SepT), alr0653-1/alr0653-2 (T25-RodA), alr0653-3/alr0653-2 (T18-RodA) and alr0653-3/alr0653-4 (RodA-T25, RodA-T18). alr5045-7/alr5045-8 (T25-Alr5045) and alr5045-9/alr5045-8 (T18-Alr5045). The resulting PCR products were cloned in pUT18, pUT18C, pKNT25 or pKT25. All the resulting plasmids were verified by sequencing. Other fusions used in this work were as previously described (20,32,36,37,40). Plasmids were transformed into *E. coli* XL1-Blue for amplification. Isolated plasmids were co-transformed into strain BTH101 (*cya*-99), and the transformants were plated on solid LB medium containing selective antibiotics and 1 % (w/v) glucose.

Co-immunoprecipitation

About 20-30 ml of culture of *Anabaena* WT or a derivative strain including plasmid pTHS143, driving the expression of SepT-GFP from P_{petE} promoter, was pelleted by centrifugation (4800 x *g*, 10 min, RT); cells were washed twice by centrifugation (4800 x *g*, 10 min, RT) with 40 ml PBS and then resuspended in 1 ml lysis buffer (PBS-N: PBS supplemented with 1% (v/v) NP-40) supplemented with protease inhibitor cocktail (PIC; cOmplete™, EDTA-free Protease Inhibitor Cocktail, Sigma-Aldrich). Cells were lysed using the VK05 lysis kit (Bertin) in a Precellys® 24 homogenizer (3 strokes for 30 seconds at 6500 rpm) and cell debris was pelleted by centrifugation (30 min, 21,100 x *g*, 4 °C). 50 µl µMACS anti-GFP MicroBeads (Miltenyi Biotec) were added to

the resulting cell-free supernatant with further incubation for 1 hour at 4 °C with mild rotation. Afterwards, the samples were loaded onto µColumns (Miltenyi Biotec), washed twice with 1 ml lysis buffer and eluted in 50 µl elution buffer (50 mM Tris HCl pH 6.8, 50 mM DTT, 1% SDS, 1 mM EDTA, 0.005% (w/v) bromophenol blue, 10% (v/v) glycerol; Miltenyi Biotec). Until further use, samples were stored at -80 °C.

Mass spectrometry analysis

Mass spectrometry was performed as previously described (20). The acquired MS/MS data were searched with the SequestHT algorithm against the entire reviewed Uniprot protein database of *Anabaena* sp. PCC 7120 including proteins encoded in plasmids (6922 sequences in total). Static modification applied was carbamidomethylation on cysteine residues, while oxidation on methionine residues was set as dynamic modification. Spectra were searched with full enzyme specificity. A MS mass tolerance of 10 ppm and a MS/MS tolerance of 0.02 Da was used. Proteins were identified with at least three unique peptides with a FDR confidence ≤ 0.01 (high).

Van-FL staining and quantification

Filaments were stained by incubation with 2 µg ml^{-1} Vancomycin-FL (Bodipy-FL conjugate, Invitrogen), and lateral and septal fluorescence were quantified with ImageJ (72) processing of fluorescence images by collecting total fluorescence in manually-defined equal square sections, as described (32). For each cell, lateral fluorescence was calculated as the mean of the values of four sections, and septal fluorescence as the mean of two sections, one at each cell pole. 20 to 30 cells were counted for each strain and condition, and the average values were calculated.

PG sacculi isolation and visualization

PG was isolated from filaments grown in BG11 medium by protease treatment and hot detergent extraction, as described (15). Aliquots of the obtained preparations were deposited on formvar-carbon film-coated copper grids and stained with 1% (wt/v) uranyl acetate and examined with a Zeiss Libra 120 plus (Zeiss) transmission electron microscope at 120 kV.

Microscopy

Cell area and cell axis length were determined automatically by processing light-microscopy images with ImageJ software, as in (31). Data were plotted using the open-source software RStudio Desktop (https://www.rstudio.com). Van-FL fluorescence was visualized with a Leica DM6000B fluorescence microscope and a FITCL5 filter (excitation band-pass, 480/40; emission band-pass, 527/30), and photographed with an ORCA-ER camera (Hamamatsu). GFP fluorescence was monitored with an Olympus TCS SP2 confocal laser-scanning microscope equipped with an HCX PLAN-APO 63x1.4 NA oil immersion objective (excitation, 488 nm;

collection, 500-540 nm for GFP or 630-700 nm for cyanobacterial autofluorescence) or with an Olympus FLUOVIEW FV3000 (hyper-resolution) confocal laser-scanning microscope equipped with an UPlanApo 60x 1.5 NA oil immersion objective (excitation, 488-nm; collection 500-540 nm for GFP or excitation, 640 nm; collection, 650-750 nm for cyanobacterial autofluorescence).

Supplemental material:

Data Set S1. xlsx file, 68 KB.

Data Set S2. txt file, 24 KB.

Data Set S3. xlsx file, 29 KB.

Data Set S4. xlsx file, 42 KB.

Figure S1. pdf file, 417 KB.

Table S1. pdf file, 95 KB.

Table S2. pdf file, 64 KB.

REFERENCES

1. Shapiro JA. 1998. Thinking about bacterial populations as multicellular organisms. Annu Rev Microbiol 52:81-104.
2. Lyons NA, Kolter R. 2015 On the evolution of bacterial multicellularity. Curr Opin Microbiol 24:21–28.
3. Flärdh K, Richards DM, Hempel AM., Howard M, Buttner MJ. 2012 Regulation of apical growth and hyphal branching in *Streptomyces*. Curr Opin Microbiol 15:737–743.
4. Flores E, Herrero A. 2010 Compartmentalized function through cell differentiation in filamentous cyanobacteria. Nat Rev Microbiol 8:39–50.
5. Hoiczyk E, Hansel A. 2000 Cyanobacterial cell walls: News from an unusual prokaryotic envelope. J Bacteriol 182:1191–1199.
6. Rippka R, Stanier RY, Deruelles J, Herdman M, Waterbury JB 1979 Generic assignments, strain histories and properties of pure cultures of cyanobacteria. Microbiology 111:1–61.
7. Herrero A, Stavans J, Flores E. 2016 The multicellular nature of filamentous heterocyst-forming cyanobacteria. FEMS Microbiol Rev 40: 831–854.
8. Zeng X, Zhang CC. 2022 The making of a heterocyst in cyanobacteria. Ann Rev Microbiol 76:597-618.
9. Mariscal V, Herrero A, Flores E. 2007 Continuous periplasm in a filamentous, heterocyst-forming cyanobacterim. Mol Microbiol 65:11-39-1145.
10. Wilk L, Strauss M, Rudolf M, Nicolaisen K, Flores E, Kühlbrandt W, Schleiff, E. 2011. Outer membrane continuity and septosome formation between vegetative cells in the filaments of *Anabaena* sp. PCC 7120. Cell Microbiol 13:1744–1754.
11. Claessen D, Rozen DE, Kuipers OP, Søgaard-Andersen L, Van Wezel GP. 2014. Bacterial solutions to multicellularity: A tale of biofilms, filaments and fruiting bodies. Nat Rev Microbiol 12:115–124.

12. Mariscal V, Nürnberg DJ, Herrero A, Mullineaux CW, Flores E. 2016. Overexpression of SepJ alters septal morphology and heterocyst pattern regulated by diffusible signals in *Anabaena*. Mol Microbiol 101:968-981.

13. Arévalo S, Nenninger A, Nieves-Morión M, Herrero A, Mullineaux CW, Flores E. 2021. Coexistence of communicating and noncommunicating cells in the filamentous cyanobacterium *Anabaena*. mSphere 6:e0109120.

14. Nürnberg DJ, Mariscal V, Bornikoel J, Nieves-Morión M, Krauß N, Herrero A, Maldener I, Flores E, Mullineaux CW. 2015. Intercellular diffusion of a fluorescent sucrose analog via the septal junctions in a filamentous cyanobacterium. mBio 6:1–12.

15. Nieves-Morión M, Mullineaux CW, Flores E. 2017. Molecular diffusion through cyanobacterial septal junctions. mBio 8:e01756-16.

16. Weiss GL, Kieninger A-K, Maldener I, Forchhammer K, Pilhofer M. 2019 Structure and function of a bacterial gap junction analog. Cell 178:374-384.e15.

17. Mullineaux CW, Mariscal V, Nenninger A, Khanum H, Herrero A, Flores E, Adams DG. 2008 Mechanism of intercellular molecular exchange in heterocyst-forming cyanobacteria. EMBO J 27:1299–1308.

18. Merino-Puerto V, Mariscal V, Mullineaux CW, Herrero A. Flores E. 2010 Fra proteins influencing filament integrity, diazotrophy and localization of septal protein SepJ in the heterocyst-forming cyanobacterium *Anabaena* sp. Mol Microbiol 75:1159–1170.

19. Flores E, Pernil R, Muro-Pastor AM, Mariscal V, Maldener I, Lechno-Yossef S, Fan Q, Wolk CP, Herrero A. 2007. Septum-localized protein required for filament integrity and diazotrophy in the heterocyst-forming cyanobacterium *Anabaena* sp. strain PCC 7120. J Bacteriol 189:3884–3890.

20. Springstein BL, Arévalo S, Helbig AO, Herrero A, Stucken K, Flores E, Dagan T. 2020. A novel septal protein of multicellular heterocystous cyanobacteria is associated with the divisome. Mol Microbiol 113:1140–1154.

21. Kieninger AK, Tokarz P, Janovic A, Pilhofer M,Weiss GL, Maldener I. 2022. SepN is a septal junction component required for gated cell-cell communication in the filamentous cyanobacterium *Nostoc*. Nature Commu 13:7486.

22. Lehner J, Berendt S, Dörsam B, Pérez R, Forchhammer K, Maldener I. 2013. Prokaryotic multicellularity: A nanopore array for bacterial cell communication. FASEB J 27:2293–2300.

23. Bornikoel J, Carrión A, Fan Q, Flores E, Forchhammer K, Mariscal V, Mullineaux CW, Pérez R, Silber N, Wolk CP, Maldener I. 2017. Role of two cell wall amidases in septal junction and nanopore formation in the multicellular cyanobacterium *Anabaena* sp. PCC 7120. Front Cell Infect Microbiol 7:386.

24. Rudolf, M., Tetik, N., Ramos-León, F., Flinner, N., Ngo, G., Stevanovic, M, Burnat M, Pernil R, Flores E, Schleiff E. 2015. The peptidoglycan-binding protein SjcF1 influences septal junction function and channel formation in the filamentous cyanobacterium *Anabaena*. mBio 6:e00376-15.

25. Ramos-León F, Ramamurthi KS. 2022. Cytoskeletal proteins: lessons learned from bacteria. Phys Biol 19:021005.

26. Esue O, Cordero M, Wirtz D, Tseng Y. 2005. The assembly of MreB, a prokaryotic homolog of actin. J Biol Chem 280:2628–2635.

27. Vollmer W, Bertsche U. 2008. Murein (peptidoglycan) structure, architecture and biosynthesis in *Escherichia coli*. Biochim Biophys Acta 1778:1714-1734.

28. Egan AJF, Errington J, Vollmer W. 2020. Regulation of peptidoglycan synthesis and remodeling. Nat Rev Microbiol 18:446-460.

29. Errington J. 2015 Bacterial morphogenesis and the enigmatic MreB helix. Nature Rev Microbiol 13:241.

30. Hu B, Yang G, Zhao W, Zhang Y, Zhao J. 2007. MreB is important for cell shape but not for chromosome segregation of the filamentous cyanobacterium *Anabaena* sp. PCC 7120. Mol Microbiol 63:1640–1652.

31. Velázquez-Suárez C, Luque I, Herrero A. 2020. The inorganic nutrient regime and the *mre* genes regulate cell and filament size and morphology in the phototrophic multicellular bacterium *Anabaena*. mSphere 5, Issue 5 e00747-20.

32. Velázquez-Suárez C, Valladares A, Luque I, Herrero A. 2022. The role of Mre factors and cell division in peptidoglycan growth in the multicellular cyanobacterium *Anabaena*. mBio 13, Issue 4. 10.1128/mbio.01165-22.

33. Velázquez-Suárez C, Luque I, Herrero A. 2022. The role of MreB, MreC and MreD in the morphology of the diazotrophic filament of *Anabaena* sp. PCC 7120. Life 12:1437.

34. Du S, Lutkenhaus J. 2017. Assembly and activation of the *Escherichia coli* divisome. Mol Microbiol 105:177-187.

35. Sakr S, Thyssen M, Denis M, Zhang CC. 2006. Relationship among several key cell cycle events in the developmental cyanobacterium *Anabaena* sp. strain PCC 7120. J Bacteriol 188:5958–5965.

36. Corrales-Guerrero L, Camargo S, Valladares A, Picossi S, Luque I, Ochoa de Alda JAG, Herrero A. 2018. FtsZ of filamentous, heterocyst-forming cyanobacteria has a conserved N-terminal peptide required for normal FtsZ polymerization and cell division. Front Microbiol 9, Article 2260.

37. Camargo S, Picossi S, Corrales-Guerrero L, Valladares A, Arévalo S, Herrero A. 2019. ZipN is an essential FtsZ membrane tether and contributes to the septal localization of SepJ in the filamentous cyanobacterium *Anabaena*. Sci Reports 9: 2744.

38. Cassier-Chauvat C, Chauvat F. 2014 Cell division in cyanobacteria. In: The Cell Biology of Cyanobacteria. Flores E, Herrero A (eds.) Norfolk, UK: Caister Academic Press, pp. 7-27.

39. Burnat M, Schleiff E, Flores E. 2014. Cell envelope components influencing filament length in the heterocyst-forming cyanobacterium *Anabaena* sp. strain PCC 7120. J Bacteriol 196:4026-4035.

40. Ramos-León F, Mariscal V, Frías JE, Flores E, Herrero A. 2015. Divisome-dependent subcellular localization of cell-cell joining protein SepJ in the filamentous cyanobacterium *Anabaena*. Mol Microbiol 96:566-580.

41. Ramos-León F, Mariscal V, Battchikova N, Aro E-M, Flores E. 2017. Septal protein SepJ from the heterocyst-forming cyanobacterium *Anabaena* forms multimers and interacts with peptidoglycan. FEBS Open Bio 7:1515-1526.

42. Springstein BL, Woehle C, Weissenbach J, Helbig AO, Dagan T, Stucken K. 2020. Identification and

characterization of novel filament-forming proteins in cyanobacteria. Sci Rep 10: 1894.

43. Springstein BL, Nürnberg DJ, Woehle C, Weissenbach J, Theune ML, Helbig A, Maldener I, Dagan T, Stucken K. 2020. Two novel heteropolymer-forming proteins maintain the multicellular shape of *Anabaena* sp. PCC 7120. FEBS J. 288:3197-3216.

44. Lupas A, Van Dyke M, Stock J. 1991. Predicting coiled coils from protein sequences. Science 252(5009):1162–1164.

45. Strunecky O, Ivanova AP, Mares J. 2023. An updated classification of cyanobacterial orders and families based on phylogenomics and polyphasic analysis. J Phycol 59:12-51.

46. Svetlitsky D, Dagan T, Ziv-Ukelson M. 2020. Discovery of multi-operon colinear syntenic blocks in microbial genomes. Bioinformatics 36:i21-i29.

47. Lutkenhaus J. 2012. The ParA/MinD family puts things in their place. Trends Microbiol 20:411–418.

48. Flaherty BL, Van Nieuwerburgh F, Head SR, Golden JW. 2011. Directional RNA deep sequencing sheds new light on the transcriptional response of *Anabaena* sp. strain PCC 7120 to combined-nitrogen deprivation. BMC Genomics 12:332.

49. Mackinney G. 1941. Absorption of light by chlorophyll solutions. J Biol Chem 140: 109-112.

50. Flores E, Wolk CP. 1985. Identification of facultatively heterotrophic, N_2-fixing cyanobacteria able to receive plasmid vectors from *Escherichia coli* by conjugation. J Bacteriol 162:1339–1341.

51. Altschul SF, Gish W, Miller W, Myers EW, Lipman DJ. 1990. Basic local alignment search tool. J Mol Biol 215:403–410.

52. Camacho C, Colouris G, Avagyan V, Ma N, Papadopoulos J, Bealer K, Madde TL. 2009. BLAST+: architecture and applications. BMC Bioinformatics 10, article 421.

53. Rice P, Longden I, Bleasby A. 2000 EMBOSS: the European Molecular Biology Open Software Suite. Trends Genet 16:276–7.

54. Katoh K, Standley DM. 2013. MAFFT multiple sequence alignement software Version 7: improvements in performance and usability. Mol Biol Evol 30:772-780.

55. Minh BQ, Schmidt HA, Chernomor O, Schrempf D, Woodhams MD, von Haeseler A, Lanfear R. 2020. IQ-TREE 2: new models and efficient methods for phylogenetic inference in the genomic era. Mol Biol Evol 37:1530-1534.

56. Le SQ, Gascuel O. 2008. An improved general amino acid replacement matrix. Mol Biol Evol 25:1307-1320.

57. Tria FDK, Landan G, Dagan T. 2017. Phylogenetic rooting using minimal ancestor deviation. Nat Ecol Evol 1:0193.

58. Marchler-Bauer A, Bo Y, Han L, He J, Lanczycki CJ, Lu S, Chitsaz F, Derbyshire MK, Geer RC, Gonzales NR, Gwadz M, Hurwitz DI, Lu F, Marchler GH, Song JS, Thanki N, Wang Z, Yamashita RA, Zhang D, Zheng C, Geer LY, Bryant SH. 2016. CDD/SPARCLE: functional classification of proteins via subfamily domain architectures. Nucleic Acids Res 45:D200–D203.

59. Sonnhammer EL, von Heijne G, Krogh A. 1998. A hidden Markov model for predicting transmembrane helices in protein sequences. Proc Int Conf Intell Sist Mol Biol 6:175–182.

60. Yu NY, Wagner JR, Laird MR, Melli G, Rey S, Lo R, Dao P, Sahinalp SC, Ester M, Foster LJ, Brinkman FSL. 2010 PSORTb 3.0: Improved protein subcellular localization prediction with refined localization subcategories and predictive capabilities for all prokaryotes. Bioinformatics 26:1608–1615.

61. Shen H-Bin, Chou KC. 2010. Gneg-mPLoc: A top-down strategy to enhance the quality of predicting subcellular localization of Gram-negative bacterial proteins. J Theor Biol 264:326–333.

62. Buchan DWA, Jones DT. 2019. The PSIPRED Protein Analysis Workbench: 20 years on. Nucleic Acids Res 47: W402–W407.

63. Käll L, Krogh A, Sonnhammer ELL. 2007. Advantages of combined transmembrane topology and signal peptide prediction-the Phobius web server. Nucleic Acids Res 35:429–432.

64. Solovyev V, Salamov A. 2011. Automatic Annotation of Microbial Genomes and Metagenomic Sequences. In Metagenomics and its Applications in Agriculture, Biomedicine and Environmental Studies. Li RW (ed.). Nova Science Publishers, Inc., pp. 61–78.

65. Black TA, Cai Y, Wolk CP. 1993. Spatial expression and autoregulation of *hetR*, a gene involved in the control of heterocyst development in *Anabaena*. Mol Microbiol 9:77-84.

66. Elhai J, Wolk CP. 1988. A versatile class of positive selection vectors based on the nonviability of palindrome-containing plasmids that allows cloning into long polylinkers. Gene 68:119-138.

67. Elhai J, Vepritskiy A, Muro-Pastor AM, Flores E, Wolk CP. 1997. Reduction of conjugal transfer efficiency by three restriction activities of *Anabaena* sp. strain PCC 7120. J Bacteriol 179:1998–2005.

68. Olmedo-Verd E, Muro-Pastor AM, Flores E, Herrero A. 2006. Localized induction of the *ntcA* regulatory gene in developing heterocysts of *Anabaena* sp. strain PCC 7120. J Bacteriol 188:6694–6699.

69. Cai YP, Wolk CP. 1990. Use of a conditionally lethal gene in *Anabaena* sp. strain PCC 7120 to select for double recombinants and to entrap insertion sequences. J Bacteriol 172:3138-3145.

70. Wolk CP, Cai Y, Cardemil L, Flores E, Hohn B, Murry M, Schmetterer G, Schrautemeier B, Wison R. 1988. Isolation and complementation of mutants of *Anabaena* sp. strain PCC 7120 unable to grow aerobically on dinitrogen. J Bacteriol 170:1239–1244.

71. Karimova G, Dautin N, Ladant D. 2005. Interaction network among *Escherichia coli* membrane proteins involved in cell division as revealed by bacterial two-hybrid analysis. J Bacteriol 187:2233-2243.

72. Schneider CA, Rasband WS, Eliceiri KW. 2012. NIH Image to ImageJ: 25 years of image analysis. Nature Methods 9: 671-675.

FIGURE LEGENDS:

Fig. 1. SepT domain distribution and phylogeny. (A) Prediction of conserved domains in SepT using the Conserved Domain Search (CDS; NCBI). Orange bars indicate the presence of the two transmembrane domains (TMDs); a Structural Maintenance of Chromosomes (SMC) domain is depicted in grey and a TerB-C domain (putative metal-chelating) domain is shown in yellow. The SMC and TerB-C domains overlap in part, which is highlighted by a mixed grey-yellow part. (B) Prediction of coiled-coil-rich regions using the COILS algorithm and three different screening windows for repetitive heptamer sequences (windows 14, 21 and 28). (C) Prediction of the structure of a SepT dimer (colored by pLDDT) according to AlphaFold algorithm. (D) Phylogenetic tree of selected SepT homologs. Heterocyst-forming species are written in black and non-heterocystous species are written in blue. *Nostoc* sp. PCC 7120 is the same strain as *Anabaena* sp. PCC 7120. Bootstrap values are shown next to ancestral node and the branch width is scaled to the bootstrap values. (E) The genomic region of *all2460* taken from the Integrated Microbial Genomes and Microbiomes (IMG/M) of the Joint Genome Institute (JGI) database.

Fig. 2. Localization of SepT-GFP in *Anabaena* PCC 7120 and BS1 mutant. Strains *Anabaena* WT, CSCV25 (expressing SepT-GFP in the wild-type background) and CSCV26 (expressing SepT-GFP in BS1 background) were grown in and transferred to BG11 medium at a cell density corresponding to 0.5 μg Chl ml^{-1} and incubated under culture conditions. After 24 h, filaments were observed by confocal microscopy with a Fluoview equipment. GFP fluorescence (green) and merged GFP and cyanobacterial autofluorescence (red) images are shown. Yellow arrows point to GFP fluorescence matching the divisome. Magnification is the same for all micrographs.

Fig. 3. Analysis of SepT interactions by BACTH. The topology of each fusion is indicated by the order of components (T18-protein and T25-protein denote the corresponding adenylate cyclase domain fused to the N-terminus of the tested protein, whereas protein-T18 and protein-T25 denote fusions to the C-terminus). (A) Interaction of protein pairs produced in *E. coli* was assayed by measurements of β-galactosidase activity (nmol ONP min^{-1} mg protein^{-1}) in liquid cultures incubated at 30 °C. Data are the mean and standard deviation of 2 to 9 determinations of the activity with the indicated protein fused to T25 (or the empty vectors pKNT25 or pKT25) and SepT-T18 (dark bars), or the indicated protein (or the empty vectors pKNT25 or pKT25) and pUT18C (clear bars); or with the indicated protein fused to T18 (or the empty vectors pUT18C or pUT18) and SepT-T25 (dark bars), or the indicated protein (or the empty vectors pUT18C or pUT18) and pKT25 (light bars). Significance of differences were assessed by Student's *t* tests. Asterisks indicate strains expressing a pair of tested proteins that exhibited β-galactosidase activity significantly different (p<0.023) from the two controls: the strains expressing each fused protein and containing the complementary empty vector. (B) *E. coli* cells were subjected to β-

galactosidase assay in triplicates from three independent colonies grown for 2 days at 20 °C. Quantitative values are given in Miller units, and the mean results from three independent colonies are presented. Negative: N-terminal T25 fusion construct of the respective protein co-transformed with empty pUT18C. Positive: Zip/Zip control. Error bars indicate standard deviations (n=3). Values indicated with asterisks are significantly different from the negative control. ***: $p<0.001$, ****: $p<0.0001$ (Dunnett's multiple comparison test and one-way ANOVA).

Fig. 4. Genomic structure and growth of strains with inactivated *sepT*. (A) Schematic of the genetic structure of strains CSCV9 and BS1 in the *sepT* genomic region. (B) Filaments of strains *Anabaena* WT, CSCV9 and BS1 were grown in BG11 medium, transferred to BG11 (containing $NaNO_3^-$) or $BG11_0$ (no combined nitrogen), at a cell density corresponding to 0.5 mg Chl ml^{-1}, and incubated under culture conditions. At the indicated times, the OD_{750} (At) was measured in aliquots of each culture. The values of 2 independent cultures of each condition (1 culture of CSCV9 under N_2) were represented and adjusted to sequential linear functions. A0 represents the OD_{750} at the start of the culture. Growth rate constant, μ (day^{-1}), corresponds to $\ln2/t_d$, where t_d is the doubling time, calculated from the increase in OD_{750} from 0-98.5 hours (exponential growth) and from 170.5-266.5 hours (slow growth) of incubation as above. Mann-Whitney tests indicated no significance of differences ($p > 0.1$) between each mutant and the WT for any time and condition.

Fig. 5. Cell size and morphology of *sepT* mutants. Filaments of *Anabaena* WT (WT-s, the parental for CSCV9; WT-k, the parental for BS1), CSCV9 (*sepT*::C.K1) and BS1 (*sepT*::C.S3) grown in BG11 medium were transferred to BG11 or $BG11_0$, at a cell density corresponding to 0.5 μg Chl ml^{-1}, and incubated under culture conditions. (A) After 48 h filaments from $BG11_0$ cultures were photographed. Purple arrows point to polar granules in heterocysts. Magnification is the same for all micrographs. (B-C) After 48 h and 216 h, aliquots of each culture were photographed and used for cell area (B) and Aspect ratio (C) determinations. 200-300 cells (vegetative cells in the diazotrophic cultures) from two different cultures of each strain and condition (150 cells for WT-k) were measured. The Aspect ratio is the result of dividing the length of the axis parallel to the filament by the length of the axis perpendicular to the filament. Notched boxplot representations of the data are shown. The mean values are represented by black dots.

Fig. 6. Localization of PG growth in *sepT* mutants. Strains *Anabaena* WT and CSCV9 grown in BG11 medium were transferred (at a cell density of 0.5 μg Chl ml^{-1}) to BG11 (A) or $BG11_0$ (B) medium and incubated under culture conditions. After 48 h, samples of filaments were stained with Van-FL and observed under a fluorescence microscope and photographed. Van-FL

fluorescence (green), cyanobacterial autofluorescence (red) and bright-field images are shown. White arrows point to heterocysts. Magnification is the same for all micrographs. After 48 and 216 h, lateral and septal fluorescence was quantified as described in Materials and Methods. Student's t test was used to assess significance of differences (Data Set S4).

Fig. 7. Localization of MreB, MreC and MreD in the absence of SepT. Strains CSCV11 (*sepT*::C.K1, *sfgfp-mreB*), CSCV12 (*sepT*::C.K1, *sfgfp-mreC*), CSCV13 (*sepT*::C.K1, *sfgfp-mreD*), and reference strains *Anabaena* WT, CSCV9 (*sepT*::C.K1), CSCV6 (*sfgfp-mreB*), CSCV7 (*sfgfp-mreC*) and CSCV8 (*sfgfp-mreD*) were grown in BG11 medium and transferred to BG11$_0$ + NH$_4^+$ (A) or BG11$_0$ medium (B), adjusted to a cell density corresponding to 0.5 µg Chl ml^{-1}. After 24 hours, aliquots of filaments were observed under a TCS confocal microscope and photographed. GFP fluorescence (green), cyanobacterial autofluorescence (red) and bright-field images are shown. Yellow arrows point to heterocysts. Magnification is the same for all micrographs.

Fig. 8. Septal nanopore array in *sepT* mutant strains. (A) Representative transmission electron microscopy images of PG sacculi septa from *Anabaena* WT and the *sepT* mutant strains CSCV9 and BS1 grown in BG11 medium (see Materials and methods for details). (B) Number of nanopores per septum and mean nanopore diameter. n, sample size (number of septal disks or nanopores, respectively). Data on *Anabaena* WT are from (13).

Fig. 1

A

SepT (426 aa)

N | | | SMC | TerB-C | > C

TMD

B

C

D

Nostoc sp. PCC 7120
90 ┌ *Nodularia spumigena* CCY9414
93 ┤
100 └ *Nodularia* sp. NIES-3585
82 *Anabaenopsis elenkinii* CCIBt3563
Anabaenopsis circularis NIES-21
49 *Nostoc azollae* PCC 0708
98 ┌ *Aphanizomenon flos-aquae* NIES-81
100 ┤
49 └ *Aphanizomenon flos-aquae* 2012/KM1/D3
80 ┌ *Tolypothrix* sp. PCC 7601
100 ┤
57 └ *Calothrix* sp. NIES-2098
Cylindrospermum sp. NIES-4074
Nostoc punctiforme PCC 73102
Fischerella thermalis
100 91 ┌ *Chlorogloeopsis fritschii* PCC 9212
100 ┤
73 └ *Chlorogloeopsis fritschii* PCC 6912
82 *Richelia intracellularis* HH01
46 *Mastigocladopsis repens* PCC 10914
64 *Scytonema hofmannii* PCC 7110
76 *Rivularia* sp. PCC 7116
Calothrix desertica PCC 7102
100 ┌ *Gloeocapsa* sp. PCC 7428
└ *Chroococcidiopsis* sp. TS-821
100 *Pleurocapsales* sp. LEGE 06147
100 *Microcoleus* sp. PCC 7113
93 *Spirulina subsalsa* PCC 9445
88 *Spirulina major* PCC 6313

0.4

E

all2460

all2459   *all2461*

Fig. 2

WT

CSCV25

10 μm

CSCV26

Fig. 3

Fig. 4

A

PCC 7120 — *all2459*, *all2460*, *all2461*

CSCV9 — C.K1

BS1 — C.S3

1 kb

B

NO_3^- — WT, BS1, CSCV9 — ln(At/A0) vs Time (h)

N_2 — ln(At/A0) vs Time (h)

- WT
- BS1
- CSCV9

	Growth rate constant (day^{-1})			
	Exponential growth		Slow growth	
	N_2	NO_3^-	N_2	NO_3^-
WT	0.326	0.598	0.036	0.072
CSCV9	0.281	0.516	0.137	0.089
BS1	0.418	0.701	0.106	0.094

Fig. 5
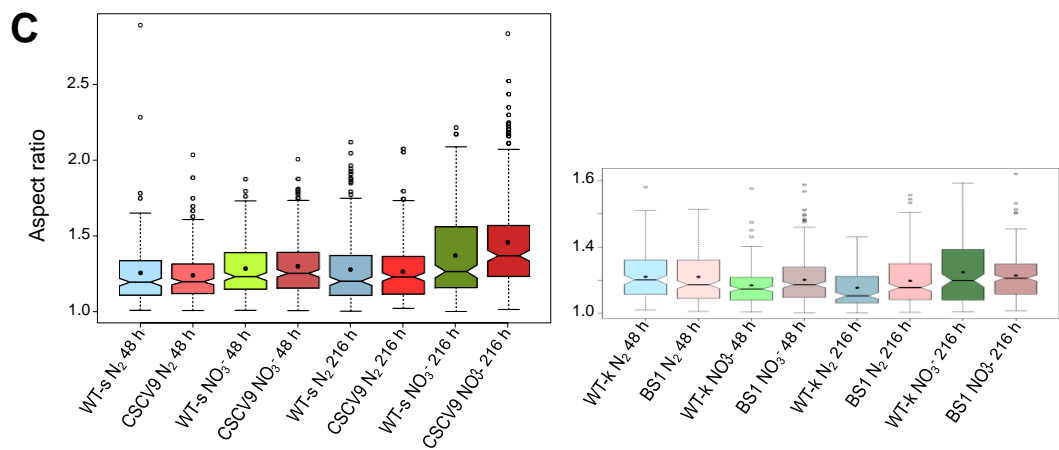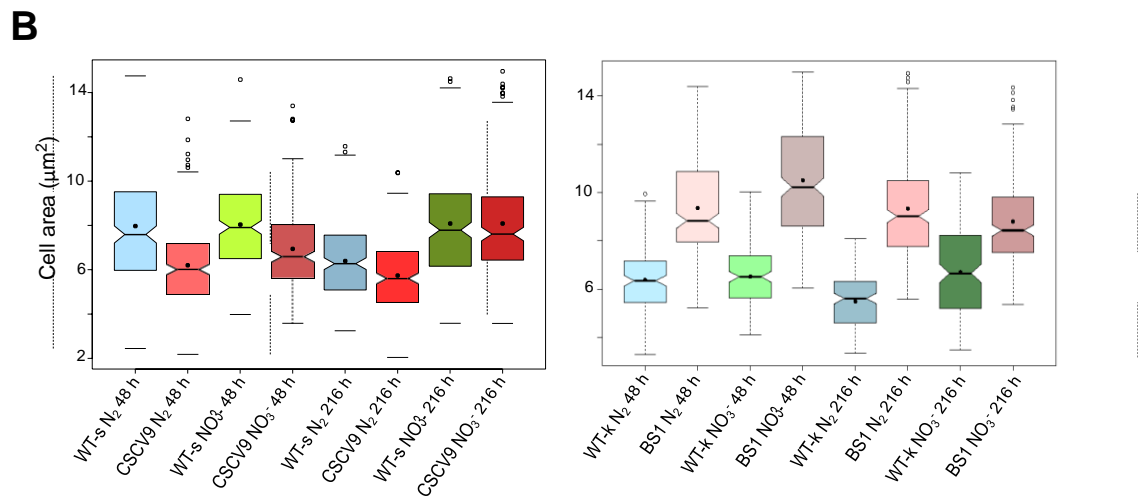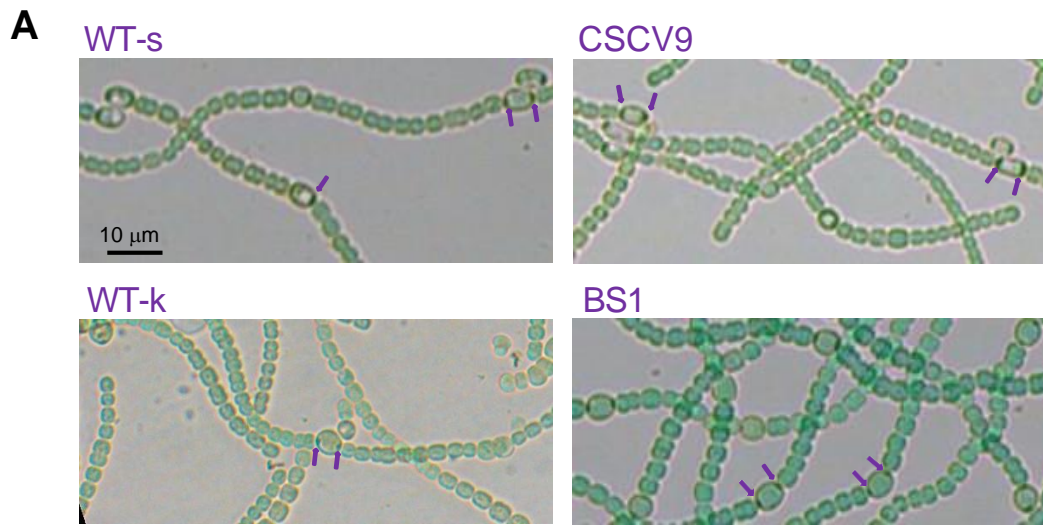
Fig. 6

A

WT   CSCV9   BS1

10 μm

Fluorescence intensity (a.u.) BG11

Time (h)	WT		CSCV9		BS1	
	Lateral	Septal	Lateral	Septal	Lateral	Septal
48	8.60	28.42	6.30	22.79	4.64	18.95
216	4.42	20.42	4.46	23.46	2.66	19.35

B

WT   CSCV9   BS1

10 μm
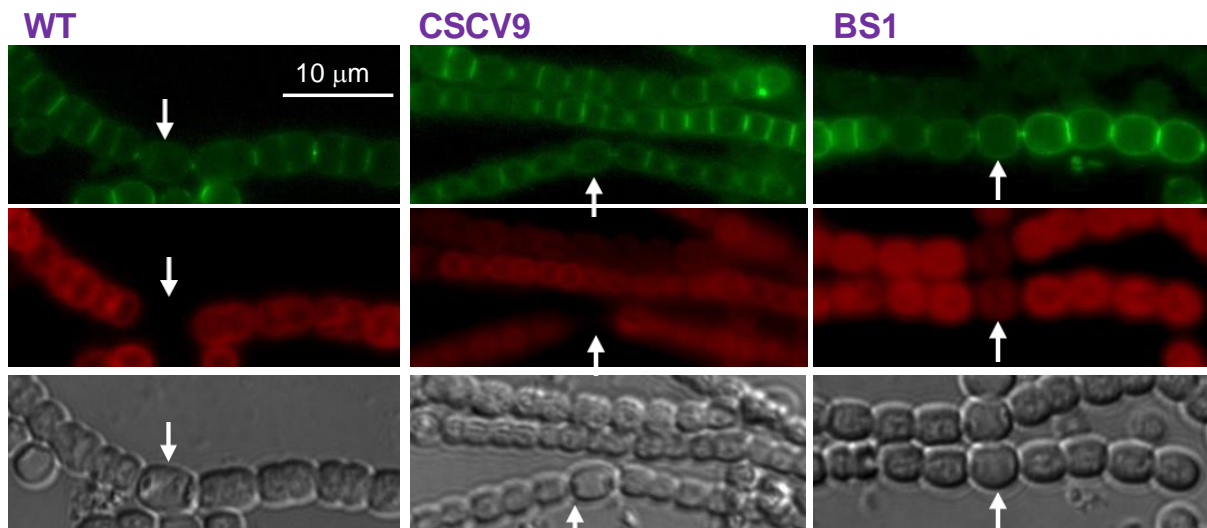
Fluorescence intensity (a.u.) BG11$_0$ (vegetative cells)

Time (h)	WT		CSCV9		BS1	
	Lateral	Septal	Lateral	Septal	Lateral	Septal
48	8.52	25.96	8.87	23.16	10.24	27.38
216	4.90	17.36	2.76	15.87	5.23	17.00

Fig. 7

A

B
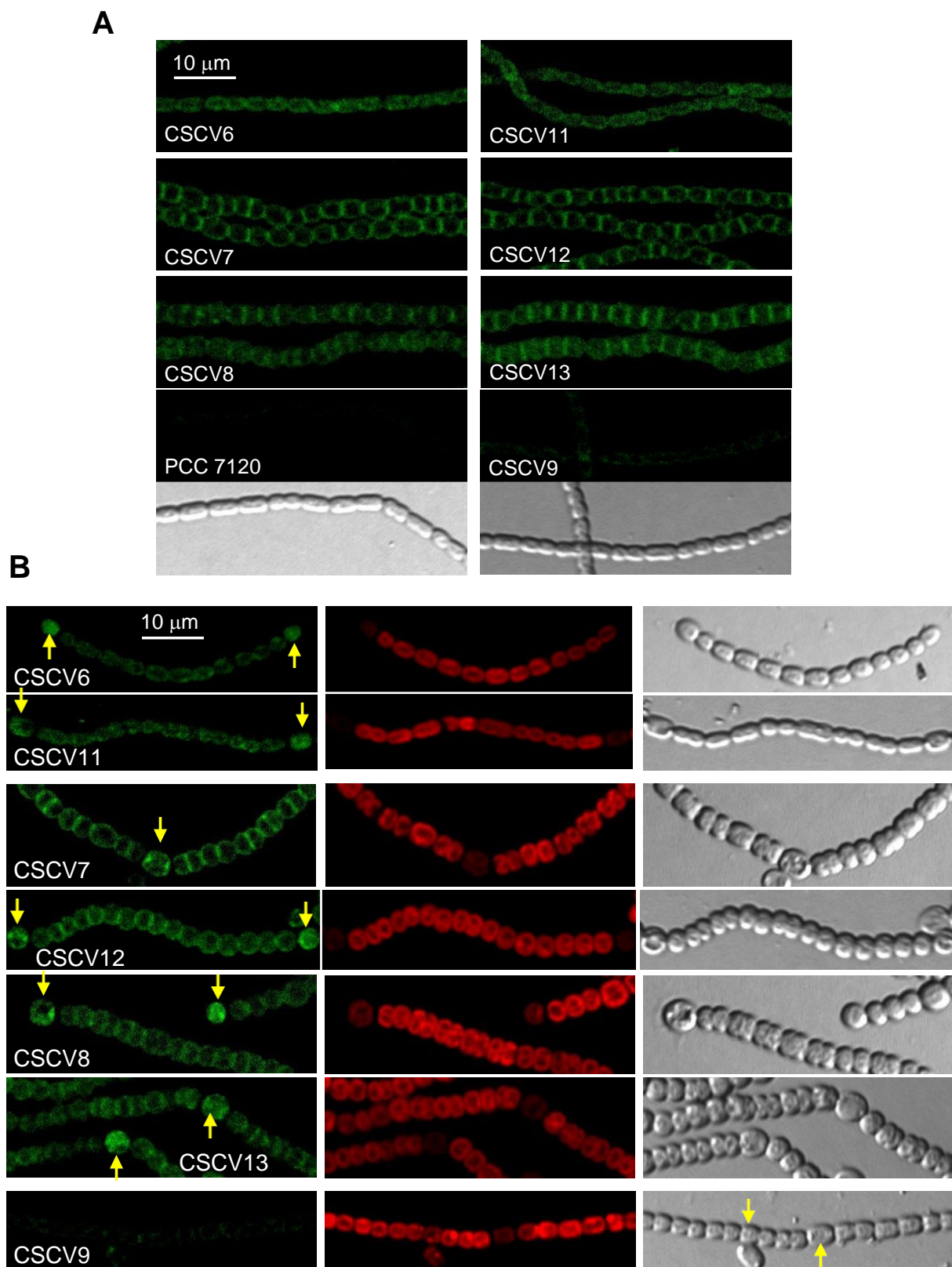
Fig. 8

A

PCC 7120   CSCV9   BS1
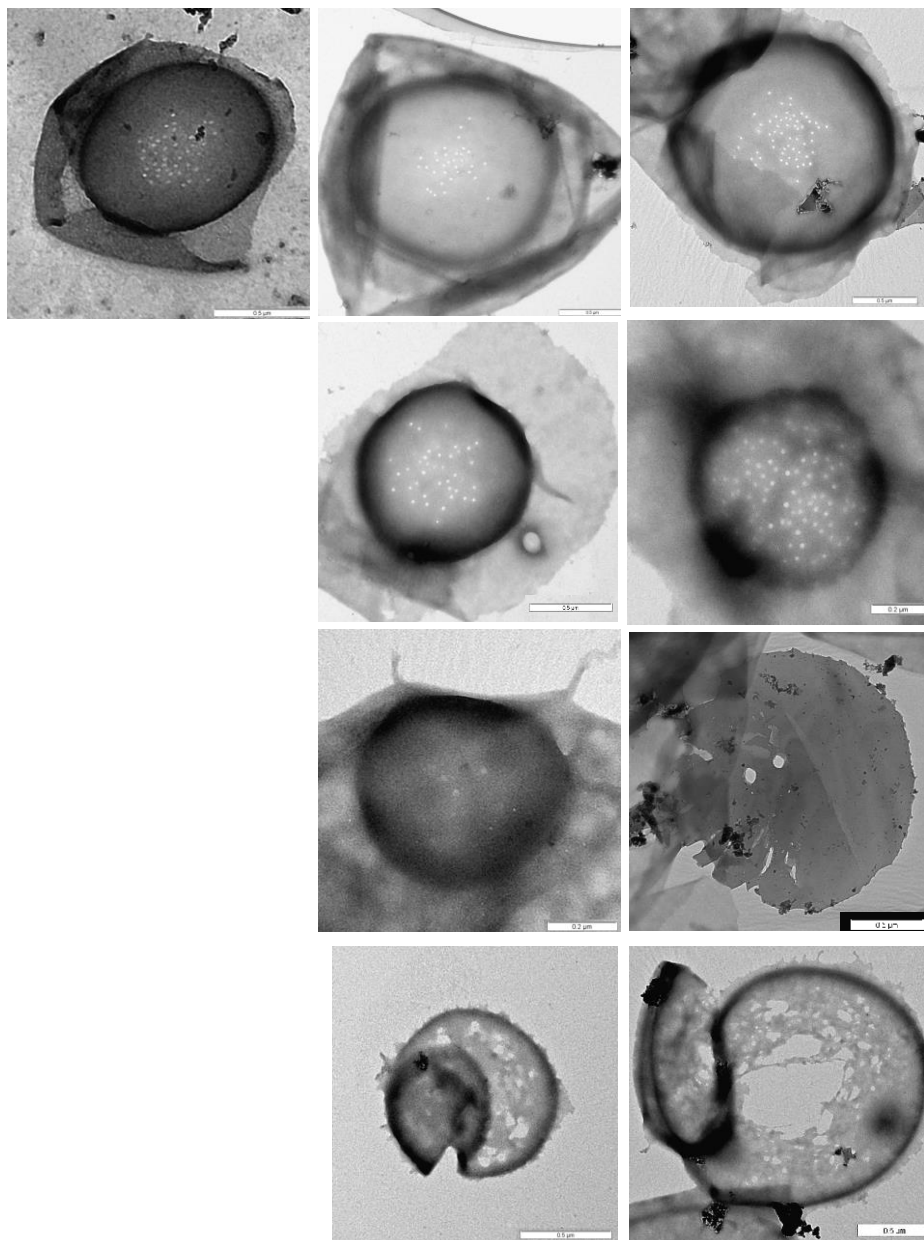
B

	Nanopores/disk mean ± SD (n)	Nanopore diameter mean ± SD (n)
PCC 7120	41.67 ± 21.85 (21)	17.06 ± 4.13 (131)
CSCV9	28 ± 17.89 (11)	15 ± 0.005 (308)
BS1	21.5 ± 21.12 (14)	15 ± 0.012 (301)

Fig. 9
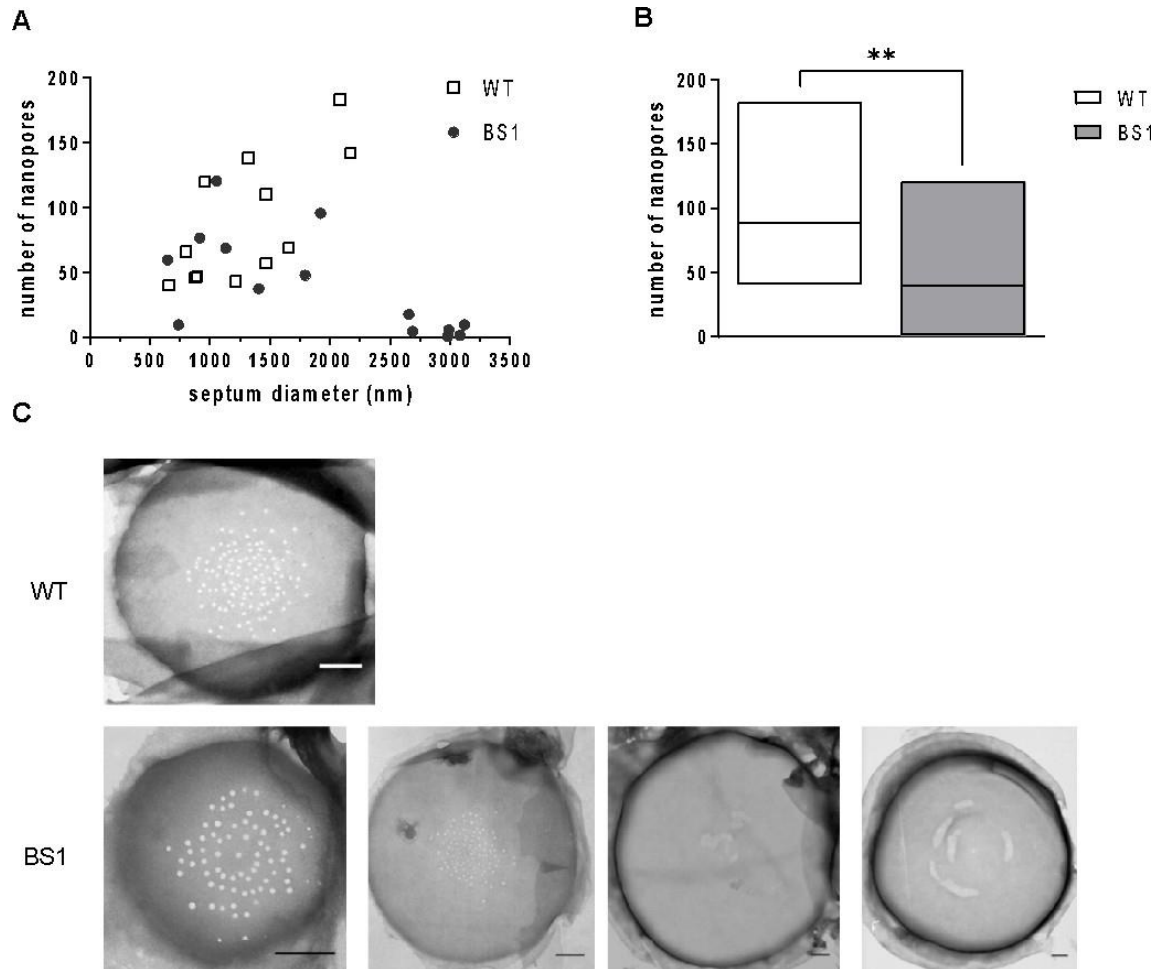
Figure S1. Septal nanopore array in strain BS1 grown on solid medium. Peptidoglycan was purified from filaments of the wild type (WT) and mutant BS1 that were grown on agar plates, and the sacculi investigated by TEM. A, The number of nanopores is shown correlated to the septum size. In contrast to the WT, the mutant shows a subset of large septa with very few nanopores. B, The number of pores per septum was analyzed. Floating bars show the mean value. Unpaired Student's *t*-test was performed (mutant vs. WT). *p*-values are indicated (**$p<0.001$). C, Representative TEM images of indicated strains are shown. Bars: 250 nm.

Methods: Transmission electron microscopy and sacculi preparation. Peptidoglycan sacculi were isolated from filaments grown on BG11 agar plates, by the method of Kühner *et al.* (2014) with the following modifications: cells were sonicated (Branson Sonifier 250; duty cycle 50%, output control 1, 2 min) prior to boiling in 1 mL 0.1 M Tris/HCl pH 6.8 with 3% SDS. After the sonifier waterbath, the sample was incubated with 600 μg α-chymotrypsin at 37° C overnight in 50 mM Na_3PO_4 buffer pH 6.8. After inactivation of the enzyme, the sample was sonified again and loaded on a formvar/carbon film coated copper grid (Science Services GmbH München) and stained with 1 % (w/v) uranyl acetate as described previously (Lehner *et al.*, 2011). Images were taken with a Philips Tecnai10 electron microscope at 80 kV.

References:
Kühner D, Stahl M, Demircioglu DD, Bertsche U. 2014. From cells to muropeptide structures in 24 h: Peptidoglycan mapping by UPLC-MS. Protocol Exchange.
Lehner J, Zhang Y, Berendt S, Rasse TM, Forchhammer K, Maldener I. 2011. The morphogene AmiC2 is pivotal for multicellular development in the cyanobacterium *Nostoc punctiforme*. Mol Microbiol 79:1655-1669.

Table S1. Cyanobacterial strains and plasmids used in this work.

Strain	Genotype	Resistance	Source
Anabaena sp. PCC 7120	WT		Pasteur Culture Collection
BS1	*sepT*::C.S3	Sm, Sp	This study
CSCV6	*thrS2*::P$_{mreB}$-*sfgfp-mreB*	Sm, Sp	Velázquez-Suárez *et al.*, 2022a
CSCV7	*thrS2*::P$_{mreB}$-*sfgfp-mreC*	Sm, Sp	Velázquez-Suárez *et al.*, 2022a
CSCV8	*thrS2*::P$_{mreB}$-*sfgfp-mreD*	Sm, Sp	Velázquez-Suárez *et al.*, 2022a
CSCV9	*sepT*::C.K1	Nm	This study
CSCV11	*thrS2*::P$_{mreB}$-*sfgfp-mreB*, *sepT*(CSCV9)	Nm, Sm, Sp	This study
CSCV12	*thrS2*::P$_{mreB}$-*sfgfp-mreC*, *sepT*(CSCV9)	Nm, Sm, Sp	This study
CSCV13	*thrS2*::P$_{mreB}$-*sfgfp-mreD*, *sepT*(CSCV9)	Nm, Sm, Sp	This study
CSCV25	P$_{sepT}$-*sepT-gfpmut3.1*	Nm	This study
CSCV26	P$_{sepT}$-*sepT-gfpmut3.1*, *sepT*(BS1)	Nm, Sm, Sp	This study

Plasmid	Description	Resistance marker	Source
pCSCV36	pRL277 carrying *sepT*::C.K1	Km, Nm	This study
pTHS109	pRL278 carrying *sepT*::C.S3	Sm, Sp	This study
pTHS240	pRL25C carrying P$_{sepT}$-*sepT-gfpmut3.1*	Km, Nm	This study
pTHS143	pRL25C carrying P$_{petE}$-*sepT-gfpmut3.1*	Km, Nm	This study

Table S2. Oligodeoxynucleotide primers used in this work.

Name	Sequence (5'-3')
842KO_2A	ATTCGATATCTAGATCTCGAGATGGATAATCCAGCAATGTCGGC
842KO_2B	AAGGTGCTGTGCACGGATCATTGCTGATTTTTAGCGTAGTTAAGCTTT
842KO_4A	CAAGGTAGTCGGCAAATAAAATTTAATATCCCTAGCTCATCGTAAAATTTTTATAAAAATATG
842KO_4B	ATGCAAGCTTTCGCGAGCTCTTTAAAACTAGAACTATGAACTAGCTCGCTAAAC
all2459-1	AATGCTGCAGCACCTTCGGCAATATCATC
all2460-1	GAATGGATCCACGGAGTGAACTTAAAAG
all2460-2	AATTGGATCCGCTAACATCACTATGCCG
all2461-1	CTTTCTGCAGCGCTTTGGCTTAACCCTC
alr0653-1	CAACTCCTGCAGGGTTATTAAAACGATCGCTTC
alr0653-2	GATGACGAATTCTAGTGGTTGGTGGTCAGT
alr0653-3	CAAAACTGCAGCTTATTAAAACGATCGCTTC
alr0653-4	GAAAGTGAATTCGTAAAATAATATTTCTGTCGTTGTC
alr5045-7	TTTAAGCTGCAGGGCTTTACTGCAACCATC
alr5045-8	TATTTAGAATTCATATTATCTGCTTTTTGC
alr5045-9	CTTTAACTGCAGTGGCTTTACTGCAACCAT
CS.3_Fwd	GATCCGTGCACAGCACCTTG
CS.3_Rev	TTATTTGCCGACTACCTTGGTGATCT
GFP_25C_R	AGGCCCTTTCGTCTTCAAGTTATTTGTATAGTTCATCCATGCCATGTGT
GFP_842_A	AGCTAGATACGCATCCGCTAGTGCATCTGCTAGTGCTAGTG
MB_25A	TGCCTGCAGGTCGACTCTAATGCAACAAGTCATAGTAAGTAATCGAT
MB_25B	TCGGTACCCGGGGATCCTCGGATGCGTATCTAGCTATTAGATGTTC
MB_26A	AGGGTCGACTCTAGAGGATATGCAACAAGTCATAGTAAGTAATCGAT
MB_26B	CTTACTTAGGTACCCGGGGGGATGCGTATCTAGCTATTAGATGTTC
MB_27A	TGCCTGCAGGTCGACTCTAATGCAACAAGTCATAGTAAGTAATCGAT
MB_27B	TCGGTACCCGGGGATCCTCGGATGCGTATCTAGCTATTAGATGTTC
MB_28A	TCTAGAGGATCCCCGGGTAATGCAACAAGTCATAGTAAGTAATCGAT
MB_28B	TCGATGAATTCGAGCTCGGGGATGCGTATCTAGCTATTAGATGTTC
Nos842_2A	TACAGGTTAGGAGAACGCCATGCAACAAGTCATAGTAAGTAATCGATT
Nos842_2B	CACTAGCAGATGCACTAGCGGATGCGTATCTAGCTATTAGATGTTC
p842_25C_long_A	TTTTGGTCATGAGATTATCAAAAAGTCTCTCTATCCCCAAGTACAATTTCTCC
petE_903_Fwd	GAGATTATCAAAAAGGATCCCAGTACTCAGAATTTTTTGCTGAGGTACT
pRL25C_F	CTTGAAGACGAAAGGGCCTCT
pRL25c_NEB_Fwd	GCTAGTGCATCTGCTAGTGCTAGTG
pRL25c_NEB_Rev	GGCGTTCTCCTAACCTGTAGTTTTATTTTTCT
pRL25C_R	CTTTTTGATAATCTCATGACCAAAATCCCTTAAC
pRL25c-903_V_F	TGGATGAACTATACAAATAAAGAATTCTTGAAGACGAAAGGGCC
pRL25c-	GCAAAAAATTCTGAGTACTGGGATCCTTTTTGATAATCTCATGACC

903_V_R	AAAATCC
pRL271_Fwd	GAGCTCGCGAAAGCTTGCATG
pRL271_Rev	CTCGAGATCTAGATATCGAATTTCTGCCAT

GENERAL REFERENCES

Aaron, M., Charbon, G., Lam, H., Schwarz, H., Vollmer, W., and Jacobs-Wagner, C. (2007) The tubulin homologue FtsZ contributes to cell elongation by guiding cell wall precursor synthesis in *Caulobacter crescentus*. *Mol Microbiol* **64**: 938–952.

Abed, R.M.M., Dobretsov, S., and Sudesh, K. (2009) Applications of cyanobacteria in biotechnology. *J Appl Microbiol* **106**: 1–12.

Ago, R. and Shiomi, D. (2019) RodZ: A key-player in cell elongation and cell division in *Escherichia coli*. *AIMS Microbiol* **5**: 358–367.

Aliashkevich, A. and Cava, F. (2022) LD-transpeptidases: the great unknown among the peptidoglycan cross-linkers. *FEBS J* **289**: 4718–4730.

Alyahya, S.A., Alexander, R., Costa, T., Henriques, A.O., Emonet, T., and Jacobs-Wagner, C. (2009) RodZ, a component of the bacterial core morphogenic apparatus. *Proc Natl Acad Sci U S A* **106**: 1239–1244.

Anderson, S.L. and McIntosh, L. (1991) Light-activated heterotrophic growth of the cyanobacterium *Synechocystis* sp. strain PCC 6803: A blue-light-requiring process. *J Bacteriol* **173**: 2761–2767.

Arends, S.J.R., Kustusch, R.J., and Weiss, D.S. (2009) ATP-binding site lesions in FtsE impair cell division. *J Bacteriol* **191**: 3772–3784.

Arévalo, S. and Flores, E. (2021) Heterocyst septa contain large nanopores that are influenced by the Fra proteins in the filamentous cyanobacterium *Anabaena* sp. strain PCC 7120. *J Bacteriol* **203**: e00081-21.

Arévalo, S., Nenninger, A., Nieves-Morión, M., Herrero, A., Mullineaux, C.W., and Flores, E. (2021) Coexistence of communicating and noncommunicating cells in the filamentous cyanobacterium *Anabaena* . *mSphere* **6**:e01091-20.

Attaibi, M. and den Blaauwen, T. (2022) An updated model of the divisome: regulation of the septal peptidoglycan synthesis machinery by the divisome. *Int J Mol Sci* **23**:3537.

Bailey, S. and Grossman, A. (2008) Photoprotection in cyanobacteria: Regulation of light harvesting. *Photochem Photobiol* **84**: 1410–1420.

Barrows, J.M. and Goley, E.D. (2021) FtsZ dynamics in bacterial division: what, how, and why? *Curr Opin Cell Biol* **68**: 163–172.

Bendezú, F.O., Hale, C.A., Bernhardt, T.G., and de Boer, P.A.J. (2009) RodZ (YfgA) is required for proper assembly of the MreB actin cytoskeleton and cell shape in *E. coli*. *EMBO J* **28**: 193–204.

Berendt, S., Lehner, J., Zhang, Y.V., Rasse, T.M., Forchhammer, K., and Maldener, I. (2012) Cell wall amidase Amic1 is required for cellular communication and heterocyst development in the cyanobacterium *Anabaena* PCC 7120 but not for filament integrity. *J Bacteriol* **194**: 5218–5227.

Bergman, B., Gallon, J.R., Rai, A.N., and Stal, L.J. (1997) N$_2$ fixation by non-heterocystous cyanobacteria. *FEMS Microbiol Rev* **19**: 139–185.

Bernhardt, T.G. and de Boer, P.A.J. (2004) Screening for synthetic lethal mutants in *Escherichia coli* and identification of EnvC (YibP) as a periplasmic septal ring factor with murein hydrolase activity. *Mol Microbiol* **52**: 1255–1269.

Beveridge, T.J. (1988) The bacterial surface: general considerations towards design and function. *Can J Microbiol* **34**: 363–372.

Billings, G., Ouzounov, N., Ursell, T., Desmarais, S.M., Shaevitz, J., Gitai, Z., and Huang, K.C. (2014) De novo morphogenesis in L-forms via geometric control of cell growth. *Mol Microbiol* **93**: 883–896.

Bisson-Filho, A.W., Hsu, Y.P., Squyres, G.R., Kuru, E., Wu, F., Jukes, C., et al. (2017) Treadmilling by FtsZ filaments drives peptidoglycan synthesis and bacterial cell division. *Science* **355**: 739–743.

Bonner, J.T. (1998) The origins of multicellularity. *Integr Biol* **1**: 27–36.

Bonner, J.T. (2003) On the origin of differentiation. *J Biosci* **28**: 523–528.

Bordowitz, J.R. and Montgomery, B.L. (2008) Photoregulation of cellular morphology during complementary chromatic adaptation requires sensor-kinase-class protein RcaE in *Fremyella diplosiphon*. *J Bacteriol* **190**: 4069–4074.

Bornikoel, J., Carrión, A., Fan, Q., Flores, E., Forchhammer, K., Mariscal, V., et al. (2017) Role of two cell wall amidases in septal junction and nanopore formation in the multicellular cyanobacterium *Anabaena* sp. PCC 7120. *Front Cell Infect Microbiol* **7**: 386.

Bramhill, D. and Thompson, C.M. (1994) GTP-dependent polymerization of *Escherichia coli* FtsZ protein to form tubules. *Proc Natl Acad Sci U S A* **91**: 5813–5817.

Bratton, B.P., Shaevitz, J.W., Gitai, Z., and Morgenstein, R.M. (2018) MreB polymers and curvature localization are enhanced by RodZ and predict *E. coli*'s cylindrical uniformity. *Nat Commun* **9**: 2797.

Brenes-Álvarez, M., Mitschke, J., Olmedo-Verd, E., Georg, J., Hess, W.R., Vioque, A., and Muro-Pastor, A.M. (2019)

Elements of the heterocyst-specific transcriptome unravelled by co-expression analysis in *Nostoc* sp. PCC 7120. *Environ Microbiol* **21**: 2544–2558.

Buikema, W.J. and Haselkorn, R. (1991) Characterization of a gene controlling heterocyst differentiation in the cyanobacterium *Anabaena* 7120. *Genes Dev* **5**: 321–330.

Büke, F., Grilli, J., Lagomarsino, M.C., Bokinsky, G., and Tans, S.J. (2022) ppGpp is a bacterial cell size regulator. *Curr Biol* **32**: 870-877.e5.

Burillo, S., Luque, I., Fuentes, I., and Contreras, A. (2004) Interactions between the nitrogen signal transduction protein PII and *N*-acetyl glutamate kinase in organisms that perform oxygenic photosynthesis. *J Bacteriol* **186**: 3346–3354.

Burnat, M., Herrero, A., and Flores, E. (2014) Compartmentalized cyanophycin metabolism in the diazotrophic filaments of a heterocyst-forming cyanobacterium. *Proc Natl Acad Sci U S A* **111**: 3823–3828.

Bush, M.J., Tschowri, N., Schlimpert, S., Flärdh, K., and Buttner, M.J. (2015) c-di-GMP signalling and the regulation of developmental transitions in streptomycetes. *Nat Rev Microbiol* **13**: 749–760.

Busiek, K.K. and Margolin, W. (2015) Bacterial actin and tubulin homologs in cell growth and division. *Curr Biol* **25**: R243–R254.

Buske, P.J. and Levin, P.A. (2012) Extreme C terminus of bacterial cytoskeletal protein FtsZ plays fundamental role in assembly independent of modulatory proteins. *J Biol Chem* **287**: 10945–10957.

Cabeen, M.T. and Jacobs-Wagner, C. (2010) The bacterial cytoskeleton. *Annu Rev Genet* **44**: 365–392.

Camargo, S., Picossi, S., Corrales-Guerrero, L., Valladares, A., Arévalo, S., and Herrero, A. (2019a) ZipN is an essential FtsZ membrane tether and contributes to the septal localization of SepJ in the filamentous cyanobacterium *Anabaena*. *Sci Rep* **9**: 2744.

Cameron, J.C., Wilson, S.C., Bernstein, S.L., and Kerfeld, C.A. (2013) Biogenesis of a bacterial organelle: the carboxysome assembly pathway. *Cell* **155**: 1131–1140.

Cameron, T.A., Anderson-Furgeson, J., Zupan, J.R., Zik, J.J., and Zambryski, P.C. (2014) Peptidoglycan synthesis machinery in *Agrobacterium tumefaciens* during unipolar growth and cell division. *mBio* **5**: e01219-14.

Canfield, D.E., Glazer, A.N., and Falkowski, P.G. (2010) The evolution and future of Earth's nitrogen cycle. *Science* **330**: 192–196.

Carballido-López, R., Formstone, A., Li, Y., Ehrlich, S.D., Noirot, P., and Errington, J. (2006) Actin homolog MreBH governs cell morphogenesis by localization of the cell wall hydrolase LytE. *Dev Cell* **11**: 399–409.

Cardemil, L. and Wolk, C.P. (1979) The polysaccharides from heterocyst and spore envelopes of a blue-green alga. Structure of the basic repeating unit. *J Biol Chem* **254**: 736–741.

Cardona, T. (2018) Early Archean origin of heterodimeric photosystem I. *Heliyon* **4**: e00548.

Carroll, S.B. (2001) Chance and necessity: the evolution of morphological complexity and diversity. *Nature* **409**: 1102–1109.

Cassier-Chauvat, C. and Chauvat, F. (2014) Cell division in cyanobacteria. In *The cell biology of Cyanobacteria*. Flores, E. and Herrero, A. (Eds.) Caister Academic Press, Norfolk, UK. Pp 7–27.

Cavalier-Smith, T. (2002) The neomuran origin of archaebacteria, the negibacterial root of the universal tree and bacterial megaclassification. *Int J Syst Evol Microbiol* **52**: 7–76.

Chaudhary, R., Mishra, S., Kota, S., and Misra, H. (2021) Molecular interactions and their predictive roles in cell pole determination in bacteria. *Crit Rev Microbiol* **47**: 141–161.

Chen, H. and Good, M.C. (2016) Size regulation: big insights from little cells. *Dev Cell* **37**: 392–394.

Chen, J.C. and Beckwith, J. (2001) FtsQ, FtsL and FtsI require FtsK, but not FtsN, for co-localization with FtsZ during *Escherichia coli* cell division. *Mol Microbiol* **42**: 395–413.

Cho, H., Wivagg, Carl N., Kapoor, M., Barry, Z., Rohs, P.D.A., Suh, H., et al. (2016) Bacterial cell wall biogenesis is mediated by SEDS and PBP polymerase families functioning semi-autonomously. *Nat Microbiol* **1**: 16172.

Choi, U. and Lee, C.R. (2019) Distinct roles of outer membrane porins in antibiotic resistance and membrane integrity in *Escherichia coli*. *Front Microbiol* **10**: 953.

Claessen, D., Rozen, D.E., Kuipers, O.P., Søgaard-Andersen, L., and van Wezel, G.P. (2014) Bacterial solutions to multicellularity: a tale of biofilms, filaments and fruiting bodies. *Nat Rev Microbiol* **12**: 115–124.

Cohen, S.E. and Golden, S.S. (2015) Circadian rhythms in cyanobacteria. *Microbiol Mol Biol Rev* **79**: 373–385.

Coleman, G.A., Davín, A.A., Mahendrarajah, T.A., Szánthó, L.L., Spang, A., Hugenholtz, P., et al. (2021) A rooted phylogeny resolves early bacterial evolution. *Science* **372**: eabe0511.

Coltharp, C., Buss, J., Plumer, T.M., and Xiao, J. (2016) Defining the rate-limiting processes of bacterial cytokinesis.

Proc Natl Acad Sci U S A **113**: E1044–E1053.

Contreras-Martel, C., Martins, A., Ecobichon, C., Trindade, D.M., Matteï, P.J., Hicham, S., et al. (2017) Molecular architecture of the PBP2-MreC core bacterial cell wall synthesis complex. *Nat Commun* **8**: 776.

Cook, J., Baverstock, T.C., McAndrew, M.B.L., Stansfeld, P.J., Roper, D.I., and Crow, A. (2020) Insights into bacterial cell division from a structure of EnvC bound to the FtsX periplasmic domain. *Proc Natl Acad Sci U S A* **117**: 28355–28365.

Corrales-Guerrero, L., Camargo, S., Valladares, A., Picossi, S., Luque, I., Ochoa de Alda, J.A.G., and Herrero, A. (2018) FtsZ of filamentous, heterocyst-forming cyanobacteria has a conserved N-terminal peptide required for normal FtsZ polymerization and cell division. *Front Microbiol* **9**: 2260.

Corrales-Guerrero, L., Mariscal, V., Flores, E., and Herrero, A. (2013) Functional dissection and evidence for intercellular transfer of the heterocyst-differentiation PatS morphogen. *Mol Microbiol* **88**: 1093–1105.

Corrales-Guerrero, L., Mariscal, V., Nürnberg, D.J., Elhai, J., Mullineaux, C.W., Flores, E., and Herrero, A. (2014) Subcellular localization and clues for the function of the HetN factor influencing heterocyst distribution in *Anabaena* sp. strain PCC 7120. *J Bacteriol* **196**: 3452–3460.

Dagan, T., Roettger, M., Stucken, K., Landan, G., Koch, R., Major, P., et al. (2013) Genomes of stigonematalean cyanobacteria (subsection V) and the evolution of oxygenic photosynthesis from prokaryotes to plastids. *Genome Biol Evol* **5**: 31–44.

Dai, K. and Lutkenhaus, J. (1991) *ftsZ* Is an essential cell division gene in *Escherichia coli*. *J Bacteriol* **173**: 3500–3506.

Daniel, R.A. and Errington, J. (2003) Control of cell morphogenesis in bacteria: two distinct ways to make a rod-shaped cell. *Cell* **113**: 767–776.

de Pedro, M.A., Donachie, W.D., Höltje, J. V., and Schwarz, H. (2001) Constitutive septal murein synthesis in *Escherichia coli* with impaired activity of the morphogenetic proteins RodA and penicillin-binding protein 2. *J Bacteriol* **183**: 4115–4126.

den Blaauwen, T., de Pedro, M.A., Nguyen-Distèche, M., and Ayala, J.A. (2008) Morphogenesis of rod-shaped sacculi. *FEMS Microbiol Rev* **32**: 321–344.

Divakaruni, A. V., Baida, C., White, C.L., and Gober, J.W. (2007) The cell shape proteins MreB and MreC control cell morphogenesis by positioning cell wall synthetic complexes. *Mol Microbiol* **66**: 174–188.

Divakaruni, A. V., Loo, R.R.O., Xie, Y., Loo, J.A., and Gober, J.W. (2005) The cell-shape protein MreC interacts with extracytoplasmic proteins including cell wall assembly complexes in *Caulobacter crescentus*. *Proc Natl Acad Sci U S A* **102**: 18602–18607.

Domínguez-Cuevas, P., Porcelli, I., Daniel, R.A., and Errington, J. (2013) Differentiated roles for MreB-actin isologues and autolytic enzymes in *Bacillus subtilis* morphogenesis. *Mol Microbiol* **89**: 1084–1098.

Dominguez-Escobar, J., Chastanet, A., Crevenna, A.H., Fromion, V., Wedlich-Söldner, R., and Carballido-López, R. (2011) Processive movement of MreB-associated cell wall biosynthetic complexes in bacteria. *Science* **333**: 225–228.

Dong, G., Yang, Q., Wang, Q., Kim, Y.I., Wood, T.L., Osteryoung, K.W., et al. (2010) Elevated ATPase activity of KaiC applies a circadian checkpoint on cell division in *Synechococcus elongatus*. *Cell* **140**: 529–539.

Du, S. and Lutkenhaus, J. (2017) Assembly and activation of the *Escherichia coli* divisome. *Mol Microbiol* **105**: 177–187.

Du, S., Pichoff, S., and Lutkenhaus, J. (2016) FtsEX acts on FtsA to regulate divisome assembly and activity. *Proc Natl Acad Sci U S A* **113**: E5052–E5061.

Dye, N.A., Pincus, Z., Theriot, J.A., Shapiro, L., and Gitai, Z. (2005) Two independent spiral structures control cell shape in *Caulobacter*. *Proc Natl Acad Sci U S A* **102**: 18608–18613.

Egan, A.J.F., Errington, J., and Vollmer, W. (2020) Regulation of peptidoglycan synthesis and remodelling. *Nat Rev Microbiol* **18**: 446–460.

Ekman, M., Picossi, S., Campbell, E.L., Meeks, J.C., and Flores, E. (2013) A *Nostoc punctiforme* sugar transporter necessary to establish a cyanobacterium-plant symbiosis. *Plant Physiol* **161**: 1984–1992.

Elhai, J., and Khudyakov, I. (2018) Ancient association of cyanobacterial multicellularity with the regulator HetR and an RGSGR pentapeptide-containing protein (PatX). *Mol Microbiol* **110**: 931–954.

Epand, R.M. and Epand, R.F. (2009) Lipid domains in bacterial membranes and the action of antimicrobial agents. *Biochim Biophys Acta* **1788**: 289–294.

Errington, J. (2015) Bacterial morphogenesis and the enigmatic MreB helix. *Nat Rev Microbiol* **13**: 241–248.

Espinosa, J., Forchhammer, K., Burillo, S., and Contreras, A. (2006) Interaction network in cyanobacterial nitrogen regulation: PipX, a protein that interacts in a 2-oxoglutarate dependent manner with PII and NtcA. *Mol Microbiol* **61**: 457–469.

Fay, P. (1992) Oxygen relations of nitrogen fixation in cyanobacteria. *Microbiol Rev* **56**: 340–373.

Fenton, A.K. and Gerdes, K. (2013) Direct interaction of FtsZ and MreB is required for septum synthesis and cell division in *Escherichia coli*. *EMBO J* **32**: 1953–1965.

Field, C.B., Behrenfeld, M.J., Randerson, J.T., and Falkowski, P. (1998) Primary production of the biosphere: integrating terrestrial and oceanic components. *Science* **281**: 237–240.

Figge, R.M., Divakaruni, A. V., and Gober, J.W. (2004) MreB, the cell shape-determining bacterial actin homologue, co-ordinates cell wall morphogenesis in *Caulobacter crescentus*. *Mol Microbiol* **51**: 1321–1332.

Flaherty, B.L., Johnson, D.B.F., and Golden, J.W. (2014) Deep sequencing of HetR-bound DNA reveals novel HetR targets in *Anabaena* sp. strain PCC7120. *BMC Microbiol* **14**: 255.

Flärdh, K. and Buttner, M.J. (2009) *Streptomyces* morphogenetics: dissecting differentiation in a filamentous bacterium. *Nat Rev Microbiol* **7**: 36–49.

Flemming, H.C., Wingender, J., Szewzyk, U., Steinberg, P., Rice, S.A., and Kjelleberg, S. (2016) Biofilms: an emergent form of bacterial life. *Nat Rev Microbiol* **14**: 563–575.

Flores, E. and Herrero, A. (1994) Assimilatory nitrogen metabolism and its regulation. In *The Molecular Biology of Cyanobacteria*. Bryant, D. A. (Ed.) Kluwer Academic Publishers, Dordrecht, The Netherlands. Pp 487–517.

Flores, E., Frías, J.E., Rubio, L.M., and Herrero, A. (2005) Photosynthetic nitrate assimilation in cyanobacteria. *Photosynth Res* **83**: 117–133.

Flores, E., Herrero, A., Wolk, C.P., and Maldener, I. (2006) Is the periplasm continuous in filamentous multicellular cyanobacteria? *Trends Microbiol* **14**: 439–443.

Flores, E. and Herrero, A. (2010) Compartmentalized function through cell differentiation in filamentous cyanobacteria. *Nat Rev Microbiol* **8**: 39–50.

Flores, E. and Herrero, A. (2014) The cyanobacteria: morphological diversity in a photoautotrophic lifestyle. *Perspect Phycol* **1**: 63–72.

Forchhammer, K. and Selim, K.A. (2020) Carbon/nitrogen homeostasis control in cyanobacteria. *FEMS Microbiol Rev* **44**: 33–53.

Garcia-Pichel, F., Lombard, J., Soule, T., Dunaj, S., Wu, S.H., and Wojciechowski, M.F. (2019) Timing the evolutionary advent of cyanobacteria and the later great oxidation event using gene phylogenies of a sunscreen. *mBio* **10**: e00561-19.

Garner, E.C., Bernard, R., Wang, W., Zhuang, X., Rudner, D.Z., and Mitchison, T. (2011) Coupled, circumferential motions of the cell wall synthesis machinery and MreB filaments in *B. subtilis*. *Science* **333**: 222–225.

Giner-Lamia, J., Robles-Rengel, R., Hernández-Prieto, M.A., Muro-Pastor, M.I., Florencio, F.J., and Futschik, M.E. (2017) Identification of the direct regulon of NtcA during early acclimation to nitrogen starvation in the cyanobacterium *Synechocystis* sp. PCC 6803. *Nucleid Acids Res* **45**: 11800–11820.

Giordano, M., Beardall, J., and Raven, J.A. (2005) CO_2 concentrating mechanisms in algae: mechanisms, environmental modulation, and evolution. *Annu Rev Plant Biol* **56**: 99–131.

Glauner, B., Holtje, J. V., and Schwarz, U. (1988) The composition of the murein of *Escherichia coli*. *J Biol Chem* **263**: 10088–10095.

Goehring, N.W. and Beckwith, J. (2005) Diverse paths to midcell: assembly of the bacterial cell division machinery. *Curr Biol* **15**: 514–526.

Goehring, N.W., Gueiros-Filho, F., and Beckwith, J. (2005) Premature targeting of a cell division protein to midcell allows dissection of divisome assembly in *Escherichia coli*. *Genes Dev* **19**: 127–137.

González-Leiza, S.M., de Pedro, M.A., and Ayala, J.A. (2011) Amph, a bifunctional DD-endopeptidase and DD-carboxypeptidase of *Escherichia coli*. *J Bacteriol* **193**: 6887–6894.

Gonzalez, A., Riley, K.W., Harwood, T. V., Zuniga, E.G., and Risser, D.D. (2019) A tripartite, hierarchical sigma factor cascade promotes hormogonium development in the filamentous cyanobacterium *Nostoc punctiforme*. *mSphere* **4**: e00231-19.

Gray, M.W. (2017) Lynn Margulis and the endosymbiont hypothesis: 50 years later. *Mol Biol Cell* **28**: 1285–1287.

Grosberg, R.K. and Strathmann, R.R. (2007) The evolution of multicellularity: a minor major transition? *Annu Rev Ecol Evol Syst* **38**: 621–654.

Gruber, N. (2004) The dynamics of the marine nitrogen cycle and its influence on atmospheric CO_2 variations. In: *The ocean carbon cycle and climate.* Follows, M., Oguz, T. (Eds.) NATO Science Series, vol 40. Springer, Dordrecht, The Netherlands. Pp 97–148.

Gruber, N. and Galloway, J.N. (2008) An Earth-system perspective of the global nitrogen cycle. *Nature* **451**: 293–296.

Gupta, R.S. (2011) Origin of diderm (Gram-negative) bacteria: antibiotic selection pressure rather than endosymbiosis

likely led to the evolution of bacterial cells with two membranes. *Antonie van Leeuwenhoek* **100**: 171–182.

Gutu, A. and Kehoe, D.M. (2012) Emerging perspectives on the mechanisms, regulation, and distribution of light color acclimation in cyanobacteria. *Mol Plant* **5**: 1–13.

Hahn, A. and Schleiff, E. (2014). The cell envelope. In *The cell biology of Cyanobacteria*. Flores, E. and Herrero, A (Eds.) Caister Academic Press, Norfolk, UK. Pp 29–87.

Harris, L.K. and Theriot, J.A. (2016) Relative rates of surface and volume synthesis set bacterial cell size. *Cell* **165**: 1479–1492.

Haselkorn, R. (2008) Cell-cell communication in filamentous cyanobacteria. *Mol Microbiol* **70**: 783–785.

Heidrich, C., Templin, M.F., Ursinus, A., Merdanovic, M., Berger, J., Schwarz, H., et al. (2001) Involvement of *N*-acetylmuramyl-L-alanine amidases in cell separation and antibiotic-induced autolysis of *Escherichia col*i. *Mol Microbiol* **41**: 167–178.

Herrero, A., Muro-Pastor, A.M., and Flores, E. (2001) Nitrogen control in cyanobacteria. *J Bacteriol* **183**: 411–425.

Herrero, A., Muro-Pastor, A.M., Valladares, A., and Flores, E. (2004) Cellular differentiation and the NtcA transcription factor in filamentous cyanobacteria. *FEMS Microbiol Rev* **28**: 469–487.

Herrero, A., Stavans, J., and Flores, E. (2016) The multicellular nature of filamentous heterocyst-forming cyanobacteria. *FEMS Microbiol Rev* **40**: 831–854.

Herrero, A., and Flores, E. (2019) Genetic responses to carbon and nitrogen availability in *Anabaena*. *Environ Microbiol* **21**: 1–17.

Herrero, A., Flores, E., and Imperial, J. (2019) Nitrogen assimilation in bacteria. In *Encyclopedia of Microbiology*. Schmidt, T.M. (Ed.), 4th ed, vol 3. Academic Press, Cambridge, USA. Pp 280–300.

Hilton, J.A., Foster, R.A., Tripp, H.J., Carter, B.J., Zehr, J.P., and Villareal, T.A. (2013) Genomic deletions disrupt nitrogen metabolism pathways of a cyanobacterial diatom symbiont. *Nat Commun* **4**: 1767.

Hohmann-Marriott, M.F. and Blankenship, R.E. (2011) Evolution of photosynthesis. *Annu Rev Plant Biol* **62**: 515–548.

Hoiczyk, E. and Hansel, A. (2000) Cyanobacterial cell walls: news from an unusual prokaryotic envelope. *J Bacteriol* **182**: 1191–1199.

Hu, B., Yang, G., Zhao, W., Zhang, Y., and Zhao, J. (2007) MreB is important for cell shape but not for chromosome segregation of the filamentous cyanobacterium *Anabaena* sp. PCC 7120. *Mol Microbiol* **63**: 1640–1652.

Huang, F., Hedman, E., Funk, C., Kieselbach, T., Schröder, W.P., and Norling, B. (2004) Isolation of outer membrane of Synechocystis sp. PCC 6803 and its proteomic characterization. *Mol Cell Proteomics* **3**: 586–595.

Hussain, S., Wivagg, C.N., Szwedziak, P., Wong, F., Schaefer, K., Izoré, T., et al. (2018) MreB filaments align along greatest principal membrane curvature to orient cell wall synthesis. *eLife* **7**: e32471.

Jeon, W.J. and Cho, H. (2022) A cell wall hydrolase MepH is negatively regulated by proteolysis involving Prc and NlpI in *Escherichia coli*. *Front Microbiol* **13**: 878049.

Jordan, A., Chandler, J., MacCready, J.S., Huang, J., Osteryoung, K.W., and Ducat, D.C. (2017) Engineering cyanobacterial cell morphology for enhanced recovery and processing of biomass. *Appl Environ Microbiol* **83**: e00053-17.

Kang, K.N. and Boll, J.M. (2022) PBP1A directly interacts with the divisome complex to promote septal peptidoglycan synthesis in *Acinetobacter baumannii*. *J Bacteriol* **204**: e00239-22.

Kaplan, A. and Reinhold, L. (1999) CO_2 concentrating mechanisms in photosynthetic microorganisms. *Annu Rev Plant Biol* **50**: 539–570.

Karl, D.M., Church, M.J., Dore, J.E., Letelier, R.M., and Mahaffey, C. (2012) Predictable and efficient carbon sequestration in the North Pacific Ocean supported by symbiotic nitrogen fixation. *Proc Natl Acad Sci U S A* **109**: 1842–1849.

Kawazura, T., Matsumoto, K., Kojima, K., Kato, F., Kanai, T., Niki, H., and Shiomi, D. (2017) Exclusion of assembled MreB by anionic phospholipids at cell poles confers cell polarity for bidirectional growth. *Mol Microbiol* **104**: 472–486.

Kerfeld, C.A. and Melnicki, M.R. (2016) Assembly, function and evolution of cyanobacterial carboxysomes. *Curr Opin Plant Biol* **31**: 66–75.

Kieninger, A.K. and Maldener, I. (2021) Cell–cell communication through septal junctions in filamentous cyanobacteria. *Curr Opin Microbiol* **61**: 35–41.

Kieninger, A.K., Tokarz, P., Janović, A., Pilhofer, M., Weiss, G.L., and Maldener, I. (2022) SepN is a septal junction component required for gated cell–cell communication in the filamentous cyanobacterium *Nostoc*. *Nat Commun* **13**: 7486.

Kim, Y., Joachimiak, G., Ye, Z., Binkowski, A., Zhang, R., Gornicki, P., et al. (2011) Structure of transcription factor HetR

required for heterocyst differentiation in cyanobacteria. *Proc Natl Acad Sci U S A* **108**: 10109–10114.

Koch, A.L. (1996) What size should a bacterium be? A question of scale. *Annu Rev Microbiol* **50**: 317–348.

Koksharova, O.A., Klint, J., and Rasmussen, U. (2007) Comparative proteomics of cell division mutants and wild-type of *Synechococcus* sp. strain PCC 7942. *Microbiology* **153**: 2505–2517.

Konovalova, A., Kahne, D.E., and Silhavy, T.J. (2017) Outer membrane biogenesis. *Annu Rev Microbiol* **71**: 539–556.

Kroth, P.G. (2015) The biodiversity of carbon assimilation. *J Plant Physiol* **172**: 76–81.

Kruse, T., Bork-Jensen, J., and Gerdes, K. (2005) The morphogenetic MreBCD proteins of *Escherichia coli* form an essential membrane-bound complex. *Mol Microbiol* **55**: 78–89.

Kumar, K., Mella-Herrera, R.A., and Golden, J.W. (2010) Cyanobacterial heterocysts. *Cold Spring Harb Perspect Biol* **2**: a000315.

Kumar, S., Mollo, A., Kahne, D., and Ruiz, N. (2022) The bacterial cell wall: from Lipid II flipping to polymerization. *Chem Rev* **122**: 8884–8910.

Kurita, K., Kato, F., and Shiomi, D. (2020) Alteration of membrane fluidity or phospholipid composition perturbs rotation of MreB complexes in *Escherichia coli*. *Front Mol Biosci* **7**: 582660.

Lake, J.A. (2009) Evidence for an early prokaryotic endosymbiosis. *Nature* **460**: 967–971.

Lamanna, M.M. and Maurelli, A.T. (2022) What is motion? Recent advances in the study of molecular movement patterns of the peptidoglycan synthesis machines. *J Bacteriol* **204**: e00598-21.

Lang, N.J., Simon, R.D., and Wolk, C.P. (1972) Correspondence of cyanophycin granules with structured granules in *Anabaena cylindrica*. *Arch Mikrobiol* **83**: 313–320.

Lawrence, T.J., Amrine, K.C.H., Swingley, W.D., and Ardell, D.H. (2019) tRNA functional signatures classify plastids as late-branching cyanobacteria. *BMC Evol Biol* **19**: 224.

Lázaro, S., Fernández-Piñas, F., Fernández-Valiente, E., Blanco-Rivero, A., and Leganés, F. (2001) *pbpB*, a gene coding for a putative penicillin-binding protein, is required for aerobic nitrogen fixation in the cyanobacterium *Anabaena* sp. strain PCC7120. *J Bacteriol* **183**: 628–636.

Leaver, M. and Errington, J. (2005) Roles for MreC and MreD proteins in helical growth of the cylindrical cell wall in *Bacillus subtilis*. *Mol Microbiol* **57**: 1196–1209.

Leganés, F., Blanco-Rivero, A., Fernández-Piñas, F., Redondo, M., Fernández-Valiente, E., Fan, Q., et al. (2005) Wide variation in the cyanobacterial complement of presumptive penicillin-binding proteins. *Arch Microbiol* **184**: 234–248.

Lehner, J., Zhang, Y., Berendt, S., Rasse, T.M., Forchhammer, K., and Maldener, I. (2011) The morphogene AmiC2 is pivotal for multicellular development in the cyanobacterium *Nostoc punctiforme*. *Mol Microbiol* **79**: 1655–1669.

Lehner, J., Berendt, S., Dörsam, B., Pérez, R., Forchhammer, K., and Maldener, I. (2013) Prokaryotic multicellularity: a nanopore array for bacterial cell communication. *FASEB J* **27**: 2293–2300.

Levin, P.A. and Angert, E.R. (2015) Small but mighty: cell size and bacteria. *Cold Spring Harb Perspect Biol* **7**: a019216.

Levin, P.A. and Janakiraman, A. (2021) Activation, assembly, and activation of the *Escherichia coli* cell division machinery. *EcoSal Plus* **9**: eESP-0022-2021.

Li, C., Zhang, H., Du, Y., Zhang, W., and Xu, X. (2021) Effects of PatU3 peptides on cell size and heterocyst frequency of *Anabaena* sp. strain PCC 7120. *J Bacteriol* **203**: e00108-21.

Liu, B., Persons, L., Lee, L., and de Boer, P.A.J. (2015) Roles for both FtsA and the FtsBLQ subcomplex in FtsN-stimulated cell constriction in *Escherichia coli*. *Mol Microbiol* **95**: 945–970.

Liu, H., Nolla, H.A., and Campbell, L. (1997) *Prochlorococcus* growth rate and contribution to primary production in the equatorial and subtropical North Pacific Ocean. *Aquat Microb Ecol* **12**: 39–47.

Liu, H., Zhang, H., Niedzwiedzki, D.M., Prado, M., He, G., Gross, M.L., and Blankenship, R.E. (2013) Phycobilisomes supply excitations to both photosystems in a megacomplex in cyanobacteria. *Science* **342**: 1104–1107.

Liu, J., Xing, W.-Y., Zhang, J.-Y., Zeng, X., Yang, Y., and Zhang, C.-C. (2021) Functions of the essential gene *mraY* in cellular morphogenesis and development of the filamentous cyanobacterium *Anabaena* PCC 7120. *Front Microbiol* **12**: 765878.

Liu, R., Yaxin, L., Liu, S., Wang, Y., Li, K., Li, N., et al. (2017) Three-Dimensional superresolution imaging of the FtsZ ring during cell division of the cyanobacterium *Prochlorococcus*. *mBio* **8**: e00657-17.

Liu, X., Biboy, J., Consoli, E., Vollmer, W., and den Blaauwen, T. (2020) MreC and MreD balance the interaction between the elongasome proteins PBP2 and RodA. *PLoS Genet* **16**: e1009276.

Llácer, J.L., Espinosa, J., Castells, M.A., Contreras, A., Forchhammer, K., and Rubio, V. (2010) Structural basis for the

regulation of NtcA-dependent transcription by proteins PipX and PII. *Proc Natl Acad Sci U S A* **107**: 15397–15402.

Loose, M. and Mitchison, T.J. (2014) The bacterial cell division proteins FtsA and FtsZ self-organize into dynamic cytoskeletal patterns. *Nat Cell Biol* **16**: 38–46.

Lopes Pinto, F., Erasmie, S., Blikstad, C., Lindblad, P., and Oliveira, P. (2011) FtsZ degradation in the cyanobacterium *Anabaena* sp. strain PCC 7120. *J Plant Physiol* **168**: 1934–1942.

López-Igual, R., Flores, E., and Herrero, A. Inactivation of a heterocyst-specific invertase indicates a principal role of sucrose catabolism in heterocysts of *Anabaena* sp. *J Bacteriol* **192**: 5526–5533.

Lovering, A.L., Safadi, S.S., and Strynadka, N.C.J. (2012) Structural perspective of peptidoglycan biosynthesis and assembly. *Annu Rev Biochem* **81**: 451–478.

Löwe, J. and Amos, L.A. (1998) Crystal structure of the bacterial cell-division protein FtsZ. *Nature* **391**: 203–206.

Luo, G., Ono, S., Beukes, N.J., Wang, D.T., Xie, S., and Summons, R.E. (2016) Rapid oxygenation of Earth's atmosphere 2.33 billion years ago. *Sci Adv* **2**: e1600134.

Lyons, N.A. and Kolter, R. (2015) On the evolution of bacterial multicellularity. *Curr Opin Microbiol* **24**: 21–28.

Macnair, C.R. and Brown, E.D. (2020) Outer membrane disruption overcomes intrinsic, acquired, and spontaneous antibiotic resistance. *mBio* **11**: e01615-20.

Magnuson, A. and Cardona, T. (2016) Thylakoid membrane function in heterocysts. *Biochim Biophys Acta* **1857**: 309–319.

Mahaffey, C., Michaels, A.F., and Capone, D.G. (2005) The conundrum of marine N_2 fixation. *Am J Sci* **305**: 546–595.

Männik, J., Bailey, M.W., O'Neill, J.C., and Männik, J. (2017) Kinetics of large-scale chromosomal movement during asymmetric cell division in *Escherichia coli*. *PLoS Genet* **13**: e1006638.

Marbouty, M., Mazouni, K., Saguez, C., Cassier-Chauvat, C., and Chauvat, F. (2009) Characterization of the *Synechocystis* strain PCC 6803 penicillin-binding proteins and cytokinetic proteins FtsQ and FtsW and their network of interactions with ZipN. *J Bacteriol* **191**: 5123–5133.

Mariscal, V., Herrero, A., and Flores, E. (2007) Continuous periplasm in a filamentous, heterocyst-forming cyanobacterium. *Mol Microbiol* **65**: 1139–1145.

Martín-Figueroa, E., Navarro, F., and Florencio, F.J. (2000) The GS-GOGAT pathway is not operative in the heterocysts. Cloning and expression of *glsF* gene from the cyanobacterium *Anabaena* sp. PCC 7120. *FEBS Lett* **476**: 282–286.

Martin, W. and Kowallik, K. (1999) Annotated English translation of Mereschkowsky's 1905 paper 'Über natur und ursprung der chromatophoren im pflanzenreiche.' *Eur J Phycol* **34**: 287–295.

Martin, W., Rujan, T., Richly, E., Hansen, A., Cornelsen, S., Lins, T., et al. (2002) Evolutionary analysis of *Arabidopsis*, cyanobacterial, and chloroplast genomes reveals plastid phylogeny and thousands of cyanobacterial genes in the nucleus. *Proc Natl Acad Sci U S A* **99**: 12246–12251.

Martins, A., Contreras-Martel, C., Janet-Maitre, M., Miyachiro, M.M., Estrozi, L.F., Trindade, D.M., et al. (2021) Self-association of MreC as a regulatory signal in bacterial cell wall elongation. *Nat Commun* **12**: 2987.

Matsuzawa, H., Asoh, S., Kunai, K., Muraiso, K., Takasuga, A., and Ohta, T. (1989) Nucleotide sequence of the *rodA* gene, responsible for the rod shape of *Escherichia coli*: *rodA* and the *pbpA* gene, encoding Penicillin-Binding Protein 2, constitute the *rodA* operon. *J Bacteriol* **171**: 558–560.

Mazouni, K., Domain, F., Cassier-Chauvat, C., and Chauvat, F. (2004) Molecular analysis of the key cytokinetic components of cyanobacteria: FtsZ, ZipN and MinCDE. *Mol Microbiol* **52**: 1145–1158.

Meeks, J.C. and Elhai, J. (2002) Regulation of cellular differentiation in filamentous cyanobacteria in free-living and plant-associated symbiotic growth states. *Microbiol Mol Biol Rev* **66**: 94–121.

Meeske, A.J., Riley, E.P., Robins, W.P., Uehara, T., Mekalanos, J.J., Kahne, D., et al. (2016) SEDS proteins are a widespread family of bacterial cell wall polymerases. *Nature* **537**: 634–638.

Megrian, D., Taib, N., Witwinowski, J., Beloin, C., and Gribaldo, S. (2020) One or two membranes? Diderm Firmicutes challenge the Gram-positive/Gram-negative divide. *Mol Microbiol* **113**: 659–671.

Megrian, D., Taib, N., Jaffe, A.L., Banfield, J.F., and Gribaldo, S. (2022) Ancient origin and constrained evolution of the *division and cell wall* gene cluster in Bacteria. *Nat Microbiol* **7**: 2114–2127.

Meisner, J., Montero Llopis, P., Sham, L.T., Garner, E., Bernhardt, T.G., and Rudner, D.Z. (2013) FtsEX is required for CwlO peptidoglycan hydrolase activity during cell wall elongation in *Bacillus subtilis*. *Mol Microbiol* **89**: 1069–1083.

Merino-Puerto, V., Mariscal, V., Mullineaux, C.W., Herrero, A., and Flores, E. (2010) Fra proteins influencing filament integrity, diazotrophy and localization of septal protein SepJ in the heterocyst-forming cyanobacterium

Anabaena sp. *Mol Microbiol* **75**: 1159–1170.

Merino-Puerto, V., Schwarz, H., Maldener, I., Mariscal, V., Mullineaux, C.W., Herrero, A., and Flores, E. (2011) FraC/FraD-dependent intercellular molecule exchange in the filaments of a heterocyst-forming cyanobacterium, *Anabaena* sp. *Mol Microbiol* **82**: 87–98.

Michie, K.A. and Löwe, J. (2006) Dynamic filaments of the bacterial cytoskeleton. *Annu Rev Biochem* **75**: 467–492.

Missiakas, D. and Schneewind, O. (2017) Assembly and function of the *Bacillus anthracis* S-layer. *Annu Rev Microbiol* **71**: 79–98.

Miyagishima, S.Y., Wolk, P.P., and Osteryoung, K.W. (2005) Identification of cyanobacterial cell division genes by comparative and mutational analyses. *Mol Microbiol* **56**: 126–143.

Mohammadi, T., van Dam, V., Sijbrandi, R., Vernet, T., Zapun, A., Bouhss, A., et al. (2011) Identification of FtsW as a transporter of lipid-linked cell wall precursors across the membrane. *EMBO J* **30**: 1425–1432.

Monteiro, J.M., Fernandes, P.B., Vaz, F., Pereira, A.R., Tavares, A.C., Ferreira, M.T., et al. (2015) Cell shape dynamics during the staphylococcal cell cycle. *Nat Commun* **6**: 8055.

Monteiro, J.M., Pereira, A.R., Reichmann, N.T., Saraiva, B.M., Fernandes, P.B., Veiga, H., et al. (2018) Peptidoglycan synthesis drives an FtsZ-treadmilling-independent step of cytokinesis. *Nature* **554**: 528–532.

Montgomery, B.L. (2016) Mechanisms and fitness implications of photomorphogenesis during chromatic acclimation in cyanobacteria. *J Exp Bot* **67**: 4079–4090.

Morcinek-Orlowska, J., Galinska, J., and Glinkowska, M. (2019) When size matters-coordination of growth and cell cycle in bacteria. *Acta Biochim Pol* **66**: 139–146.

Morè, N., Martorana, A.M., Biboy, J., Otten, C., Winkle, M., Serrano, C.K.G., Motón Silva, A., et al. (2019) Peptidoglycan remodeling enables *Escherichia coli* to survive severe outer membrane assembly defect. *mBio* **10**: e02729-18.

Morgenstein, R.M., Bratton, B.P., Nguyen, J.P., Ouzounov, N., Shaevitz, J.W., and Gitai, Z. (2015) RodZ links MreB to cell wall synthesis to mediate MreB rotation and robust morphogenesis. *Proc Natl Acad Sci U S A* **112**: 12510–12515.

Moslavac, S., Bredemeier, R., Mirus, O., Granvogl, B., Eichacker, L.A., and Schleiff, E. (2005) Proteomic analysis of the outer membrane of *Anabaena* sp. strain PCC 7120. *J Proteome Res* **4**: 1330–1338.

Mueller, E.A. and Levin, P.A. (2020) Bacterial cell wall quality control during environmental stress. *mBio* **11**: e02456-20.

Mukherjee, A. and Lutkenhaus, J. (1998) Dynamic assembly of FtsZ regulated by GTP hydrolysis. *EMBO J* **17**: 462–469.

Mullineaux, C.W., Mariscal, V., Nenninger, A., Khanum, H., Herrero, A., Flores, E., and Adams, D.G. (2008) Mechanism of intercellular molecular exchange in heterocyst-forming cyanobacteria. *EMBO J* **27**: 1299–1308.

Muñoz-Dorado, J., Marcos-Torres, F.J., García-Bravo, E., Moraleda-Muñoz, A., and Pérez, J. (2016) Myxobacteria: moving, killing, feeding, and surviving together. *Front Microbiol* **7**: 781.

Muñoz-García, J. and Ares, S. (2016) Formation and maintenance of nitrogen-fixing cell patterns in filamentous cyanobacteria. *Proc Natl Acad Sci U S A* **113**: 6218–6223.

Muñoz-Marín, M.C., Luque, I., Zubkov, M. V., Hill, P.G., Diez, J., and García-Fernández, J.M. (2013) *Prochlorococcus* can use the Pro1404 transporter to take up glucose at nanomolar concentrations in the Atlantic Ocean. *Proc Natl Acad Sci U S A* **110**: 8597–8602.

Muro-Pastor, M.I., Reyes, J.C., and Florencio, F.J. (2001) Cyanobacteria perceive nitrogen status by sensing intracellular 2-oxoglutarate levels. *J Biol Chem* **276**: 38320–38328.

Muro-Pastor, A.M., Valladares, A., Flores, E., and Herrero, A. (2002) Mutual dependence of the expression of the cell differentiation regulatory protein HetR and the global nitrogen regulator NtcA during heterocyst development. *Mol Microbiol* **44**: 1377–1385.

Murry, M.A. and Wolk, C.P. (1989) Evidence that the barrier to the penetration of oxygen into heterocysts depends upon two layers of the cell envelope. *Arch Microbiol* **151**: 469–474.

Navarro, P.P., Vettiger, A., Ananda, V.Y., Llopis, P.M., Allolio, C., Bernhardt, T.G., and Chao, L.H. (2022) Cell wall synthesis and remodelling dynamics determine division site architecture and cell shape in *Escherichia coli*. *Nat Microbiol* **7**: 1621–1634.

Newitt, J.A., Ulbrandt, N.D., and Bernstein, H.D. (1999) The structure of multiple polypeptide domains determines the signal recognition particle targeting requirement of *Escherichia coli* inner membrane proteins. *J Bacteriol* **181**: 4561–4567.

Nicolaisen, K., Hahn, A., and Schleiff, E. (2009a) The cell wall in heterocyst formation by *Anabaena* sp. PCC 7120. *J Basic Microbiol* **49**: 5–24.

Nicolaisen, K., Mariscal, V., Bredemeier, R., Pernil, R., Moslavac, S., López-Igual, R., et al. (2009b) The outer membrane

of a heterocyst-forming cyanobacterium is a permeability barrier for uptake of metabolites that are exchanged between cells. *Mol Microbiol* **74**: 58–70.

Nieves-Morión, M., Lechno-Yossef, S., López-Igual, R., Frías, J.E., Mariscal, V., Nürnberg, D.J., et al. (2017) Specific glucoside transporters influence septal structure and function in the filamentous, heterocyst-forming cyanobacterium *Anabaena* sp. strain PCC 7120. *J Bacteriol* **199**: e00876-16.

Nieves-Morión, M., Flores, E., Whitehouse, M.J., Thomen, A., and Foster, R.A. (2021) Single-cell measurements of fixation and intercellular exchange of C and N in the filaments of the heterocyst-forming cyanobacterium *Anabaena* sp. strain PCC 7120. *mBio* **12**: e01314-21.

Nowicka, B. and Kruk, J. (2016) Powered by light: Phototrophy and photosynthesis in prokaryotes and its evolution. *Microbiol Res* **186**–**187**: 99–118.

Nürnberg, D.J., Mariscal, V., Bornikoel, J., Nieves-Morión, M., Krauß, N., Herrero, A., et al. (2015) Intercellular diffusion of a fluorescent sucrose analog via the septal junctions in a filamentous cyanobacterium. *mBio* **6**: e02109-14.

Ochoa de Alda, J.A.G., Esteban, R., Diago, M.L., and Houmard, J. (2014) The plastid ancestor originated among one of the major cyanobacterial lineages. *Nat Commun* **5**: 4937.

Ojkic, N. and Banerjee, S. (2021) Bacterial cell shape control by nutrient-dependent synthesis of cell division inhibitors. *Biophys J* **120**: 2079–2084.

Ojkic, N., Serbanescu, D., and Banerjee, S. (2022) Antibiotic resistance via bacterial cell shape-shifting. *mBio* **13**: e00659-22.

Oliva, M.A., Cordell, S.C., and Löwe, J. (2004) Structural insights into FtsZ protofilament formation. *Nat Struct Mol Biol* **11**: 1243–1250.

Ortiz, C., Natale, P., Cueto, L., and Vicente, M. (2015) The keepers of the ring: regulators of FtsZ assembly. *FEMS Microbiol Rev* **40**: 57–67.

Ouzounov, N., Nguyen, J.P., Bratton, B.P., Jacobowitz, D., Gitai, Z., and Shaevitz, J.W. (2016) MreB orientation correlates with cell diameter in *Escherichia coli*. *Biophys J* **111**: 1035–1043.

Özbaykal, G., Wollrab, E., Simon, F., Vigouroux, A., Cordier, B., Aristov, A., et al. (2020) The transpeptidase PBP2 governs initial localization and activity of the major cell-wall synthesis machinery in *E. coli*. eL*ife* **9**: e50629.

Partensky, F., Hess, W.R., and Vaulot, D. (1999) *Prochlorococcu*s, a marine photosynthetic prokaryote of global significance. *Microbiol Mol Biol Rev* **63**: 106–127.

Pazos, M., Peters, K., Casanova, M., Palacios, P., van Nieuwenhze, M., Breukink, E., et al. (2018) Z-ring membrane anchors associate with cell wall synthases to initiate bacterial cell division. *Nat Commun* **9**: 5090.

Pernil, R., Herrero, A., and Flores, F. (2010) Catabolic function of compartmentalized alanine dehydrogenase in the heterocyst-forming cyanobacterium *Anabaena* sp. strain PCC 7120. *J Bacteriol* **192**: 5165–5172.

Petiti, M., Serrano, B., Faure, L., Lloubes, R., Mignot, T., and Duché, D. (2019) Tol energy-driven localization of Pal and anchoring to the peptidoglycan promote outer-membrane constriction. *J Mol Biol* **431**:3275–3288.

Pichoff, S. and Lutkenhaus, J. (2005) Tethering the Z ring to the membrane through a conserved membrane targeting sequence in FtsA. *Mol Microbiol* **55**: 1722–1734.

Pichoff, S., Shen, B., Sullivan, B., and Lutkenhaus, J. (2012) FtsA mutants impaired for self-interaction bypass ZipA suggesting a model in which FtsA's self-interaction competes with its ability to recruit downstream division proteins. *Mol Microbiol* **83**: 151–167.

Picossi, S., Montesinos, M.L., Pernil, R., Lichtlé, C., Herrero, A., and Flores, E. (2005) ABC-type neutral amino acid permease N-I is required for optimal diazotrophic growth and is repressed in the heterocysts of *Anabaena* sp. strain PCC 7120. *Mol Microbiol* **57**: 1582–1592.

Picossi, S., Flores, E., and Ekman, M. (2013) Diverse roles of the GlcP glucose permease in free-living and symbiotic cyanobacteria. *Plant Signal Behav* **8**: e27416.

Picossi, S., Flores, E., and Herrero, A. (2014) ChIP analysis unravels an exceptionally wide distribution of DNA binding sites for the NtcA transcription factor in a heterocyst-forming cyanobacterium. *BMC Genom* **15**: 22.

Pogliano, J. (2008) The bacterial cytoskeleton. *Curr Opin Cell Biol* **20**: 19–27.

Ponce-Toledo, R.I., Deschamps, P., López-García, P., Zivanovic, Y., Benzerara, K., and Moreira, D. (2017) An early-branching freshwater cyanobacterium at the origin of plastids. *Curr Biol* **27**: 386–391.

Popa, R., Weber, P.K., Pett-Ridge, J., Finzi, J.A., Fallon, S.J., Hutcheon, I.D., et al. (2007) Carbon and nitrogen fixation and metabolite exchange in and between individual cells of *Anabaena oscillarioides*. *ISME J* **1**: 354–360.

Porter, K.J., Cao, L., and Osteryoung, K.W. (2023) Dynamics of the *Synechococcus elongatus* cytoskeletal GTPase FtsZ yields mechanistic and evolutionary insight into cyanobacterial and chloroplast FtsZs. *J Biol Chem* **299**: 102917.

Price, G.D., Badger, M.R., Woodger, F.J., and Long, B.M. (2008) Advances in understanding the cyanobacterial CO_2-

concentrating-mechanism (CCM): functional components, Ci transporters, diversity, genetic regulation and prospects for engineering into plants. *J Exp Bot* **59**: 1441–1461.

Qiao, Y., Srisuknimit, V., Rubino, F., Schaefer, K., Ruiz, N., Walker, S., and Kahne, D. (2017) Lipid II overproduction allows direct assay of transpeptidase inhibition by β-lactams. *Nat Chem Biol* **13**: 793–798.

Raetz, C.R.H. and Whitfield, C. (2002) Lipopolysaccharide endotoxins. *Annu Rev Biochem* **71**: 635–700.

Ramirez-Diaz, D.A., García-Soriano, D.A., Raso, A., Mücksch, J., Feingold, M., Rivas, G., and Schwille, P. (2018) Treadmilling analysis reveals new insights into dynamic FtsZ ring architecture. *PLoS Biol* **16**: e2004845.

Ramos-León, F., Mariscal, V., Frías, J.E., Flores, E., and Herrero, A. (2015) Divisome-dependent subcellular localization of cell-cell joining protein SepJ in the filamentous cyanobacterium *Anabaena*. *Mol Microbiol* **96**: 566–580.

Ranjit, D.K. and Young, K.D. (2013) The Rcs stress response and accessory envelope proteins are required for *de novo* generation of cell shape in *Escherichia coli*. *J Bacteriol* **195**: 2452–2462.

Raven, J.A. and Allen, J.F. (2003) Genomics and chloroplast evolution: what did cyanobacteria do for plants? *Genome Biol* **4**: 209.

Redick, S.D., Stricker, J., Briscoe, G., and Erickson, H.P. (2005) Mutants of FtsZ targeting the protofilament interface: effects on cell division and GTPase activity. *J Bacteriol* **187**: 2727–2736.

Resch, C.M. and Gibson, J. (1983) Isolation of the carotenoid-containing cell wall of three unicellular cyanobacteria. *J Bacteriol* **155**: 345–350.

Rippka, R. (1972) Photoheterotrophy and chemoheterotrophy among unicellular blue-green algae. *Arch Mikrobiol* **87**: 93–98.

Rippka, R. and Waterbury, J.B. (1977) The synthesis of nitrogenase by non-heterocystous cyanobacteria. *FEMS Microbiol Lett* **2**: 83–86.

Rippka, R., Deruelles, J., Waterbury, J.B., Herdman, M., and Stanier, R.Y. (1979) Generic assignments, strain histories and properties of pure cultures of cyanobacteria. *J Gen Microbiol* **111**: 1–61.

Risser, D.D., Wong, F.C.Y., and Meeks, J.C. (2012) Biased inheritance of the protein PatN frees vegetative cells to initiate patterned heterocyst differentiation. *Proc Natl Acad Sci U S A* **109**: 15342–15347.

Rohs, P.D.A. and Bernhardt, T.G. (2021) Growth and division of the peptidoglycan matrix. *Annu Rev Microbiol* **75**: 315–336.

Rohs, P.D.A., Buss, J., Sim, S.I., Squyres, G.R., Srisuknimit, V., Smith, M., et al. (2018) A central role for PBP2 in the activation of peptidoglycan polymerization by the bacterial cell elongation machinery. *PLoS Genet* **14**: e1007726.

Rohs, P.D.A., Qiu, J.M., Torres, G., Smith, M.D., Fivenson, E.M., and Bernhardt, T.G. (2021) Identification of potential regulatory domains within the MreC and MreD components of the cell elongation machinery. *J Bacteriol* **203**: e00493-20.

Ruiz, N. (2008) Bioinformatics identification of MurJ (MviN) as the peptidoglycan lipid II flippase in *Escherichia coli*. *Proc Natl Acad Sci U S A* **105**: 15553–15557.

Sagan, L. (1967) On the origin of mitosing cells. *J Theor Biol* **14**: 255–274.

Sakr, S., Jeanjean, R., Zhang, C.C., and Arcondeguy, T. (2006) Inhibition of cell division suppresses heterocyst development in *Anabaena* sp. strain PCC 7120. *J Bacteriol* **188**: 1396–1404.

Salje, J., van den Ent, F., de Boer, P., and Löwe, J. (2011) Direct membrane binding by bacterial actin MreB. *Mol Cell* **43**: 478–487.

Sarcina, M. and Mullineaux, C.W. (2000) Effects of tubulin assembly inhibitors on cell division in prokaryotes *in vivo*. *FEMS Microbiol Lett* **191**: 25–29.

Savage, D.F., Afonso, B., Chen, A.H., and Silver, P.A. (2010) Spatially ordered dynamics of the bacterial carbon fixation machinery. *Science* **327**: 1258–1261.

Schaechter, M., Maaloe, O., and Kjeldgaard, N. O. (1958) Dependecy on medium and temperature of cell size and chemical composition during balanced growth of *Salmonella typhimurium*. *J Gen Microbiol* **19**: 592–606.

Scheffers, D.J., de Wit, J.G., den Blaauwen, T., and Driessen, A.J.M. (2002) GTP hydrolysis of cell division protein FtsZ: evidence that the active site is formed by the association of monomers. *Biochemistry* **41**: 521–529.

Schirrmeister, B.E., Antonelli, A., and Bagheri, H.C. (2011) The origin of multicellularity in cyanobacteria. *BMC Evol Biol* **11**: 45.

Schirrmeister, B.E., de Vos, J.M., Antonelli, A., and Bagheri, H.C. (2013) Evolution of multicellularity coincided with increased diversification of cyanobacteria and the Great Oxidation Event. *Proc Natl Acad Sci U S A* **110**: 1791–1796.

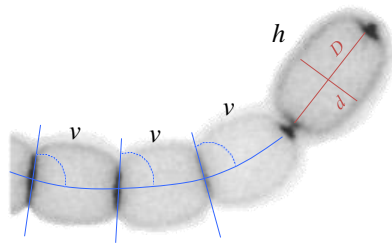Schirrmeister, B.E., Gugger, M., and Donoghue, P.C.J. (2015) Cyanobacteria and the Great Oxidation Event: evidence

from genes and fossils. *Palaeontology* **58**: 769–785.

Schirrmeister, B.E., Sanchez-Baracaldo, P., and Wacey, D. (2016) Cyanobacterial evolution during the Precambrian. *Int J Astrobiol* **15**: 187–204.

Schopf, J.W. (2011) The paleobiological record of photosynthesis. *Photosynth Res* **107**: 87–101.

Schulz-Vogt, H.N., Angert, E.R., and Garcia-Pichel, F. (2007) Giant Bacteria. In *Encyclopedia of Life* Sciences. John Wiley & Sons, Ltd.

Schulz, H.N. and Jørgensen, B.B. (2001) Big Bacteria. *Annu Rev Microbiol* **55**: 105–137.

Schumacher, M.A., Ohashi, T., Corbin, L., and Ericksona, H.P. (2020) High-resolution crystal structures of *Escherichia coli* FtsZ bound to GDP and GTP. *Acta Crystallogr F Struct Biol Commun* **76**: 94–102.

Shaku, M., Ealand, C., Matlhabe, O., Lala, R., and Kana, B.D. (2020) Peptidoglycan biosynthesis and remodeling revisited. *Adv Appl Microbiol* **112**: 67–103.

Shapiro, J.A. (1988) Bacteria as multicellular organisms. *Sci Am* **256**: 82–89.

Shi, H., Quint, D.A., Grason, G.M., Gopinathan, A., and Huang, K.C. (2020) Chiral twisting in a bacterial cytoskeletal polymer affects filament size and orientation. *Nat Commun* **11**: 1408.

Shih, P.M., Wu, D., Latifi, A., Axen, S.D., Fewer, D.P., Talla, E., et al. (2013) Improving the coverage of the cyanobacterial phylum using diversity-driven genome sequencing. *Proc Natl Acad Sci U S A* **110**: 1053–1058.

Si, F., Le Treut, G., Sauls, J.T., Vadia, S., Levin, P.A., and Jun, S. (2019) Mechanistic origin of cell-size control and homeostasis in bacteria. *Curr Biol* **29**: 1760-1770.e7.

Silale, A., and van den Berg, B. (2023) TonB-dependent transport across the bacterial outer membrane. *Annu Rev Microbiol* **77**: 67–88.

Singh, S.K., SaiSree, L., Amrutha, R.N., and Reddy, M. (2012) Three redundant murein endopeptidases catalyse an essential cleavage step in peptidoglycan synthesis of *Escherichia coli* K12. *Mol Microbiol* **86**: 1036–1051.

Singh, S.P. and Montgomery, B.L. (2011) Determining cell shape: adaptive regulation of cyanobacterial cellular differentiation and morphology. *Trends Microbiol* **19**: 278–285.

Singh, S.P. and Montgomery, B.L. (2014) Morphogenes *bolA* and *mreB* mediate the photoregulation of cellular morphology during complementary chromatic acclimation in *Fremyella diplosiphon*. *Mol Microbiol* **93**: 167–182.

Sjodt, M., Rohs, P.D.A., Gilman, M.S.A., Erlandson, S.C., Zheng, S., Green, A.G., et al. (2020) Structural coordination of polymerization and crosslinking by a SEDS–bPBP peptidoglycan synthase complex. *Nat Microbiol* **5**: 813–820.

Söderström, B., Skoog, K., Blom, H., Weiss, D.S., von Heijne, G., and Daley, D.O. (2014) Disassembly of the divisome in *Escherichia coli*: evidence that FtsZ dissociates before compartmentalization. *Mol Microbiol* **92**: 1–9.

Söderström, B., Mirzadeh, K., Toddo, S., von Heijne, G., Skoglund, U., and Daley, D.O. (2016) Coordinated disassembly of the divisome complex in *Escherichia coli*. *Mol Microbiol* **101**: 425–438.

Sohlenkamp, C. and Geiger, O. (2015) Bacterial membrane lipids: diversity in structures and pathways. *FEMS Microbiol Rev* **40**: 133–159.

Soo, R.M., Hemp, J., Parks, D.H., Fischer, W. W., and Hugenholtz, P. (2017) On the origin of oxygenic photosynthesis and Cyanobacteria. *Science* **355**: 1436–1440.

Springstein, B.L., Arévalo, S., Helbig, A.O., Herrero, A., Stucken, K., Flores, E., and Dagan, T. (2020a) A novel septal protein of multicellular heterocystous cyanobacteria is associated with the divisome. *Mol Microbiol* **113**: 1140–1154.

Springstein, B.L., Weissenbach, J., Koch, R., Stücker, F., and Stucken, K. (2020b) The role of the cytoskeletal proteins MreB and FtsZ in multicellular cyanobacteria. *FEBS Open Bio* **10**: 2510–2531.

Springstein, B.L., Nürnberg, D.J., Weiss, G.L., Pilhofer, M., and Stucken, K. (2020c) Structural determinants and their role in cyanobacterial morphogenesis. *Life* **10**: 355.

Springstein, B.L., Nürnberg, D.J., Woehle, C., Weissenbach, J., Theune, M.L., Helbig, A.O., et al. (2021) Two novel heteropolymer-forming proteins maintain the multicellular shape of the cyanobacterium *Anabaena* sp. PCC 7120. *FEBS J* **288**: 3197–3216.

Stanier, R.Y. and Cohen-Bazire, G. (1977) Phototrophic prokaryotes: the Cyanobacteria. *Annu Rev Microbiol* **31**: 225–274.

Strahl, H. and Errington, J. (2017) Bacterial membranes: structure, domains, and function. *Annu Rev Microbiol* **71**: 519–538.

Sun, J., Rutherford, S.T., Silhavy, T.J., and Huang, K.C. (2022) Physical properties of the bacterial outer membrane. *Nat Rev Microbiol* **20**: 236–248.

Szczepaniak, J., Holmes, P., Rajasekar, K., Kaminska, R., Samsudin, F., Inns, P.G., et al. (2020) The lipoprotein Pal stabilises the bacterial outer membrane during constriction by a mobilisation-and-capture mechanism. *Nat Commun* **11**: 1305.

Szwedziak, P., Wang, Q., Freund, S.M., and Löwe, J. (2012) FtsA forms actin-like protofilaments. *EMBO J* **31**: 2249–2260.

Tang, S., Pichugin, Y., and Hammerschmidt, K. (2023) An environmentally induced multicellular life cycle of a unicellular cyanobacterium. *Curr Biol* **33**: 764-769.e5.

Thomas, J., Meeks, J.C., Wolk, C.P., Shaffer, P.W., Austin, S.M., and Chien, W.S. (1977) Formation of glutamine from [^{13}N]ammonia, [^{13}N]dinitrogen, and [^{14}C]glutamate by heterocysts isolated from *Anabaena cylindrica*. *J Bacteriol* **129**: 1545–1555.

Tocheva, E.I., Ortega, D.R., and Jensen, G.J. (2016) Sporulation, bacterial cell envelopes and the origin of life. *Nat Rev Microbiol* **14**: 535–542.

Tomitani, A., Knoll, A.H., Cavanaugh, C.M., and Ohno, T. (2006) The evolutionary diversification of cyanobacteria: molecular-phylogenetic and paleontological perspectives. *Proc Natl Acad Sci U S A* **103**: 5442–5447.

Tsang, M.J. and Bernhardt, T.G. (2015) A role for the FtsQLB complex in cytokinetic ring activation revealed by an *ftsL* allele that accelerates division. *Mol Microbiol* **95**: 925–944.

Tsang, M.J., Yakhnina, A.A., and Bernhardt, T.G. (2017) NlpD links cell wall remodeling and outer membrane invagination during cytokinesis in *Escherichia coli*. *PLoS Genet* **13**: e1006888.

Typas, A., Banzhaf, M., Gross, C.A., and Vollmer, W. (2012) From the regulation of peptidoglycan synthesis to bacterial growth and morphology. *Nat Rev Microbiol* **10**: 123–136.

Uehara, T., Dinh, T., and Bernhardt, T.G. (2009) LytM-domain factors are required for daughter cell separation and rapid ampicillin-induced lysis in *Escherichia coli*. *J Bacteriol* **191**: 5094–5107.

Urrejola, C., von Dassow, P., van den Engh, G., Salas, L., Mullineaux, C.W., Vicuña, R., and Sánchez-Baracaldo, P. (2020) Loss of filamentous multicellularity in *Cyanobacteria*: the extremophile *Gloeocapsopsis* sp. strain UTEX B3054 retained multicellular features at the genomic and behavioral levels. *J Bacteriol* **202**: e00514-19.

Ursell, T.S., Nguyen, J., Monds, R.D., Colavin, A., Billings, G., Ouzounov, N., et al. (2014) Rod-like bacterial shape is maintained by feedback between cell curvature and cytoskeletal localization. *Proc Natl Acad Sci U S A* **111**: E1025–E1034.

Valladares, A., Maldener, I., Muro-Pastor, A.M., Flores, E., and Herrero, A. (2007) Heterocyst development and diazotrophic metabolism in terminal respiratory oxidase mutants of the cyanobacterium *Anabaena* sp. strain PCC 7120. *J Bacteriol* **189**: 4425–4430.

Valladares, A., Flores, E., and Herrero, A. (2008) Transcription activation by NtcA and 2-oxoglutarate of three genes involved in heterocyst differentiation in the cyanobacterium *Anabaena* sp. strain PCC 7120. *J Bacteriol* **190**: 6126–6133.

Valladares, A., Rodríguez, V., Camargo, S., Martínez-Noël, G.M.A., Herrero, A., and Luque, I. (2011) Specific role of the cyanobacterial PipX factor in the heterocysts of *Anabaena* sp. strain PCC 7120. *J Bacteriol* **193**: 1172–1182.

Valladares, A., Velázquez-Suárez, C., and Herrero, A. (2020) Interactions of PatA with the divisome during heterocyst differentiation in *Anabaena*. *mSphere* **5**: e00188-20.

van den Ent, F., Johnson, C.M., Persons, L., de Boer, P., and Löwe, J. (2010) Bacterial actin MreB assembles in complex with cell shape protein RodZ. *EMBO J* **29**: 1081–1090.

van den Ent, F., Izoré, T., Bharat, T.A.M., Johnson, C.M., and Löwe, J. (2014) Bacterial actin MreB forms antiparallel double filaments. *eLife* **2014**: e02634.

van der Ploeg, R., Verheul, J., Vischer, N.O.E., Alexeeva, S., Hoogendoorn, E., Postma, M., et al. (2013) Colocalization and interaction between elongasome and divisome during a preparative cell division phase in *Escherichia coli*. *Mol Microbiol* **87**: 1074–1087.

van Teeffelen, S., Wang, S., Furchtgott, L., Huang, K.C., Wingreen, N.S., Shaevitz, J.W., and Gitai, Z. (2011) The bacterial actin MreB rotates, and rotation depends on cell-wall assembly. *Proc Natl Acad Sci U S A* **108**: 15822–15827.

van Teeseling, M.C.F., de Pedro, M.A., and Cava, F. (2017) Determinants of bacterial morphology: from fundamentals to possibilities for antimicrobial targeting. *Front Microbiol* **8**: 1264.

van Teeseling, M.C.F. (2021) Elongation at midcell in preparation of cell division requires FtsZ, but not MreB nor PBP2 in *Caulobacter crescentus*. *Front Microbiol* **12**: 732031.

Vázquez-Bermúdez, M.F., Herrero, A., and Flores, E. (2003) Carbon supply and 2-oxoglutarate effects on expression of nitrate reductase and nitrogen-regulated genes in *Synechococcus* sp. strain PCC 7942. *FEMS Microbiol Lett* **221**: 155–159.

Videau, P., Rivers, O.S., Ushijima, B., Oshiro, R.T., Kim, M.J., Philmus, B., and Cozy, L.M. (2016) Mutation of the *murC*

and *murB* genes impairs heterocyst differentiation in *Anabaena* sp. strain PCC 7120. *J Bacteriol* **198**: 1196–1206.

Vigouroux, A., Cordier, B., Aristov, A., Alvarez, L., Özbaykal, G., Chaze, T., et al. (2020) Class-A penicillin binding proteins do not contribute to cell shape but repair cell-wall defects. *eLife* **9**: e51998.

Volland, J.M., Gonzalez-Rizzo, S., Gros, O., Tyml, T., Ivanova, N., Schulz, F., et al. (2022) A centimeter-long bacterium with DNA contained in metabolically active, membrane-bound organelles. *Science* **376**: 1453–1458.

Vollmer, W. (2012) Bacterial growth does require peptidoglycan hydrolases. *Mol Microbiol* **86**: 1031–1035.

Wachi, M., Doi, M., Tamaki, S., Park, W., Nakajima-Iijima, S., and Matsuhashi, M. (1987) Mutant isolation and molecular cloning of *mre* genes, which determine cell shape, sensitivity to mecillinam, and amount of penicillin-binding proteins in *Escherichia coli*. *J Bacteriol* **169**: 4935–4940.

Wagstaff, J. and Löwe, J. (2018) Prokaryotic cytoskeletons: protein filaments organizing small cells. *Nat Rev Microbiol* **16**: 187–201.

Wagstaff, J.M., Tsim, M., Oliva, M.A., García-Sanchez, A., Kureisaite-Ciziene, D., Andreu, J.M., and Löwe, J. (2017) A polymerization-associated structural switch in FtsZ that enables treadmilling of model filaments. m*Bio* **8**: e00254-17.

Walsby, A.E. (2007) Cyanobacterial heterocysts: terminal pores proposed as sites of gas exchange. *Trends Microbiol* **15**: 340–349.

Wang, L., Niu, T.C., Valladares, A., Lin, G.M., Zhang, J.Y., Herrero, A., et al. (2021) The developmental regulator PatD modulates assembly of the cell-division protein FtsZ in the cyanobacterium *Anabaena* sp. PCC 7120. *Environ Microbiol* **23**: 4823–4837.

Ward, J.E. and Lutkenhaus, J. (1985) Overproduction of FtsZ induces minicell formation in *E. coli*. *Cell* **42**: 941–949.

Weiss, G.L., Kieninger, A.K., Maldener, I., Forchhammer, K., and Pilhofer, M. (2019) Structure and function of a bacterial gap junction analog. *Cell* **178**: 374-384.e15.

Westfall, C.S. and Levin, P.A. (2017) Bacterial cell size: multifactorial and multifaceted. *Annu Rev Microbiol* **71**: 499–517.

Whitley, K.D., Jukes, C., Tregidgo, N., Karinou, E., Almada, P., Cesbron, Y., et al. (2021) FtsZ treadmilling is essential for Z-ring condensation and septal constriction initiation in *Bacillus subtilis* cell division. *Nat Commun* **12**: 2448.

Wildon, D.C. and Mercer, F. V. (1963) The ultrastructure of the heterocyst and akinete of the blue-green algae. *Arch Mikrobiol* **47**: 19–31.

Wilk, L., Strauss, M., Rudolf, M., Nicolaisen, K., Flores, E., Kühlbrandt, W., and Schleiff, E. (2011) Outer membrane continuity and septosome formation between vegetative cells in the filaments of *Anabaena* sp. PCC 7120. *Cell Microbiol* **13**: 1744–1754.

Williams, M.A., Aliashkevich, A., Krol, E., Kuru, E., Bouchier, J.M., Rittichier, J., et al. (2021) Unipolar peptidoglycan synthesis in the *Rhizobiales* requires an essential class A penicillin-binding protein. *mBio* **12**: e02346-21.

Willis, L. and Huang, K.C. (2017) Sizing up the bacterial cell cycle. *Nat Rev Microbiol* **15**: 606–620.

Winkenbach, F. and Wolk, C.P. (1973) Activities of enzymes of the oxidative and the reductive pentose phosphate pathways in heterocysts of a blue-green alga. *Plant Physiol* **52**: 480–483.

Witwinowski, J., Sartori-Rupp, A., Taib, N., Pende, N., Tham, T.N., Poppleton, D., Ghigo, J.-M., et al. (2022) An ancient divide in outer membrane tethering systems in bacteria suggests a mechanism for the diderm-to-monoderm transition. *Nat Microbiol* **7**: 411–422.

Woese, C.R. (1987) Bacterial evolution. *Microbiol Rev* **51**: 221–271.

Wolk, C.P. (1967) Physiological basis of the pattern of vegetative growth of a blue-green alga. *Proc Natl Acad Sci U S A* **57**: 1246–1251.

Wolk, C.P., Shaffer, P.W. (1976) Heterotrophic micro- and macrocultures of a nitrogen-fixing cyanobacterium. *Arch Microbiol* **110**: 145–147.

Wolk, C.P., Thomas, J., Shaffer, P.W., Austin, S.M., and Galonsky, A. (1976) Pathway of nitrogen metabolism after fixation of ^{13}N labeled nitrogen gas by the cyanobacterium, *Anabaena cylindrica*. *J Biol Chem* **251**: 5027–5034.

Wong, F., Garner, E.C., and Amir, A. (2019) Mechanics and dynamics of translocating MreB filaments on curved membranes. *eLife* **8**: e40472.

Xing, W.Y., Liu, J., Zhang, J.Y., Zeng, X., and Zhang, C.C. (2022) A proteolytic pathway coordinates cell division and heterocyst differentiation in the cyanobacterium *Anabaena* sp. PCC 7120. *Proc Natl Acad Sci U S A* **119**: e2207963119.

Xu, Q., Sun, N., Xiao, Q., Huang, C., Xu, M., Zhang, W., et al. (2022) The crystal structure of MreC provides insights into polymer formation. *FEBS Open Bio* **12**: 340–348.

Xu, X., Elhai, J., and Wolk, C.P. (2008) Transcriptional and developmental responses by *Anabaena* to deprivation of fixed nitrogen. In *The Cyanobacteria: molecular biology, genomics and evolution*. Herrero, A. and Flores, E. (Eds.) Caister Academic Press, Norfolk, UK. Pp 383-422.

Xu, X., Risoul, V., Byrne, D., Champ, S., Douzi, B., and Latifi, A. (2020) HetL, HetR and PatS form a reaction-diffusion system to control pattern formation in the cyanobacterium *nostoc* PCC 7120. *eLife* **9**: e59190.

Yakhnina, A.A. and Bernhardt, T.G. (2020) The Tol-Pal system is required for peptidoglycan-cleaving enzymes to complete bacterial cell division. *Proc Natl Acad Sci U S A* **117**: 6777–6783.

Yang, D.C., Peters, N.T., Parzych, K.R., Uehara, T., Markovski, M., and Bernhardt, T.G. (2011) An ATP-binding cassette transporter-like complex governs cell-wall hydrolysis at the bacterial cytokinetic ring. *Proc Natl Acad Sci U S A* **108**: E1052–E1060.

Yang, Q., Pando, B.F., Dong, G., Golden, S.S., and Van Oudenaarden, A. (2010) Circadian gating of the cell cycle revealed in single cyanobacterial cells. *Science* **327**: 1522–1526.

Yang, X., Lyu, Z., Miguel, A., McQuillen, R., Huang, K.C., and Xiao, J. (2017) GTPase activity–coupled treadmilling of the bacterial tubulin FtsZ organizes septal cell wall synthesis. *Science* **355**: 744–747.

Yoon, H.S. and Golden, J.W. (2001) PatS and products of nitrogen fixation control heterocyst pattern. *J Bacteriol* **183**: 2605–2613.

Yoshii, Y., Niki, H., and Shiomi, D. (2019) Division-site localization of RodZ is required for efficient Z ring formation in *Escherichia coli*. *Mol Microbiol* **111**: 1229–1244.

Young, K. D. (2006) The selective value of bacterial shape. *Microbiol Mol Biol Rev* **70**: 660–703.

Zehr, J.P. (2011) Nitrogen fixation by marine cyanobacteria. *Trends Microbiol* **19**: 162–173.

Zehr, J.P. and Capone, D.G. (2020) Changing perspectives in marine nitrogen fixation. *Science* **368**: eaay9514.

Zeng, X. and Zhang, C.C. (2022) The making of a heterocyst in cyanobacteria. *Annu Rev Microbiol* **76**: 597–618.

Zeng, X., Huang, M., Sun, Q.-X., Peng, Y.-J., Xu, X., Tang, Y.-B., et al. (2023) A c-di-GMP binding effector controls cell size in a cyanobacterium. *Proc Natl Acad Sci* **120**: e2221874120.

Zhang, J.Y., Lin, G.M., Xing, W.Y., and Zhang, C.C. (2018) Diversity of growth patterns probed in live cyanobacterial cells using a fluorescent analog of a peptidoglycan precursor. *Front Microbiol* **9**: 791.

Zhang, L.C., Chen, Y.F., Chen, W.L., and Zhang, C.C. (2008) Existence of periplasmic barriers preventing green fluorescent protein diffusion from cell to cell in the cyanobacterium *Anabaena* sp. strain PCC 7120. *Mol Microbiol* **70**: 814–823.

Zhang, L., Zhou, F., Wang, S., and Xu, X. (2017) Processing of PatS, a morphogen precursor, in cell extracts of *Anabaena* sp. PCC 7120. *FEBS Lett* **591**: 751–759.

Zhao, M.X., Jiang, Y.L., He, Y.X., Chen, Y.F., Teng, Y. B., Chen, Y., et al. (2010) Structural basis for the allosteric control of the global transcription factor NtcA by the nitrogen starvation signal 2-oxoglutarate. *Proc Natl Acad Sci U S A* **107**: 12487–12492.

Zheng, Z., Omairi-Nasser, A., Li, X., Dong, C., Lin, Y., Haselkorn, R., and Zhao, J. (2017) An amidase is required for proper intercellular communication in the filamentous cyanobacterium *Anabaena* sp. PCC 7120. *Proc Natl Acad Sci U S A* **114**: E1405–E1412.

Zusman, D.R., Scott, A.E., Yang, Z., and Kirby, J.R. (2007) Chemosensory pathways, motility and development in *Myxococcus xanthus*. *Nat Rev Microbiol* **5**: 862–872.

Anabaena sp. PCC 7120

h

D

d

v

v

v

mreD mutant

h

D

d

v

v

v